

DEPARTMENT OF
SYSTEMS ENGINEERING AND AUTOMATION
UNIVERSITY OF MALAGA



PhD THESIS

SMART CAMERA ROBOTIC ASSISTANT FOR LAPAROSCOPIC SURGERY

Author: Ms. Irene Rivas Blanco

Supervisor: Prof. Mr. Víctor Muñoz Martínez


Co-supervisor: Dr. Giuseppe Tortora

MÁLAGA, June 7th, 2017



UNIVERSIDAD
DE MÁLAGA

AUTOR: Irene Rivas Blanco

 <http://orcid.org/0000-0002-6936-1918>

EDITA: Publicaciones y Divulgación Científica. Universidad de Málaga



Esta obra está bajo una licencia de Creative Commons Reconocimiento-NoComercial-SinObraDerivada 4.0 Internacional:

<http://creativecommons.org/licenses/by-nc-nd/4.0/legalcode>

Cualquier parte de esta obra se puede reproducir sin autorización pero con el reconocimiento y atribución de los autores.

No se puede hacer uso comercial de la obra y no se puede alterar, transformar o hacer obras derivadas.

Esta Tesis Doctoral está depositada en el Repositorio Institucional de la Universidad de Málaga (RIUMA): riuma.uma.es



D. Víctor Muñoz Martínez, Catedrático de Universidad adscrito al Departamento de Ingeniería de Sistemas y Automática de la Universidad de Málaga, y D. Giuseppe Tortora, doctor en Biorrobótica y adscrito al Instituto de Biorrobótica (The Biorobotics Institute) de la Universidad de Pisa, Italia, hacen constar

QUE

Ambos son directores de la tesis titulada “SMART CAMERA ROBOTIC ASSISTANT FOR MINIMALLY INVASIVE SURGERY”, realizada por Dña. Irene Rivas Blanco, y que dicha autora ha llevado a cabo los objetivos de investigación propuestos para la completa elaboración de la Tesis, y que se encuentra en disposición de la defensa de la misma ante el Tribunal Examinador.

Málaga, 07 de junio de 2017

Fdo. Víctor F. Muñoz Martínez

Fdo. Giuseppe Tortora

A mi madre

Agradecimientos - Acknowledgments

Esta tesis doctoral ha sido un largo camino que, por suerte, no he realizado sola. En primer lugar quiero agradecer a Lucas y a Nara toda la energía que me han dado, desde dentro y desde fuera, en esta última etapa de la tesis. Ellos han sido mi principal motivación para culminar este trabajo.

A Salva, por aguantarme todos estos años y escuchar estoicamente una y otra vez todas las presentaciones que he realizado durante esta tesis. A mi familia, por apoyarme y animarme durante todo este tiempo. Especialmente a mi madre, que me ha ayudado a sacar el tiempo necesario para terminar esta memoria.

A mis amigas, que se han hartado de escuchar la palabra tesis durante estos años. Especialmente a Desirée, por esas largas horas de desahogo al teléfono.

A mis compañeras y compañeros de laboratorio por todo el apoyo técnico y moral que me han dado en este tiempo, y a todo el departamento de Ingeniería de Sistemas y Automática. A Pablo por los sabios consejos que siempre ha dado. A mis compañeras y compañeros del PTA, María, Kike, Belén y Mari Carmen, por su ayuda en los aspectos técnicos de este trabajo y sobre todo por aguantar mis brotes de estrés, que no han sido pocos. Y a todas mis compañeras y compañeros de industriales, especialmente a Isabel y a Carlos, por todos los consejos que me han dado.

A Arianna Menciassi, per avermi dato la possibilità di realizzare un trimestre di ricerca presso L'Istituto di Biorobotica della Scuola Superiore Sant'Anna, e a tutte le persone con cui ho condiviso quei tre mesi a Pontedera. Particolarmente a Giuseppe Tortora, per avirno accolto con tanta gentilezza, e per tutte le cose che mi ha insegnato con molta pazienza.

Por último, quería agradecer a Víctor Muñoz que confiara en mí y me diera la oportunidad de realizar esta tesis doctoral. Por todo el tiempo que me ha dedicado, por todos los consejos que me ha dado, y por tratar de convertirme en una buena científica. Espero haber estado a la altura.

Resumen

En las últimas décadas, la cirugía laparoscópica se ha convertido en una práctica habitual en los quirófanos de todo el mundo, cuya evolución está tendiendo hacia técnicas cada vez menos invasivas. En este escenario, la robótica ha encontrado un gran campo de aplicación, que va desde sistemas robóticos que actúan como sistemas esclavos que replican los movimientos del cirujano hasta sistemas capaces de actuar con cierto grado de autonomía asistiendo al cirujano en determinadas maniobras quirúrgicas, o bien realizando tareas completas de forma autónoma. Sin embargo, estos sistemas requieren la supervisión directa del cirujano y su capacidad de toma de decisiones y de adaptación a un entorno tan dinámico como es una intervención quirúrgica es aún muy limitada.

Esta tesis doctoral presenta el diseño e implementación de un asistente robótico inteligente para colaborar con el cirujano en un entorno quirúrgico real. En primer lugar, se presenta el diseño de un sistema robótico camarógrafo novedoso que permite aumentar las capacidades de los sistemas actuales. Dicho sistema robótico está basado en un robot cámara intra-abdominal que se introduce por completo en el abdomen del paciente y se puede mover libremente a lo largo de toda la cavidad abdominal mediante interacción magnética con un imán externo. Con el objetivo de dotar a la cámara de autonomía, el imán externo se encuentra acoplado al efector final de un brazo robótico, que controla el desplazamiento de la cámara. De esta manera, el asistente robótico que se propone en esta tesis cuenta con seis grados de libertad, permitiendo obtener no solo un mayor campo de visión que con los sistemas de visión actuales, sino también la posibilidad de observar una misma escena desde nuevas perspectivas.

Por otro lado, la inteligencia del sistema robótico se basa en una arquitectura cognitiva especialmente diseñada para la colaboración autónoma con el cirujano en entornos quirúrgicos reales. La arquitectura propuesta trata de simular el comportamiento de un asistente humano, de manera que la comunicación con el cirujano sea lo más natural posible, así como el tipo de colaboración. La arquitectura cognitiva incluye mecanismos de aprendizaje para que el robot pueda adaptar su comportamiento a las particularidades del personal quirúrgico, así como mejorar su comportamiento a través de la experiencia, tal y como lo haría un asistente humano.

Los conceptos teóricos de esta tesis se han validado tanto mediante experimentación in-vitro en los laboratorios de robótica médica de la Universidad de Málaga, como en experimentación in-vivo con modelos porcinos en el Centro IACE (Instituto Andaluz de Cirugía Experimental) llevada a cabo por cirujanos expertos.

Abstract

In the last decades, laparoscopic surgery has become a daily practice in operating rooms worldwide, which evolution is tending towards less invasive techniques. In this scenario, robotics has found a wide field of application, from slave robotic systems that replicate the movements of the surgeon to autonomous robots able to assist the surgeon in certain maneuvers or to perform autonomous surgical tasks. However, these systems require the direct supervision of the surgeon, and its capacity of making decisions and adapting to dynamic environments is very limited.

This PhD dissertation presents the design and implementation of a smart camera robotic assistant to collaborate with the surgeon in a real surgical environment. First, it presents the design of a novel camera robotic assistant able to augment the capacities of current vision systems. This robotic assistant is based on an intra-abdominal camera robot, which is completely inserted into the patient's abdomen and it can be freely moved along the abdominal cavity by means of magnetic interaction with an external magnet. To provide the camera with the autonomy of motion, the external magnet is coupled to the end effector of a robotic arm, which controls the shift of the camera robot along the abdominal wall. This way, the robotic assistant proposed in this dissertation has six degrees of freedom, which allow providing a wider field of view compared to the traditional vision systems, and also to have different perspectives of the operating area.

On the other hand, the intelligence of the system is based on a cognitive architecture specially designed for autonomous collaboration with the surgeon in real surgical environments. The proposed architecture simulates the behavior of a human assistant, with a natural and intuitive human-robot interface for the communication between the robot and the surgeon. The cognitive architecture also includes learning mechanisms to adapt the behavior of the robot to the different ways of working of surgeons, and to improve the robot behavior through experience, in a similar way as a human assistant would do.

The theoretical concepts of this dissertation have been validated both through in-vitro experimentation in the labs of medical robotics of the University of Malaga and through in-vivo experimentation with pigs in the IACE Center (Instituto Andaluz de Cirugía Experimental), performed by expert surgeons.

CONTENT

1	Introduction	1
1.1	Background and motivation	1
1.2	Contributions.....	3
1.3	Context	5
1.4	Thesis outline	5
2	State of the art	7
2.1	Introduction.....	7
2.2	Intra-abdominal magnetic devices	11
2.3	Automation of surgical tasks	17
2.4	Cognitive robot architectures	22
2.5	Conclusion	30
3	Control system of the robotic assistant	33
3.1	Introduction.....	33
3.2	General description of the camera robotic assistant.....	34
3.2.1	Cable-driven actuation mechanism	37
3.3	Geometric model of the task	40
3.4	Control system.....	43
3.4.1	Hybrid force-position control with torque compensation	45
3.5	Conclusion	52
4	Robot cognition	53
4.1	Introduction.....	53
4.2	Description of the cognitive architecture.....	54
4.3	Semantic memory	57
4.4	Procedural memory	60
4.5	Reinforcement learning.....	64
4.6	Conclusion	69
5	Implementation and experiments	71
5.1	Introduction.....	71

5.2 Implementation of the robotic assistant	72
5.2.1 Experimental prototype of the camera robot	74
5.2.2 Hardware architecture	76
5.2.3 Software architecture	77
5.3 In-vivo validation of the camera robot	80
5.4 Force-position control	84
5.4.1 Experimental setup	85
5.4.2 Stiffness matrix estimation	85
5.4.3 Experimental results	87
5.5 Smart camera navigation	87
5.5.1 Experimental task	87
5.5.2 Analysis of the cable-driven mechanism	91
5.5.3 Semantic knowledge	92
5.5.4 Experiment 1: navigation behaviors comparison	95
5.5.5 Experiment 2: learning evaluation	102
5.6 Conclusion	107
6 Conclusion and future work	109
6.1 Conclusion	109
6.2 Future work	112
A Intuitive teleoperation control	113
A.1 Control scheme	114
A.2 Experimental validation	115
A.2.1 Modular robotic platform	116
A.2.2 Kinematics configuration	117
A.2.3 Experiments	118
B The cisobot platform	121
C Robotic operating system (ROS)	125
DSOAR Cognitive Architecture	127
Resumen de la Tesis Doctoral	131
Glossary of terms	145

Notations	147
References	149

LIST OF FIGURES

Figure 2.1 Close proximity of instruments and camera in SPAS.	8
Figure 2.2 Da Vinci Surgical System (Intuitive Surgical Inc.).....	9
Figure 2.3 Integration of key technologies to develop a smart robotic assistant..	10
Figure 2.4 Tissue retractor based on local magnetic actuation proposed by (Garbin et al. 2015).	12
Figure 2.5 Retraction system with a screw-drive mechanism to adapt for different thickness of abdominal wall developed by (Brancadoro et al. 2017).....	13
Figure 2.6 Magnetic anchoring robotic platforms: (a) dexterous miniature robot (Lehman et al. 2009); (b) Modular robotic platform (Tognarelli et al. 2015).	14
Figure 2.7 Magnetic anchoring camera robot designed by (Cadeddu et al. 2009).	14
Figure 2.8 Magnetically activated stereoscopic vision system proposed by (Simi et al. 2013).	16
Figure 2.9 Laparoscopic camera based on an orthogonal magnet arrangement proposed by (Garbin et al. 2016).....	16
Figure 2.10 The Berkeley Surgical Robots performing knot-tie (Van den Berg et al. 2010).	19
Figure 2.11 Automated suturing on a pig using the STAR robot (Shademan et al. 2016).	19
Figure 2.12 Illustration of the tasks performed by the collaborative framework of (Padoy and Hager 2011).	21
Figure 2.13 The SOAR cognitive architecture (Laird 2008).	25
Figure 2.14 The ACT-R cognitive architecture (Kajdoci and Pozna 2014).	26
Figure 2.15 The CLARION cognitive architecture (Sun, Wilson, and Lynch 2016).	27
Figure 2.16 Human-robot interaction architecture for camera guidance in LS proposed by (Ko et al. 2005).	28
Figure 2.17 Cognitive architecture proposed by (Weede et al. 2013).	29
Figure 2.18 SOAR-based cognitive framework for smart robotic assistants.	31
Figure 3.1 General description of the camera robotic assistant.	35
Figure 3.2 (a) Top view of the camera robot; and (b) coupling mechanism between components of the robotic assistant.	35
Figure 3.3 Actuation of the DoFs: (a) external DoFs; and (b) internal DoFs.....	36
Figure 3.4 Cable-driven actuation system: (a) driven side; and (b) driver side. ..	39
Figure 3.5 Motion transmission of the cable-driven actuation system particularized for the roll rotation: (a) initial position, (b) clockwise rotation, and (c) counterclockwise rotation.....	40
Figure 3.6 Geometric model of the task.	41

Figure 3.7 Effect of the robotic assistant DoFs on the camera view.	42
Figure 3.8 Control system of the robotic assistant.	43
Figure 3.9 Roll and tilt control scheme.....	44
Figure 3.10 Camera displacement along the abdominal wall.....	45
Figure 3.11 Control scheme for the displacement of the camera along the abdominal wall.....	46
Figure 3.12 Orientation control of the external robot: (a) holder parallel to the contact surface, (b) holder not parallel to the contact surface, (c) action to correct the robot orientation.	47
Figure 3.13 Control scheme of the torque compensation.	48
Figure 3.14 Control scheme of the hybrid force-position control.....	49
Figure 4.1 Global cognitive architecture.	55
Figure 4.2 Semantic memory codification as a database.	57
Figure 4.3 Camera navigation strategy.....	61
Figure 4.4 Procedural memory control scheme.	62
Figure 4.5 Camera robot displacement computation.	63
Figure 4.6 Reinforcement learning algorithm.....	65
Figure 4.7 Membership functions of input and output variables of the reward fuzzy model: (a) noCorrections, (b) time, (c) satisfaction, and (d) reward...	68
Figure 4.8 Fuzzy model surfaces: (a) satisfaction vs noCorrections, and (b) satisfaction vs time.	69
Figure 5.1 Camera robotic assistant experimental setup.	73
Figure 5.2 CISOBOT platform.	74
Figure 5.3 Design of the intra-abdominal device: top view (left), and front view (right).	75
Figure 5.4 Experimental prototype of the intra-abdominal device: (a) intra- abdominal device, (b) external motors, and (c) HD miniature camera.....	75
Figure 5.5 Hardware architecture of the experimental setup.....	77
Figure 5.6 ROS architecture.	78
Figure 5.7 Snapshot of the Human-Machine Interface.....	80
Figure 5.8 In-vivo experimentation in a pig: (a) insertion procedure, (b) snapshot of the operating room during the experiment, and (c) snapshot of the camera robot inside the abdominal cavity.	81
Figure 5.9 Comparison between images provided by the camera robot (left) and a conventional endoscope (right).	83
Figure 5.10 Experimental setup for the force-position control validation.....	84
Figure 5.11 Stiffness matrix estimation.	85
Figure 5.12 Results of the force-position control experiment: (a) position tracking, (b) force tracking, and (c) torque tracking.....	86
Figure 5.13 Snapshot of the task platform.....	89
Figure 5.14 State diagram of the overall task.	90

Figure 5.15 Distribution of the experimental data for the analysis of repeatability of cable-driven DoFs: (a) roll; (b) tilt.	91
Figure 5.16 Colored markers stored in the semantic memory.....	93
Figure 5.17 Snapshot of the camera view for each state of the task.....	94
Figure 5.18 Admissible area within no camera displacement is necessary.....	96
Figure 5.19 Results of Experiment 1: (a) mean performance time; (b) mean number of corrections.	98
Figure 5.20 Comparison of the performance of a particular user during the five trials: time (up) and number of commands (down).	99
Figure 5.21 Marker tracking and camera displacement in State 2 in a normal situation.....	100
Figure 5.22 Marker tracking and camera displacement in State 2 during an unexpected situation.....	101
Figure 5.23 Customized values for K_r for each user and each state.....	104
Figure 5.24 Frequency of the customized value for the 15 trials performed by each user.	105
Figure 5.25 Reinforcement learning algorithm analysis for State 4 of User 4: K_r and reward for each trial of the experiment.....	106
Figure A.1 Intuitive teleoperation of the surgical tools.	114
Figure A.2 Intuitive teleoperation control scheme.....	115
Figure A.3 Modular robotic platform developed by (Tortora, Dario, and Menciassi 2014).	116
Figure A.4 Modular robotic units: (a) electro-cutter robot, and (b) grasper robot.	117
Figure A.5 Task protocol: (a) state 1, (b) state 2, and (c) state 3.....	119
Figure A.6 Learning curve associated with the teleoperated system.	120
Figure B.1 Robotnik modular arm.....	122
Figure B.2 Inverse kinematics solutions: (a) $b = 1, c = 1$, (b) $b = 1, c = -1$, (c) $b = -1, c = 1$, and (d) $b = -1, c = -1$	123
Figure C.1 ROS network.....	126

LIST OF TABLES

Table 4.1 Semantic learning algorithm.	60
Table 4.2 Procedural memory with reinforcement learning algorithm.	67
Table 5.1 Discrete steps of the robotic assistant DoFs with the HMI.	90
Table 5.2 Knowledge stored in semantic unit S_1	92
Table 5.3 Knowledge stored in semantic unit S_2	94
Table 5.4 Knowledge stored in semantic unit S_3	94
Table 5.5 Description of the procedure of Experiment 1.	96
Table A.1 Denavit-Hartenberg parameters of the robotic units.	118
Table A.2 Inverse kinematics of the robotic units.	118
Table A.3 Dexterity evaluation experimental results.	120
Table B.1 Denavit-Hartenberg parameters of the Robotnik modular arms.	123
Table B.2 Inverse kinematics of the Robotnik modular arms.	124

1 INTRODUCTION

1.1 Background and motivation

In the last few decades, the field of surgery has evolved towards minimally invasive techniques that are aimed at reducing the invasiveness of the interventions. Laparoscopic surgery (LS) involves operating through small incisions performed on the patient's abdominal wall whereby the instruments and a camera are introduced. This form of operating offers numerous advantages for patients, including cosmetic and recovery benefits (Romanelli, Mark, and Omotosho 2008). However, they imply new challenges for surgeons, who require longer training periods to become skilled in performing operations following this approach. Laparoscopic procedures have evolved to new less invasive techniques that improve the cosmetic advantages for patients but increase the difficulties for surgeons: Single Port Access Surgery (SPAS) and Natural Orifice Transluminal Endoscopic Surgery (NOTES). SPAS makes use of a single incision whereby all the working instruments and the endoscope are introduced (Gascón Hove et al. 2014). This technique requires the use of special semi-flexible or curved instruments that increase the surgeons' learning curve (Bucher, Pugin, and Morel 2008). Moreover, this way of operating reduces the instruments workspace due to the “sword fighting” effect, i.e. tools easily collide inside and outside the abdomen. Furthermore, the close proximity of the instruments and the endoscope entails a loss of triangulation, which translates to a loss of depth sensation. On the other hand, in NOTES procedures special flexible instruments are introduced into the abdominal cavity through natural orifices of the body (Wang et al. 2016). However, this technique is stagnant due to the lack of suitable instruments (Trejos et al. 2011).

In this sense, robotics has encountered a wide field of application in order to overcome the limitations of laparoscopic procedures described above by enhancing surgeons' abilities in terms of high precision and more intuitive movements of the

surgical tools. Surgical robots can be defined as robotic systems that work cooperatively with surgeons, and they can be classified into two main groups: surgeon extenders and auxiliary surgical supports (Taylor 2006). The first group are directly operated by the surgeon and are conceived to augment surgeons' abilities to manipulate surgical instruments. The market for these kinds of surgical assistants has been monopolized by Intuitive Surgical Inc., who developed the da Vinci Surgical System, a three or four-armed teleoperated platform. The company has sold more than 3,000 units worldwide, and more than 1.5 million surgeries have been performed with this platform. In fact, approximately 90% of the prostatectomies are performed using the da Vinci system (Haidegger, Sándor, and Benyó 2011). However, the main limitation of these kinds of robots is that they are not able to perform autonomous tasks to help the surgeon during the intervention. Thus, they act as a robotic tool rather than as a robotic partner for the surgeon. On the other hand, auxiliary surgical supports, also called surgical robotic assistants, work side-by-side with the surgeon and perform functions such as endoscope holding or retraction.

In order to augment the capabilities of surgical robotic assistants, many authors have addressed the development of autonomous and semi-autonomous systems able to perform automatic tasks that relieve the surgeon of performing some maneuvers and reduces his or her workload during laparoscopic procedures. There have been proposed methods for automatic camera guidance (Ko et al. 2005; Weede et al. 2011), and for autonomous performance of complete surgical tasks such as suturing (Kang and Wen 2001), tissue retraction (Patil and Alterovitz 2010) or motion planning for needle insertion (Alterovitz et al. 2009). Other authors have proposed collaborative scenarios in which the robot performs some parts of a maneuver while the surgeon performs the more challenging states (Bauzano et al. 2015; Padoy and Hager 2011). However, these systems still require a lot of attention from surgeons and they are limited to performing preprogrammed motions. Thus, they lack the intelligence and awareness to be considered autonomous (Pandya et al. 2014).

Therefore, the evolution of surgical robots should be aimed toward the development of co-worker robotic assistants that work side-by-side with the surgeon in a similar way as a human assistant. Cognitive architectures provide the required infrastructure to endow robots with human capabilities. There are numerous standard cognitive architectures that have been applied to different fields such as mobile robots (Janrathitikarn and Long 2008; Laird et al. 2012), games theory (Choi et al. 2011; Kirk, Mininger, and Laird 2016) and modelling human behavior (Liu et al. 2016; Zhang et al. 2014). However, the concept of co-worker robot in minimally invasive surgery is an open research field in which there is still much work to be done. These kinds of robots require the interaction of different technologies that provide the robot the means necessary to reason and make

decisions, and to perform surgical tasks autonomously. Thus, navigation technologies must be combined with a natural human-robot interaction that emulates human communication, all integrated into a cognitive architecture that provides the robot with the capabilities for performing high-level task planning through reasoning and an appropriate knowledge base.

1.2 Contributions

This PhD dissertation offers theoretical and experimental results related to a smart camera robotic assistant that works side-by-side with the surgeon during minimally invasive interventions. This robotic assistant is conceived to substitute the endoscope and to provide autonomous assistance to the surgeon. This work proposes a novel concept of a camera robot that enhances the capabilities of current approaches of surgical vision systems. Moreover, the robotic assistant is designed following a cooperative philosophy, involving natural communication with the surgeon that emulates human surgical team interaction. Thus, the intelligence of the system is based on a cognitive architecture with learning capabilities that provides the robot with decision-making and autonomous navigation capabilities. In particular, aside from an in-depth analysis of the current state of the art, this PhD dissertation offers the following contributions:

1. Novel concept of camera robotic assistant for minimally invasive surgery without holonomic constraints

This work proposes a novel concept of camera robotic assistant for minimally invasive surgery without holonomic constraints of its movement. The camera robotic assistant is composed of an external robotic arm and an intra-abdominal camera robot, which is guided along the abdominal wall via magnetic interaction with the external robot. Thus, the camera can be freely moved within the abdominal cavity thanks to the six degrees of freedom of the robotic assistant: two shifts along the abdominal wall and a pan rotation, which are actuated by the external robot, and two internal rotations, roll and tilt, and a digital zoom, which are actuated by the intra-abdominal device. This system approach enhances the field of view of the operating area compared to conventional endoscopes and it is able to provide different perspectives of the anatomical structures, helping surgeons to overcome the loss of depth perception of planar images and offering a more natural view of the anatomical structures. Moreover, this approach allows autonomous camera navigation, releasing the surgeon from this task and avoiding the need of a human assistant to handle the camera.

2. Force-position control with torque compensation able to adapt the motion of the camera to the anatomy of the abdominal wall

Shifting of the camera along the abdominal wall requires an active orientation control able to adapt the motion of the robot to the anatomy of the abdominal wall, assuring that the motion of the camera does not cause any harm to the patient. With this aim, a hybrid force-position control with a torque compensation module that assures a proper robot orientation is proposed. Thus, the force-position scheme controls the displacement of the robot in the tangent directions of the contact surface (abdominal wall) while controlling the force exerted in the normal direction. On the other hand, the torque compensation module assures that the end effector of the external robot stays parallel to the abdominal wall during the displacement, which anatomy is a priori unknown and differs from one patient to another.

3. Design of a cognitive architecture with learning capabilities that emulates human behavior for surgical applications

Cognitive architectures provide robotic systems with human functionalities, such as reasoning, learning, problem-solving and decision making. A standard cognitive architecture has been adapted to provide the camera robotic assistant with a natural human-robot interaction, along with decision-making and autonomous navigation capabilities to work side-by-side with the surgeon in a similar way as a human assistant would do. The cognitive architecture also includes learning mechanisms that allow the system to augment its base of knowledge and to improve its behavior over time.

4. Implementation of the smart camera robotic assistant and experimental results

The cognitive architecture and the hybrid force-position control have been validated through a set of in-vitro experiments that demonstrate the feasibility of the theoretical concepts proposed in this PhD dissertation. The design of the camera robotic assistant has also been tested through an in-vivo experiment in a pig in the Center IACE (Instituto Andaluz de Cirugía Experimental), through which the main features of the robot have been analyzed.

1.3 Context

This thesis has been conducted within the context of the research lines of the research group of medical robotics of the Department of Systems Engineering and Automation of the University of Malaga. Furthermore, the author spent a three-month research stay at the laboratories of The Birobotics Institute of the Scuola Superiore Sant'Anna (Pisa, Italy).

The first primary achievement of the author's research group was the design and implementation of a camera robotic assistant that was successfully used in human surgery (Munoz et al. 2006). After this achievement, the group focused its research on the development of a robotic platform able to autonomously collaborate with the surgeon in surgical tasks (Bauzano 2012), and in the development of a surgeons' gesture recognition system (Estebanez 2013). The last PhD dissertation of the group was focused on the navigation of surgical instruments for Single Port Access Surgery (Pérez del Pulgar 2015). Thus, this PhD dissertation is a step forward in smart surgical robotics systems.

This doctoral thesis has been supported by a doctoral grant given by the Spanish Ministry of Economy and Competitiveness (EEBB-I-13-07552) associated with the National Project DPI2010-21126-C03-01, with the main goal being to develop a robotic assistant for SPAS/NOTES surgical techniques. The research stay was also supported by the Spanish Ministry of Economy and Competitiveness in the context of research stay grants for doctoral students.

1.4 Thesis outline

This thesis is divided into six chapters, four appendices, and bibliographical references. Except for this chapter and the one related to the conclusions and future work, each chapter starts with an introduction that states the problem to solve and ends with the conclusions that highlight the contributions and/or the results that have been obtained.

Chapter 2, *State of the art*, offers an up-to-date state of the robotic solutions applied to the needs of current surgical techniques, including the current state of the art regarding surgical robot skills. A revision of the most significant cognitive architectures is later discussed, along with the application of each one. The chapter ends with the global proposal of this PhD dissertation that goes a step further beyond the current state of the art.

Chapter 3, *Control system of the robotic assistant*, presents the control scheme of the camera robotic assistant. It starts with a general description of the robotic assistant along with the specifications of the design of the camera robot, followed by the geometric model of the task. Then, it delves into the control scheme of the system, which is divided into the control of the cable-driven actuation mechanism of the camera robot, and a hybrid force-position control with torque compensation for the external displacement of the robot.

Chapter 4, *Robot cognition*, describes the cognitive architecture implemented for the smart camera robotic assistant. First, a general overview of the architecture is presented, followed by an in-depth analysis of the robot cognition system. Then, the semantic memory and the procedural memory of the system are described, along with the reinforcement learning mechanism to improve the robot behavior.

Chapter 5, *Implementation and experiments*, describes the implementation of the theoretical concepts described in the previous chapters and presents the experimental results of this work. After the description of the robotic assistant employed for the experiments, the software architecture based on a ROS network is described. Then, an in-vivo validation of the camera robot in a pig is presented. After that, experiments that validate the force-position control for the camera displacement are analyzed. Finally, experiments to validate the smart camera navigation proposed in this work are exposed. These experiments are divided into a comparison among different robotic assistant behaviors, and an evaluation of the learning mechanism.

Chapter 6, *Conclusion and future work*, highlights the most relevant contributions of this thesis and proposes future research topics.

Finally, the appendices provide a further analysis of the teleoperation control used in the experimentation and the theoretical concepts of the programming tools used for the implementation of this work.

2 STATE OF THE ART

2.1 Introduction

Nowadays, Minimally Invasive Surgery (MIS) or Laparoscopic Surgery (LS) is a widely accepted technique all over the world, not only by surgeons but also by patients who benefit from its better cosmetic outcomes. Although LS has a steep learning curve compared to conventional open surgery, and unexpected complications are not infrequent, it leads to a shorter recovery time, less use of analgesic and tissue trauma, and a reduced risk of post-operative complications (Romanelli, Mark, and Omotosho 2008; Shah and Shah 2008; Varela, Wilson, and Nguyen 2010). LS involves the use of special surgical instruments that are inserted into the abdominal cavity through small incisions in the abdominal wall, along with a camera that provides visual feedback of the operating area. The natural evolution of laparoscopic procedures has led to new less invasive techniques:

- Single Port Access Surgery (SPAS): this technique involves having all instruments entering the abdominal wall through a single portal entry, typically the navel. Unlike the traditional multi-port LS, it does not leave any visible scar (Gascón Hove et al. 2014).
- Natural Orifice Transluminal Endoscopic Surgery (NOTES): in this new procedure, access to the abdominal cavity is gained through natural orifices of the body. NOTES has the advantages of avoiding incision scars on the abdomen, but it is limited by the lack of suitable flexible instruments (Wang et al. 2016).

Despite the medical and aesthetical advantages of these techniques for patients, the difficulties derived from the manipulation of laparoscopic instruments by means

of a standard video image feedback implies a long training period for surgeons to become skilled enough to successfully perform these techniques (Park et al. 2009; Zhang and Tanigawa 2009). In fact, the surgeon learning curve significantly increases from LS to NOTES. Difficulties derive not only from the narrow field of view offered by endoscopes and the planar vision they provide but also from the lack of natural perspective of the operating area and the limited motion of the camera, restricted by the entry port. Moreover, the entry port also hinders instrument manipulation due to the motion inversion as a consequence of the fulcrum effect. Furthermore, the nature of laparoscopy requires the use of at least three instruments at the same time: two for manipulation and the camera. Therefore, the surgeon needs an assistant, who usually handles the endoscope. Thus, the cooperation of the medical staff is essential for a successful operation.

These LS limitations increase with the reduction of invasiveness. In SPAS, the close proximity of the instruments and the camera entails extra challenges for this type of procedure. First, the close proximity of the instruments severely restricts the range of motion of the tools (Figure 2.1). This fact reveals the need of special semi-flexible or curved laparoscopic instruments (Bucher, Pugin, and Morel 2008) so that a larger space can be achieved inside the patient without the tools running into each other. Second, the close proximity between the instruments and the camera entails a loss of triangulation, which translates into a loss of 3D perception in the image. NOTES represents the more challenging MIS technique, which has a limited application due to the lack of actual suitable instruments. Limitations of the existing instruments for NOTES include a reduced number of channels of small size, instability, triangulation issues, inability to apply retraction and the difficulty in the instrument handling (Trejos et al. 2011).

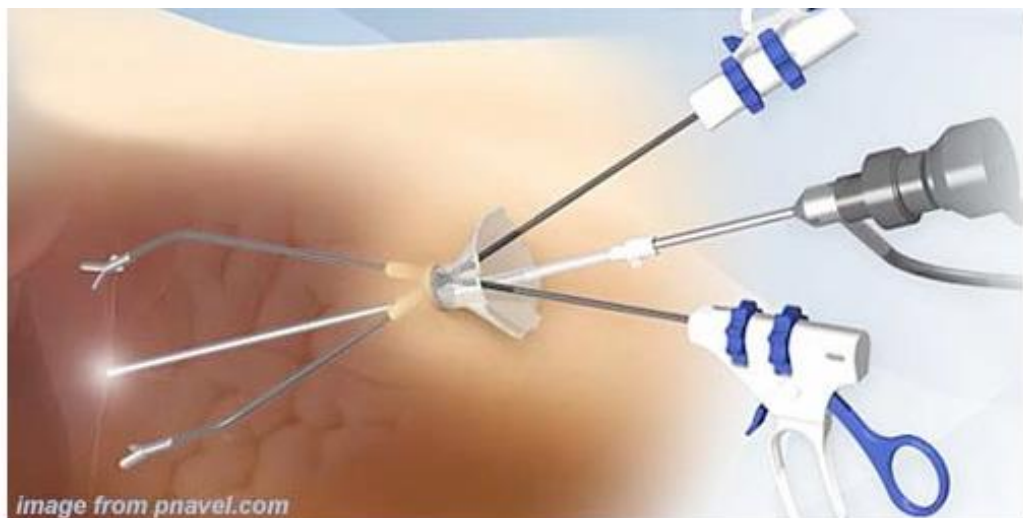


Figure 2.1 Close proximity of instruments and camera in SPAS.



Figure 2.2 Da Vinci Surgical System (Intuitive Surgical Inc.).

In this context, teleoperated platforms have emerged as a robotic solution for the above limitations, providing more accuracy and a more intuitive motion of the instruments, and a three-dimensional view of the operating area. Although these systems have become a daily reality in operating rooms all over the world (Haidegger, Sándor, and Benyó 2011), this market is actually stagnant with the available teleoperated robotic systems on the market, with the main reference worldwide being the da Vinci System (Figure 2.2). Although this system enhances surgeons' abilities in terms of accuracy, accessibility and dexterity, it requires long training periods, adapting the operating rooms for its integration, and the challenging surgical tasks remain tedious and time-consuming. Its teleoperated schemes do not provide the required assistance and human support for collaborating with surgeons during an intervention; they limit to replicate the surgeons' movements. In other words, the da Vinci System acts as a robotic tool for the surgeon, but not as a robotic partner.

In order to augment surgical robot capabilities, many authors have developed strategies for automatic motion of surgical tools, such as reactive methods for obstacle avoidance in surgical tool navigation (Bauzano, Muñoz, and Garcia-Morales 2010; Shiller, Gal, and Rimon 2010) or autonomous camera navigation based on instrument tracking (Casals, Amat, and Laporte 1996; Voros et al. 2010). These methods have been improved with predictive navigation techniques that consider the future motion of humans and/or other obstacles to foresee future situations (Foka and Trahanias 2010; Weede et al. 2011). Other authors employ learning from demonstration techniques for the automation of surgical tasks (Reiley, Plaku, and Hager 2010). (Leonard et al. 2014) propose a surgical robot for automatic planar suturing, and (Bauzano et al. 2015) propose a motion planner to assist surgeons during a collaborative suture. However, an active collaboration requires adapting robots to dynamic environments and being able to react to unexpected situations.

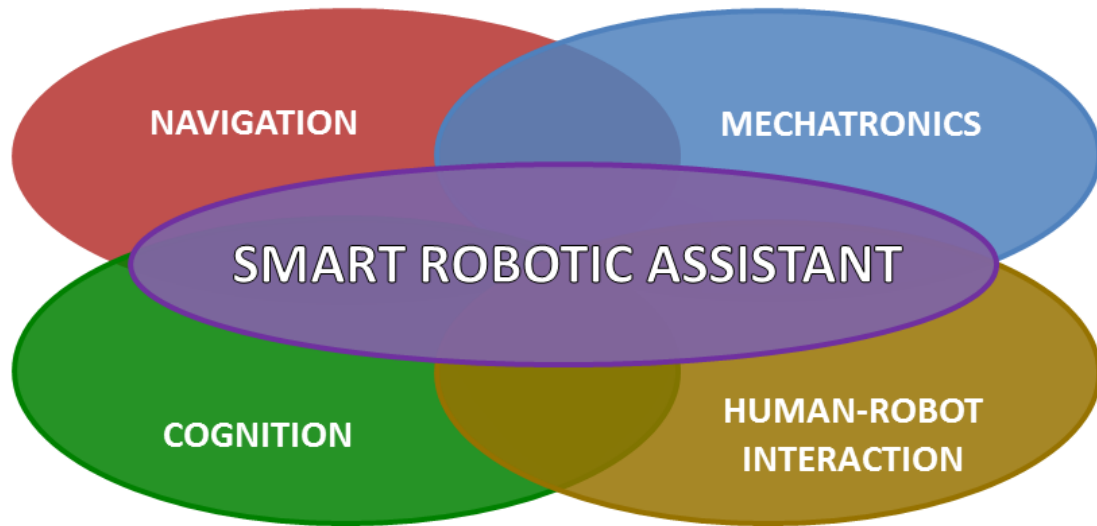


Figure 2.3 Integration of key technologies to develop a smart robotic assistant.

According to the above considerations, it is clear that the evolution of surgical robotics must move in the direction of developing a new concept of surgical robot that combines human and robot capabilities under the co-worker concept (Haddadin et al. 2011). These new robotic assistants must work side-by-side with surgeons, collaborating with them in a natural and autonomous way, as a human assistant would do. The development of such robotic assistants requires the integration of the following key technologies, depicted in Figure 2.3: navigation, mechatronics, human-robot interaction, and cognition.

Current navigation methods are constrained by the fulcrum point, i.e. the point at which the surgical instruments are inserted. This hugely limits the range of motion of the tools and reduces their reachable workspace. This effect could be avoided with new mechatronic solutions that lead to unconstrained robotic systems able to reach any point within the abdominal cavity. Some steps have been taken in this sense, with the development of intra-abdominal robots based on external magnetic guidance (Best et al. 2012; Lehman et al. 2008).

On the other hand, human-robot interaction technologies must offer a natural way of communication that goes a step further than the current direct control interfaces, such as teleoperation or bilateral control provided with force-feedback (Hagn et al. 2010; Yoon, Kim, and Lee 2015), voice commands (Kraft et al. 2004; Munoz et al. 2006; Voros et al. 2010), head movements (Gilbert 2009; Stolzenburg et al. 2011) or gaze-contingent control (Noonan et al. 2008, 2010). Gesture recognition is a more natural human-machine interface that allows the robot to identify the maneuvers the surgeon is performing and thus to follow the surgical workflow without direct commands from the surgeon (Estebanez et al. 2010). This

approach requires a robot knowledge base that stores, among other things, surgical protocols and maneuvers. Moreover, a smart robotic assistant must be endowed with a cognitive infrastructure with decision-making and high-level planning capabilities, as well as learning mechanisms, that allow the robot to collaborate with the surgeon in a dynamic environment without direct supervision and to react to situations that have not been preprogrammed.

This chapter offers the state of the art of the key technologies depicted in Figure 2.3. Firstly, a revision of the new intra-abdominal magnetic devices proposed in the literature is presented. Then, Section 2.3 discusses the automation of surgical tasks and its current limitations, and Section 2.4 reviews the most significant standard robot cognitive architectures and the application of cognitive frameworks in surgical robotics. Finally, conclusions are reported.

2.2 Intra-abdominal magnetic devices

The new laparoscopic techniques SPAS and NOTES require the design of new robotic approaches that overcome the limitations derived from the reduced degree of invasiveness of this new form of operating. Thus, the new research line of surgical robotics is geared towards the development of intra-abdominal devices, also called miniature robots, which are fully introduced into the human body and operate directly from inside the patient. These devices are introduced into the abdominal cavity through one of the incisions the surgeons make to insert the surgical tools or through natural orifices, commonly the esophagus. Different forms of attachment to the abdominal wall have been explored, such as suturing (Hu et al. 2009) or needle locking (Castro et al. 2012), but magnetic interaction is the only one that allows continuous motion of the devices (Leong et al. 2016). In this last approach, also called Magnetic Anchoring and Guidance Systems (MAGS), a permanent magnet is embedded into the devices, and an external magnet placed onto the abdominal wall is used to guide and reposition the intra-abdominal devices. Hence, this solution makes it possible to reach areas unattainable for conventional laparoscopic tools and to release an entry port, which can be used for an additional tool if required. MAGS found in literature include robotic platforms with miniature tools for manipulation (Lehman et al. 2011; Park et al. 2007; Tortora et al. 2013), intra-abdominal camera robots (Best et al. 2012), surgical retractors (Brancadoro et al. 2017), and surgical cauterizers (Zeltser et al. 2007).

(Garbin et al. 2015) proposed a tissue retractor based on local magnetic actuation (LMA). This approach, shown in Figure 2.4, combines two pairs of magnets: the anchoring unit and the actuation unit. The former provides the anchoring to the



Figure 2.4 Tissue retractor based on local magnetic actuation proposed by (Garbin et al. 2015).

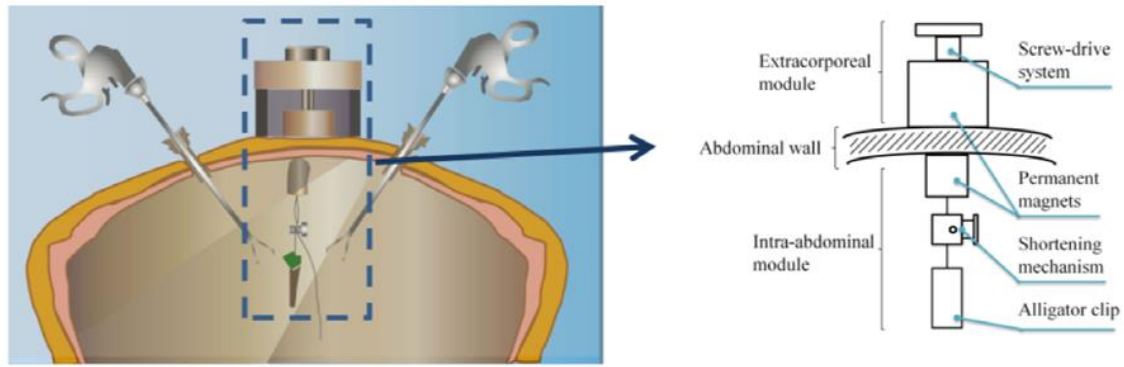


Figure 2.5 Retraction system with a screw-drive mechanism to adapt for different thickness of abdominal wall developed by (Brancadoro et al. 2017).

Regarding robotic platforms for MIS, (Lehman et al. 2009) have developed a dexterous six DoFs robot consisting of a central body and two arms fitted with cautery and forceps end-effectors (Figure 2.6.a). The robot enters the abdominal cavity through the esophagus with the arms unfolded, and once inside, the arms are refolded and the robot is attached to the abdominal wall through external magnetic interaction. The surgeon remotely controls the actuation of the robot using an external console provided with two joysticks, which also serves as the external magnetic handle. The efficacy of the robot was validated in three procedures in a porcine model, namely, abdominal exploration, bowel manipulations, and cholecystectomy. Under the same concept, (Tognarelli et al. 2015) have developed an endoluminal modular robotic platform for NOTES composed of a set of miniaturized robotic units (Figure 2.6.b). The triangular-shaped anchoring frame enters the abdominal cavity through a 17 mm esophageal access port in an open configuration. Once inside the abdomen, Shape Memory Alloy actuators are used to reach the triangular configuration (Salerno et al. 2013). An external magnetic component guarantees a stable adhesion of the frame to the abdominal wall, and a dedicated docking mechanism allows the anchoring of a set of modular robotic units (Tortora et al. 2011). This system has also been validated in an in-vivo experiment with a porcine model.

Although the previous systems enhance the capabilities of surgical robotic systems by augmenting the reachable workspace by the instruments, the close and fixed relative position of the camera with respect to the working tools results in triangulation problems and a limited perspective of the operating area. Thus, some authors have developed miniature camera robots with magnetic anchoring to the abdominal wall. With this kind of vision system, the surgeon operates with conventional laparoscopic tools, but visual feedback is obtained through a miniature robot provided with a high-resolution camera, instead of through a conventional endoscope. It has been demonstrated that these camera robots provide a wider field

of view with respect to fixed devices, as the camera can be moved independently from the instruments by external displacement of the magnetic holder (Fakhry et al. 2009).

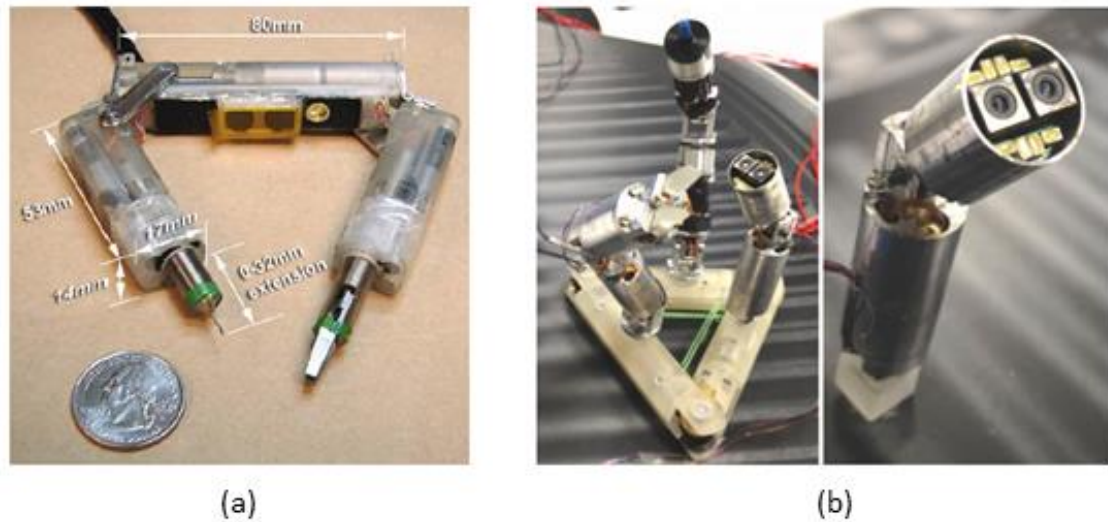


Figure 2.6 Magnetic anchoring robotic platforms: (a) dexterous miniature robot (Lehman et al. 2009); (b) Modular robotic platform (Tognarelli et al. 2015).



Figure 2.7 Magnetic anchoring camera robot designed by (Cadeddu et al. 2009).

(Cadeddu et al. 2009) have demonstrated the feasibility of using an intra-abdominal camera robot in human minimally invasive interventions, in particular, it has been used during laparoscopic nephrectomy and appendectomy. The robot, which is inserted into the abdominal cavity through a 2.5 cm incision, has a commercial camera and two high-intensity light-emitting diodes to provide onboard illumination (Figure 2.7). Power supply and signal transmission are provided by

external wires. To avoid the mobility limitations derived from the use of wires, some authors have proposed cable-free camera robots (Li, Mancini, and Tan 2016; Zhuang et al. 2014). The problems of these systems are that they are powered by batteries, which may be an issue especially in long interventions, and wireless cameras do not have the same quality as conventional wired ones.

To increase the capabilities of surgical vision systems, other authors have proposed camera robots with internal DoFs in order to augment the visual capabilities of the robots. (Lehman et al. 2008) propose an imaging robot with panning and tilting capabilities activated with internal permanent magnet direct current micromotors. Panning is accomplished by rotating a planet gear about a stationary sun gear fixed to the outer tube, and tilting is actuated with a micromotor. The intra-abdominal device is designed with a diameter of 12 mm so it can be inserted through a standard trocar. Another camera robot with active pan and tilt capabilities activated with internal motors has been proposed in (Fowler et al. 2010). (Simi et al. 2013) have designed a vision platform with two internal actuated DoFs, which combines motorized and magnetic actuation (Figure 2.8). The tilt DoF is actuated by an internal mechanism consisting of a motor connected to an internal magnet, which allows a maximum bending of 80° . The drawback of this system is that bending of the robot brings the camera closer to the anatomical structures, reducing the field of view. (Garbin et al. 2016) presented an orthogonal magnet arrangement for pan and tilt of an intra-abdominal camera device with a mechanical auto-flip that compensates for dipole-dipole singularity (Figure 2.9). The mechanism consists of two internal permanent magnets and an external one coupled with a motor. The mechanical auto-flip avoids the need of using software for correcting the image if necessary.

Summarizing, current intra-abdominal robotic solutions are provided with two active DoFs, pan and tilt, and two passive DoFs, roll and shift in two directions, which are actuated by hand motion of the external magnet. Thus, although magnetically guided camera robots augment the field of view of conventional endoscopes and provide a stable anchoring to the abdominal wall for high-quality image retransmission, the current approaches require a human assistant to control the external handle. Therefore, at present, it is not possible to implement an autonomous navigation in order to actively collaborate with surgeons in real interventions. Thus, a new approach in which the external handle could be controlled autonomously would augment the capacities of miniature camera robots and would make them suitable for integration in a co-worker scenario.

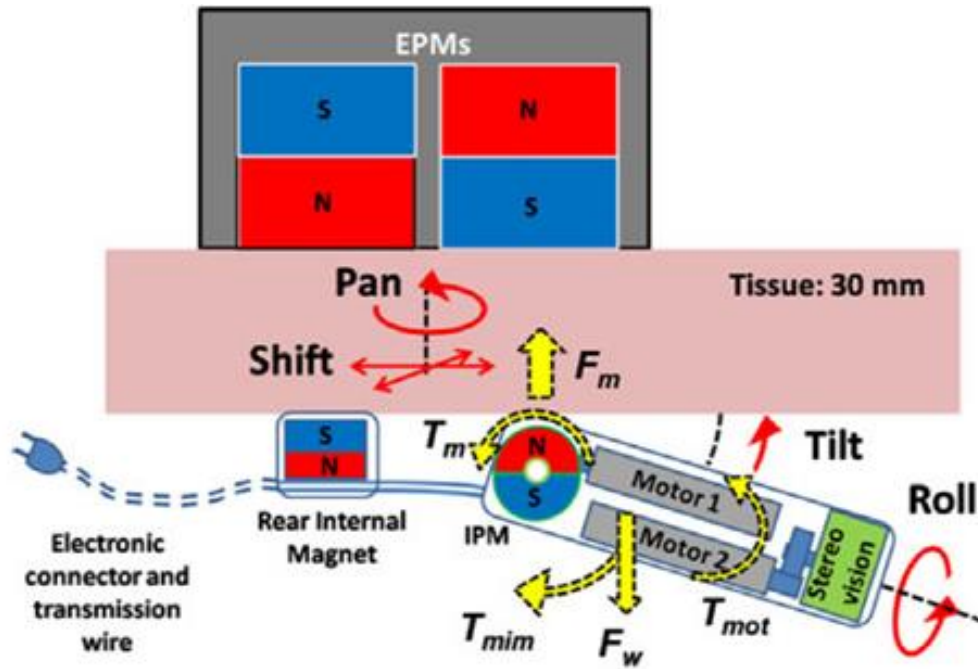


Figure 2.8 Magnetically activated stereoscopic vision system proposed by (Simi et al. 2013).

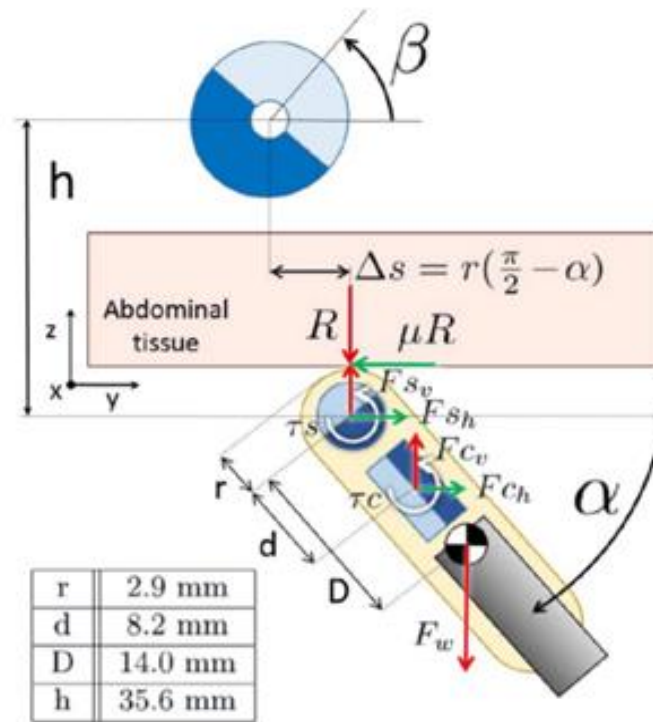


Figure 2.9 Laparoscopic camera based on an orthogonal magnet arrangement proposed by (Garbin et al. 2016).

2.3 Automation of surgical tasks

Most of the current robotic systems employed in surgical environments are teleoperated platforms, from external platforms such as the da Vinci surgical system (Haidegger, Sándor, and Benyó 2011) or the SPRINT robot (Niccolini et al. 2012), to the new intra-abdominal robotic platforms developed by (Lehman et al. 2009) or (Tognarelli et al. 2015). These systems enhance surgeons' abilities in terms of accuracy, instrument handling, tremor filtering and force sensing. However, they do not provide real assistance to the surgeon; they simply replicate the motions performed by the surgeon on a master console into a slave platform. Hence, researchers have focused their efforts on developing automatic ways of assistance in order to reduce the surgeon's workload during the interventions. The current trends can be divided into camera guidance, automation of subtasks, and automation of complete task (Elek et al. 2016).

Camera guidance is one of the most significant tasks to be automated, as it considerably reduces the cognitive load on the surgeon. Natural human interfaces are common methods for indirectly commanding the robot where to move the camera. Among these methods, the most relevant are voice commands (Kraft et al. 2004; Muñoz et al. 2005; Voros et al. 2010), head movements (Gilbert 2009; Stolzenburg et al. 2011) and gaze-contingent camera control (Noonan et al. 2008, 2010). Although these methods have succeeded in substituting medical staff, they introduce extraneous devices that may result uncomfortable for surgeons. Moreover, surgeons must pay attention in order to say the correct commands or to execute a particular head motion, which may distract them from the important surgical task.

Instrument tracking is a camera guidance approach consisting in following the tip of the surgical instruments with the camera (Azizian et al. 2014). The first examples of automatic camera guidance based on instrument tracking date back to the 1990s (Casals, Amat, and Laporte 1996). Visual servoing has also been used for the automatic positioning of surgical instruments. (Krupa et al. 2003) used this technique to move a surgical instrument around the area of an organ, and to place the instrument inside the camera field of view when it was out the camera view. (Hynes, Dodds, and Wilkinson 2005) used visual servoing to perform automatic stitching. Most of these methods employ color markers to identify the surgical tools, although (Voros et al. 2010) have implemented a tracking method based on the information of the 3D positions of the insertion point of the instruments and shape considerations. (Weede et al. 2011) improved tracking methods with the long-term prediction of the surgical instruments motion. This method is based on building a knowledge base of the position of the instruments for a particular procedure from recordings of former interventions. Using Markov chains, the system predicts the

area where the surgical tools are going to move. The ideal field of view includes all predicted points and both tools' tips.

Other surgical tasks of interest for automation are tissue retraction (Patil and Alterovitz 2010), suturing (Kang and Wen 2001), knot tying (Chow and Newman 2013), autonomous surgical debridement (Kehoe et al. 2014), cochleostomy (Brett et al. 2007) and motion planning for needle insertion for biopsies, anesthesia drug injections or brachytherapy cancer treatments (Alterovitz et al. 2009). In this sense, (Jansen et al. 2009) proposed an algorithm to generate stable and secure grasp and retraction trajectories with a 3D finite element simulation to certify the quality of the trajectories. (Jackson and Cavusoglu 2013) proposed a preliminary study of automatic suture needle driving using preplanned motion combined with visual servoing and force and torque measurements. The problem of automating the stitching task has also been addressed by (Nageotte et al. 2009). (Brett et al. 2007) developed the first autonomous surgical robot for cochleostomy. This robot navigates using transients of the reactive drilling forces to discriminate cutting conditions, the state of the tissue and the detection of the medial surface before drill break-out occurs.

(Muradore et al. 2011) discussed the application of formal methods for the verification of properties of autonomous surgical robots. They state that task automation requires progress in knowledge representation and the development of reasoning methods capable of dealing with various knowledge types in static and dynamic environments. Modeling of surgical tasks can be done manually or using machine learning strategies. One of the most common approaches is teaching the robot by imitation. (Mayer et al. 2008) proposed an approach for human-machine skill transfer. User demonstrations are decomposed into meaningful primitives by matching user patterns against features in the trajectory. They tested this method in an autonomous knot-tying task. (Osa, Sugita, and Mamoru 2014) improved this approach by proposing a method for learning time-and-space-dependent trajectories able to on-line adaptation to changes in the environment. This system, which was tested in a da Vinci system in a double loop and pick and pull tasks, can learn particular gestures and reproduce them with different initial conditions. (Van den Berg et al. 2010) have proposed a learning approach to autonomously execute specific trajectories with superhuman performance in terms of speed and smoothness by recording a set of trajectories. The important parameters maximized during the learning process are smoothness and speed of task execution. The approach is implemented on the Berkeley Surgical Robot and applied in two tasks: drawing figures on a magnetic wire-board and knot-tying (Figure 2.10).

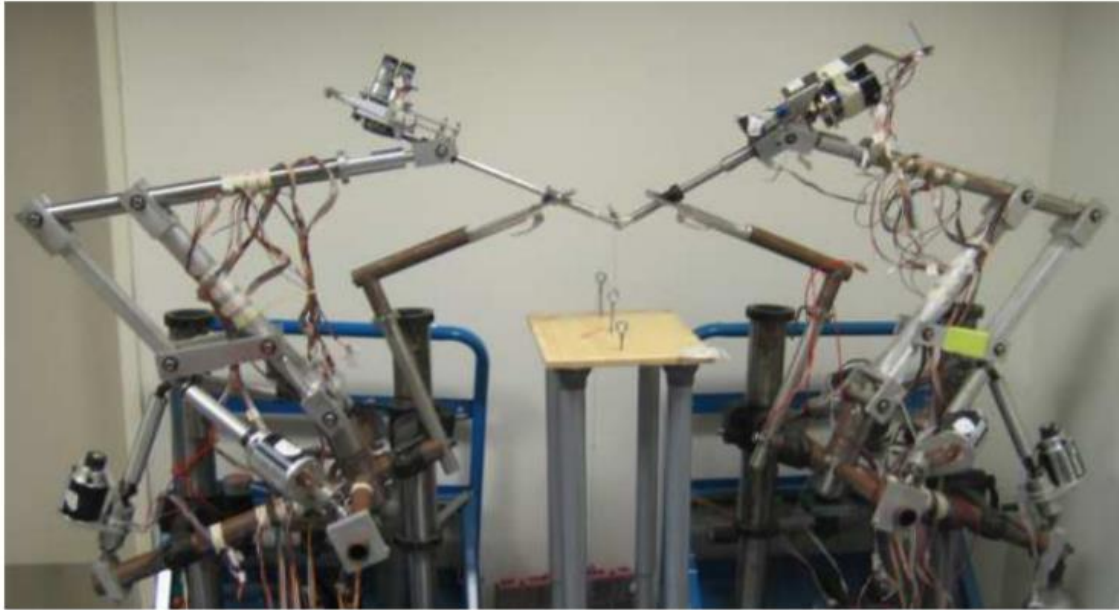


Figure 2.10 The Berkeley Surgical Robots performing knot-tie (Van den Berg et al. 2010).

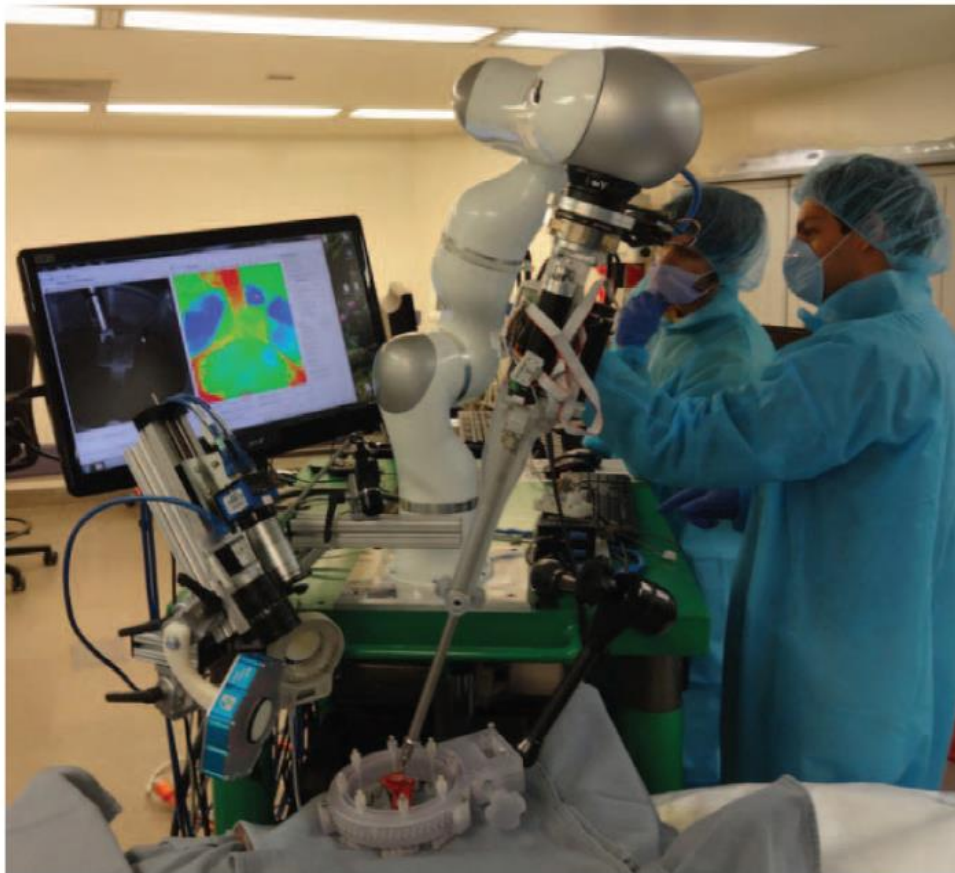


Figure 2.11 Automated suturing on a pig using the STAR robot (Shademan et al. 2016).

The ENDOBOT is the first surgical robot that can autonomously perform a suturing without surgeon supervision (Kang and Wen 2001). This robot was designed with three modes of operating: manual mode, in which the controller only provides gravity compensation, shared control, in which the surgeon controls some axes while the other axes are controlled automatically, and autonomous mode. The Stapbot is an autonomous robot for suturing using staples (Baili, Tazi, and Salih Alj 2014). The system is composed of a sensing module that collects data to detect the position and characteristics of the wound, a software analysis system to translate data into specific instructions, and the execution unit that performs the stapling. Recently, (Shademan et al. 2016) achieved the first semi-automated reconnection of bowel segments during a live pig surgery. They designed the Smart Tissue Autonomous Robot (STAR), combining smart imaging technologies and fluorescent markers to navigate and adapt to the complexities of the tissue (Figure 2.11).

Other authors propose a semiautonomous robotic system that can collaborate with surgeons during a laparoscopic procedure performing simple tasks, instead of automating a complete task. This approach requires an exhaustive modeling of the complete task and the robot must be able to follow the surgical workflow to be able to participate without direct orders from the surgeon. In this sense, (Padoy and Hager 2011) propose a collaborative system in which portions of the task are performed by the surgeon manually, and other portions are performed autonomously by the robot. It uses Hidden Markov Models (HMM) for the recognition of task completion and temporal curve averaging for learning the executed motions. The approach is validated using the da Vinci research interface in a pin task and in a suturing task, where the left tool is automated and the right one is handled by the surgeon (Figure 2.12). Based on this paradigm, (Bauzano et al. 2015) have proposed a collaborative robot for surgical procedures based on gesture recognition. A suturing task is modeled with a state diagram in which transition from one state to the following is triggered by a gesture recognition. Thus, the robot is able to follow the surgery workflow and to execute preprogrammed behaviors depending on the actual state of the task.

(Hu et al. 2015) proposed a semiautonomous neurosurgical procedure of brain tumor ablation using the RAVEN robot. The task is represented using behavior trees, in which each subtask is expressed as a leaf and relation between leafs is modeled through higher order nodes. Semi-autonomous tasks are also being studied with miniature robots. (Dumpert et al. 2009) proposed to automate the achievement of particular points the surgeon marks in the image using an overhead camera for tracking the position of the robot and a PI controller for position control of the robot joints.

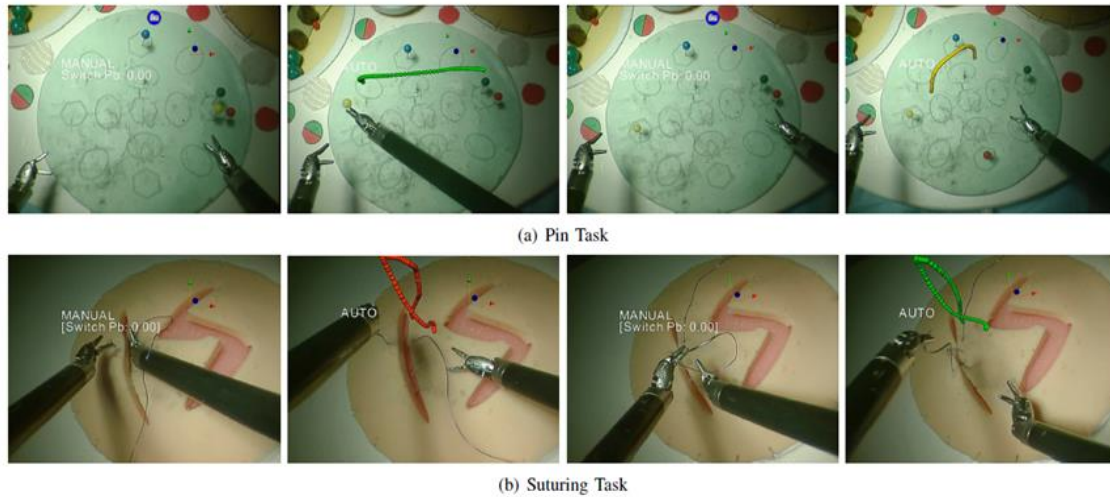


Figure 2.12 Illustration of the tasks performed by the collaborative framework of (Padoy and Hager 2011).

According to the state of the art reported above, current surgical robots have different grades of automation, from camera guidance to automation of specific surgical tasks. However, they lack the abilities to provide the required assistance to work side-by-side with the surgeon in a co-worker surgical scenario. Such a robot must have the capacity to react to unexpected situations, a knowledge base to be able to interpret the environment and to perform reasoning functions, and learning mechanisms to improve and adapt its behavior to the ways of operating of different surgeons. Thus, a smart robotic assistant must go a step further in the current abilities of surgical robots to be able to autonomously collaborate with surgeons in a real environment. First, it must be able to react to unexpected or unplanned situations and to adapt to the way of operating of different users. Second, interaction with the medical personnel must be as natural as possible, getting as close as possible to human communication. Thus, it must be provided with the surgical knowledge to be able to follow the surgery workflow by interpreting the maneuvers the surgeon performs, but it must also allow direct control interfaces, such as voice commands, to correct the behavior of the robot and to be used as inputs to the learning mechanisms. In regards to the cognitive level, a smart robotic assistant must be able to interpret its environment and to reason about it, to acquire new knowledge from the perception system and/or direct human commands, and to improve and learn new behaviors from past experiences. Cognitive architectures provide the means to manage all these abilities in order to simulate human behavior. Thus, endowed with an appropriate cognitive architecture, surgical robots could take over the simpler parts of a task and allow surgeons to focus on the more crucial and complex parts of the procedure (Kassahun et al. 2016).

2.4 Cognitive robot architectures

A cognitive architecture is a theoretical/computational model that describes the underlying infrastructure of cognitive systems, i.e. humans. Thus, it can be said that a cognitive architecture is an integration of modules or components that produces human-like behavior (Butt et al. 2013). A variety of cognitive architectures can be defined depending on the features required for each particular application. However, all of them share the following characteristics:

- **Memory structures.** Memory structures are a pivotal attribute of each biological or artificial cognitive system. They are the precondition for cognitive processes such as the acquisition of new knowledge, learning, planning, and reasoning (Kleinmann and Mertsching 2011). For psychologists, the term memory covers three aspects of information processing: encoding, storage, and retrieval (Matlin 2005). Encoding is the process of receiving and processing the incoming information, storage is the process of creating a record in a memory structure during a period of time, and retrieval is the process of getting back information. Psychologists distinguish two memory structures according to the duration of the storage: short-term memory (minutes) and long-term memory (days and years). Short-term memory, also called working memory, is viewed as a temporary store of information, but unlike the instantaneous sensory register, it holds the information in consciousness for a short period of time so that it can be processed (Woolley 2011). Conversely, long-term memory is a permanent memory store, where information transferred from working memory is organized and stored indefinitely. Long-term memory is usually broken down into semantic, procedural and episodic memory. Semantic memory stores declarative knowledge about factual information; procedural memory stores knowledge about how to perform particular behaviors such as using a pencil or driving a car; and episodic memory stores events and past experiences.
- **Knowledge representation.** Knowledge is the awareness or understanding of facts, objects or skills, and it is the main characteristic of human cognition. Knowledge is the base for other human skills such as reasoning, planning and interpreting the world we perceive. Thus, an autonomous system must have a knowledge base with the knowledge it needs to reason and interact with its environment. The content of this knowledge base would depend on the particular environment the robot is working in and the particular task it has to perform. Knowledge representation is the symbolic encoding of the propositions the cognitive agent knows. In human cognition, there are three main ways in which information can be encoded: visual, in the form of

pictures; acoustic, in the form of sounds; or semantic, in terms of the meaning of the information. In computer cognition, the knowledge representation approach depends on the type of knowledge to model and the type of information the system needs. Procedural knowledge is usually encoded as production systems containing the set of behaviors of the robot, while for semantic knowledge, the two dominant approaches are semantic networks and semantic spaces (Griffiths, Steyvers, and Tenenbaum 2007).

- **Perception.** Perception is essential to perceive the environment robots work in. We humans have multiple senses to perceive data from the environment, such as sight, hearing, taste, smell, and touch. Robots use different kinds of sensors to acquire data from the environment, such as cameras, range sensors, acoustics, force sensors, etc. Sensing ability is essential to work in highly dynamic and a priori unknown environments. Moreover, perception is one of the main mechanisms cognitive agents use to acquire new knowledge.
- **Reasoning and planning.** One of the essential high-level cognitive functions for cognitive agents is reasoning about its actions and the change that these actions cause in the environment. Planning is one of the most important reasoning tasks in robotic agents, and allow them to autonomously find a sequence of actions to execute to reach a given goal from an initial state (Dogmus, Erdem, and Patoglu 2013). The reasoning process needs to perceive the current conditions of the environment, the list of actions that can be executed, and how these actions affect the world. For this purpose, actions are usually described in a logic-based formalism so that the agent can autonomously perform reasoning tasks by based on logic-based algorithms.
- **Learning.** Learning is a pivotal process in human cognition that allows us to acquire new knowledge and to modify our behavior based on past experiences. In artificial intelligence, knowledge acquisition can be performed manually by the designer, i.e. directly entering new code in the system, or in a more dynamic way using learning mechanisms. Machine learning tasks are typically classified into three broad categories: supervised learning, unsupervised learning and reinforcement learning. In supervised learning, the system infers a function from labeled training data, so the goal is to learn patterns that can be recognized in the future. Hidden Markov Models is a widely used technique for modeling tasks for autonomous robots (Rosen et al. 2006). Conversely, unsupervised learning is a technique used to infer a function to describe hidden structure from data, and it is used in a wide range of applications such as clustering spam emails (Alishahi, Mejri, and Tawbi 2015), online topological map construction (Chin and Loo 2013) or online prediction of trajectories (Bascetta et al. 2011). Finally, in reinforcement

learning the agents take actions in an environment so as to maximize some notion of cumulative reward. This learning mechanism is used in many disciplines such as game theory (Chen et al. 2006), control theory (Anderlini et al. 2016; Jagodnik et al. 2016), multi-agent systems (Dimeas and Hatziaargyriou 2010) and swarm intelligence (Iima and Kuroe 2015).

There are many standard frameworks of cognitive architectures that offer different functionalities. The most relevant ones are SOAR, ACT-R, ICARUS, CLARION, and LIDA. SOAR is the most general cognitive architecture and its main characteristic is its flexibility. It is designed following a symbolic paradigm based on production rules. Besides its flexibility, the main advantages of SOAR are the multiple learning mechanisms it implements and a low-level planning that makes it especially suitable for robotic control applications. Thanks to its characteristics, it has a full range of applications for intelligent behavior. ACT-R is also a rule-based architecture that implements a learning mechanism that makes it possible to learn new rules from sample solutions over a process of production compilation. However, it differs from SOAR in its strong emphasis on producing a psychologically motivated cognitive model. Along with ACT-R, ICARUS and CLARION have a strong emphasis on cognitive psychology. ICARUS is characterized by a hierarchical organization that separates concepts from skills, while CLARION is based on neural networks. CLARION's on-line bottom-up learning allows agents to adapt to dynamic changes in the environment without pre-existing knowledge. Finally, LIDA is a broad-based architecture aimed at modeling the mind but puts special emphasis on human intention. Next, further details of each of these architectures and its applications are described.

SOAR is one of the most famous cognitive architectures and was developed by John E. Laird in 1983. Currently, SOAR is running its Version 9. The primary principle of SOAR is that all decisions are made through a combination of relevant knowledge at run-time. Every decision is based on the current interpretation of sensory data, the contents of working memory created by prior problem solving, and any relevant knowledge retrieved from long-term memory (Laird 2008). The SOAR architecture is depicted in Figure 2.13, consisting of various memory structures, divided into a long-term memory and a working memory, and a decision-making mechanism linking perception to action. The working memory in SOAR houses all the knowledge that is relevant to the current situation. It contains the goals, perceptions, the hierarchy of states, and operators. SOAR has many kinds of learning mechanisms: reinforcement learning, semantic learning, episodic learning, and chunking learning. SOAR has been implemented in a tabletop robot that learns new tasks from online interactive language instructions (Kirk, Mininger, and Laird 2016). (Raza and Sastry 2008) use SOAR to represent human behavior in military situations. This architecture has also been implemented in robust control of mobile

robots, taking advantage of its multiple learning mechanisms (Hanford 2011; Laird et al. 2012).

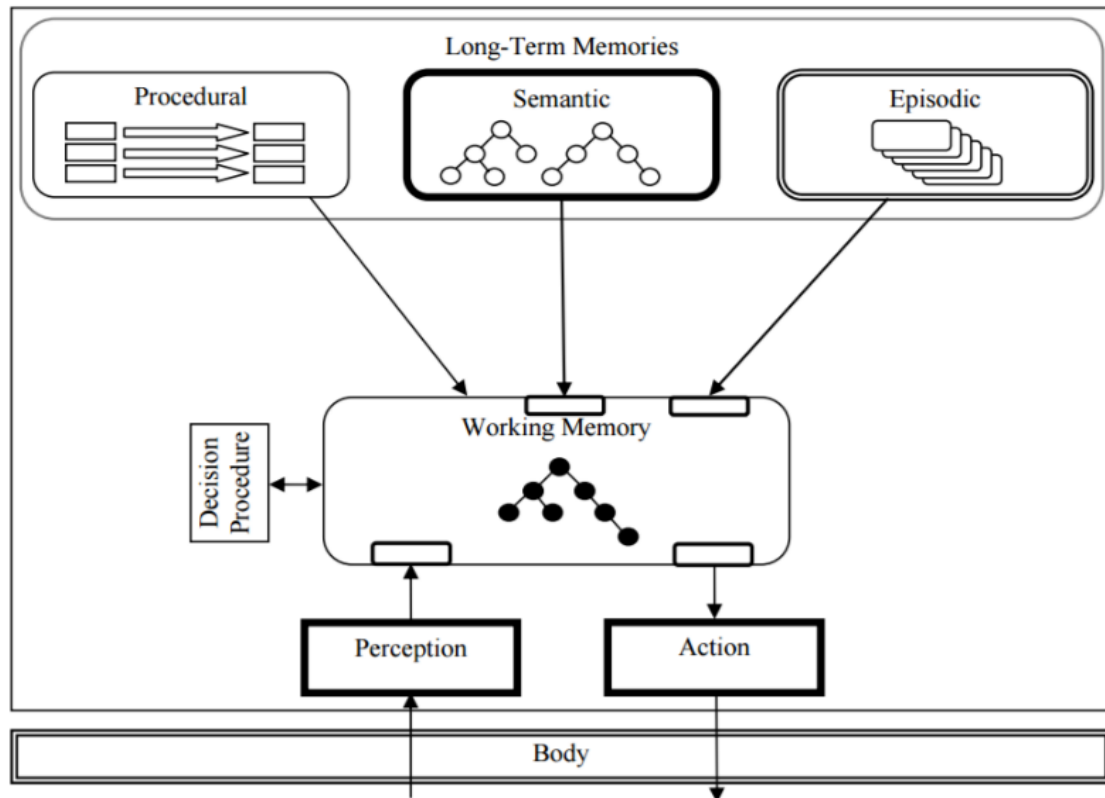


Figure 2.13 The SOAR cognitive architecture (Laird 2008).

The ACT-R (Adaptative Control of Thought-Rational) is a modular cognitive architecture that offers a theory of how cognition modules are integrated to produce coherent cognition. Each model processes a different kind of information (Figure 2.14). The vision module determines objects; the motor module is responsible for controlling the robot; the declarative module retrieves information from the long-term memory; and the goal module keeps track of the internal state when solving a problem. The fifth module, the production system, coordinates the operation of the other four modules by using the module buffers to exchange information (Profanter 2012). ACT-R is used to model a variety of aspects of human behavior, as well as to control mobile robots that interact with humans. For example, (Liu et al. 2016) employ ACT-R to model astronauts' cognitive behavior while (Xue et al. 2012) model the processes of civil aviation pilots.

ICARUS is a hierarchical cognitive architecture that aims at unifying reactive and deliberative problem-solving, as well as symbolic and numeric reasoning (Adam et al. 2016). ICARUS is composed of four main components: the perceptual buffer,

the conceptual memory, the skill memory, and the motor buffer. It operates on a recognize-act cycle: the architecture locates the descriptions of visible objects in the perceptual buffer, compares primitive concepts to precepts, and adds the matched instances to the short-term memory as beliefs (Langley, Laird, and Rogers 2009). As a learning mechanism, it supports means-ends problem-solving. The main application of this architecture is in problem-solving and learning in humanoid robots (Choi et al. 2011).

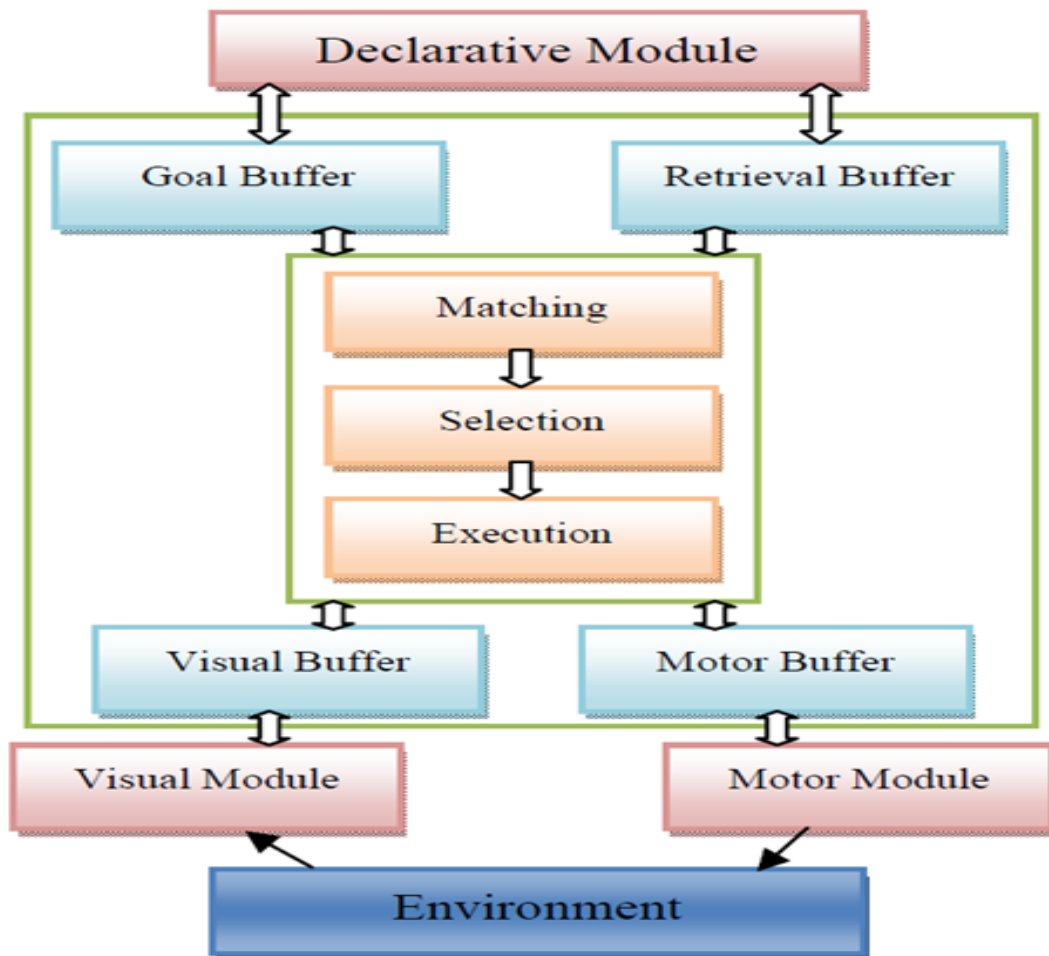


Figure 2.14 The ACT-R cognitive architecture (Kajdoci and Pozna 2014).

CLARION models essential psychological mechanisms and processes (Sun and Helie 2015). This architecture is composed of four distinct subsystems (Figure 2.15): action-centered subsystem (ACS), non-action-centered subsystem (NACS), motivational subsystem (MS) and meta-cognitive subsystem (MCS). The role of the ACS is to control actions, while the NACS maintains the general knowledge. The MS provides underlying motivations for perception, action, and cognition, and the MCS monitors and regulates the operations of the other subsystems

dynamically (Sun, Wilson, and Lynch 2016). Each subsystem consists of two levels: a top level that contains prepositional rules of explicit symbolic knowledge, and a bottom level containing procedural knowledge that uses subsymbolic neural mechanisms (Chong, Tan, and Ng 2007). Several simulations have been carried out within CLARION. For example, (Wilson and Sun 2014) show how CLARION may be used to capture the emotional dynamics of victims of school bullying. (Sun and Wilson 2011) implements CLARION to simulate human motivation and personality, and (Sun, Wilson, and Lynch 2016) employ CLARION to capture a variety of important aspects of emotion.

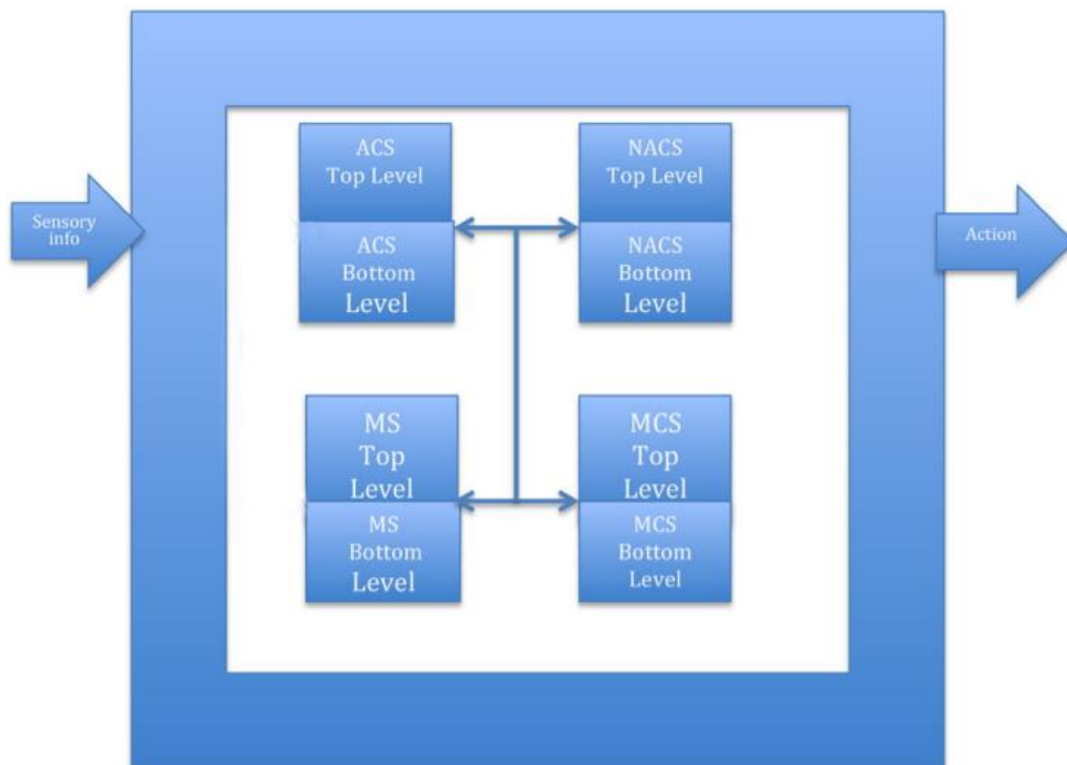


Figure 2.15 The CLARION cognitive architecture (Sun, Wilson, and Lynch 2016).

Finally, the LIDA (Learning Intelligent Distribution Agent) model of cognition is a fully integrated artificial cognitive system capable of reaching across a broad spectrum of cognition, from low-level perception/action to high-level reasoning (Faghihi and Franklin 2012). LIDA affords intention, action selection and human-like learning intended for use in controlling cognitive agents that replicate human experiments as well as performing real-world tasks (Franklin et al. 2014). One of the main characteristics of LIDA is that it features many learning processes: perceptual learning that allows the robot to construct its own representation of the environment, the episodic learning that learns from experience, the procedural

memory that learns new actions, and the attentional learning that allows restoring content to consciousness. In the area of medicine, LIDA has been implemented in a system of cognitive robots and as a supervisor that gathers both logistical and medical information in hospital Emergency Departments (Wilkes et al. 2010). The triage team and patients interact with the robots to register and make initial assessments. The robots are able to help patients and family to register their information and update patients on current wait times, while the triage team uses the robots to visually inspect and listen to the waiting room and can alert clinicians in case a patient requires immediate clinical attention. Recently, (Becker et al. 2015) developed a “conscious” mobile robot using LIDA to simplify decision-making processes during navigation.

Although standard cognitive architectures have been employed in numerous fields, such as modeling human behavior, game theory and mobile robots, the EuRoSurge European Project (The EUROSURGE Project 2016) is the only project that has addressed the specifications of a cognitive architecture for surgical robots. The goal of EuRoSurge is to facilitate the development of new products and their integration into surgical robots endowed with cognitive capabilities, thus establishing the new field of cognitive robotic surgery. Thus, there is an open research line in developing cognitive architectures for surgical co-worker robotic scenarios. To date, works endowing surgical robots with cognitive properties employ cognitive architectures designed for very specific applications.

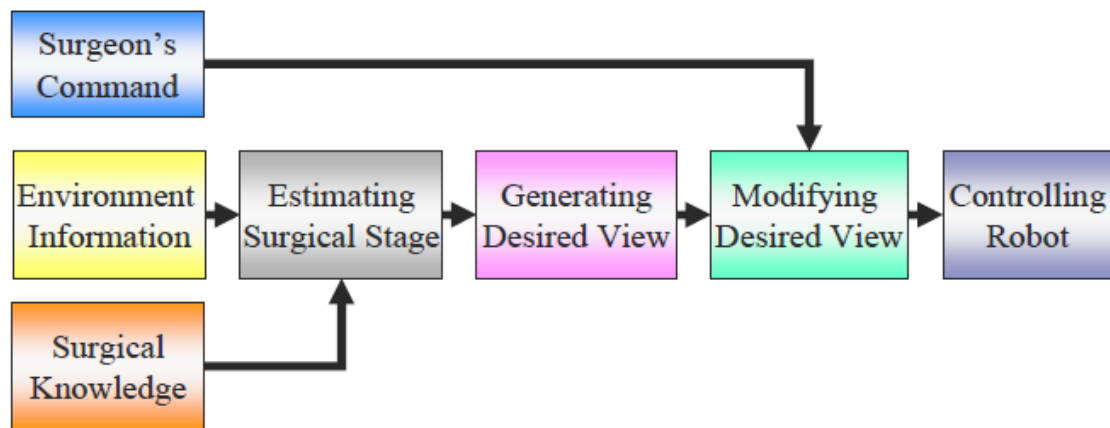


Figure 2.16 Human-robot interaction architecture for camera guidance in LS proposed by (Ko et al. 2005).

(Ko et al. 2005) propose to augment the intelligence of a camera robotic assistant with an intelligent human-robot interaction architecture (Figure 2.16). The goal of this work is to provide a particular camera view autonomously, depending on the state of the procedure. Robot surgical knowledge consists in modeling the surgical

task into a sequence of states characterized by the instrument used in each of them. The camera view can be set on a surgical site of interest or it can track the surgical tools. In case the surgeon disagrees with the camera view generated by the robot, he or she can use voice commands to modify the camera position.

(Chui, Nguyen, and Wen 2014) have presented on-going research about a cognitive surgical system, that comprises a cognitive engine to understand the operating room model and workflow and to model human behavior. This engine enables the robot to be aware of its environment and to make decisions about the actions to perform. They propose to model the biomechanics of biological tissue for the autonomous planning of surgical tasks. However, the application of this proposal to routine medical care remains a great challenge.

(Weede et al. 2013) and (Bihlmaier and Worn 2015) also propose a cognitive system for a surgical robot and present two examples of application: autonomous camera guidance and planning of trocar positions. Figure 2.17 shows the knowledge-based architecture proposed in these works for the robotic assistant. Perception has an attention process that filters the essential information, which is interpreted as a state of the world. The knowledge base distinguishes between procedural and declarative knowledge. By decision-making and planning aims are generated which can be interpreted and evaluated in a cyclic loop. Finally, decision-making results in an action taken by the robot. The camera guidance application is based on predicting the future position of the tools to provide a stable camera view.

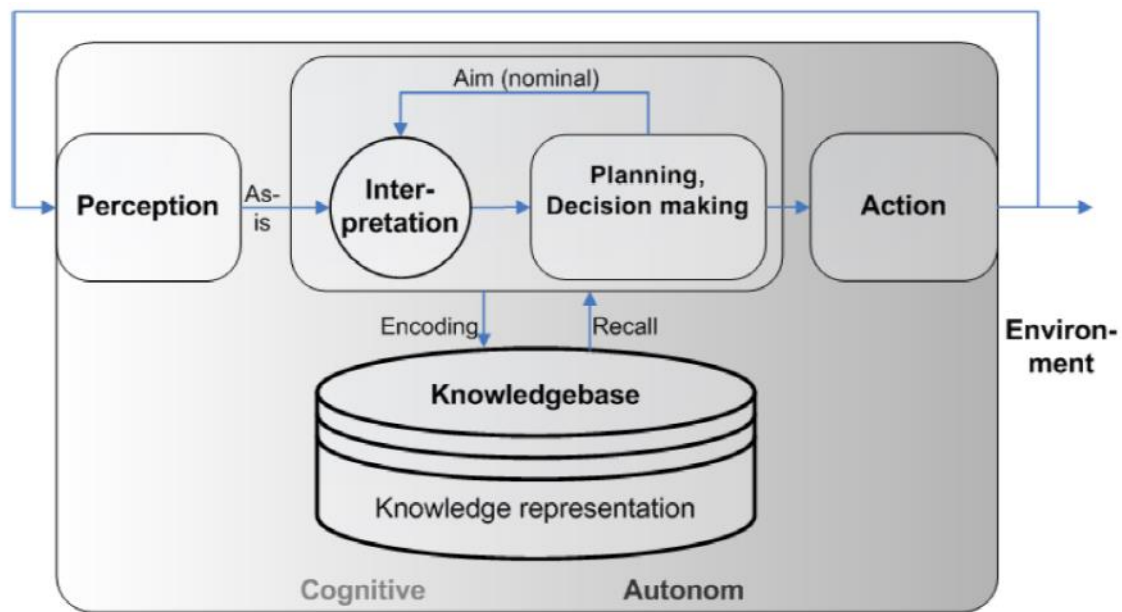


Figure 2.17 Cognitive architecture proposed by (Weede et al. 2013).

2.5 Conclusion

Most current surgical robots, as with the da Vinci system, follow a classical teleoperated scheme. These kinds of systems offer effective assistance to the surgeon as robotic tools that enhance his or her abilities, but they lack the required intelligence to act as a robotic partner for the surgeon, providing a collaborative assistance that reduces the surgeon workload during laparoscopic interventions. Moreover, traditional mechatronic solutions, based on external robots that handle laparoscopic tools, are no longer valid for new surgical techniques. Thus, researchers are focusing on the development of intra-abdominal devices that reduce the grade of invasiveness and overcome the new laparoscopic limitations by avoiding motion constraints due to the entry port. However, current approaches of this new kind of robots still require a human assistant to control the position of the intra-abdominal robots, limiting their applicability in co-worker scenarios where the robots can work with autonomy.

Many authors have addressed the problem of autonomy in surgical robots by developing systems for autonomous camera guidance and automation of surgical tasks. However, these works still require surgeons' supervision and their decisional capacity and their adaptability to dynamic scenarios are very limited. A smart robotic assistant able to collaborate with the surgeon in a co-worker scenario must go a step further in the current abilities of surgical robots, endowing the system with human-like cognitive features, such as knowledge representation, reasoning and planning, environment interpretation and learning algorithms. Some authors have designed specific cognitive architectures for surgical applications, such as endoscope guidance, but none of these works include learning mechanisms, an essential cognitive ability. Adapting a standard cognitive architecture for surgical applications would provide a general framework that could be employed for different surgical tasks and would lay the foundations of smart robotic assistants for co-worker surgical scenarios.

Analyzing the particular features of standard cognitive architectures described in the previous section, SOAR seems to be the most appropriate basis for building a general framework for smart robotic assistants. SOAR provides the required flexibility and modularity to be implemented in a full range of applications, from simpler ones such as acting in response to specific commands, to more complex collaborative scenarios in which autonomous assistance and reasoning are required. It offers different levels of long-term memory to store a wide range of knowledge: procedural memory makes it possible to store the robot behaviors; semantic memory makes it possible to store surgical knowledge such as tasks protocols or even a semantic representation of the environment; and episodic memory makes it possible

to store and recover past experiences related with, for example, unexpected situations that may occur or particular ways of operating of different surgeons. Moreover, SOAR offers a variety of learning mechanisms that allow the system to improve its behavior over time and to add new knowledge throughout the lifetime of the robotic assistant. Finally, SOAR is designed to allow an easy integration with other components, such as robots or sensors.

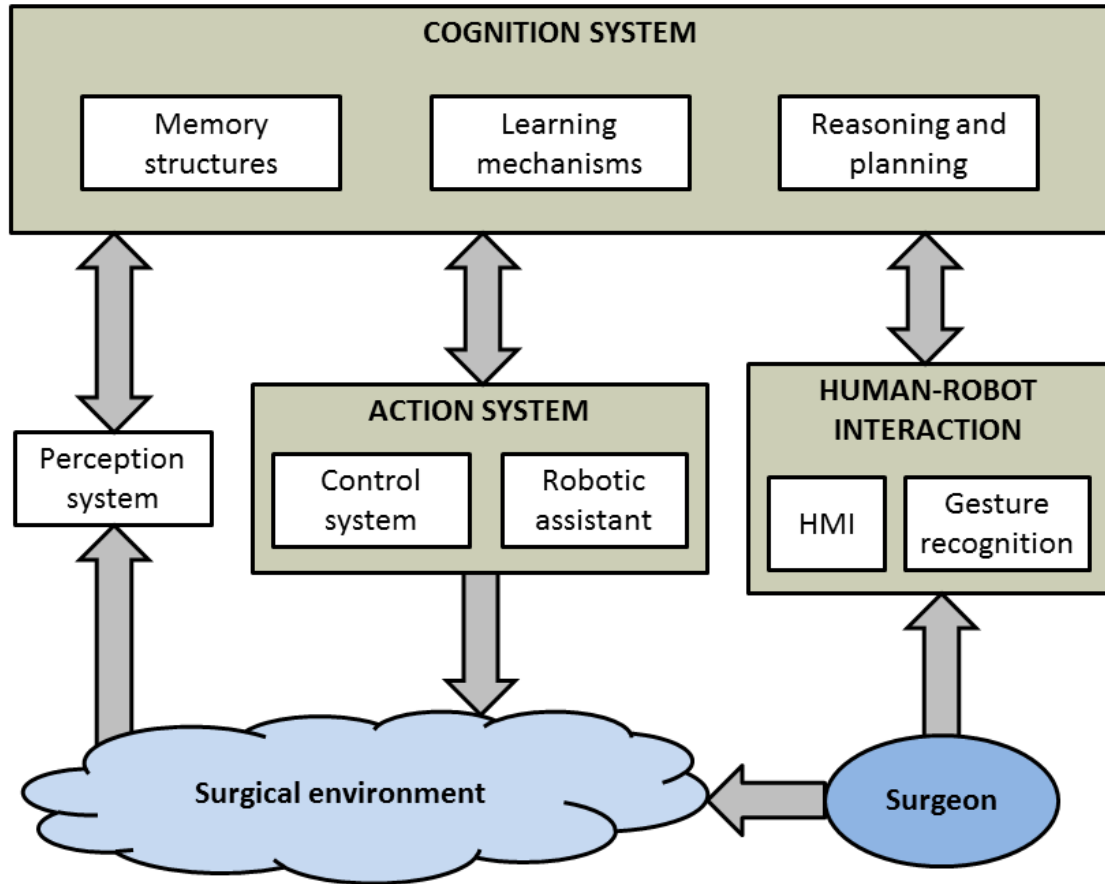


Figure 2.18 SOAR-based cognitive framework for smart robotic assistants.

Thus, this PhD dissertation proposes the SOAR-based general cognitive framework for smart robotic assistants depicted in Figure 2.18. The cognition system is composed of the required memory structures to store the robot knowledge base, learning mechanisms, and reasoning and planning algorithms. This cognition system makes use of the information provided by the perception system, which gathers sensorial data from the dynamic surgical environment and sends the corresponding planned robot behaviors to the action system. This action system is composed of two modules: the physical robotic assistant and its control system. Finally, the human-robot interaction module allows for communication between the cognition system and the surgeon. The basic way of interaction is through a Human

Machine Interface (HMI) that allows the surgeon to directly command particular motions or behaviors to the robot through voice commands, direct teleoperation, or a graphical interface. However, a smart robotic assistant aimed at emulating human behavior requires a more natural way of communication. This intuitive and natural human-robot interaction is performed through a gesture recognition system, which interprets the surgeon's maneuvers in order to follow the surgery workflow. This architecture is implemented for the particular application of a camera robotic assistant in a general open-source framework that allows easy integration of different robotic and sensorial components.

3 CONTROL SYSTEM OF THE ROBOTIC ASSISTANT

3.1 Introduction

Visual information is essential for surgeons to perform a surgical procedure. In laparoscopic surgery, surgical instruments are introduced into the abdominal cavity through small incisions. Thus, an endoscope is mandatory to provide visual feedback to the surgeon. Traditionally, a human assistant is in charge of holding the endoscope. This is a complex and tedious task, especially in long interventions, where the assistant must keep the endoscope in the same position during long periods. Fatigue and stress adversely affect image stability and accuracy of the endoscope position. Robot characteristics including tremor filtering and high accuracy help to overcome these limitations. Conventional camera robotic assistants consist of a robotic arm that holds the endoscope and moves it in response to specific commands (Gilbert 2009; Kraft et al. 2004; Munoz et al. 2006; Polet and Donnez 2008; Stolzenburg et al. 2011; Voros et al. 2010). Although these kinds of robots have succeeded in substituting medical staff, they do not tackle the narrow field of view inherent to laparoscopic procedures.

To deal with the limitations of laparoscopic vision, many researchers have designed intra-abdominal devices equipped with high-resolution cameras (Best et al. 2012; Garbin et al. 2016). These devices are completely introduced into the abdominal cavity and can be moved freely along the abdominal wall by means of magnetic interaction with an external magnet. This solution enhances the traditional narrow field of view of laparoscopic interventions, making it possible to

reach areas inaccessible for conventional endoscopes. However, current intra-abdominal camera robots are guided by hand. Thus, they still require an assistant to move the camera, or the surgeon must release the surgical tools to change the camera view.

This chapter presents the general description of the camera robotic assistant proposed in this PhD dissertation, followed by the geometric model of the task. Afterward, the control scheme is described. This control includes a hybrid force-position control for the shift of the camera along the abdominal wall and a cable-driven actuation system for the control of the internal DoFs. Finally, a summary of the conclusions of the chapter is presented.

3.2 General description of the camera robotic assistant

The camera robotic assistant proposed in this work, depicted in Figure 3.1, is composed of three components: an external robot, a magnetic holder, and a camera robot. The camera robot is composed of a high-resolution camera and a set of permanent magnets (Figure 3.2.a). This device is inserted into the abdominal cavity through one of the entry ports created by the surgeon to introduce the surgical tools. Once inside, it is attached to the abdominal wall through magnetic interaction with the external magnetic holder. The magnetic holder is a device composed of a set of magnets that couple with the magnets of the camera robot (Figure 3.2.b). Hence, the magnetic holder and the camera robot move together when the holder is displaced along the abdominal wall. To allow autonomous positioning of the camera, the holder is attached to the end effector of an external robot. The external robot attachment component allows easy mechanical coupling and decoupling with the holder. This mechanism provides more flexibility to the system, allowing manual handling of the magnetic holder if required or even to control more than one camera robot with the same external robot.

Unlike traditional endoscopes, whose motion is restricted to four DoFs due to the constraints at the entry port, the camera robotic assistant proposed in this work has six DoFs, depicted in Figure 3.1: two shifts along the abdominal wall, three rotations (roll, tilt, and pan) and a digital zoom, that performs the inward/outward motion of conventional endoscopes. As shown in Figure 3.3, these DoFs can be divided into external and internal ones, depending on the nature of its actuation. The external DoFs, the two shifts (d_x and d_y) and the pan rotation (φ), are actuated with the external robot, that controls the motion of the magnetic handle, while the internal DoFs, the roll rotation (α) and the tilt rotation (β), are actuated with an internal cable-driven mechanism, described in Section 3.2.1.

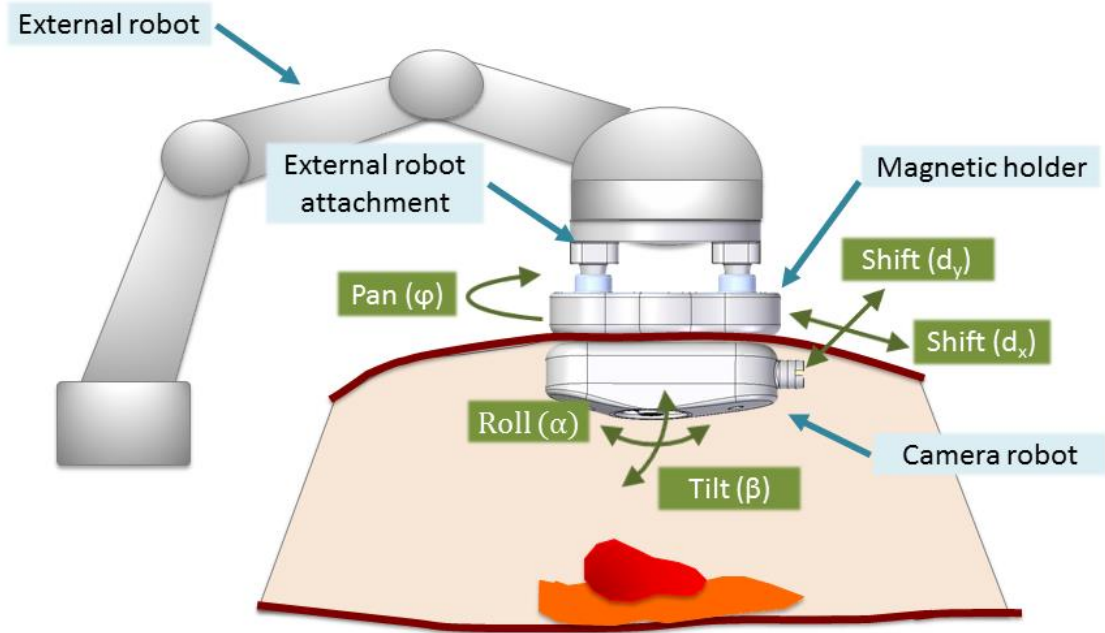


Figure 3.1 General description of the camera robotic assistant.

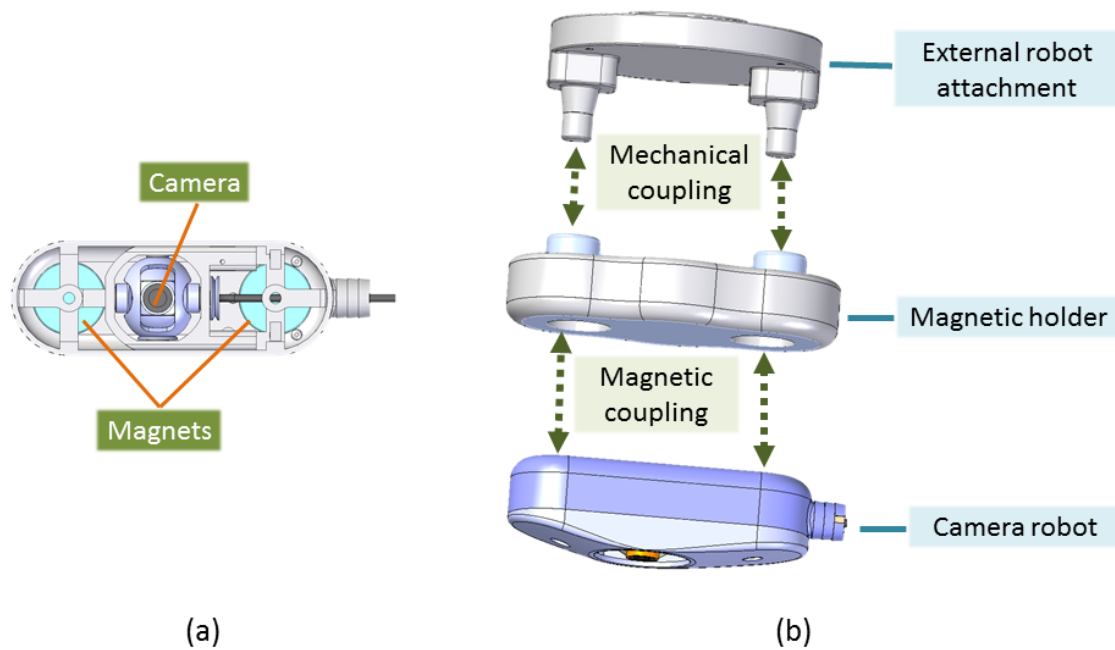


Figure 3.2 (a) Top view of the camera robot; and (b) coupling mechanism between components of the robotic assistant.

The two shifts allow the camera robot to reach almost any area inside the abdominal cavity, while the pan rotation has to do with the image horizon, i.e. a pan rotation provokes a rotation of the image. The most natural and intuitive way

of operating is following the hand-eye configuration, i.e. to have the camera between the active surgical tools and with a natural horizon (it would be quite difficult for a surgeon to operate with an inverted image). Hence, the pan rotation allows the image horizon to adapt to the position of the surgeon. On the other hand, tilt and roll rotations deal with the camera perspective. With traditional endoscopes, the angle from which an anatomical structure is viewed highly depends on the endoscope entry port. However, these two internal DoFs make it possible to view an organ from different angles of view. This fact is especially important in planar images, where one dimension is lost. Finally, the digital zoom allows the image to be focused on a particular area. Although digital zoom reduces the quality of the image, with the high quality of the actual cameras and the distance from the camera to the image plane (about 10 cm), a sufficient zoom can be applied without a loss of quality.

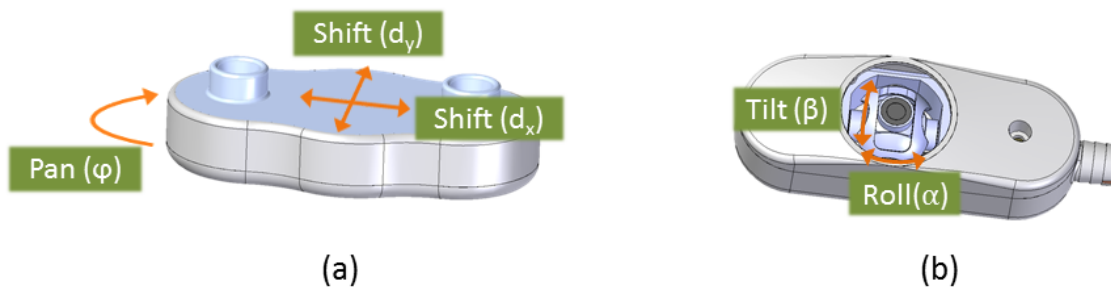


Figure 3.3 Actuation of the DoFs: (a) external DoFs; and (b) internal DoFs.

With these considerations, the advantages of the camera robotic assistant presented above can be summarized in the following points:

1. **Enhancement of the field of view.** One of the main problems of laparoscopic procedures is that the field of view is limited by the motion restrictions of the endoscope, which limits the accessible areas by the camera. However, the intra-abdominal camera robot can be freely displaced along the abdominal wall, making it possible to reach almost any area within the abdominal cavity.
2. **Enhancement of the camera perspective.** The internal DoFs of the robotic assistant allow the camera perspective to be changed easily, making it possible to view an anatomical structure from different angles. This fact is especially important in planar images, where one dimension is lost. Thus, depth perception can be improved if a particular image can be viewed from different angles. The main purpose of the camera robotic assistant is to substitute the conventional endoscope as a vision system. However, the

camera robot can also be used as a complementary vision system, allowing the operation to be performed with an endoscope as the main vision source, and using the intra-abdominal device to view unreachable areas by the endoscope or to view an organ from a different perspective. Furthermore, several camera robots could be used to create a global vision system that would provide a visual feedback as similar as possible to the vision surgeons have during an open surgery procedure (Rivas-Blanco et al. 2016).

3. **Recovery of triangulation in SPAS.** In single port access surgery, the surgical tools and the camera are all introduced through the same incision. This situation provokes a loss of triangulation between the camera and the working ports, which translates to an aggravation of the loss of depth sensation, inherent to any laparoscopic procedure. The possibility of moving the camera separately from the instruments restores the triangulation and therefore, improves the depth sensation.
4. **Automatic navigation.** All intra-abdominal devices found in the literature are controlled manually by hand motion of the magnetic holder. This implies that either a surgeon's assistant is required to perform this task or the surgeon must release the instruments every time he or she needs to change the camera position. The solution of attaching the magnetic holder to an external robot allows an automatic navigation of the camera, releasing the surgeon or an assistant from this tedious task.

3.2.1 Cable-driven actuation mechanism

The camera robot is the main component of the robotic assistant and it has the most restrictive design conditions, as its purpose is to be introduced into the abdominal cavity. Hence, for its design the following requisites must be considered:

1. **Small size.** The device is inserted into the abdomen through one of the incisions performed for the surgical instruments. Thus, the diameter of the camera robot is restricted by the size of the entry port. The maximum acceptable diameter of the device is 3 cm, as it is the size of the incisions performed in SPAS (Best et al. 2012).
2. **Low weight.** Magnetic interaction force required to keep the camera robot attached to the abdominal wall surface depends on the width of the abdominal wall, which depends on the individual characteristics of each patient and on the weight the magnets have to support. The lower the weight of the device, the less magnetic force is necessary, and therefore,

smaller magnets can be used. This is an important fact to take into account when designing the actuation of the internal DoFs and when selecting the device components.

3. **Lighting system.** A light source is mandatory in laparoscopic procedures to illuminate the working area. Some cameras have their own built-in light source. Otherwise, the device must be provided with an independent light source. White LEDs have demonstrated to be appropriate to illuminate the abdominal cavity (Cadeddu et al. 2009; Lehman et al. 2009).
4. **Power supply and image transmission.** Active components of the device (the camera, the lighting system and motors in case they are needed for the actuation of the DoFs) require a power supply to work. Components can be powered with an external power source using wires, or with internal batteries. Similarly, image transmission from the camera to the monitor that displays the image can be done using a wired transmission, or with a wireless camera. Hence, an important design decision is whether it is advisable to have a wireless device or not. On the one hand, the main advantage of a wireless device is that it frees up an entry port. However, wires usually have a small diameter so they can exit through one of the cannulas of a multi-port device or through a small incision closed with purse-string sutures to seal the tissue around the wire. Furthermore, wireless devices have the following disadvantages: batteries have a limited lifetime and their size and weight increase both the device dimensions and the total weight, and image transmission with wireless cameras is slower than with wired communication, causing image delays that are not acceptable in surgical environments. Moreover, for safety reasons, intra-abdominal devices must have a mechanism that allows them to be picked up in case the magnetic interaction is lost and the device falls. A wire exiting the device can be very useful in such cases to manipulate the device.

Under the above considerations, the camera robot has been designed with an internal cable-driven mechanism. Thus, no motors are required, that would have increased both the size and weight of the device and would have required additional power supply. This actuation mechanism is described in Figure 3.4. The driven side is composed of two concentric mechanisms (roll mechanism and tilt mechanism) that move the camera in the two directions indicated by rotations α and β , while the driver side is composed of two motors (motor 1 and motor 2) in charge of actuating the system. The actuation system is based on motion transmission between two driver pulleys (pulley 1 and pulley 2) and two driven pulleys (pulley 3 and pulley 4). On the driven side, blue and red cables are attached to the pulley of the roll mechanism (pulley 3), green and orange cables are attached to the pulley

of the tilt mechanism (pulley 4). On the opposite side, the driver side, blue and red cables are attached to the pulley of motor 1 (pulley 1), and green and orange cables are attached to the pulley of motor 2 (pulley 2).

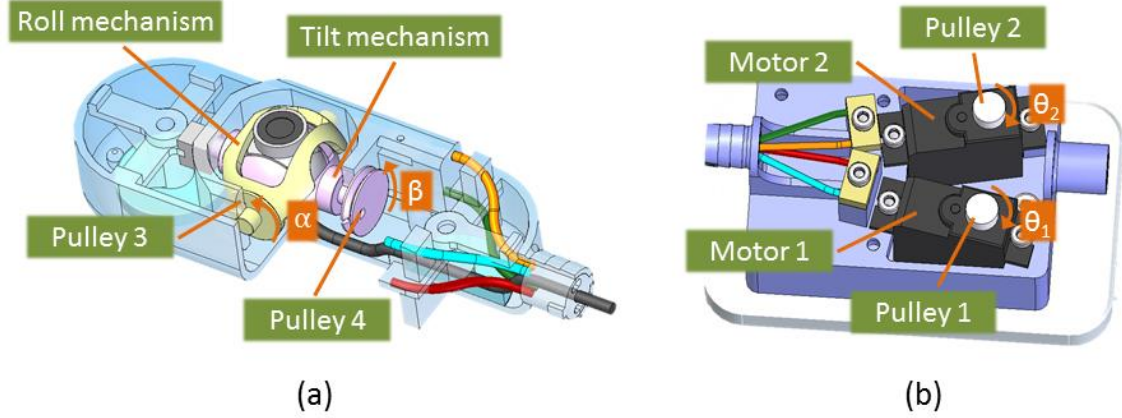


Figure 3.4 Cable-driven actuation system: (a) driven side; and (b) driver side.

Cables are tied to the pulleys so that all of them are tight in the initial position of the motors, which is made coincident with null values of α and β . Figure 3.5 shows the motion transmission of the system, particularized for the roll rotation. Figure 3.5.a depicts the initial position, for $\theta_1 = 0$ and $\alpha = 0$. A clockwise rotation of motor 1, and consequently of pulley 1, causes the red cable to move pulley 3 in the same sense, augmenting the value of α and therefore provoking a clockwise roll motion of the camera (Figure 3.5.b). Analogously, as depicted in Figure 3.5.c, a counterclockwise rotation of motor 1 causes a roll rotation of the camera in the opposite direction.

Thus, an incremental rotation θ_1 of motor 1 transmits an incremental rotation α of the roll mechanism, and an incremental rotation θ_2 of motor 2 transmits an incremental rotation β of the tilt mechanism. Assuming no slip of the cables in the mechanisms and negligible cables thickness, the equations describing the transmission of motion from the driver side to the driven side are:

$$\alpha = \frac{D_1}{D_3} \theta_1 \quad (3.1)$$

$$\beta = \frac{D_2}{D_4} \theta_2 \quad (3.2)$$

where D_1 , D_2 , D_3 , and D_4 are the diameters of pulley 1, pulley 2, pulley 3, and pulley 4, respectively.

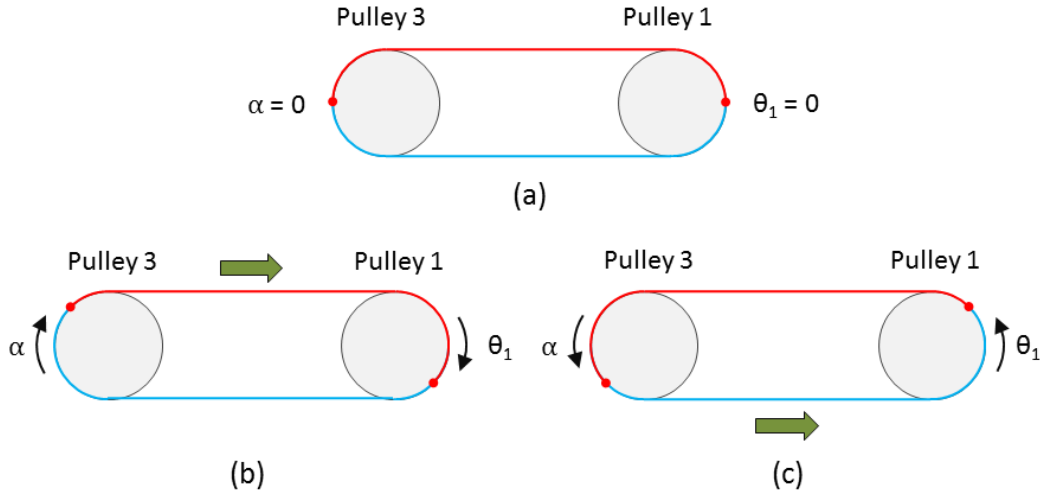


Figure 3.5 Motion transmission of the cable-driven actuation system particularized for the roll rotation: (a) initial position, (b) clockwise rotation, and (c) counterclockwise rotation.

3.3 Geometric model of the task

The task of the camera robotic assistant is to provide the surgeon with a particular camera view. Figure 3.6 depicts the geometric model of the task, where $\{0\}$ is the global reference frame, $\{E\}$ and $\{H\}$ are the reference frame of the robot's end effector and the magnetic holder, respectively, $\{C\}$ is the reference frame of the camera, and $\{I\}$ is the image reference frame. The global system $\{0\}$ coincides with the external robot reference frame, and its origin is placed at the center of its base. The origin of systems $\{E\}$, $\{H\}$ and $\{C\}$ are located at the center of the end effector, the bottom of the holder and the center of the camera lens, respectively.

Rotation matrix between systems $\{E\}$ and $\{H\}$, $\{H\}$ and $\{C\}$, and $\{C\}$ and $\{I\}$, ${}^E R_H$, ${}^H T_C$, ${}^C R_I$ are constant and correspond with the identity matrix, as shown in Figure 3.6. The relative position between these systems also remains constant, and are computed as follows:

$${}^C O_I = \begin{pmatrix} -w/2 \\ -h/2 \\ d_I \end{pmatrix}; \quad {}^C O_H = \begin{pmatrix} 0 \\ 0 \\ d_c + d_a + d_h \end{pmatrix}; \quad {}^H O_E = \begin{pmatrix} 0 \\ 0 \\ d_e \end{pmatrix} \quad (3.3)$$

where ${}^C O_I$, ${}^C O_H$ and ${}^H O_E$ are the origin of systems $\{I\}$, $\{C\}$ and $\{H\}$ with respect to systems $\{C\}$, $\{H\}$ and $\{E\}$, respectively, and d_I , d_c , d_a , d_h and d_e are the height from the camera to the image plane, the height of the camera robot, the width of the abdominal wall, the height of the holder and the height of the external robot attachment component, respectively. Conversely, transformation matrix between $\{0\}$ and $\{E\}$, ${}^0 T_E(q)$, is a function of the robot articular configuration q .

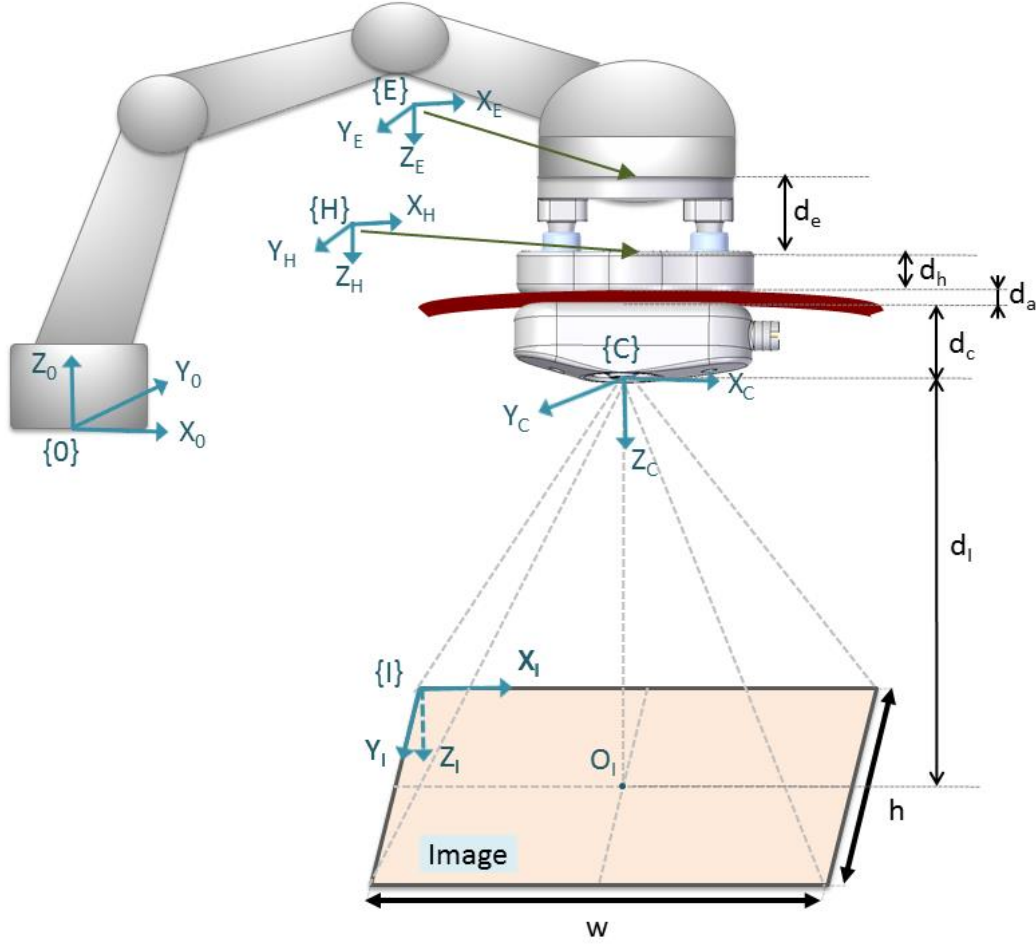


Figure 3.6 Geometric model of the task.

As the camera provides planar images, Z_I component of points of the image is equal to 0. The center of the image is denoted as O_I , and it is located in the point $(w/2, h/2, 0)$ of system $\{I\}$, where w and h are the image width and height, respectively, whose value depends on the image resolution. Please note that system $\{I\}$ associated with the image is expressed in different units of measures than the rest of systems: while points in $\{0\}$, $\{E\}$, $\{H\}$ and $\{C\}$ are expressed in Cartesian units, in particular in mm, points referred to system $\{I\}$ are expressed in image units, i.e. in pixels.

The camera view in a particular instant depends on the value of the six DoFs of the robotic assistant: d_x , d_y , α , β , φ , and zoom. Figure 3.7 depicts the effect of each DoF on the camera view, where *image* represents the camera view for the initial value of the DoFs, and *image'* represents the camera view for a particular value of every DoF. First, digital zoom is performed by displaying a smaller area ($w_z \times h_z$) of the overall image (Figure 3.7.a). Thus, it is computed as follows:

$$\begin{pmatrix} w_z \\ h_z \end{pmatrix} = \frac{1}{\text{zoom}} \begin{pmatrix} w \\ h \end{pmatrix} \quad (3.4)$$

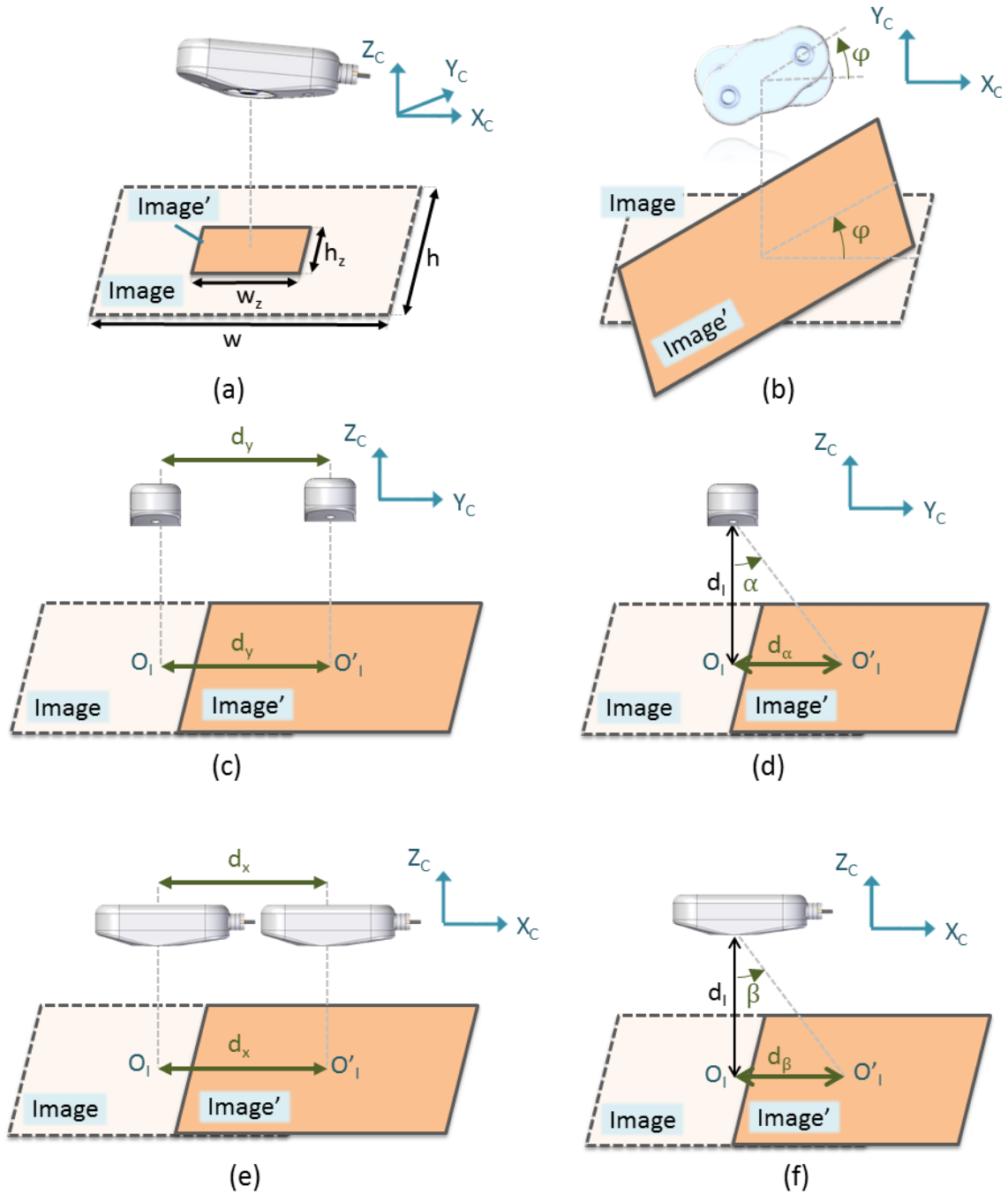


Figure 3.7 Effect of the robotic assistant DoFs on the camera view.

Second, pan rotation α affects the image horizon, i.e. it causes a rotation of the image in the plane X_c - Y_c (Figure 3.7.b). Shifts d_x and d_y are carried out along axis Y_c and X_c , respectively, and cause a displacement of the center of the image O_I along the respective axis (Figure 3.7.c and Figure 3.7.e, respectively). Finally, roll and tilt rotations cause a displacement of O_I along axis Y_c and X_c , respectively, which size depends on the distance from the camera to the image plane H (Figure 3.7.d and Figure 3.7.f, respectively). These displacements are computed as follows:

$$d_\alpha = d_I \cdot \tan(\alpha) \quad (3.5)$$

$$d_\beta = d_I \cdot \tan(\beta) \quad (3.6)$$

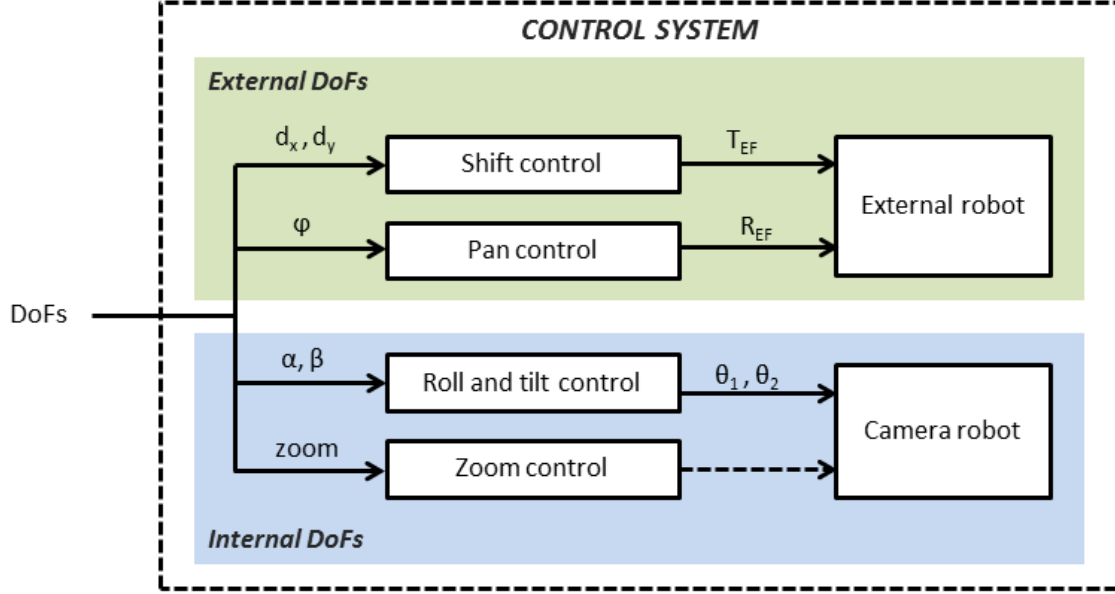


Figure 3.8 Control system of the robotic assistant.

3.4 Control system

The control system of the robotic assistant receives the value of the six DoFs (d_x , d_y , α , β , φ , and zoom) and executes the corresponding motion of the external robot and the camera robot (Figure 3.8). The shift control is done using a hybrid force-position controller that controls both the displacement of the robot and the force exerted on the abdominal wall. This control, further described in the following subsection, outputs the transformation matrix T_{EF} of the end effector of the external robot. The pan rotation φ is also performed with the external robot. It consists in a rotation φ around axis Z_C (Figure 3.7.b). Thus, it does not affect the robot position P_{EF} , only the orientation R_{EF} . The robot orientation in a particular instant k , $R_{EF}(k)$, is computed by applying a rotation $R_z(\varphi)$ to the previous robot orientation $R_{EF}(k-1)$:

$$R_{EF}(k) = R_z(\varphi) \cdot {}^C R_0 \cdot R_{EF}(k-1) \quad (3.7)$$

where ${}^C R_0$ is the rotation matrix between system $\{C\}$ associated with the camera and the global reference system $\{0\}$. This matrix is necessary because R_z is expressed with respect to $\{C\}$, and R_{EF} has to be commanded referred to system

$\{0\}$. Matrix $R_z(\varphi)$ has the following value:

$$R_z(\varphi) = \begin{pmatrix} \cos(\varphi) & -\sin(\varphi) & 0 \\ \sin(\varphi) & \cos(\varphi) & 0 \\ 0 & 0 & 1 \end{pmatrix} \quad (3.8)$$

On the other hand, roll and tilt rotations are performed with the cable-driven actuation system and are controlled following the scheme shown in Figure 3.9. It inputs the desired roll and tilt values, α_d and β_d , respectively, and computes the corresponding motors control. According to equations (3.1) and (3.2), rotations of motors 1 and 2, θ_1 and θ_2 , respectively, to get the roll and tilt rotations α_d and β_d , respectively, are computed as follows:

$$\theta_1 = \frac{D_3}{D_1} \alpha_d \quad (3.9)$$

$$\theta_2 = \frac{D_4}{D_2} \beta_d \quad (3.10)$$

These motor rotations transmit the motion to the camera robot, as described in Section 3.2. Real values of roll and tilt rotations, α and β , respectively, are difficult to obtain, as it is not possible to include any additional sensor in the environment and image analysis techniques would lead to large errors due to the highly dynamic nature of the environment. Therefore, the loop is closed by the surgeon (man-in-the-loop), who can correct these DoFs by commanding a particular value of the rotations.

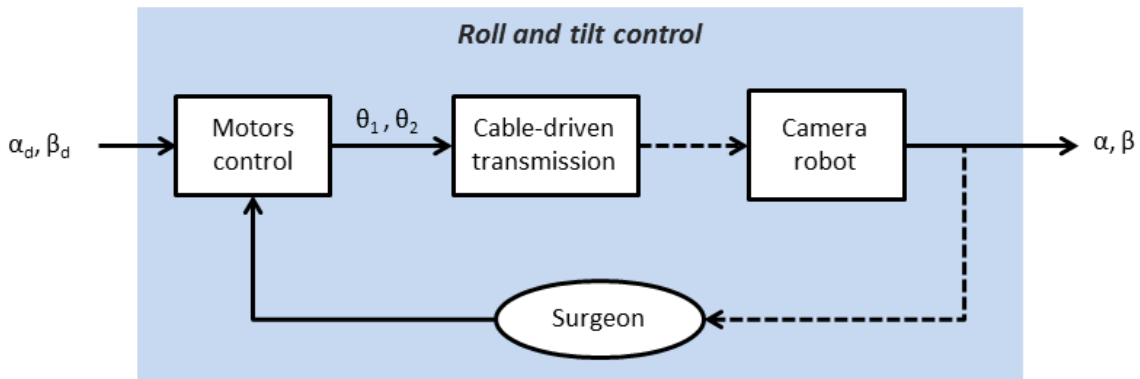


Figure 3.9 Roll and tilt control scheme.

Finally, the zoom control applies equation (3.4) to obtain the range of the image to display depending on the desired zoom level. Next, the hybrid force-position control with torque compensation that controls displacements d_x and d_y of the external robot is further described.

3.4.1 Hybrid force-position control with torque compensation

Displacement of the camera robot along the abdominal wall has some challenges that must be taken into account when designing the shift control. First, shifting must be carried out to preserve the magnetic interaction between the camera robot and the external holder, and second, it must assure that the devices do not cause any damage to the patient, internally or externally. To guarantee these issues, the displacement must be carried out in the tangential directions of the contact surface. This way, a smooth motion of the holder and the camera robot is assured, avoiding possible cuts on the patient's skin, as well as a continuous magnetic interaction. As depicted in Figure 3.10, when the holder surface is parallel to the contact surface (abdominal wall), the magnetic interaction is assured by the equal interaction of the two magnets of the devices. This way, the force due to the device weight, F_g , is balanced by the magnetic forces F_m , keeping the camera robot attached to the abdominal wall. However, if the displacement is not carried out parallel to the contact surface, magnetic interaction in one of the magnets is lost, and the other magnetic force will not be able to balance the device weight, causing it to fall. Moreover, to assure that magnetic forces F_m are enough to keep the magnetic interaction between both devices, a minimum contact force of the holder in the normal direction of the contact surface must also be assured.

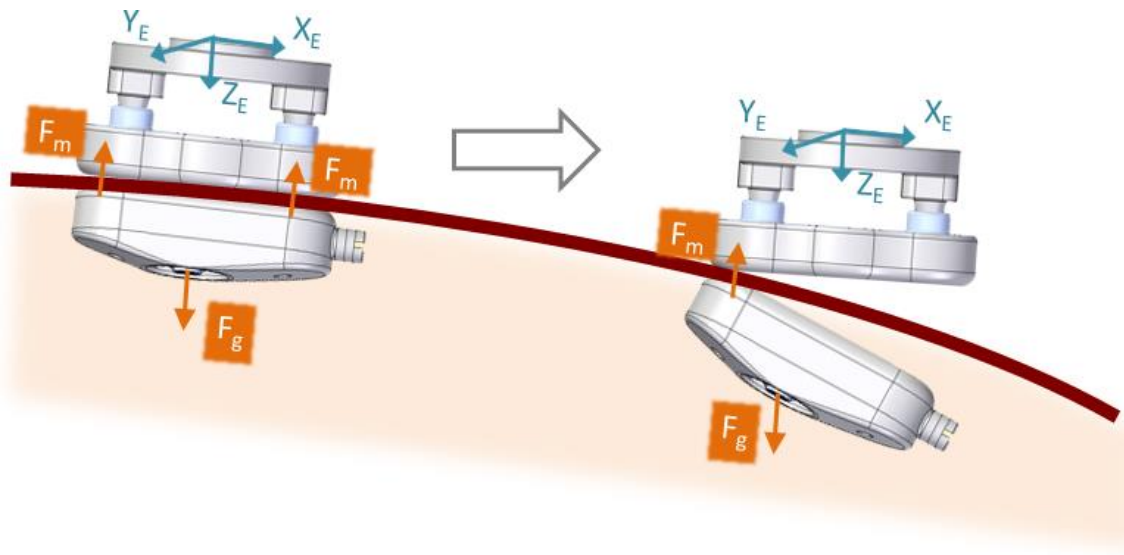


Figure 3.10 Camera displacement along the abdominal wall.

Hence, the problem of the control of DoFs d_x and d_y , i.e. the shift of the camera robot along the abdominal wall, consists in displacing the robot on the tangent plane to the contact point while exerting a particular force in the normal direction. The main challenge of this issue is that the abdominal wall is not a plane surface

and its shape is unknown for the system. Modeling the abdominal wall surface would be quite difficult, first of all, because it differs greatly from one patient to another, and second, because it is affected by a variety of external and dynamic factors. On the one hand, it is affected by how much the abdominal cavity is insufflated. On the other hand, the location of the entry ports and the external motion of the surgical tools may also affect the shape of the abdominal wall in particular areas. Thus, a reference frame associated with the abdominal wall must be dynamically computed. One approach to do this is to maintain the external robot's end effector parallel to the contact surface at all times. As the orientation of the holder is the same as the orientation of the end effector, keeping the end effector parallel to the contact surface will assure that the holder also stays parallel to the abdominal wall during the displacement. Thus, the orientation of the reference frame associated with the abdominal wall coincides with the orientation of system $\{E\}$.

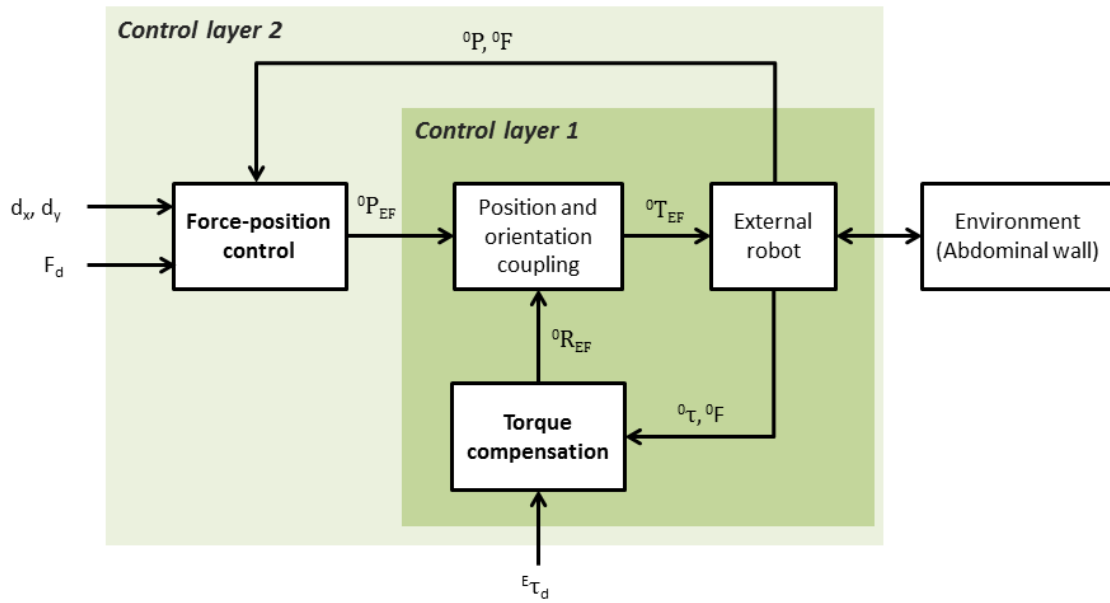


Figure 3.11 Control scheme for the displacement of the camera along the abdominal wall.

Under these considerations, the shift control is carried out following the control scheme of Figure 3.11. It is composed of two control layers: control layer 1 is executed every system cycle and it is in charge of assuring that the robot's end effector is parallel to the contact surface, and control layer 2 is in charge of performing the displacement of the robot, and it is executed with a higher sampling time so as to assure a steady-state of control layer 1 before sending a new position reference. Thus, the motion of the external robot is decoupled into an orientation

reference, ${}^0R_{EF}$, managed by control layer 1, and a position reference, ${}^0P_{EF}$, managed by control layer 2. Then, position and orientation are coupled to provide a single input to the robot in the form of transformation matrix ${}^0T_{EF}$, as:

$${}^0T_{EF} = \begin{pmatrix} {}^0R_{EF} & {}^0P_{EF} \\ 0 & 1 \end{pmatrix} \quad (3.11)$$

Orientation control is done with a torque compensation algorithm that inputs the desired torque, ${}^E\tau_d$, and real force and torque at the end effector, ${}^0\tau$ and 0F , respectively, and outputs the corresponding orientation R_{EF} to keep the end effector parallel to the contact surface. On the other hand, the position control is done with a hybrid force-position control that inputs a shift reference, d_x and d_y , a force reference, F_d , and real position and force at the end effector, 0P and 0F , respectively, and outputs the corresponding position reference ${}^0P_{EF}$ to the robot. Inputs to the control scheme are given with respect to system $\{E\}$ because the control is performed over the end effector system. However, robot inputs and outputs variables are referred to its base reference frame, which is coincident with the global reference frame $\{0\}$. Next, torque compensation and force-position control are described in detail.

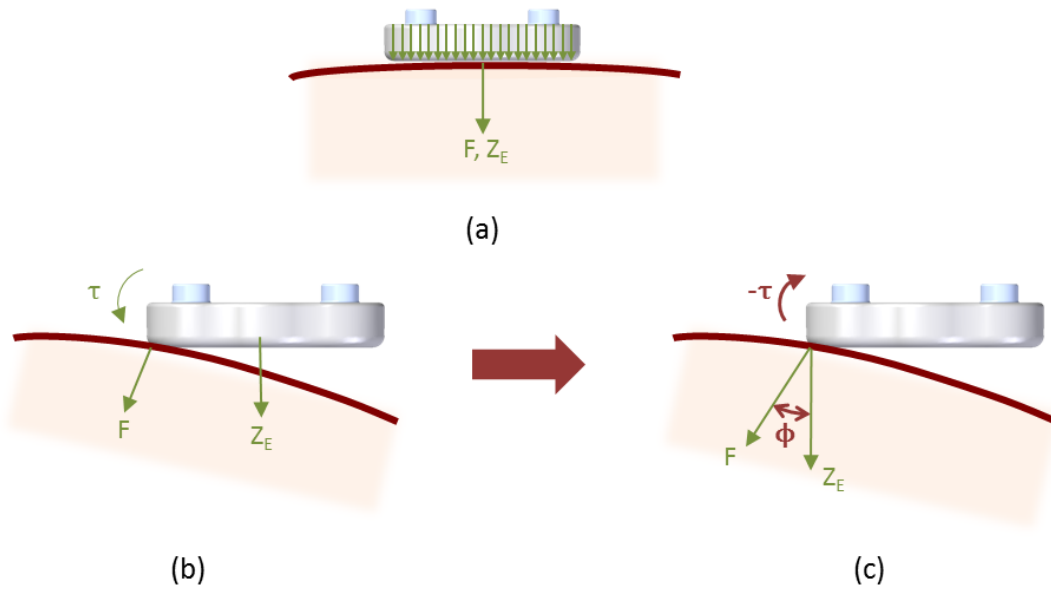


Figure 3.12 Orientation control of the external robot: (a) holder parallel to the contact surface, (b) holder not parallel to the contact surface, (c) action to correct the robot orientation.

When the external robot's end effector, and therefore the holder, is parallel to the contact surface, the contact force is uniformly distributed along the bottom

surface of the holder, creating a resultant force F in the same direction of axis Z_E , i.e., perpendicular to the contact surface (Figure 3.12.a). However, if the end effector is not parallel to the contact surface, it is produced the situation of Figure 3.12.b, in which the contact force F , which is always perpendicular to the contact surface at the contact point, is not parallel to axis Z_E , thus generating a torque τ . To get back to the situation depicted in Figure 3.12.a, the orientation of the robot must be corrected by performing a rotation of magnitude ϕ (angle formed by force F and axis Z_E) in the opposite direction of the torque vector τ . This orientation correction is depicted in Figure 3.12.c.

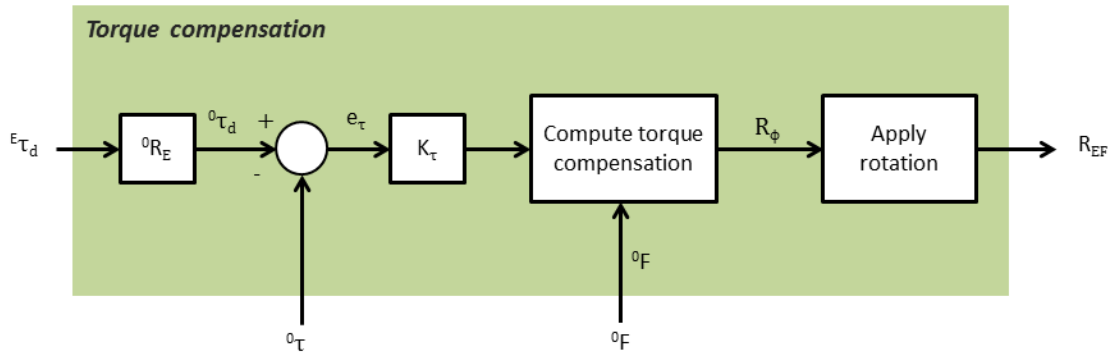


Figure 3.13 Control scheme of the torque compensation.

Hence, the control scheme of the torque compensation that corrects the robot orientation is shown in Figure 3.13, in which the torque reference, ${}^E\tau_d$, is a null vector, which leads to having the robot's end effector parallel to the contact surface. This reference is transformed from system $\{E\}$ to system $\{0\}$ through the rotation matrix 0R_E in order to compute the torque error, e_τ , which is controlled by a proportional controller of gain K_τ . Then, the torque compensation is computed as the rotation matrix that performs a rotation ϕ around the opposite axis to the torque error, R_ϕ . Firstly, angle α is computed as:

$$\phi = \arccos\left(\frac{{}^0F \cdot Z_E}{|{}^0F| \cdot |Z_E|}\right) \quad (3.12)$$

Then, the vector of rotation is computed as:

$$u = -\|e_\tau\| \quad (3.13)$$

Finally, matrix R_ϕ is computed as follows:

$$R_\phi = \begin{pmatrix} u_x^2(1 - c_\phi) + c_\phi & u_x u_y(1 - c_\phi) - u_z s_\phi & u_x u_z(1 - c_\phi) + u_y s_\phi \\ u_x u_y(1 - c_\phi) + u_z s_\phi & u_y^2(1 - c_\phi) + c_\phi & u_y u_z(1 - c_\phi) - u_x s_\phi \\ u_x u_z(1 - c_\phi) - u_y s_\phi & u_y u_z(1 - c_\phi) + u_x s_\phi & u_z^2(1 - c_\phi) + c_\phi \end{pmatrix} \quad (3.14)$$

where $s_\phi = \sin(\phi)$, $c_\phi = \cos(\phi)$, and $u = (u_x, u_y, u_z)$.

Once the torque compensation matrix R_ϕ has been computed, this rotation has to be applied to the actual orientation of the robot. Thus, orientation reference of the robot, R_{EF} , is computed as the current robot orientation, 0R_E , by matrix R_ϕ . Thus:

$$R_{EF} = {}^0R_E \cdot R_\phi \quad (3.15)$$

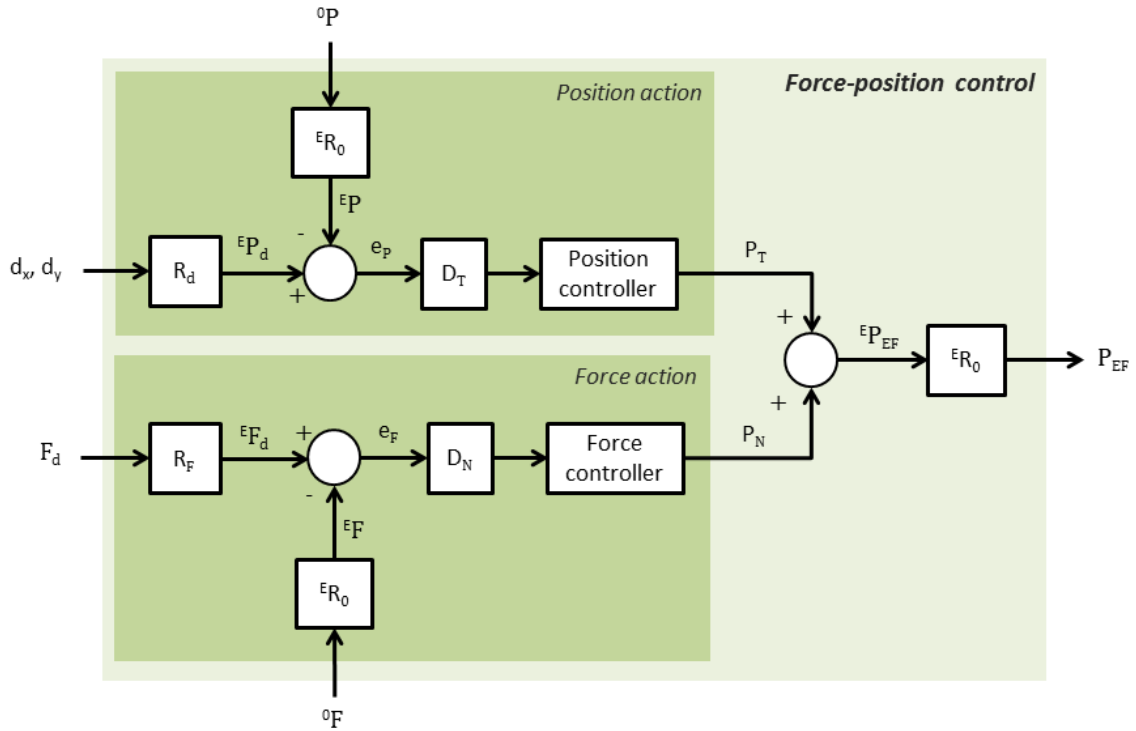


Figure 3.14 Control scheme of the hybrid force-position control.

On the other hand, the hybrid force-position control to displace the camera along the tangent surface of the abdominal wall while exerting a force on the normal direction is performed with the control scheme of Figure 3.14. This control assumes that the torque compensation control, which acts with a smaller sampling time, ensures that the end effector is parallel to the contact surface. Thus, X_E - Y_E is the contact plane, where position action takes place, and Z_E is the normal vector to the contact surface, where the force action occurs. Hence, position and force actions are decoupled through matrixes D_T and D_N , avoiding interferences between the two controllers. Thus:

$$D_T = \begin{pmatrix} 1 & 0 & 0 \\ 0 & 1 & 0 \\ 0 & 0 & 0 \end{pmatrix} \quad (3.16)$$

$$D_N = I - D_T = \begin{pmatrix} 0 & 0 & 0 \\ 0 & 0 & 0 \\ 0 & 0 & 1 \end{pmatrix} \quad (3.17)$$

With this decoupling, position action outputs a position reference P_T in which the z component is null, and force action outputs a position reference P_N in which x and y components are null. Thus, the sum of P_T and P_N provides a complete position reference ${}^E P_{EF}$, which once transformed to the global reference frame, can be sent to the robot. Position action inputs the value of DoFs d_x and d_y , which are transformed into a position vector through matrix R_d as follows:

$${}^E P_d = R_d \cdot \begin{pmatrix} d_x \\ d_y \end{pmatrix} = \begin{pmatrix} 1 & 0 \\ 0 & 1 \\ 0 & 0 \end{pmatrix} \cdot \begin{pmatrix} d_x \\ d_y \end{pmatrix} \quad (3.18)$$

The position controller ensures an accurate position reference tracking. This is done with a PI (proportional-integral) controller of gains K_P and K_I as:

$$P_T(t) = K_P \cdot e_p(t) + K_I \cdot \int e_p(t) dt \quad (3.19)$$

Robot dynamics are forced to follow a first order behavior (Munoz et al. 2006), so PI controller gains are designed following the Ackerman's methodology for poles assignment, according to a dead-beat strategy. Thus:

$$K_P = \frac{1 + e^{-(T/T_\tau)}}{1 - e^{-(T/T_\tau)}} \quad (3.20)$$

$$K_I = \frac{1}{e^{-(T/T_\tau)} - 1} \quad (3.21)$$

where T is the sampling time of the position controller, and T_τ is a time constant. On the other hand, the force action ensures a particular contact force during the robot displacement. Reference force F_d must be chosen to assure a safe contact of the magnetic holder on the abdominal wall so as not to lose the magnetic interaction with the intra-abdominal device and to not damage the patient, since if the force is too large it may cause necrosis on the patient. This force value is transformed into a force vector through matrix R_F as follows:

$${}^E F_d = R_F \cdot F_d = \begin{pmatrix} 0 \\ 0 \\ 1 \end{pmatrix} \cdot F_d \quad (3.22)$$

The force controller translates a force reference into a position reference. For the force controller design, an elastic interaction model has been assumed between the

robot and the surface. Thus:

$$e_F(t) = K_x \cdot (P_N(t) - P_N(t-1)) \quad (3.23)$$

where K_x is the stiffness matrix of the contact surface. Estimation of this parameter will be discussed below. Hence, the position reference in the normal direction, P_N , to exert a force F_d on the abdominal wall is computed as:

$$P_N(t) = P_N(t-1) + \frac{1}{K_x} e_F(t) \quad (3.24)$$

Stiffness matrix estimation

The stiffness matrix of the contact surface, i.e. the abdominal wall, depends on the particular characteristics of each patient, such as the thickness of each person's abdominal wall, which differs greatly between slim and obese people. Therefore, an accurate model of this value would be both quite complex and useless from the moment that we change the patient. Thus, K_x is estimated for each patient before the intervention with a recurrent least squares algorithm (RLS). This method employs measures of position and force obtained during the normal working of the system to update the stiffness matrix value K_x in real time (Martínez Rodríguez 2004). Thus, new values of K_x are estimated based on the previously computed values, corrected with an update factor M as follows:

$$K_x(t+1) = K_x(t) + M(t) \cdot (e_F(t+1) - P_N(t+1) \cdot K_x(t)) \quad (3.25)$$

where M is computed as:

$$M(t) = \frac{N(t) \cdot P_N(t+1)}{1 + N(t) \cdot (P_N(t+1))^2} \quad (3.26)$$

where N is a variable that has to be updated once performed the iteration as:

$$N(t+1) = \frac{N(t)}{1 + N(t) \cdot (P_N(t+1))^2} \quad (3.27)$$

3.5 Conclusion

This chapter has described a six DoFs camera robotic assistant that merges the advantages of conventional robotic camera holders and the new concept of intra-abdominal device. First, the use of an intra-abdominal device provided with a high-resolution camera, called camera robot, enhances the field of view if compared with a conventional endoscope, as the camera motion is not restricted by the entry port, so it can reach any area inside the abdominal cavity. Second, having the magnetic holder attached to the end effector of an external robot allows autonomous camera navigation, releasing the surgeon or an assistant from the task of moving the camera. Furthermore, the two internal DoFs of the camera robot, roll and tilt rotations, enhance the camera perspective, allowing an anatomical structure to be viewed from different angles. As in planar images one dimension is lost, perspective is especially important, as tasks involving depth perception become very challenging. A more natural perspective than the one obtained with an endoscope helps to recover depth perception. The internal DoFs of the robotic assistant are actuated by a cable-driven system that avoids the need of having motors onboard, which would increase both the size and the weight of the device. This system makes it possible to control the internal DoFs easily from outside.

This chapter also analyzes the control system of the robotic assistant. It details a hybrid force-position control with torque compensation for the displacement of the robot along the abdominal wall. Torque compensation ensures that the end effector of the external robot remains parallel to the contact surface. This is essential to ensure magnetic interaction between the external holder and the camera robot and also to assure a safe and smooth displacement of both devices along the abdominal wall. Then, the position and force actions can be decoupled into a displacement along the contact surface, and a force in the perpendicular direction to the surface. For the force controller, an elastic interaction model between the robot and the surface has been assumed, where the stiffness matrix is estimated with a RLS algorithm that updates the value of K_x with new measures taken during the normal working of the robotic assistant. Thus, the controller considers particular characteristics of each patient's abdominal wall, and it is also able to correct the value during the robot motion.

4 ROBOT COGNITION

4.1 Introduction

A cognitive architecture can be seen as an integration of modules or components that produce a behavior. A variety of cognitive architectures can be defined depending on the features required for each particular application. Different cognitive architectures have been proposed in fields such as mobile robots (Kleinmann and Mertsching 2011; Laird et al. 2012; Wolf and Sukhatme 2008; Zhang et al. 2010), optimization problem solving (Al-Dujaili, Subramanian, and Suresh 2015; Tanweer, Suresh, and Sundararajan 2014; Yu and Mang 2002), humanoid robots (Burghart et al. 2005; Cangelosi 2010) and human behavior mimicking (Infantino et al. 2005). However, few cognitive architectures have been proposed for surgical robots. (Bihlmaier and Worn 2015) and (Ko et al. 2005) have proposed cognitive architectures for camera guidance in laparoscopic surgery based on a surgical knowledge base, and reasoning and planning capabilities. However, these works propose very specific architectures and none of them include learning abilities, an essential characteristic of cognitive agents.

The previous chapter has described the design and control features of a camera robotic assistant, while the present chapter delves deeper into the system cognition. It describes a cognitive architecture that provides the robot with the means to work side by side with surgeons in a collaborative way, behaving as similar as possible to a human assistant. Firstly, it describes the global cognitive architecture of the system, aimed at providing an efficient and autonomous camera view during a laparoscopic procedure. Then, it expands into the robot cognition and its codification. In particular, it analyzes the long-term memory of the system, i.e. the semantic memory, which stores declarative knowledge, and the procedural memory,

which stores implicit knowledge of the robot. Furthermore, it describes the reinforcement learning algorithm of the system, which allows the robot to improve its behavior over time. Finally, conclusions are reported.

4.2 Description of the cognitive architecture

Figure 4.1 shows the cognitive architecture proposed for the smart camera robotic assistant. The aim of this architecture is to provide the robot with the means to assist the surgeon autonomously during a laparoscopic procedure, providing an efficient camera view adapted to the task conditions in every instant of time. The architecture is composed of two main modules: a cognition system, where the robot base of knowledge and reasoning functions are implemented, and the action system, described in the previous chapter, which controls the execution of motion of the robotic assistant. Moreover, a perception system makes it possible to perceive changes in the environment (the patient's abdominal cavity), and a human-robot interaction system allows the surgeon to interact with the robot in a natural and intuitive way.

The cognition system is the major module of the cognitive architecture. It contains the two memory structures (long-term memory and working memory), and the learning mechanisms. Long-term memory is broken down into semantic memory and procedural memory, each one containing a different type of knowledge. On the one hand, the semantic memory contains general knowledge that forms the base of the robot's world understanding, including concept hierarchy, causal relations, and association rules. The semantic learning allows the system to acquire new knowledge during the lifetime of the robot. On the other hand, the procedural memory contains the basic knowledge of how to select and perform basic actions or behaviors, i.e. it contains the sequences of situation-action rules to perform navigation routines. The reinforcement learning allows the system to improve the behavior of the robot by an iterative process based on rewards associated with the action rules that form the base of the procedural knowledge.

The perception system manages the data incoming from the sensors and sends it to the working memory so it can be processed. Sensing is an essential function to detect changes in a dynamic environment. In the particular context of this work, the main sensor for perceiving changes in the operating area is the camera. Thus, the perception system is based on vision algorithms that process the incoming information from the camera. Other works use 3D trackers to locate the surgical tools, but this method requires some kind of markers to be attached to the tools, which may result uncomfortable for surgeons (Bauzano et al. 2015). Vision

algorithms provide all the information the robotic assistant requires to decide on the best camera view in every instant of the procedure (tools position and detection of other areas of interest such as anatomical structures), and this method does not require any additional device. However, the main limitation of this approach is that it is only possible to track objects within the camera field of view, although predicting algorithms can be integrated to estimate the location of the tools out of the image field. There are numerous works in the literature related to object identification in real applications, such as automatic gauze detection (Garcia-Martinez et al. 2015), needle detection (Rodriguez-Molares et al. 2015) or automatic surgical tool tracking (Sahu et al. 2017; Zhang et al. 2017). There are also studies addressing the problem of bleeding detection in real environments (Deeba et al. 2016).

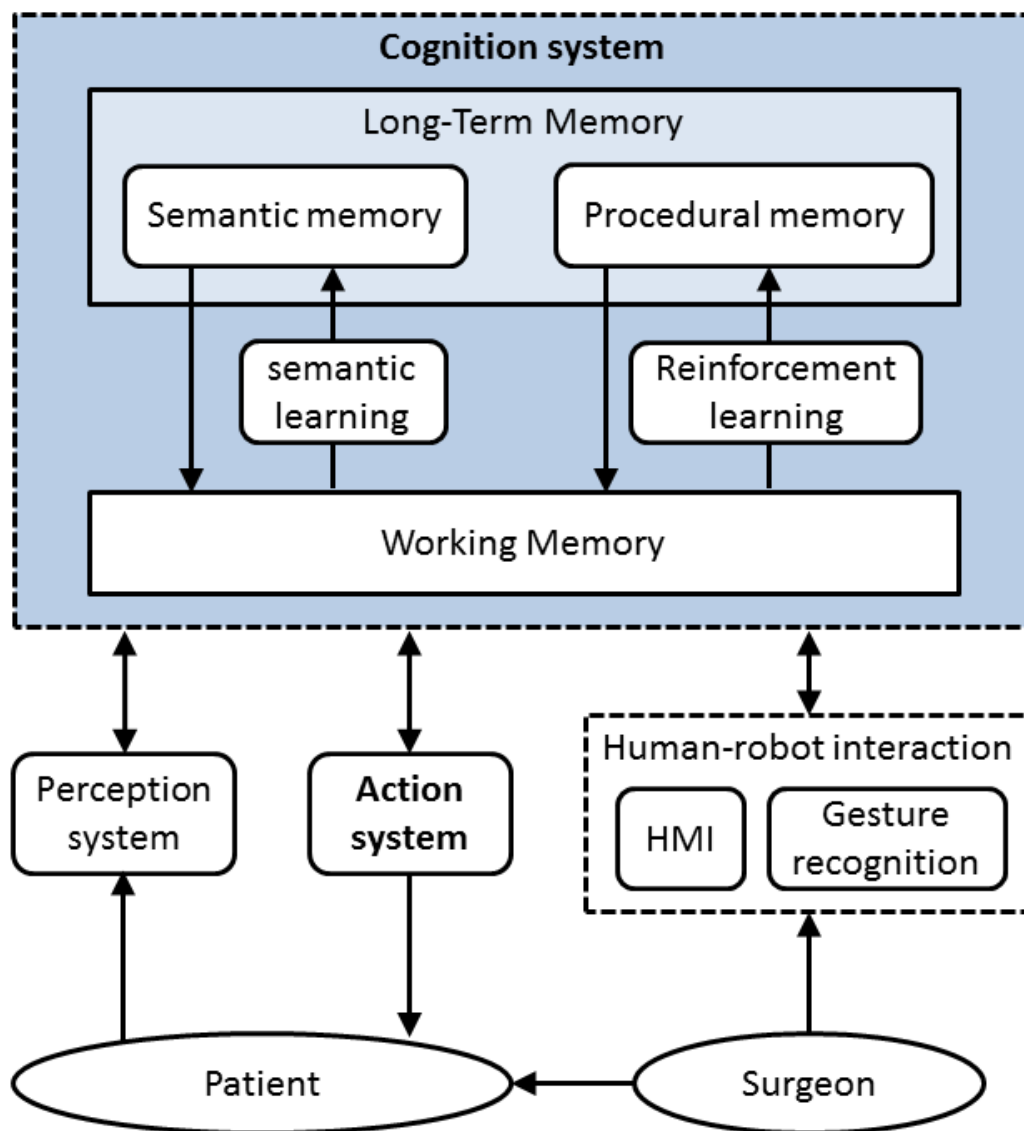


Figure 4.1 Global cognitive architecture.

On the other hand, the action system is the part of the architecture in charge of executing a motion of the robotic assistant. Thus, it receives a motion command planned in the robot cognition system, and performs the corresponding motion of the external robot and the camera robot, following the control scheme described in Figure 3.8. Although the motion of the robotic assistant is autonomous, for the sake of patients' safety and the successful performance of the surgical task, the surgeon must have the means to directly actuate on the robot to change the camera view or even to take control in the case of an emergency. This is done with a Human-Machine Interface (HMI), as a part of the human-robot interaction system, allowing the surgeon to change the value of any of the robot DoFs at any time during the procedure. The surgeon's commands will always have priority over the outgoing commands the robot cognition system.

Finally, decision making in autonomous robots largely depends on the current conditions of the environment, which in the particular context of a surgical procedure determine the actual state of the surgical task the surgeon is performing. Most surgical tasks can be described following a standardized protocol in which the global task is divided into a set of subtasks or states, modeled as a state diagram, where evolution to a particular state is triggered by a transition condition. Transition conditions can be determined using the information of the previous task state and the surgical instrument in use (Ko et al. 2005), but the most common way of modeling surgical tasks is depending on the interaction between the surgical tools (Rosen et al. 2006). Each state is modeled as a particular interaction between the instruments, called gestures. Thus, transition conditions from one step to the following in a particular surgical protocol are triggered when it is detected that a particular gesture has been completed (Estebanez et al. 2010, 2012). This process is performed in two steps: an off-line training process in which each gesture is modeled using Hidden Markov Models, and an on-line recognition system that triggers the transition conditions. This gesture recognition system has been studied in a previous thesis within the research group of the medical robotics of the University of Malaga (Estebanez 2013). Thus, although this module is needed for the overall working of the global cognitive architecture, it is out of the scope of this thesis proposal, as it is a scientific problem that has already been solved.

The following sections expand into the mathematical formulation of the robot cognition system. First, the semantic memory codification is described, along with its semantic learning mechanism. Second, the procedural memory and the reinforcement learning algorithm are described.

4.3 Semantic memory

Semantic memory plays a critical role in reasoning and decision-making, as it enables an agent to abstract useful knowledge (Wang, Tan, and Teow 2016). A human surgical assistant must have specific knowledge that makes him or her capable of assisting the surgeon during a surgical procedure. First, the assistant must be able to identify the different objects involved, in particular, he or she must be able to recognize the surgical tools and the different anatomical structures within the abdominal cavity. Second, he or she must have surgical knowledge to be able to follow the task workflow and act in consequence. Finally, to be able to anticipate to the surgeon requests, a human assistant also knows the way of operating of the surgeon he or she is assisting and his or her preferences regarding the assistance that must be provided during each state of the task. Thus, a smart surgical robotic assistant should have all this declarative knowledge to be able to assist the surgeon in an efficient and really autonomous way.

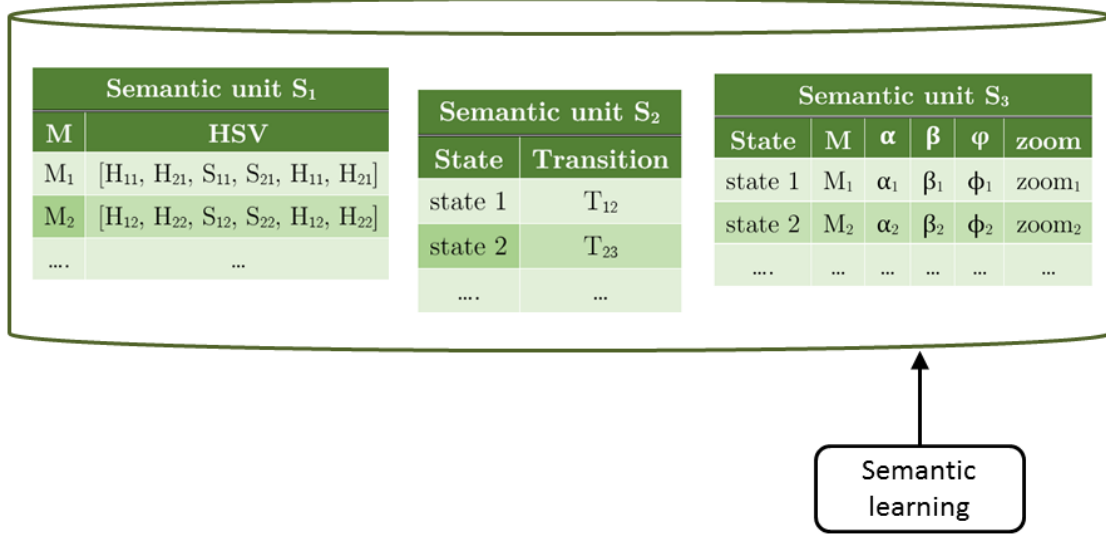


Figure 4.2 Semantic memory codification as a database.

Hence, the semantic memory is modeled as a database composed of three semantic units: S_1 , S_2 and S_3 . A semantic unit is defined as a table containing specific knowledge useful for a particular reasoning or planning function: S_1 stores the knowledge necessary to identify the different objects of the operating area; S_2 stores knowledge about the surgical protocol workflow; and S_3 stores knowledge about the expected camera behavior for each state of the protocol (Figure 4.2). Thus, each semantic unit is defined by a set of attributes (columns), and each row stores information of a particular object, event or state. As will be explained below,

semantic learning only acts on S_3 , as S_1 and S_2 are filled in off-line by manual entries.

The most natural and simple way of recognizing objects is by vision. Moreover, as the location of the objects will only be used to select a particular camera view, and the image of the camera is planar, 2D information is enough for the task concerning this work. In this work, color markers are used to identify the surgical instruments and other objects of interest by vision algorithms. A color can be represented by its RGB (red-green-blue) components or its HSV (hue-saturation-value) coordinates. In laparoscopic surgery, it is desirable that the image segmentation results be insensitive to the strength of illumination. Thus, the HSV representation is more suitable in this context (Wei, Arbter, and Hirzinger 1997). Therefore, semantic unit S_1 contains the HSV components for each color marker the system has to recognize. Formally, each row i of S_1 is defined with the following attributes:

$$S_{1i} := \langle M_i, HSV_i \rangle \quad (4.1)$$

where M_i is the color marker to be tracked, and HSV_i is a tuple containing the HSV coordinates for the marker color. In particular, $HSV_i = [H_{1i}, H_{2i}, S_{1i}, S_{2i}, V_{1i}, V_{2i}]$, being the hue, saturation and value coordinates for the color marker M_i in the range $[H_{1i} - H_{2i}]$, $[S_{1i} - S_{2i}]$, and $[V_{1i} - V_{2i}]$, respectively. Hence, S_1 will contain at least two rows, one for each marker stuck to the surgical tools.

Besides recognizing the objects of the scene, a smart robotic assistant must also have surgical knowledge to be able to follow the task workflow. As mentioned above, a surgical task or protocol can be modeled as a state-transition diagram. The gesture recognition system triggers the transition from one state to another, but the semantic memory must store the sequence of states and the relation between them, i.e. the transitions that connect the states among each other. This information is stored in semantic unit S_2 . Formally, each row i of S_2 is defined as follows:

$$S_{2i} := \langle state_i, transition_i \rangle \quad (4.2)$$

where $state_i$ represents the state number of the protocol, and $transition_i$ defines the trigger condition to jump from $state_i$ to $state_{i+1}$.

With this previous knowledge, the robotic assistant is able to follow the task workflow and to identify the actual state of the task. Then, the last thing the robot must know to provide an efficient assistance is how to actuate in every state of the procedure, i.e. which camera view is expected by the surgeon. Let's remember from Chapter 3 that the robotic assistant has six DoFs: shift in two directions along the abdominal wall that set the camera position (d_x and d_y), a pan rotation that sets

the image horizon (α), tilt and roll rotations that set the camera perspective (β and φ , respectively), and the camera zoom that sets the image region displayed on the monitor. Then, for each state of the protocol, the semantic memory must store the desired value of pan, tilt, and roll rotations, and the zoom level. However, camera displacements d_x and d_y cannot be set a priori as these are relative variables that depend on the initial position of the robot, and the final desired position of the camera. It makes more sense to define where the camera should point at during each state. Thus, instead of defining a particular value for DoFs d_x and d_y , semantic memory stores which object the camera should point at for each state of the task. Formally, each row i of S_3 is defined with the following attributes:

$$S_{3i} := \langle state_i, M_i, \alpha_i, \beta_i, \varphi_i, zoom_i \rangle \quad (4.3)$$

where M_i must be one of the objects defined in semantic unit S_1 so that the system can recognize it.

Semantic units S_1, S_2 and S_3 are the bases of the semantic memory, and they are filled in off-line by the system designer. S_1 and S_2 contain objective data related to object recognition and the protocol workflow. However, data of S_3 is highly dependent on the preferences and the way of operating of each particular surgeon. For example, it has been demonstrated that eye gaze patterns are different for expert surgeons than for novices: while expert surgeons tend to maintain eye gaze on the target, novices usually switch eye gaze between the instruments and the target (Wilson et al. 2010). Thus, although S_3 data entered by the designer serves as the default camera view parameters value, it is likely that each user (or each user profile such as expert or novice) may prefer to set his or her particular preferences. Therefore, a mechanism is necessary that allows data to be added to the semantic memory. This process is called semantic learning and allows a user to create a new semantic unit based on S_3 (i.e. with the same attributes) filled in with his or her particular preferences.

The complete process of the semantic learning is described in Table 4.1. When a new user is detected, the system creates a semantic unit called S_{userID} with the same attributes of semantic unit S_3 (subscript *userID* is a string containing the name or the profile of the user). Then, for each state of the task, the system will wait until the transition to jump to the next step is triggered, which means that the current state has finished. During the state, the user performs the corresponding task and manually sets the camera view, using the HMI. Once the state has finished, the values of DoFs α, β, φ and zoom set by the user are stored in the corresponding row of S_{userID} . Finally, the color marker at which the camera should point during each state must be set. To do this, the system will compute the distance from every marker M_j of semantic unit S_1 to the image center O_i using equation (4.4) and will store the marker with the minimum distance to the center in S_{userID} .

$$d_i = \sqrt{(M_{jx} + M_{jy})^2 + (O_{Ix} + O_{Iy})^2} \quad (4.4)$$

where (M_{jx}, M_{jy}) and (O_{Ix}, O_{Iy}) are the position of marker M_j and the center of the image, respectively, in the image reference frame $\{I\}$.

Table 4.1 Semantic learning algorithm.

```

1: if new user is detected
2:   create semantic unit  $S_{\text{userID}}$  based on  $S_3$ 
3:   for each state  $i$  of the task do
4:     wait for state transition
5:     store  $\alpha, \beta, \varphi$  and zoom values in row  $i$  of  $S_{\text{userID}}$ 
6:     for each marker  $M_j$  of  $S_1$  do
7:       compute distance to center of the image using equation (4.4)
8:     end for
9:     store  $M_j$  with minimum distance in row  $i$  of  $S_{\text{userID}}$ 
10:  end for
11: end if

```

4.4 Procedural memory

The procedural memory contains the navigation routines of the robotic assistant. Current navigation strategies for camera guidance in laparoscopic surgery are divided into two groups: a reactive behavior based on instrument tracking (Azizian et al. 2014; Casals, Amat, and Laporte 1996) and a proactive behavior based on the surgery workflow (Ko et al. 2005). Both of these approaches are based on very rigid preprogrammed behaviors, and they lack the intelligence and awareness to be considered autonomous (Pandya et al. 2014). While a reactive behavior has enough flexibility to track the surgical tools wherever they are, it lacks the capacity to adapt the viewpoint depending on the task currently being performed. On the other hand, a proactive camera behavior has the flexibility to offer different camera views depending on the task state, but the behavior within a particular state cannot be changed. Thus, a camera navigation strategy that combines both approaches would be able to offer a proactive behavior without losing the advantages of the reactive tracking of the instruments. The proactive behavior is important because the camera view during an intervention not only depends on the position of the surgical tools, but it is highly affected by the particular task the surgeon is performing. Depending on it, the surgeon may prefer to focus his or her attention on one of the

tools instead of on both tools, to zoom in the image during a challenging task, or to have a particular perspective of an anatomical structure. On the other hand, a reactive behavior that tracks the surgical tools is of great importance to be able to adapt the camera view to the particular circumstances of every instant of the procedure, and to not lose the tools from the sight of view of the camera, especially in the complex environment we are working in.

Under these considerations, the navigation strategy proposed for the camera guidance is described in Figure 4.3, which combines a proactive and a reactive behavior. Due to its nature, each behavior has a different execution cycle: while the proactive behavior runs every time the gesture recognition system triggers a transition to jump to the following state, the reactive behavior runs every system cycle. When a transition is triggered by the gesture recognition system, the cognition system infers the next state of the task according to the data stored in the semantic unit S_2 (equation (4.2)). With the current state of the task, the system infers the values of DoFs α, β, ϕ , and zoom according to data stored in the semantic unit S_3 (equation (4.3)), and sends it to the control system in order to execute the corresponding robot action. Moreover, the current state is also used to send to the perception system the HSV coordinates of the marker to track, according to the information stored in the semantic unit S_1 (equation (4.1)). The state is also sent to the reinforcement learning module, which along with a reward value computes the value of constants K_r and K_p , needed in the procedural memory module. These two modules will be described below.

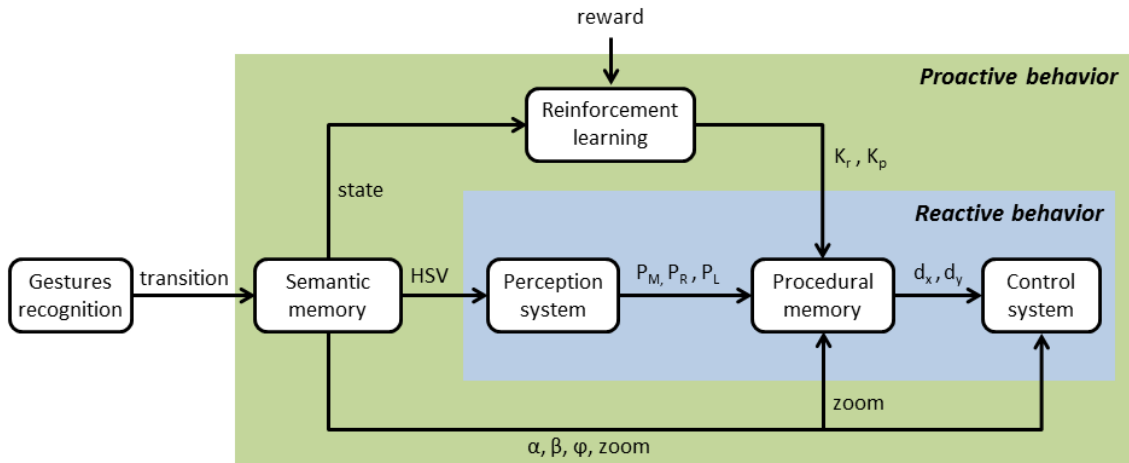


Figure 4.3 Camera navigation strategy.

Then, in each cycle of the system, the perception system outputs the instantaneous position of the marker tracked in the actual state, P_M , and the position of the tip of the right and left tools, P_R and P_L , respectively. These variables

are used along with the zoom value to compute the corresponding displacement of the camera robot, d_x and d_y , which is sent to the control system. Please note that P_M may coincide with P_R or P_L in case that for the actual state, M_i of semantic unit S_3 coincides with the marker of one of the surgical tools.

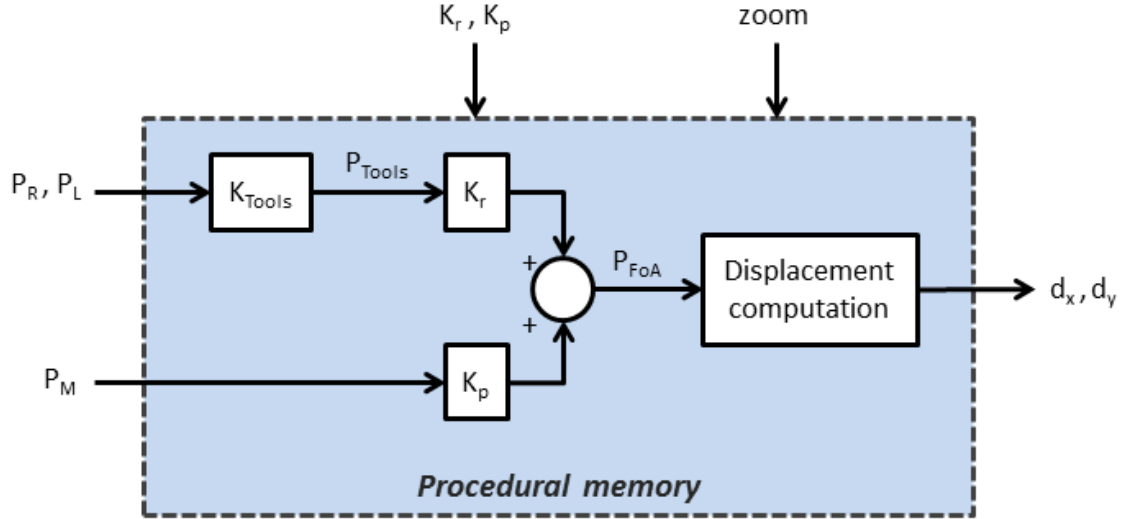


Figure 4.4 Procedural memory control scheme.

The control scheme of the procedural memory module of Figure 4.3 is described in Figure 4.4. The aim of this control is to compute the external robot displacements d_x and d_y so that the camera keeps in its field of view the marker set in the semantic memory for the actual state and the surgical tools. When a surgical tool is moving, it would be very dangerous to lose sight of it, as it could cause damage to a tissue or an organ. However, it is very common to keep one tool holding an anatomical structure to have access to a particular organ, and then operate with the other tool in a separate area. Thus, it would not make sense to try to keep both the moving tool and the static one in the field of view. First, because it may be unfeasible, and second, because despite being feasible, it would require having the working tool in one extreme of the image, when the surgeon may prefer to have that tool centered in the image to focus all of his or her attention on it. Thus, P_{Tools} , defined as the image point to be tracked regarding only the surgical tools, is computed as follows:

$$P_{Tools} = K_{Tools} \begin{pmatrix} P_R \\ P_L \end{pmatrix} \quad (4.5)$$

where $K_{Tools} = \frac{1}{\delta_R + \delta_L} (\delta_R \quad \delta_L)$, being δ_R and δ_L two binary variables that are true when right tool and left tool, respectively, are moving, and are false when they are not.

Then, P_{Tools} has to be weighted with P_M in order to provide a global point to

track that combines the proactive and the reactive behaviors. This weighting is done using constants K_r and K_p , that weight the contribution of the reactive and the proactive behavior, respectively, to the global behavior of the robotic assistant. Thus, the global point to track, i.e. the global focus of attention of the image P_{FoA} , is computed as:

$$P_{FoA} = K_r \cdot P_{Tools} + K_p \cdot P_M \quad (4.6)$$

where $K_r, K_p \in [0,1]/K_r + K_p = 1$. These values are learned with the reinforcement learning algorithm described in the following section. Finally, point P_{FoA} has to be transformed into camera displacements. This computation is graphically described in Figure 4.5. The center of the image is the point O_I :

$$O_I = \frac{1}{2} \begin{pmatrix} w_z \\ h_z \end{pmatrix} \quad (4.7)$$

where w_z and h_z are the width and height, respectively, of the zoomed image. According to equation (3.4), O_I is expressed as a function of the zoom value as:

$$O_I = \frac{1}{zoom} \frac{1}{2} \begin{pmatrix} w \\ h \end{pmatrix} \quad (4.8)$$

where w and h are the width and height, respectively, of the original image, i.e., with $zoom = 1$.

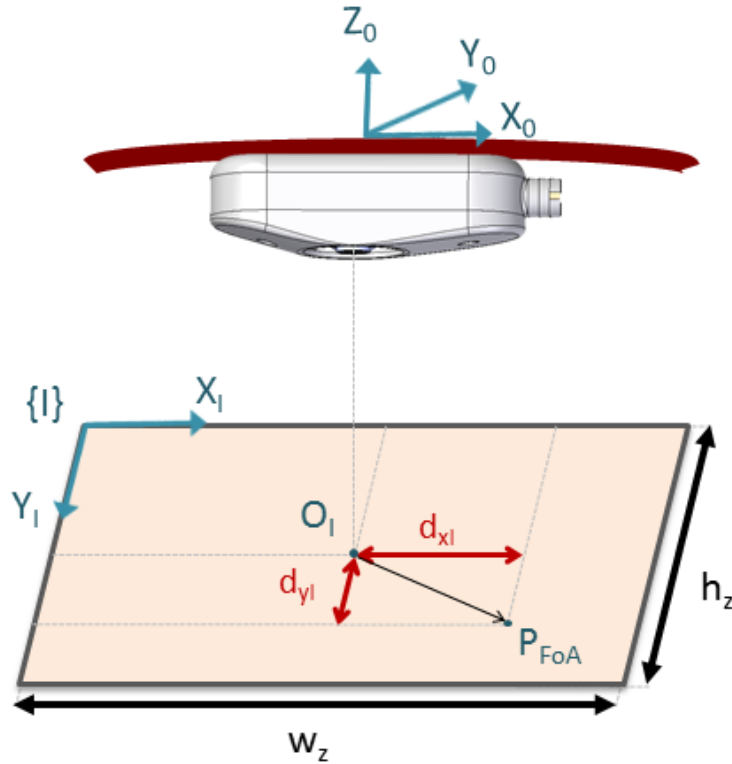


Figure 4.5 Camera robot displacement computation.

According to Figure 4.5, the distance between the center of the image O_I and the point at which the camera should be pointing at P_{FoA} referred to the image reference frame $\{I\}$ is:

$$\begin{pmatrix} d_{xI} \\ d_{yI} \end{pmatrix} = P_{FoA} - O_I = P_{FoA} - \frac{1}{zoom} \frac{1}{2} \begin{pmatrix} w \\ h \end{pmatrix} \quad (4.9)$$

where d_{xI} and d_{yI} represent the displacements of the camera along axis x_I and y_I , respectively, so that the camera points at P_{FoA} , i.e. having this point at the center of the image. As a final step, these displacements have to be transformed to the end effector reference frame $\{E\}$, as it is the component that executes the motion of the holder. Thus d_x and d_y are computed as:

$$\begin{pmatrix} d_x \\ d_y \end{pmatrix} = K_{pm} {}^E R_I \left(P_{FoA} - \frac{1}{zoom} \frac{1}{2} \begin{pmatrix} w \\ h \end{pmatrix} \right) \quad (4.10)$$

where K_{pm} is a constant to convert a distance in the image space (given in pixels) into the Cartesian space (given in mm), and ${}^E R_I$ is the rotation matrix between systems $\{E\}$ and $\{I\}$.

4.5 Reinforcement learning

As seen in the previous section, robot behavior highly depends on the weights of reactive and proactive behaviors, K_r and K_p , respectively: high values of K_r allow the camera to follow the instruments independently of the current state of the task, a behavior that is usually more comfortable for novices, while low values of K_r (and therefore high values of K_p) make the navigation strategy highly dependent on the actual state of the task, a behavior that expert surgeons usually prefer. Therefore, the system must learn the customized values of K_r and K_p for each user to provide the best robot behavior during each state of the task. This learning process is performed using a reinforcement learning algorithm. Reinforcement learning is a type of machine learning in which an agent seeks an effective policy for solving a sequential decision task. Such a policy dictates how the agent should behave in each state it may encounter (Whiteson 2010). The agent's actions affect not only the immediate reward but also future opportunities for reward. Hence, a reinforcement learning agent seeks a policy that maximizes the total reward accumulated over the long term. Reinforcement learning is used in a wide range of applications such as gamer agents (Kamei and Kakizoe 2016), multi-agent cooperation (Lei and Yu 2016), weather forecasting applications (Yan, Zhang, and Guo 2016), or dynamic pricing and energy consumption scheduling (Kim et al. 2016).

The reinforcement learning module is implemented following the Q-learning technique (Song et al. 2012). In this method, each rule R_h has a numerical value associated with it, Q_h , called utility, which is a measurement of the expected utility of a particular action. The complete process of the reinforcement learning algorithm is described in Figure 4.6. Production rules R_h are composed of two parts: a precondition (“IF”) and an action (“THEN”). Preconditions depend on the actual state of the task, while actions store the possible values of K_r and K_p , which are discretized as follows:

$$\begin{aligned} K_r &= \{K_{r1}, K_{r2}, \dots, K_{rm}\} \\ K_p &= \{K_{p1}, K_{p2}, \dots, K_{pm}\} \end{aligned} \quad (4.11)$$

where $K_{pi} = 1 - K_{ri}$. Therefore, each production rule R_h has the following syntax:

$$R_h: \text{IF state} = i \text{ THEN } K_r = K_{rj} \text{ and } K_p = K_{pj} \quad (4.12)$$

where $1 \leq i \leq n$, with n being the number of states of the task, and $1 \leq j \leq m$, and with m being the number of intervals in which K_r is discretized. Thus, the production system is composed of a total of $n \times m$ rules. According to equation (4.12), an action is defined as a particular pair of values of K_r and K_p .

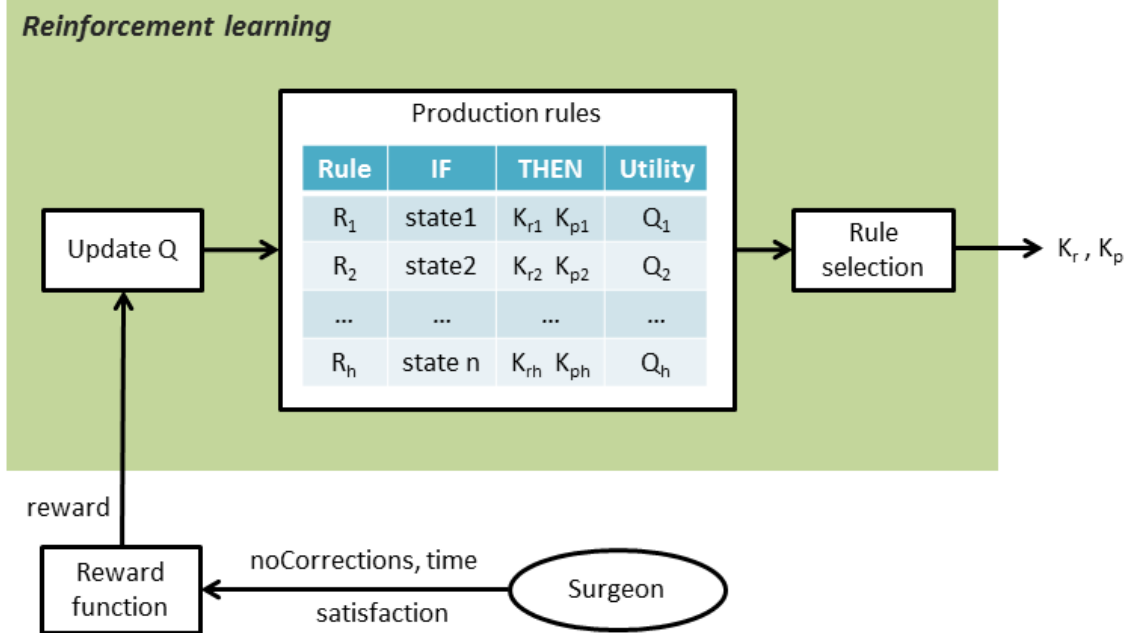


Figure 4.6 Reinforcement learning algorithm.

The final goal of the learning process is to infer the action that maximizes the global behavior of the robot for each state. Thus, the reward value is computed every time the surgeon finished a particular state. The reward function is designed

as a fuzzy model that evaluates the robot behavior during the performance of a particular task:

$$reward = \text{fuzzy}(\text{noCorrections}, \text{time}, \text{satisfaction}) \quad (4.13)$$

where *noCorrections* is the total number of corrections the surgeon commands the robot to adapt the camera view (using the HMI), *time* is the total time the surgeon spends in completing the state, and *satisfaction* is a subjective feedback that measures how satisfied is the surgeon with the robot behavior. This fuzzy model will be further described below.

The reward value is used to update the utility Q_h of each rule of the production system, following the equation:

$$Q_{h_new} = (1 - \rho) \cdot Q_{h_old} + \rho \cdot (reward + \mu \cdot EFR) \quad (4.14)$$

where Q_{h_new} and Q_{h_old} are the updated and the current utility values, respectively, $0 \leq \rho \leq 1$ is the learning rate, $0 \leq \mu \leq 1$ is the discount factor, and EFR is the expected future reward. On the one hand, the learning rate ρ models the importance of newly acquired information over old information. A value of $\rho = 0$ makes the agent not considered new information, while a value of $\rho = 1$ means that the agent only considers the most recent information, and forgets the old one. On the other hand, the discount factor μ determines the importance of future rewards. A value of $\mu = 0$ makes the agent only considers the current reward, while a discount factor approaching to 1 will make it strive for a long-term high reward.

Finally, rule selection is done using the ϵ -greedy policy (Tokic and Palm 2011). This policy is a way of selecting random actions with uniform distribution from a set of available actions. With this policy, a random rule is selected with ϵ probability, and the rule with highest utility value is selected with probability $1 - \epsilon$. Thus, rule selection is performed as follows:

$$rule\ selection = \begin{cases} random\ rule, & \text{if } \xi < \epsilon \\ rule\ with\ maximum\ utility\ Q_h & otherwise \end{cases} \quad (4.15)$$

where $0 \leq \epsilon \leq 1$ is the probability of selecting a random rule, and $0 \leq \xi \leq 1$ is a uniform random number drawn at each time step.

In summation, the process of procedural memory with reinforcement learning follows the algorithm described in Table 4.2. When a new transition condition is triggered by the gesture recognition system, the system infers the new task state using data from the semantic memory, in particular, using equation (4.2). With the new state, the system retrieves the object to track in the new state, M , and the value of the robotic assistant DoFs α , β , φ , and zoom using equation (4.3). Then, using equation (4.1), the HSV value of object M is retrieved so that the perception

system can track the object. Then, the reward value associated with the last state is computed using the fuzzy model described in equation (4.13). With this reward value, the system updates the utility value of each rule in the production system using equation (4.14). And finally, the system selects the following action, i.e. the values of K_r and K_p for the next state, using equation (4.15). Then, for each system cycle, the system computes the camera displacements d_x and d_y using equation (4.10).

Table 4.2 Procedural memory with reinforcement learning algorithm.

```

1: if new transition condition do
2:   infer next task state using equation (4.2)
3:   retrieve  $M$ ,  $\alpha$ ,  $\beta$ ,  $\phi$  and zoom using equation (4.3)
4:   retrieve HSV components of object  $M$  using equation (4.1)
5:   compute reward with fuzzy model of equation (4.13)
6:   update utility value of the production rules using equation (4.14)
7:   select a rule following policy of equation (4.15) and output  $K_r$  and  $K_p$ 
8:   for each system cycle do
9:     compute camera displacement  $d_x$  and  $d_y$  using equation (4.10)
10:  end for
11: end if

```

Reward function

As mentioned above, the reward value is computed following a fuzzy model, built with a Mamdani inference system with three input variables (noCorrections, time and satisfaction) and a single output (reward). Membership functions of variables of the fuzzy model designed are represented in Figure 4.7. Variable noCorrections is composed of three membership functions: two triangular functions to define few and many number of corrections, and a trapezoidal function to define a medium number of corrections. Variable time is also composed of three membership functions: two trapezoidal functions to define a fast and a slow performance, and a triangular one to define a normal performance. These variables represent objective values that depend on the surgeon's performance. On the other hand, satisfaction is a subjective variable through which the surgeon gives feedback about his or her degree of satisfaction with the robot behavior. It is composed of three triangular membership functions to express a high degree of satisfaction (verySatisfied), a normal satisfaction (satisfied), and a high degree of dissatisfaction (notSatisfied). Finally, the reward output by the fuzzy system according to a set of predefined fuzzy rules is composed of seven triangular membership functions: three to express

penalization, i.e. negative values of reward (N1, N2, and N3), the central one (M), and another three for positive reward values (P1, P2, P3). It has been chosen to define three functions for positive and negative values to be able to express more nuances in the model. The reward range has been defined between -10 and 10.

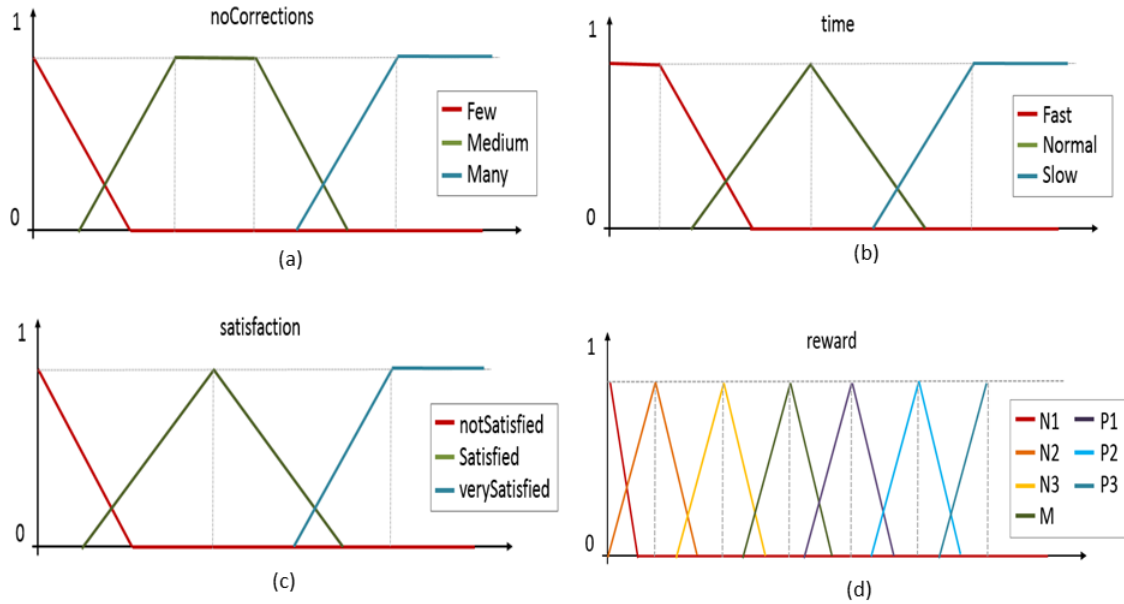


Figure 4.7 Membership functions of input and output variables of the reward fuzzy model: (a) noCorrections, (b) time, (c) satisfaction, and (d) reward.

Fuzzy rules are designed so that the user satisfaction predominates over the other two variables. Time performance and the number of corrections gives an idea about if the camera behavior has helped the surgeon during the task. However, these two variables are highly affected by the surgeon's dexterity and the particular conditions in which the task is performed, especially in the unpredictable environments of surgical interventions. Thus, although these two variables are taken into account to adjust the reward, this value is highly related to the surgeon's satisfaction. This can be clearly appreciated in Figure 4.8, that shows the behavior of the fuzzy model: the reward is maximum for maximum satisfaction value, getting slightly lower with the number of corrections and the performance time, and the reward is minimum for minimum satisfaction and maximum number of corrections and performance time. For intermediate values of satisfaction, the reward value follows a similar tendency for the number of corrections and the performance time: it falls with the user satisfaction.

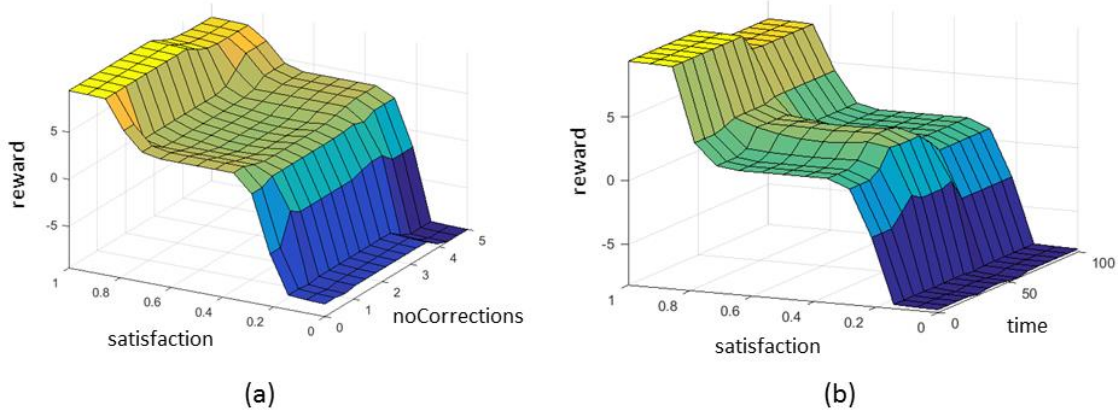


Figure 4.8 Fuzzy model surfaces: (a) satisfaction vs noCorrections, and (b) satisfaction vs time.

4.6 Conclusion

This chapter has described a cognitive architecture for a smart camera robotic assistant that allows the system to collaborate with surgeons in a surgical co-worker scenario. The architecture, based on the general framework SOAR (Laird 2012), is composed of a cognition system as the main component for knowledge storage and reasoning, perception and action systems for the interaction with the patient, and a human-robot interaction system for the communication with the surgeon. This architecture offers an easy integration of the different modules and an easy adaptation for other surgical tasks, although this work is focused on collaborative camera navigation. The cognition system makes it possible to store different kinds of knowledge, reason about them and make decisions regarding the environment according to the information received from the patient and the surgeon.

The semantic memory stores the declarative knowledge of the system, essential to be able to reason and make decisions, as it contains the basic information to be able to follow the surgery workflow. This knowledge is encoded as a database containing object identification data, the surgery workflow, and the camera behavior expected during each state of the task. A semantic learning algorithm allows new information to be added to the knowledge base in order to acquire knowledge about different surgeons' preferences and work styles.

On the other hand, the procedural memory contains the navigation strategy. Camera navigation has been improved with respect to previous work in the literature by combining a reactive behavior that tracks the surgical tools with a proactive behavior that adapts the camera view to the surgery workflow. Thus, navigation follows a more flexible algorithm that allows the robot to adapt to

different ways of working and to react to unforeseen situations. This navigation method is improved with a reinforcement learning module that learns the contribution of reactive and proactive behaviors to the global robot performance that is best suited for each state of the task and for each particular surgeon. Learning capabilities are essential for a real cognitive agent, and as far as the author's knowledge, no previous work has contemplated incorporating learning techniques with the camera navigation strategies.

5 IMPLEMENTATION AND EXPERIMENTS

5.1 Introduction

Previous chapters have described the theoretical concepts of a smart camera robotic assistant for minimally invasive surgery. In particular, Chapter 3 describes the design aspects of a camera robotic assistant of six DoFs, two of which are controlled with a cable-driven system actuation. Chapter 4 proposes a cognitive architecture for autonomous camera navigation and details the cognitive aspects of the robot along with the theoretical concepts of the actuation system that executes the motion of the robot.

This chapter describes the implementation of the methodologies proposed in previous chapters. It describes the robotic platform in which the theoretical concepts of this thesis project have been implemented, including the description of the hardware architecture of the experimental setup and the software architecture implemented in a ROS (Robotic Operating System) network. Next, the experiments that validate the work presented in this thesis are exposed. First, an in-vivo experiment to demonstrate the feasibility of the experimental prototype of the camera robot is presented. Then, experiments to validate the hybrid force-position control with torque compensation are described, along with a stiffness matrix estimation analysis. Finally, a set of experiments to validate the smart camera navigation strategy described in the previous chapter are presented. These experiments include a comparison between the different camera robotic assistant and an evaluation of the reinforcement learning algorithm. The chapter concludes

with a discussion of the experiments.

5.2 Implementation of the robotic assistant

The theoretical concepts proposed in this work have been implemented in the robotic platform shown in Figure 5.1. The robotic assistant is composed of the camera robot described in Section 3.2 (not seen in the image because it is inside the abdominal simulator), and a Barret WAM robot (WAMTM Arm, Barrett Technology, Inc.). The WAM robot is a seven DoFs backdrivable manipulator that exhibits zero backlash, low inertia, and low friction, and uses a patented cable-driven technology to facilitate kinematic motion when used as a manipulator or active resistance when used as a haptic device (WAM ARM datasheet 2016). Its high backdrivability makes this robot inherently safe for humans and very useful for applications that combine manual and automatic control. Thus, the robot can be easily moved by hand to the desired position, and then return to joint control. The WAM has a self-contained six axis force-torque sensor that provides real-time measurements (F/T Sensor datasheet 2016). The patient's abdominal cavity is simulated with a methacrylate box with a flexible cover that simulates the abdominal wall.

For the experimental setup, instead of using conventional surgical tools manually moved by the surgeon, it has been chosen to use a robotic platform to teleoperate the tools. This has been done for safety and practical reasons. First, the working workspace in a surgical intervention is quite limited. Thus, if the surgeon directly operated the surgical tools, he or she and the WAM robot would have to share a reduced space, with the consequent safety and comfort inconveniences. Second, using a teleoperating system provides more computerized information of the tools position, orientation, velocity, state of the tips, etc., which is very useful for the cognitive system to augment its knowledge about the state of the environment, and therefore, to augment its reasoning capabilities. Moreover, a three-arm configuration, one to handle the camera and the other two for surgical tools, replicates the da Vinci robot configuration. This has two main advantages: this configuration is widely accepted by clinicians all over the world, and the theoretical approaches presented in this thesis project could be easily extrapolated to a da Vinci with minimum changes to the real system.

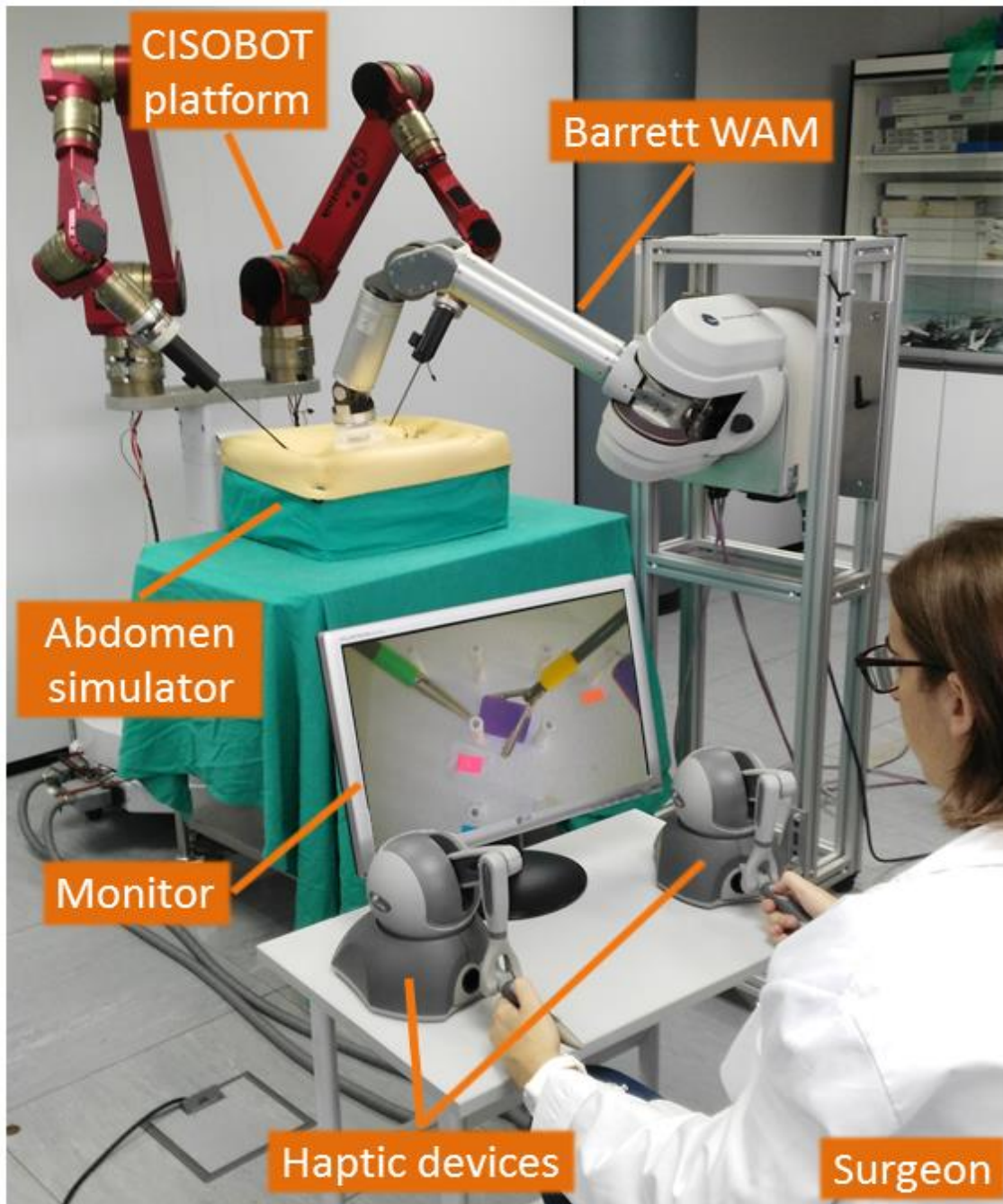


Figure 5.1 Camera robotic assistant experimental setup.

The robotic platform used to teleoperate the surgical tools is the CISOBOT platform, shown in Figure 5.2. This platform, developed by the research group of medical robotics of the University of Malaga, is composed of two commercial six DoFs manipulators manufactured by Robotnik Automation S.L, mounted on a structure that provides high stability to the platform. Two customized robotic graspers have been coupled to the end effector of each manipulator. The robotic graspers, manufactured by the Spanish company Ingenieria Uno, are made with commercial laparoscopic tools mounted on a spring system actuated by a

servomotor that allows opening and closing of the grasper tip. The CISOBOT platform is teleoperated with two haptic devices that control the motion of each manipulator and the opening and closing of the graspers tip. For natural and intuitive teleoperation of the surgical tools, the configuration of the haptic devices and the monitor follows a hand-eye configuration, as shown in Figure 5.2, i.e. the monitor is placed in front of the surgeon's eyes and between both haptic devices. Moreover, an intuitive teleoperation control, described in detail in Appendix A, has been implemented in order to transform the motion of the haptic devices into natural and intuitive motion of the robotic graspers tip.

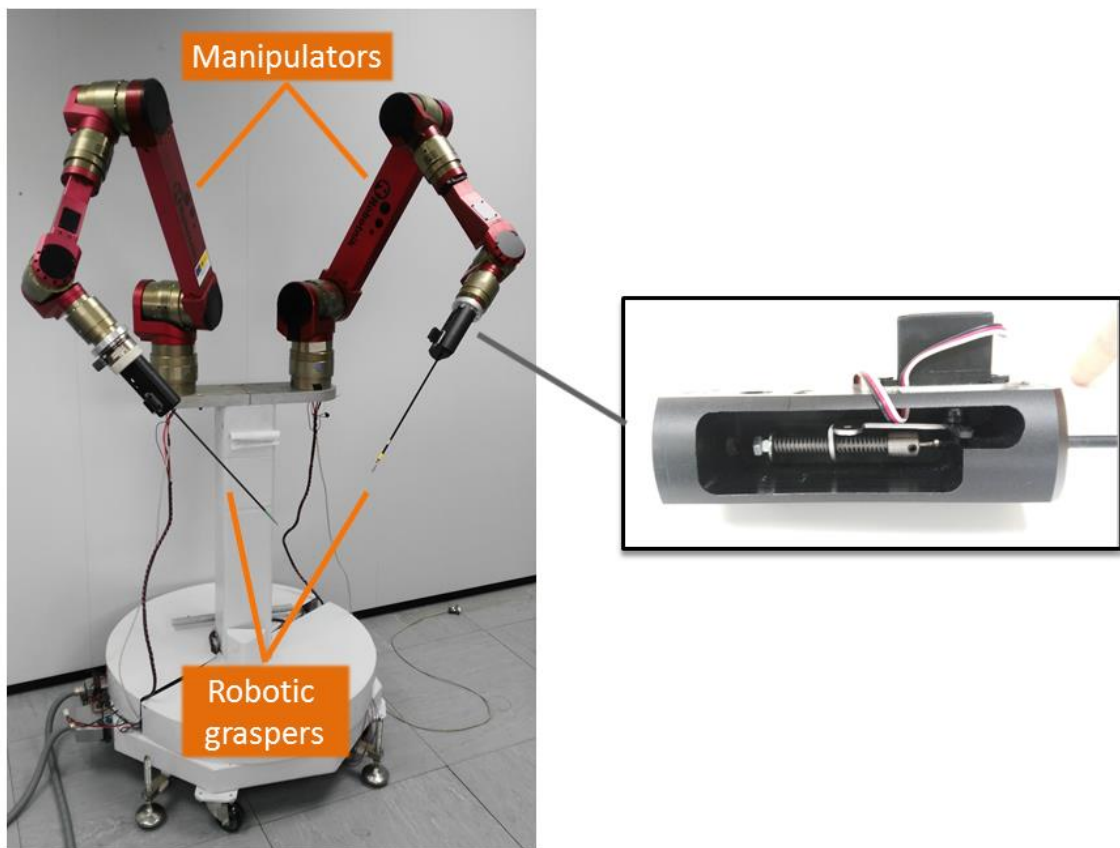


Figure 5.2 CISOBOT platform.

5.2.1 Experimental prototype of the camera robot

According to the requirements specified in Chapter 3, the camera robot has been designed with a size of 30 x 27 x 88 mm, and a cylindrical shape to facilitate its introduction through the entry port (Figure 5.3). This size fits into the 3 cm incisions performed in SPAS (Best et al. 2012). The camera, with an onboard lighting source, is placed at the central part of the device body, and a camera wire

exits the device through an opening in one of the ends. Two cylindrical permanent magnets, with 20 mm in diameter and 5 mm height, are placed symmetrically at the bottom of the device. The internal DoFs, tilt and roll rotations, are actuated with a cable-driven system. Thus, no motors are required, which would have increased both the size and weight of the device and would have required additional power supply.

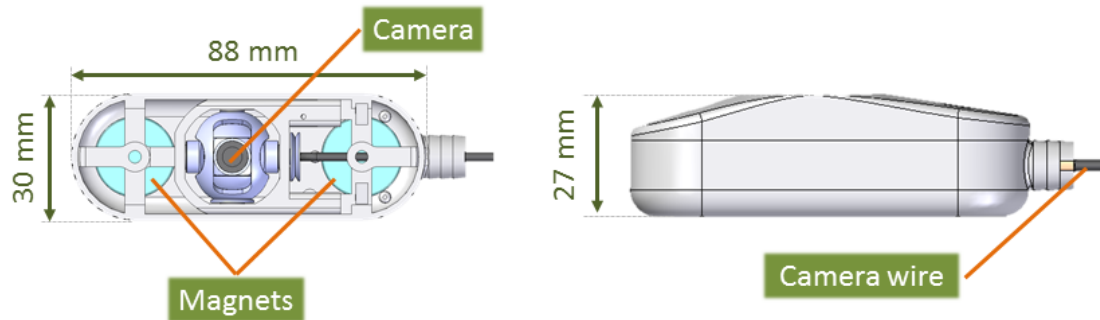


Figure 5.3 Design of the intra-abdominal device: top view (left), and front view (right).

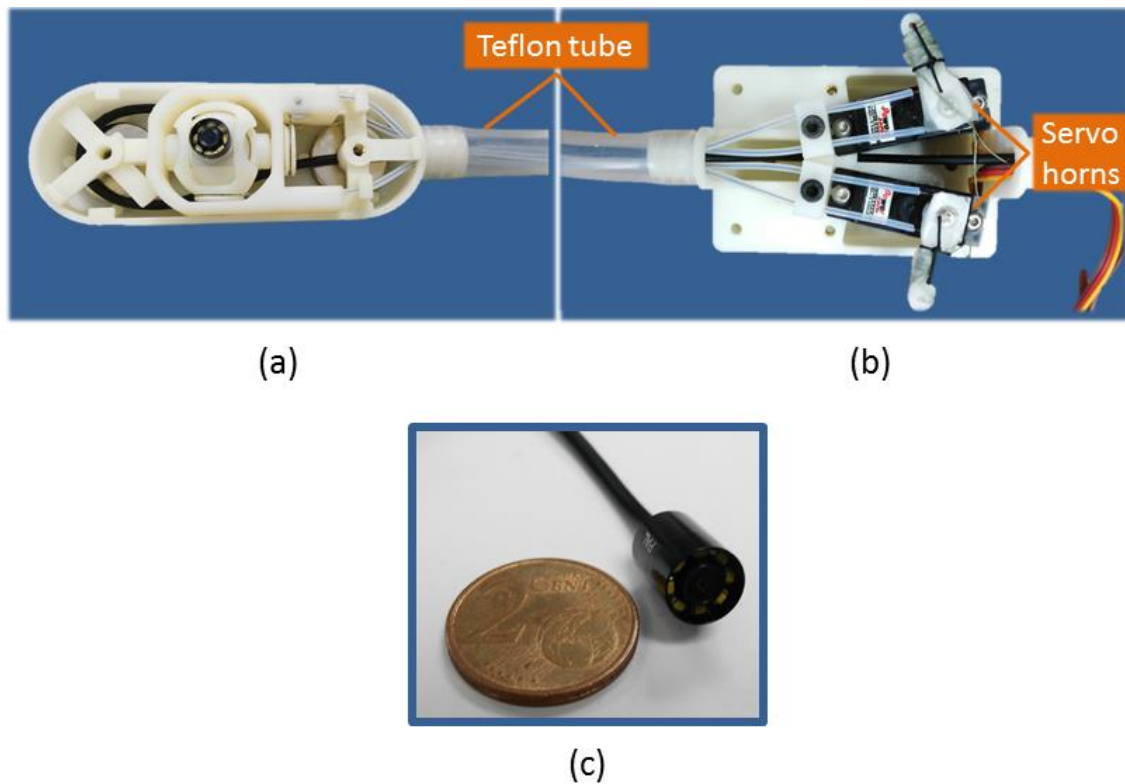


Figure 5.4 Experimental prototype of the intra-abdominal device: (a) intra-abdominal device, (b) external motors, and (c) HD miniature camera.

Figure 5.4 shows the experimental prototype manufactured for the experiments. The total weight of the device is 35 grams. Neodymium magnets (Webcraft GmbH, Germany) have a low weight of 12 grams each, a strength of approximately 6 kg and magnetization N42. The high-resolution miniature camera (model MO-F3506LSC-3T, Misumi Electronics Corp., Taiwan) is only 8 mm in diameter and has a height of 5 mm (Figure 5.4.c). The camera has a resolution of 400 TV lines and a frame rate of 50 frames per seconds. It has been designed with a focus distance between 5 and 10 cm, appropriate to provide high-resolution images in the small workspace of a peritoneal cavity. The camera has six white LEDs onboard, placed symmetrically and coaxially to the lens. Thus, no additional light source is required during an intervention. Maximum roll and tilt rotations are $\pm 30^\circ$.

Motors (power HD Mini Servo HD-1160A, Pololu Robotics & Electronics) have a maximum speed of 0.11 seconds/ 60° , and a maximum torque of $2.7 \text{ kg} \cdot \text{cm}$ (Figure 5.4.b). Servo horns are used for the cables tying. Due to its breaking and knotting strength characteristics, cables of the actuation system are made of fishing line. These cables along with the camera cable are embedded into a Teflon tube. This material is very flexible and offers a low friction coefficient.

5.2.2 Hardware architecture

Hardware connections of the experimental setup are shown in Figure 5.5. The system is managed by three personal computers: PC1, which manages the cognitive system, PC2, that runs the interaction with the environment, and PC3, that controls the teleoperation platform. Thus, PC1 implements the cognition and the action system of the cognitive architecture of Figure 4.1, PC2 the perception system and the HMI modules, and PC3 the interaction surgeon-patient. PC1 sends position and orientation references to the Barrett WAM Arm through a CANbus connection, while roll and tilt rotations of the camera robot are commanded through a microcontroller (Arduino UNO), which sends the corresponding rotations to the external motors that control the internal DoFs of the camera robot through the cable-driven actuation. On the other hand, PC2 is connected to the camera of the intra-abdominal device, so this computer is in charge of displaying the camera image on the monitor and running the vision algorithms of the perception system. Finally, PC3 runs the teleoperation control of the CISOBOT platform through a NI-PXI (National Instruments Corporation), a real-time hardware that provides an interface between PC3 and the robot joint controllers, using a CANbus connection. The haptic devices (Phantom Omni, Sensable Inc.) are connected through a FireWire connection, and the robotic graspers opening and closing functions are controlled with a micro servo controller (Micro Maestro 6, Pololu Corporation).

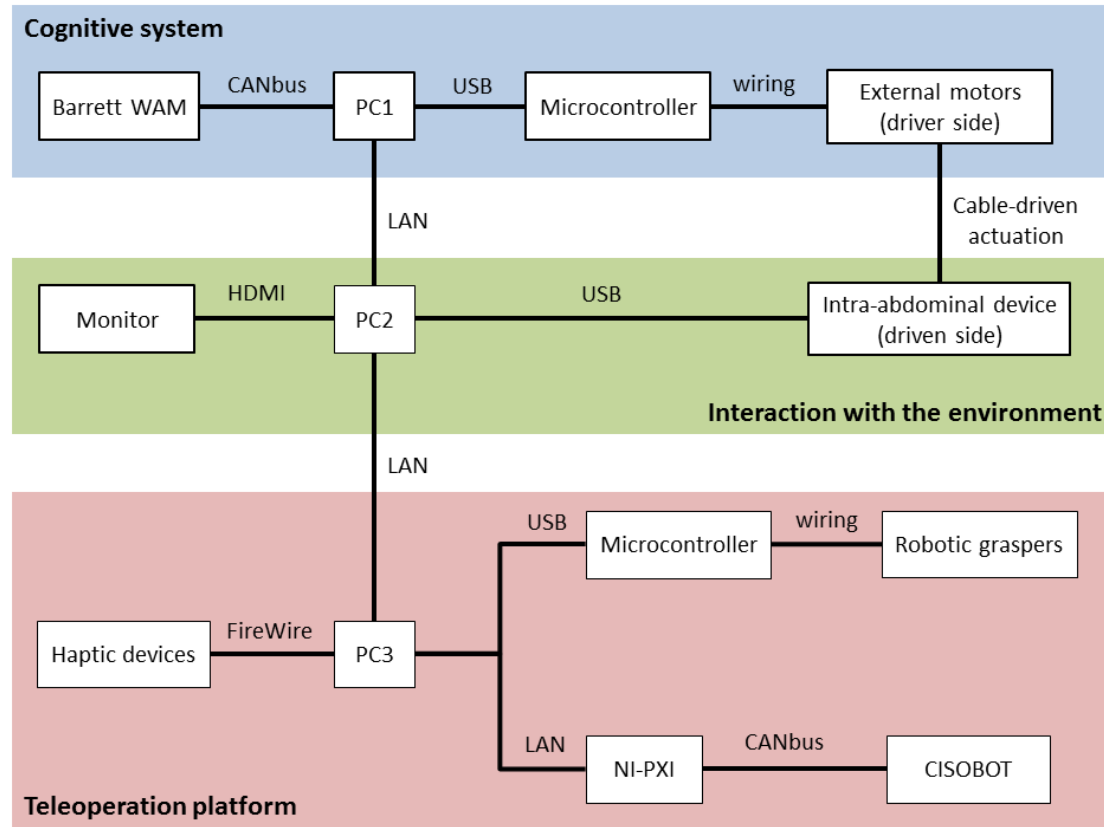


Figure 5.5 Hardware architecture of the experimental setup.

Next, the ROS architecture that implements the software of the system is described.

5.2.3 Software architecture

The software of the system has been implemented in ROS (Robotic Operating System), an open-source framework specially designed for writing robotic software (Koubaa 2016). A ROS architecture is composed of a set of programs or processes, called nodes, that communicate with each other through streaming topics using a publisher/subscriber communication. The main advantage of ROS is that its distributed and modular design allow an easy integration of the different components of a robotic system, as each element of the system is controlled by a different node. It also allows easy integration of new elements without modifying the current software structure of the system. Further details of ROS components and communications are given in Appendix C.

The ROS architecture implemented for the experimental setup described above is shown in Figure 5.6. The ROS Master is the core element of a ROS architecture,

as it enables individual nodes to locate one another. The ROS architecture is composed of eight nodes: robot cognition node, reward node, motors node and WAM node, that run in PC1, HMI node and Vision node, implemented in PC2, and Teleoperation node and Robotic graspers node, running in PC3. Next, implementation details of each node are described.

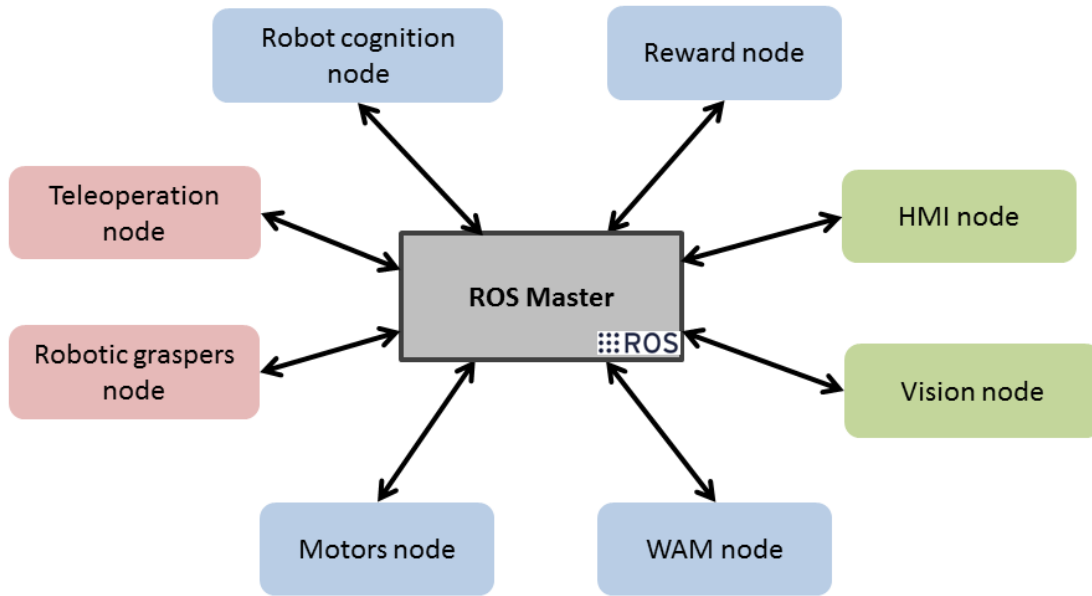


Figure 5.6 ROS architecture.

- **Robot cognition node.** The cognition system of the robot is implemented in the general framework SOAR (Laird 2012). Soar has a working memory that represents the current problem-solving situation, and a long-term knowledge represented as production rules. It also has a reinforcement learning mechanism that tunes knowledge selection based on a given reward function. Further details of SOAR are given in Appendix D. This node inputs a reward value from the Reward node, the position of the objects of the scene from the Vision node, and the transitions from one state to the following, which are triggered manually, and outputs the value of the robotic assistant DoFs (d_x , d_y , α , β , ϕ and zoom) at every system cycle.
- **Reward node.** This node implements the fuzzy model described in Section 4.5. Thus, when the current state is finished, it inputs the number of corrections the surgeon has performed, the time spent in completing the task and the surgeon satisfaction feedback regarding the camera view and outputs the numerical value of the reward corresponding to the last state. This node is implemented in a MATLAB environment using the Fuzzy Logic Toolbox.

- **HMI node.** The human-machine interface that allows the surgeon to directly command a specific value of the robot DoFs is implemented in MATLAB using the GUI Layout Toolbox. A snapshot of the HMI is shown in Figure 5.7. In the top left corner, the user introduces his or her name or profile so that the system can retrieve his or her particular camera view preferences from the semantic memory, as described in the algorithm in Table 4.1. The transitions between states are triggered using the pushbuttons labeled with *State i*. The interfaces allow the position to be modified by commanding the WAM a motion to the right or to the left, corresponding to a camera motion on the axis X_I , or moving up or down, which moves the camera on the axis Y_I . It also allows the zoom level of the image to be changed, and to increase or decrease the tilt, roll and pan rotations. Pushbuttons labeled as *IdleWam* and *HoldWam* allow the external robot joints to idle so that they can be moved by hand to be placed in the desired location and to hold joints for automatic control, respectively.
- **Vision node.** This node receives the signal from the camera and runs the code to display the image on the monitor and the color segmentation algorithm for object detection. The code is written in C++ using the real-time control computer vision library *OpenCV*. The code contains the HSV components of every color marker used in the experiment and outputs the X and Y coordinates of the markers centroid referred to the image system $\{I\}$. In case a marker is not identified by the vision algorithm, the node outputs a (-1, -1) position, meaning that the marker is not visible. Thus, a recognition error does not interrupt the vision process.
- **WAM node.** This node inputs the value of the robotic assistant DoFs that are performed by the external robot, i.e. d_x , d_y , and ϕ , and executes the corresponding motion of the camera robotic assistant and the hybrid force-position control with torque compensation described in Section 3.4. It is implemented in C++ using the real-time control library *libbarrett*, written and maintained by Barrett Technology, Inc.
- **Motors node.** This node controls the rotation of the motors of the cable-driven system that actuates the internal DoFs of the intra-abdominal device. It inputs the value of the roll and tilt rotations, α and β , respectively, and outputs the corresponding motor rotations, θ_1 and θ_2 , according to equations (3.9) and (3.10). This code is written in the Arduino environment using the servo motors control library called *servo*.
- **Robotic graspers node.** This node runs the opening and closing function of the robotic graspers, performed through the two servomotors of Figure 5.2.

This code is written in C++ using the same library as in the previous node, *servo*.

- **Teleoperation node.** This is the node in charge of controlling the CISOBOT platform, including processing the inputs from the haptic device, computing the teleoperation control described in Appendix A, and sending the corresponding motion to the robot joints. This code is implemented using a Simulink real-time windows target (SRTWT), that provides runtime for the Microsoft Windows operating system that is able to execute Simulink diagrams in real-time. The haptic devices are connected to SRTWT using a C++ application as a gateway between both haptic devices and the SRTWT.

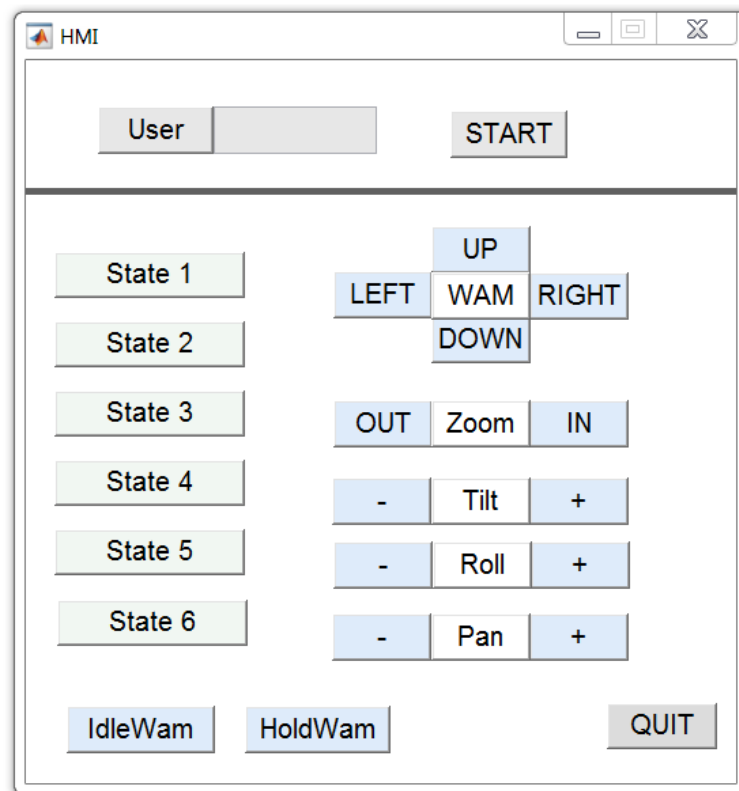


Figure 5.7 Snapshot of the Human-Machine Interface.

5.3 In-vivo validation of the camera robot

Validation of the camera robot has been carried out in an in-vivo experiment with a pig in the Center IACE (Instituto Andaluz de Cirugía Experimental) of Malaga. The experiment was performed by Dr. Eduardo Sánchez de Badajoz and Dr. Pilar Sánchez Gallegos, professors at the University of Málaga and experts in

laparoscopy. The main goals of the experiment were to demonstrate the viability of using a camera robot with magnetic anchoring to the abdominal wall and to test the quality of the camera in a real environment. Furthermore, the possibilities of the device providing more camera views than a traditional endoscope were also tested. The experiment consisted of performing a laparoscopic varicocelectomy (removal of varicoceles). For the intervention, the surgeons used conventional laparoscopic tools and a conventional endoscope (KARL STORZ H3Z HD) to acquire images of the camera robot inside the abdomen and to be able to compare the images provided by the two devices.

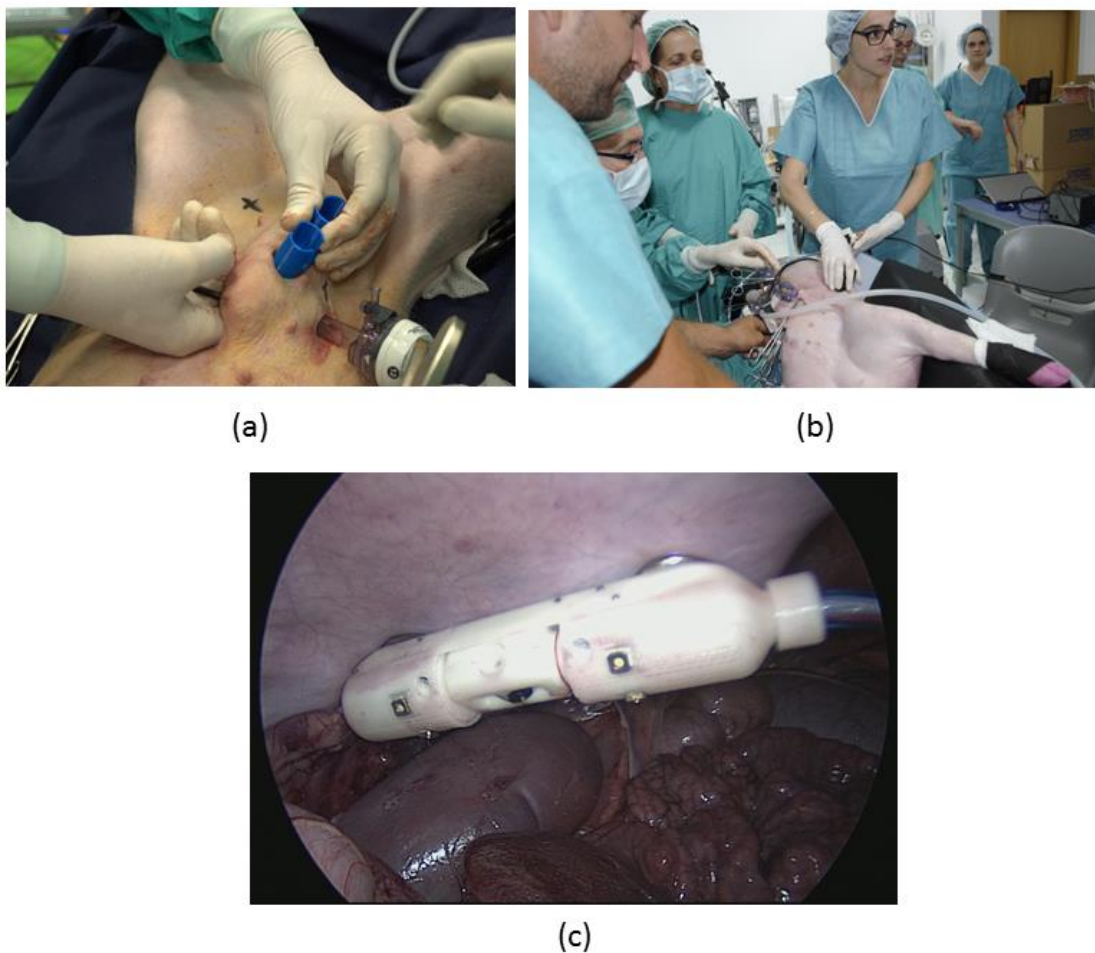


Figure 5.8 In-vivo experimentation in a pig: (a) insertion procedure, (b) snapshot of the operating room during the experiment, and (c) snapshot of the camera robot inside the abdominal cavity.

The camera robot was introduced into the abdominal cavity through an incision of around 3 cm (Figure 5.8.a). Insertion of the robot was easy and did not cause any damage to the skin of the patient thanks to the oval shape of the device. The insertion procedure was performed before the abdomen was insufflated, as during

this process the gas would escape through the incision. The camera robot wire exited the abdomen through the incision. Thus, in order to avoid gas leaks, the incision was closed with a purse-string suture to seal the tissue around the wire. No problems of gas leakage occurred during the experiment. Once the abdomen was insufflated with CO₂ to introduce the laparoscopic instruments, the camera had to be cleaned with a gauze using a conventional laparoscopic grasper tool due to the contact of the camera with organs during the process. No more cleaning was necessary during the experiment, as the camera did not come into contact with any organ again. On the contrary, as it usually occurs in normal laparoscopy procedures, the endoscope had to be removed and cleaned very often in order to maintain a sharply-focused image.

Figure 5.8.b shows a snapshot of the operating room during the experiment. As this experiment was aimed at evaluating the camera robot and not the whole robotic assistant, the magnetic holder was handled manually by one of the surgeons. A snapshot of a first prototype of the camera robot is shown in Figure 5.8.c. This prototype was designed with magnets 3 mm high and 20 mm in diameter, which resulted insufficient for the attachment of the device to the abdominal wall. Thus, as it can be appreciated in Figure 5.8.c, additional magnets of 2 mm height were necessary. Thus, this in-vivo experiment served to assess the dimension of the magnets, and consequently, the device was modified to contain magnets with a height of 5 mm. This magnet dimension results in an appropriate magnetic interaction between the internal device and the external holder, maintaining the device attached to the abdominal wall, and allows easy displacement of the holder without causing injury nor necrosis to the patient.

Figure 5.9 shows a comparison between images provided by the camera robot (on the left) and images provided by the endoscope (on the right). Although the images from the endoscope are slightly better, the quality of the camera robot is good enough to perform laparoscopic tasks. Images on the top correspond to the same instant in time (as well as images on the bottom). This way, points of view of the camera robot and the endoscope can be compared. In general, during the intervention, images of the camera robot were more intuitive and natural than the laparoscopic ones, as they come from above, providing a more similar perspective to a laparotomy, where the surgeon's eyes are always above the operating area. Although this was noticed and appreciated by the medical staff, it was especially relevant for the technical staff present in the operating room, who were not familiar with endoscopic procedures. For them, it was much easier to follow the intervention looking at the camera robot images. At the end of the intervention, the cold light of the endoscope was turned off to check if the onboard lights of the camera provided enough illumination to have a high-quality image. It was proved that the quality of the image was not affected by the endoscope light.

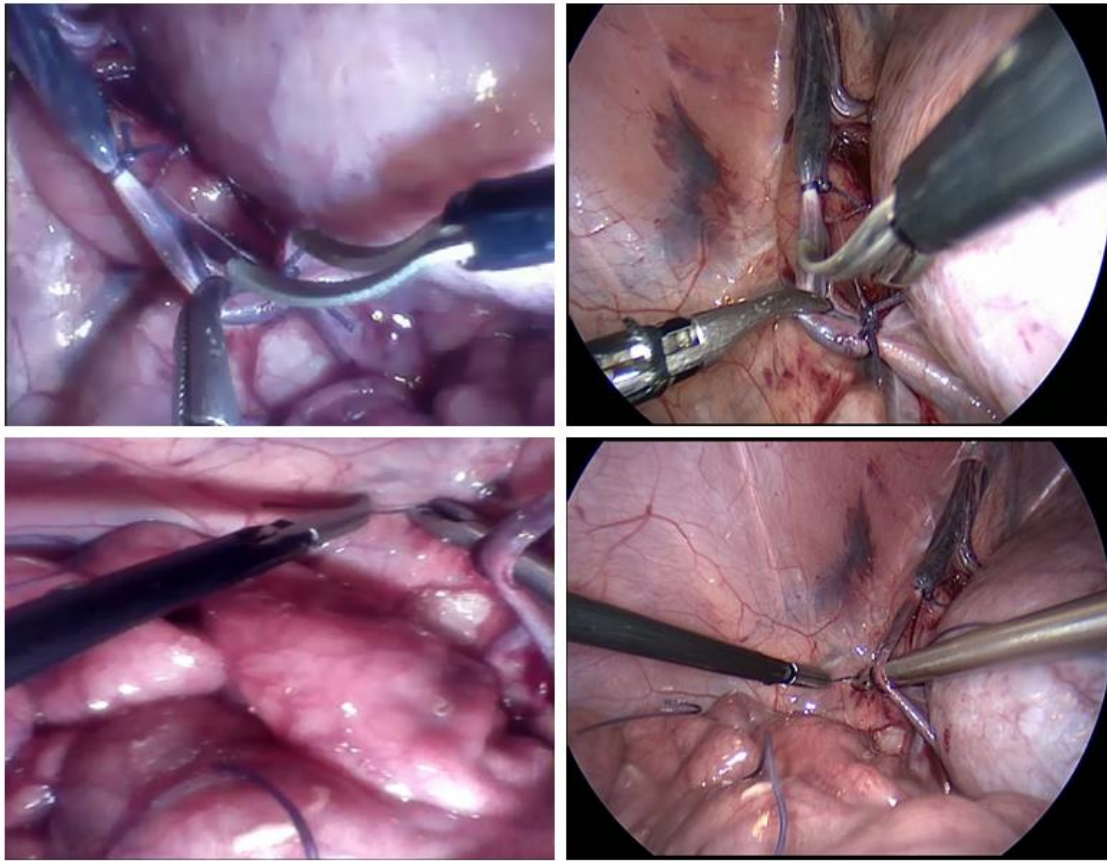


Figure 5.9 Comparison between images provided by the camera robot (left) and a conventional endoscope (right).

Summarizing, the in-vivo experiment demonstrated the viability of introducing a camera device into the abdominal cavity with no medical complications. Magnetic interaction has proven to be an appropriate guidance method in laparoscopic procedures, which does not cause any damage to the patient. The experiment reveals that the weak point of the camera robot is the image quality. However, surgeons reported that, although not comparable with an endoscope, the camera robot provides a stable image with sufficient quality to perform a real operation. Moreover, image stability with the camera robot was better than with the conventional endoscope, as the latter suffers from the inherent instability of human holding. On the other hand, the strengths of the camera robot are the field of view and the camera handling. As the motion of the camera is not restricted by the entry port, it can provide more points of view than a conventional endoscope, making it possible to reach areas inaccessible for endoscopes. As regards camera handling, although the camera robot has a more tedious insertion procedure, once inside the abdominal cavity it can be easily moved along the abdominal wall, and the camera does not fog up during the intervention. By contrast, the conventional endoscope fogs up very frequently, forcing surgeons to remove them for cleaning during surgery.

5.4 Force-position control

The hybrid force-position control with torque compensation described in Section 3.4.1 has been validated through an in-vitro experiment. This section describes the experiment setup, followed by the stiffness matrix estimation and the results obtained during the experiment.

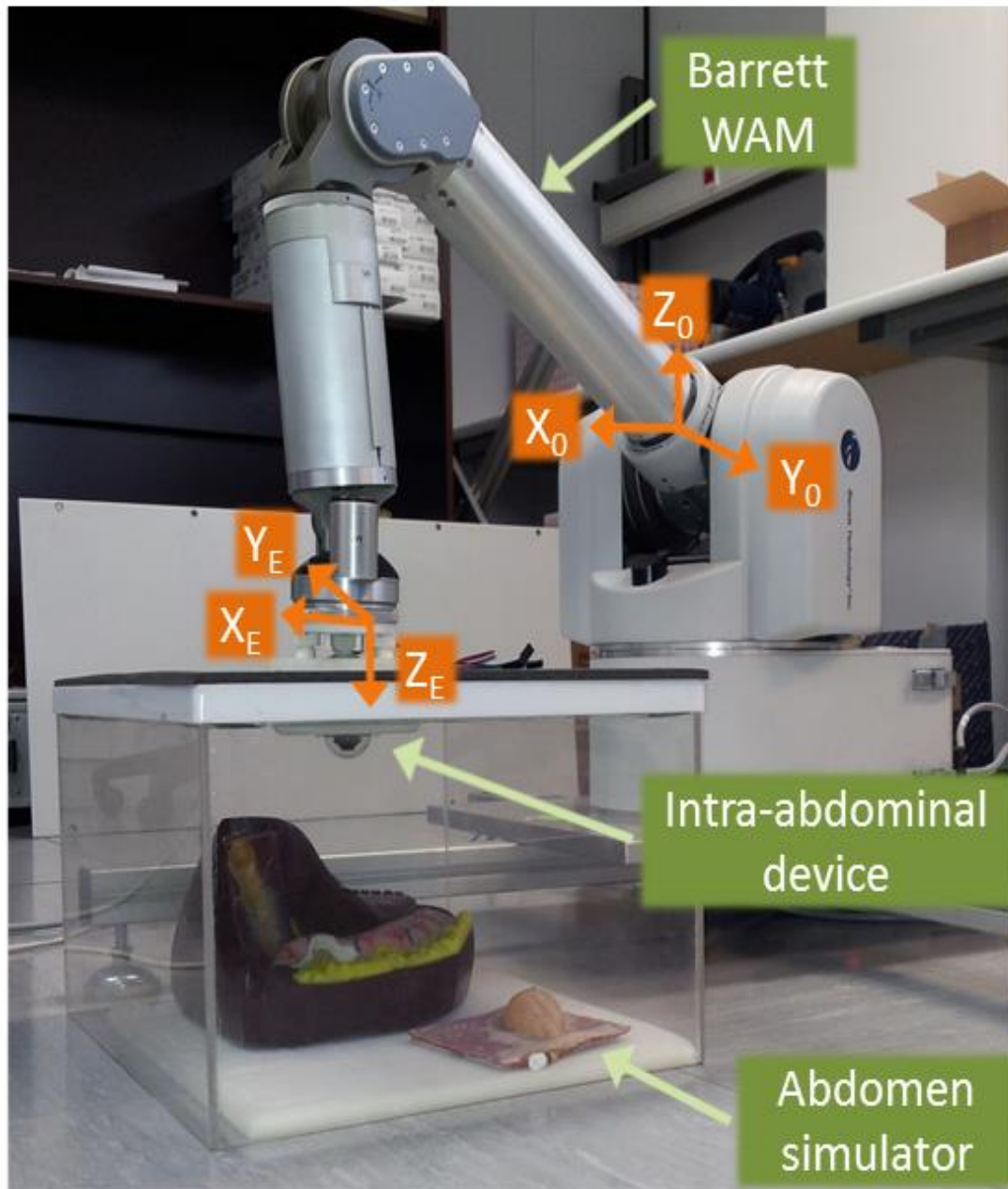


Figure 5.10 Experimental setup for the force-position control validation.

5.4.1 Experimental setup

The experimental setup for the validation of the hybrid force-position control that controls the displacement of the camera along the abdominal wall is shown in Figure 5.10. The patient abdomen is simulated with a methacrylate box, covered with a neoprene layer that emulates an elastic model of the contact surface. The external robot is a Barrett WAM Arm. The reference frame of the robot base, $\{0\}$, and the end effector, $\{E\}$, are also represented in the figure.

5.4.2 Stiffness matrix estimation

Before performing the force-position control validations, the stiffness matrix K_x has to be estimated, using the RLS algorithm described in Section 3.4.1. The experiment for K_x estimation consists in pushing the end effector of the Barrett WAM by hand in order to exert a particular force on the surface. During this process, measures of force and end effector position are measured, and equation (3.25) is applied to estimate the value of the stiffness matrix at every iteration. This process has been repeated three times. Results are shown in Figure 5.11.

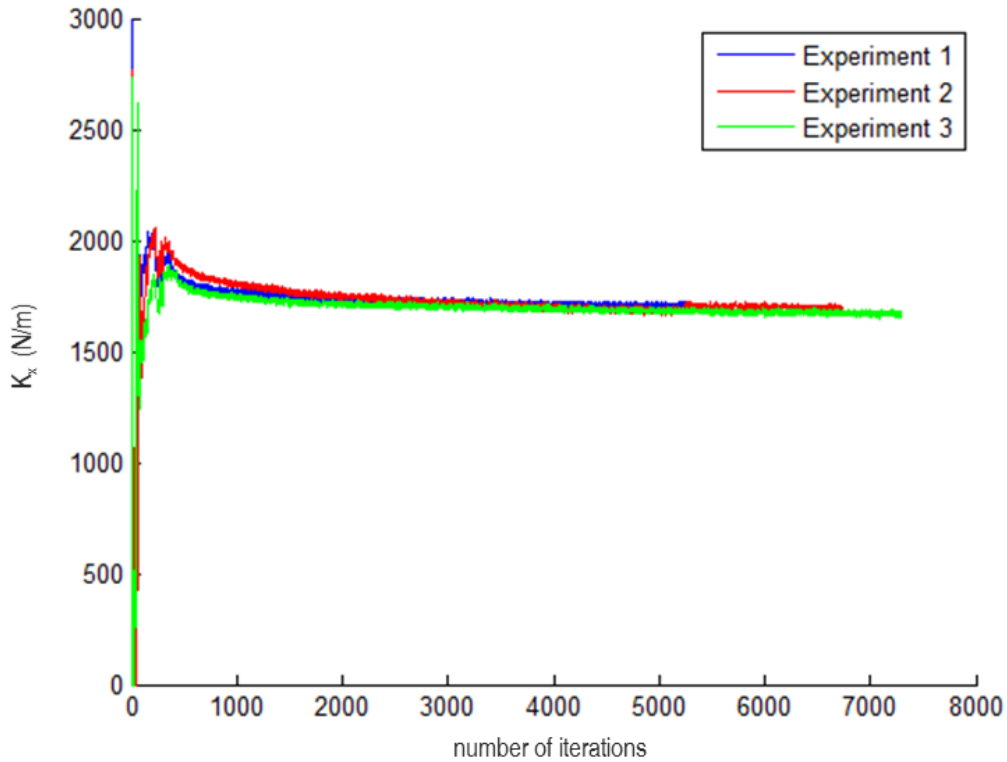
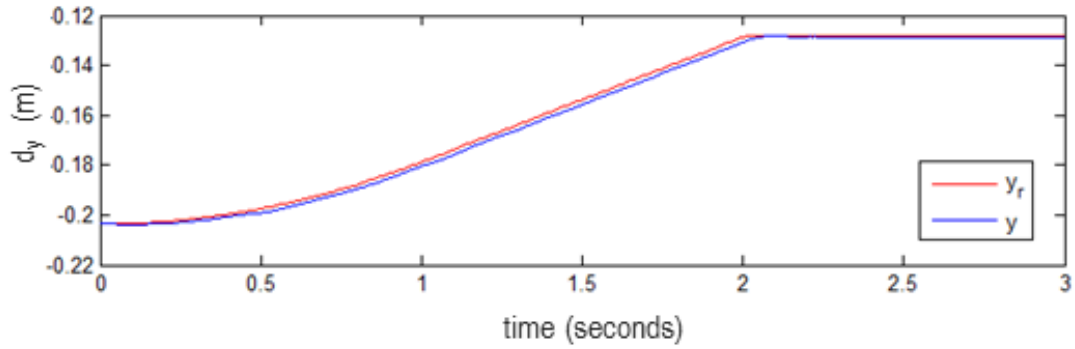
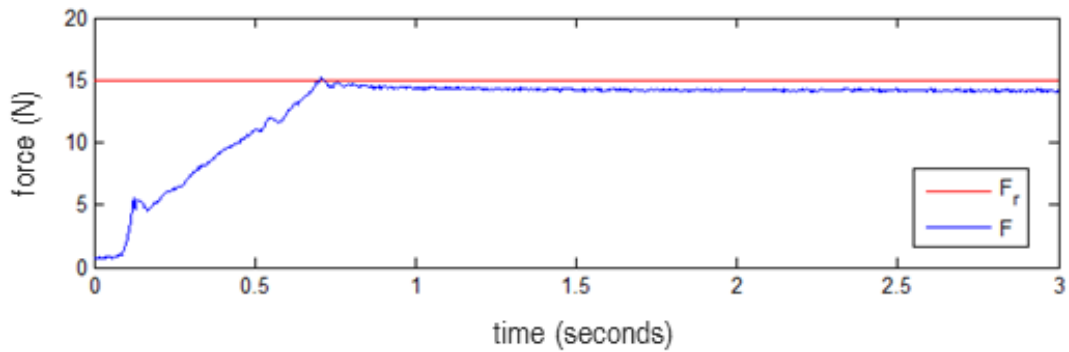


Figure 5.11 Stiffness matrix estimation.

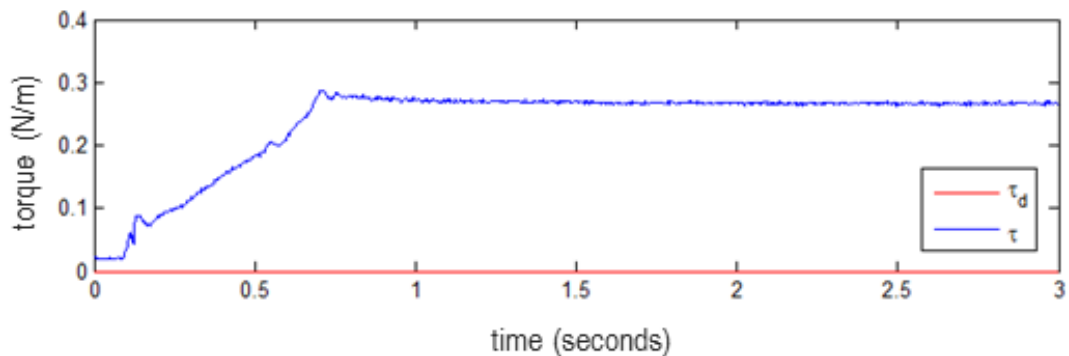
As it can be seen, the stiffness value of the three experiments stabilizes at a constant value of 1727.7 N/m for experiments 1 and 2, and at 1691.5 N/m for the third experiment. High values of the stiffness parameter are due to the high rigidity of the surface. At the beginning of the experiment, a large noise is appreciated until the values begin to converge to a stable value. This is mainly due to the small quantities of position measured due to the high rigidity of the surface.



(a)



(b)



(c)

Figure 5.12 Results of the force-position control experiment: (a) position tracking, (b) force tracking, and (c) torque tracking.

5.4.3 Experimental results

The experiment performed to validate the force-position control consists in displacing the camera robot 75 mm along the y direction, i.e. $d_x = 75$ mm, while exerting a force of 15 N on the surface simulating the abdominal wall. This force value corresponds with a weight of 1.5 kg on the surface, which is a small enough weight to not damage the surface, and high enough to assure magnetic interaction between the external holder and the intra-abdominal device. The system time constant of the first-order behavior imposed on the robot dynamics is $T_\tau = 0.01$ seconds. PI gains in the position controller, computed following Ackerman's methodology for poles assignment, according to equations (3.20) and (3.21), are $K_P = 10.0333$ and $K_I = -5.5167$. And the gain of torque compensation control is $K_\tau = 100$.

Figure 5.12 shows position, force and torque references tracking. Movement along the y direction is done following a trapezoidal velocity profile, with a maximum velocity of 0.05 m/s, to obtain a smooth movement. As it can be observed in Figure 5.12.a, tracking of the position reference is done accurately with a small delay during the transient-state. On the other hand, penetration on the surface is done following a linear profile, as it can be appreciated in the force response in Figure 5.12.b. Force and torque errors are mainly due to the inaccuracies of the force-torque sensor, which has an output resolution of 12 bits, with a noise of 2 bits. Figure 5.12.c shows that torque norm starts with a null value when there is no contact with the surface, and then stabilizes at around 0.3 N/m when force reaches the steady-state at the desired force.

5.5 Smart camera navigation

This section describes the experimental results that validate the smart camera navigation strategy described in Chapter 4. First, the experiment design is described, followed by the experimental results. Finally, results are discussed in detail and conclusions of the experiments are presented.

5.5.1 Experimental task

The aim of the experiments regarding the smart camera navigation strategy is to validate the theoretical concepts described in Chapter 4, i.e. to evaluate the cognitive architecture of Figure 4.1. The experimental task has been designed under the following criteria: task must be as real as possible to be extrapolated to real

surgical environments, but easy enough to be performed by non-expert personnel and to be repeated a significant number of times so that results are reliable. Under these considerations, the experiment is inspired by the first task of the SAGES manual skills in laparoscopic surgery (Choy and Okrainec 2012), peg transfer. This task involves the transfer of six rubber triangular rings across a board with 12 pegs fixed into it. The user would begin by picking up the rings with their non-dominant hand, transfer them to their dominant hand, and then place them onto a peg on the opposite side of the pegboard. The main purpose of this training task is to exercise depth perception in a two-dimensional environment. Thus, it is a suitable task to validate if the navigation strategy proposed in this thesis project helps users to perform the task, as depth perception, and therefore the performance of the task is highly affected by the point of view provided by the camera.

Figure 5.13 shows a snapshot of the task platform. The task is performed over a commercial pegboard from Medical Simulator, with two cylindrical rubber rings (ring 1 and ring 2). Color markers (pink marker, blue marker, orange marker, and green marker) have been used to identify particular areas within the pegboard. The experiment consists in performing a pick and place task with each ring using the robotic graspers of Figure 5.2. The initial setup of the task is as depicted in Figure 5.13, with ring 1 placed on the peg labeled peg 1, and ring 2 onto the peg labeled peg 3. As it can be seen, the original pegboard setup has been slightly modified to increase the depth perception difficulty in order to give even more importance to the camera view and the perspective during the performance of the task. Hence, two metallic hooks have been stuck to peg 3 and peg 4, in order to increase the complexity of the picking and placing tasks. The overall task has been divided into the following six states, where the first three are performed with ring 1 and the following three with ring 2 (Figure 5.14):

- State 1 (picking state): the first state consists of picking ring 1 from peg 1 with the left tool. The state is done when the ring is completely out of the peg. Transition to State 2 is triggered by T_{12} .
- State 2 (transferring state): this state consists of transferring ring 1 from the left tool to the right tool. The state is considered finished when the ring is held by the right tool and the left tool is not in contact with the ring. Transition to State 3 is triggered by T_{23} .
- State 3 (placing state): the last state performed with ring 1 consists of placing it onto peg 4. The state is done when the ring is on peg 4 and the right tool is not touching it. Transition to State 4 is triggered by T_{34} .
- State 4 (picking state): State 4 is a picking state similar to state 1 but in this case ring 2 has to be picked from peg 3 with the right tool. As in State 1, the

state is done when the ring is completely out of the peg. Transition to the next state is triggered by T_{45} .

- State 5 (transferring state): this state consists of transferring the ring from the right tool to the left tool. It is considered finished under the same criteria of State 2. Transition to State 6 is triggered by T_{56} .
- State 6 (placing state): the last state of the task consists of placing ring 2 onto peg 2. After this state is completed the task is considered finished.

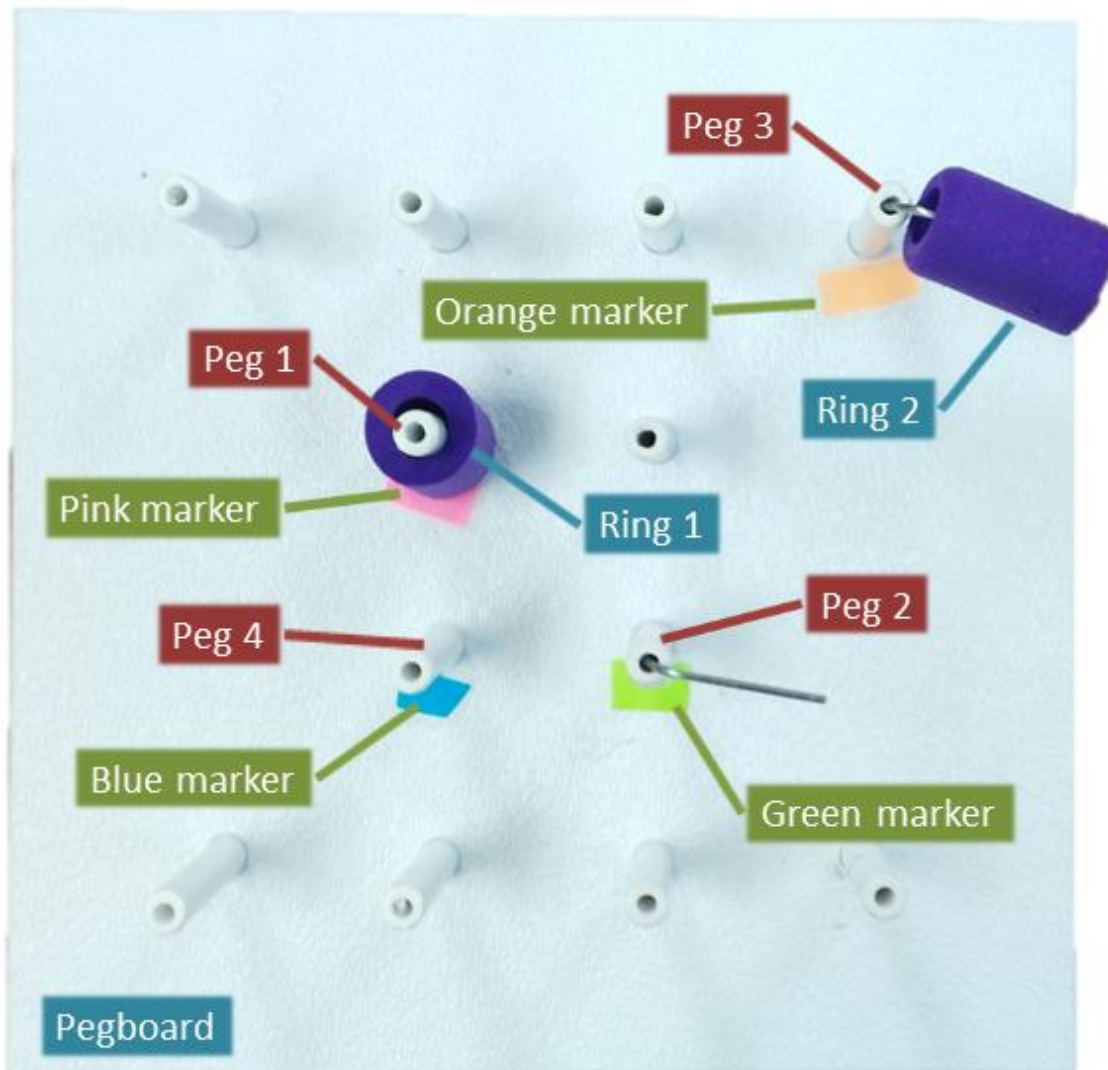


Figure 5.13 Snapshot of the task platform.

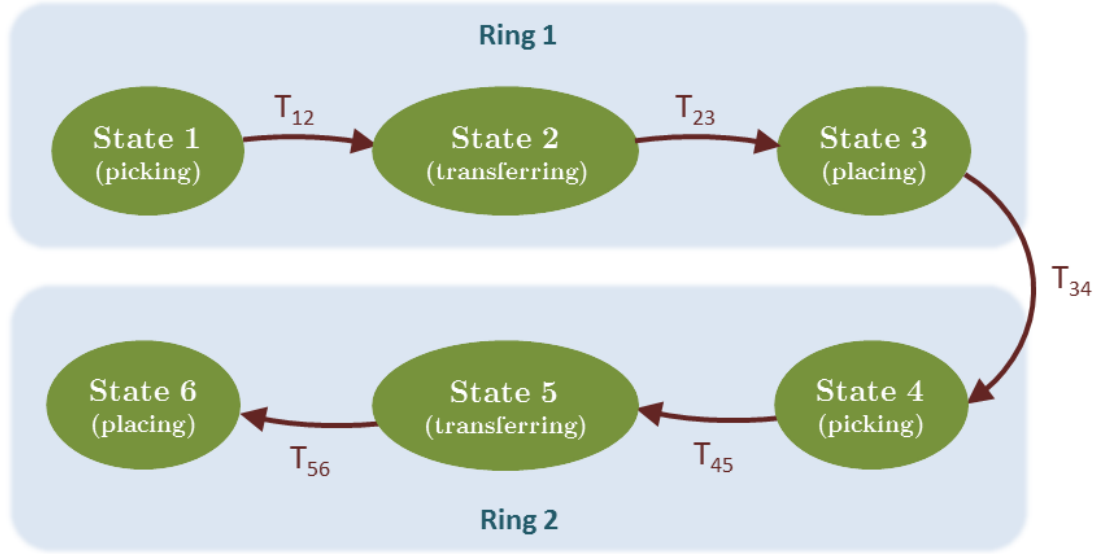


Figure 5.14 State diagram of the overall task.

As described in Section 5.2.3, the surgeon can directly modify the camera view through the HMI depicted in Figure 5.7, by changing the value of the following parameters: external robot displacement, zoom level, roll (α), tilt (β), and pan (φ) rotations. These parameters are changed through discrete steps, resulting in a trade-off between motion accuracy and practical steps that do not imply large commands to perform a motion. Table 5.1 shows the value of the discrete steps of each DoF using the HMI. Displacements of the robots are of 10 mm in each direction, while the zoom level is increased or decreased by 10% when zoomed in or out with the HMI. Finally, the three rotations can be modified using steps of 10 degrees each. Due to constraints on the driven side, roll and tilt range is $\pm 60^\circ$, as the range of the motors is 180° . For both motors, the rest position has been defined at 90° . Thus, for $\theta_1 = 90^\circ$ and $\theta_2 = 90^\circ$, $\alpha = 0^\circ$ and $\beta = 0^\circ$, respectively. Thus, according to equations (3.1) and (3.2), maximum and minimum values of α and β are $\pm 60^\circ$, where $D_1 = D_2 = 8$ mm, $D_3 = 11$ mm, and $D_4 = 12$ mm. On the other hand, pan rotations are performed by rotating the external robot end effector. Hence, the range of pan rotations is $\pm 180^\circ$.

Table 5.1 Discrete steps of the robotic assistant DoFs with the HMI.

DoF	Step
Displacement	10 mm
Zoom	10%
Roll	10°
Tilt	10°
Pan	10°

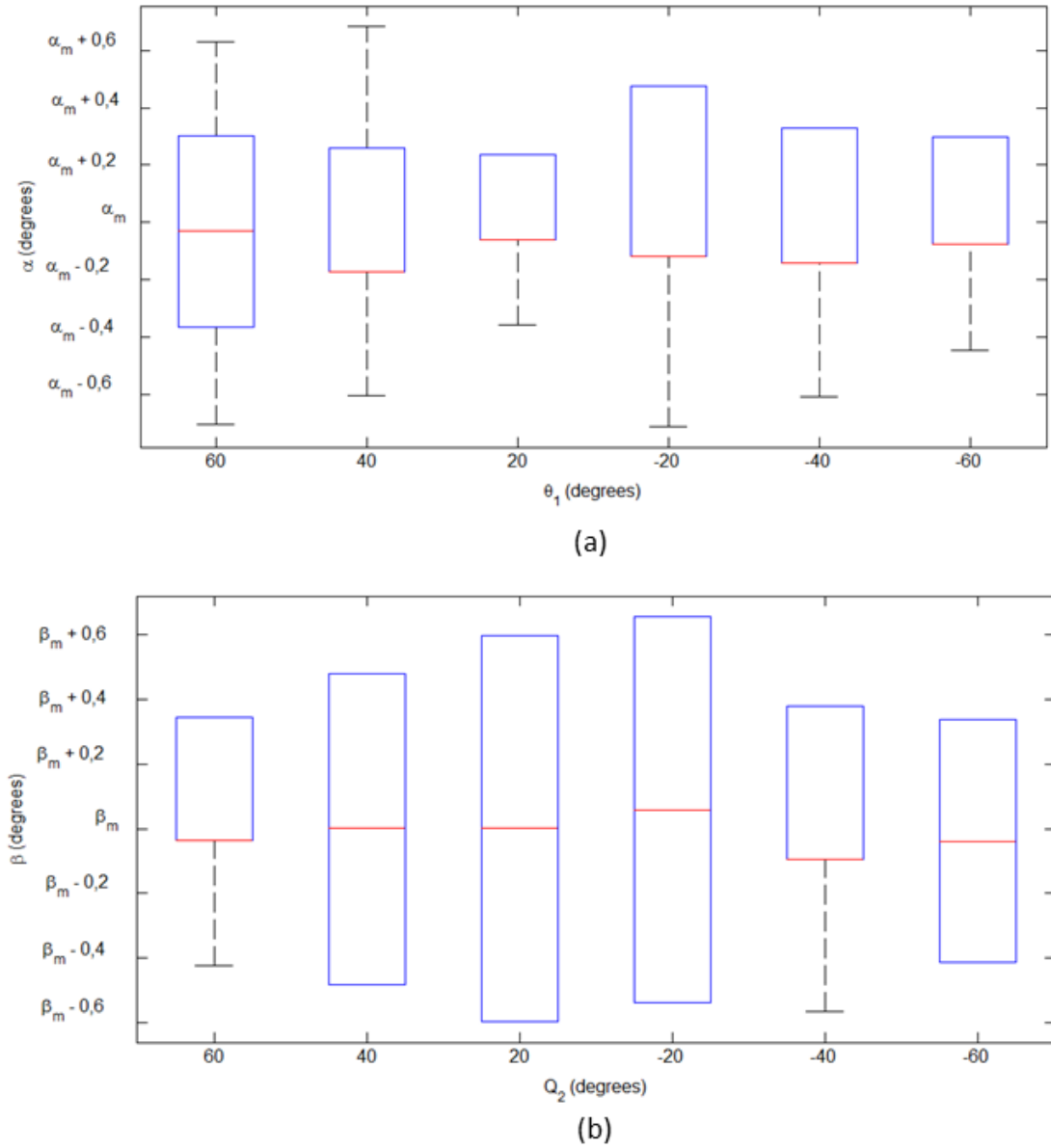


Figure 5.15 Distribution of the experimental data for the analysis of repeatability of cable-driven DoFs: (a) roll; (b) tilt.

5.5.2 Analysis of the cable-driven mechanism

In regards to the performance of the cable-driven DoFs of the intra-abdominal device, control of these roll and tilt rotations is performed in an open loop due to the lack of mechanisms to measure the orientation of the camera in a real environment. Thus, an analysis of repeatability of each DoF has been carried out in order to evaluate the actuation system. For this experiment, motor angles θ_1 and θ_2 have been computed with the following equations, derived from equations (3.1) and (3.2), for each desired value of α and β :

$$\theta_1 = \frac{D_3}{D_1} \alpha \quad (5.1)$$

$$\theta_2 = \frac{D_4}{D_2} \beta \quad (5.2)$$

Six particular positions of the motors 1 and 2, θ_1 and θ_2 , respectively, were chosen, namely $\pm 60^\circ$, $\pm 40^\circ$, and $\pm 20^\circ$. Each of these positions was repeated ten times, measuring α and β for each of them, for motor 1 and 2, respectively. Figure 5.15 shows the distribution of the experimental data for each DoF, where α_m and β_m represent the mean value of α and β , respectively, for each set of data. As it can be appreciated in the figure, the values measured are in the range $[\alpha_m - 0.7, \alpha_m + 0.7]$ and $[\beta_m - 0.6, \beta_m + 0.65]$, for α and β , respectively. Taking into account that maximum values of α and β are ± 30 degrees for both angles, the maximum errors are 2.3% and 2% for α and β , respectively. These are acceptable errors for moving the camera in a surgical intervention, as this task does not require an accuracy as high as is required for other surgical tasks, such as moving the instruments. In fact, for a standard camera height of approximately 10 cm, an error of 0.7° in the orientation of the camera means an error of 1.22 millimeters in the area displayed by the camera, which can be considered a negligible error.

Table 5.2 Knowledge stored in semantic unit S_1 .

M	HSV
M_1	[14, 29, 135, 255, 73, 255, 42, 201]
M_2	[42, 70, 109, 197, 87, 137]
M_3	[152, 179, 51, 194, 171, 255]
M_4	[90, 149, 148, 255, 0, 255]
M_5	[0, 19, 103, 157, 183, 255]
M_6	[90, 101, 200, 255, 130, 218]

5.5.3 Semantic knowledge

This section describes the knowledge stored in the semantic memory, following the formulation presented in Section 4.3. As shown in Figure 4.2, the semantic memory is composed of three semantic units: S_1 , that stores knowledge to identify the different objects of the operating area, S_2 , that stores knowledge about the surgical protocol workflow, and S_3 , that stores knowledge about the camera behavior for each state of the protocol. Table 5.2 shows the knowledge stored in the semantic unit S_1 , where each row contains the HSV coordinates of each color

marker used to perform the experiments. As shown in Figure 5.17, six color markers have been used: one to identify each surgical tool, and another four to identify the significant pegs.

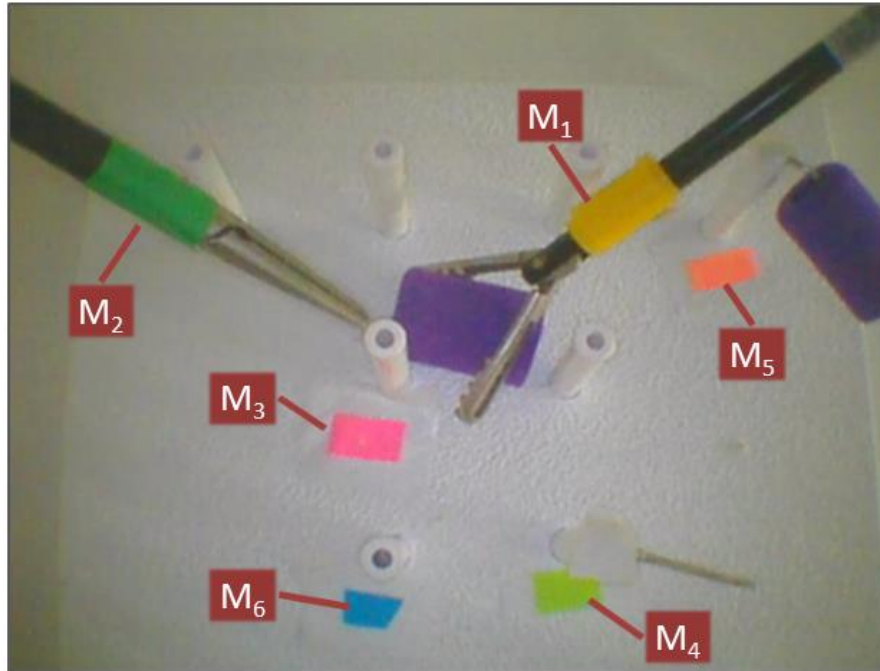


Figure 5.16 Colored markers stored in the semantic memory.

On the other hand, Table 5.3 contains the sequential set of states in which the overall task has been divided, along with the transition triggers to jump from one step to the following, according to the diagram depicted in Figure 5.14. T_{end} represents the trigger that states the end of state 6, and therefore, the completion of the task. Finally, Table 5.4 contains the values of semantic unit S_3 for one of the users that performed the experiment. Figure 5.18 shows a snapshot of the camera view described by Table 5.4 for each state, starting from the initial view depicted in Figure 5.13. As it can be seen, the user has adapted the camera view depending on the task to be performed in every state. Roll rotation allows for a more natural perspective of the working area, which helps the users to tackle the lack of depth perception. Tilt rotation is used in State 3 and State 4 to complement the perspective given by the roll rotation. On the other hand, the pan rotation is not used during the experiment, as the camera is located in a position so that the image horizon results natural for the tool handling. Finally, picking and placing tasks (State 1, State 3, State 4 and State 6) are performed with higher zoom, as the user focuses his or her attention only on the ring that he or she is managing, however, for transferring tasks (State 2 and State 5) zooming is out as the user usually prefers to have an overall view that covers both tools.

Table 5.3 Knowledge stored in semantic unit S_2 .

State	Transition
State 1	T_{12}
State 2	T_{23}
State 3	T_{34}
State 4	T_{45}
State 5	T_{56}
State 6	T_{end}

Table 5.4 Knowledge stored in semantic unit S_3 .

State	M	α	β	ϕ	zoom
State 1	M_3	30°	0°	0°	1.46
State 2	M_3	30°	0°	0°	1.00
State 3	M_4	50°	10°	0°	1.33
State 4	M_5	30°	30°	0°	1.21
State 5	M_6	30°	0°	0°	1.00
State 6	M_6	30°	0°	0°	1.21

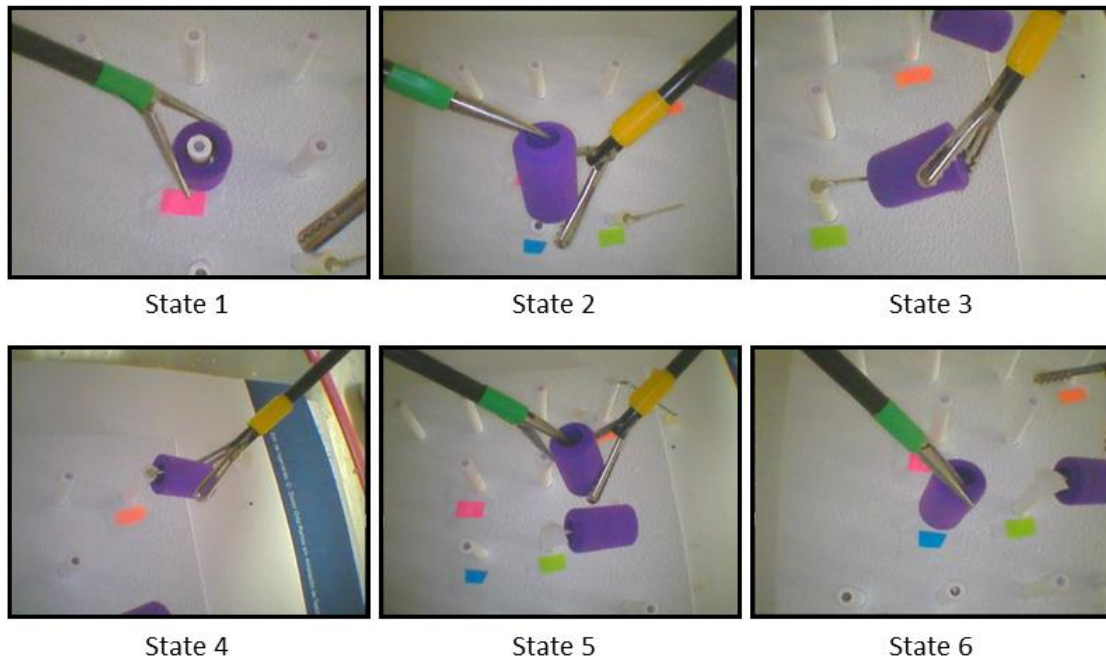


Figure 5.17 Snapshot of the camera view for each state of the task.

5.5.4 Experiment 1: navigation behaviors comparison

This section describes the first experiment of the smart camera navigation strategy, aimed at comparing the different behaviors of the camera robotic assistant. First, the objective of the experiment is stated, followed by the detailed description of the procedure and the variables used to evaluate the results. Finally, the results are exposed and discussed.

5.5.4.1 Objective

As described in Section 4.4, the camera navigation strategy combines two types of behaviors: a reactive behavior, that tracks the surgical tools, and a proactive behavior, that modifies the camera view depending on the current state of the task. Thus, camera position depends on the contribution of each behavior to the global comportment of the robotic assistant, according to equation (4.6), in which the contribution of the reactive and the proactive behaviors are denoted by parameters K_r and K_p , respectively. This approach is based on the hypothesis that combining the advantages of these two behaviors allows the robotic assistant to provide a real autonomous camera navigation that spares the surgeon from having to give direct commands to the assistant, and that provides an efficient camera view that improves the task performance.

The objective of this first experiment is to validate the previous hypothesis by comparing the task performance results using different behavior contribution parameters K_r and K_p in the robotic camera assistant navigation strategy.

5.5.4.2 Procedure

The experiment has been performed by five users with no experience in surgical procedures. Each user has performed a total of 20 trials of the task described in Section 5.5.1. The experiment has been divided into sets of five trials, each of them with a different predefined robotic assistant behavior, as described in Table 5.5. The first five trials are performed with $K_r = 0$ and $K_p = 0$, i.e. camera view is directly controlled by the surgeon, who can change the camera position and orientation using the HMI. The next five trials are performed with $K_r = 1$ and $K_p = 0$, i.e. using a pure reactive control to navigate the camera. In this case, information of the current task state is not taken into account to position the camera. Conversely, the next five trials are performed with $K_r = 0$ and $K_p = 1$, i.e. adapting the camera view for each state only depending on the pre-defined data

stored in semantic unit S_3 . In this case, the camera view is static during the performance of each state. The last five trials are performed with $K_r = 0.5$ and $K_p = 0.5$, i.e. with an equal contribution of the reactive and proactive behavior to the global camera positioning. For simplicity reasons, each pair of values of K_r and K_p has been labeled with an identifying string, shown in Table 5.5. From now on, these labels will be used to name each set of trials.

Table 5.5 Description of the procedure of Experiment 1.

K_r	K_p	# Trials	Label
0	0	5	Manual control
1	0	5	Reactive control
0	1	5	Proactive control
0.5	0.5	5	Dual control

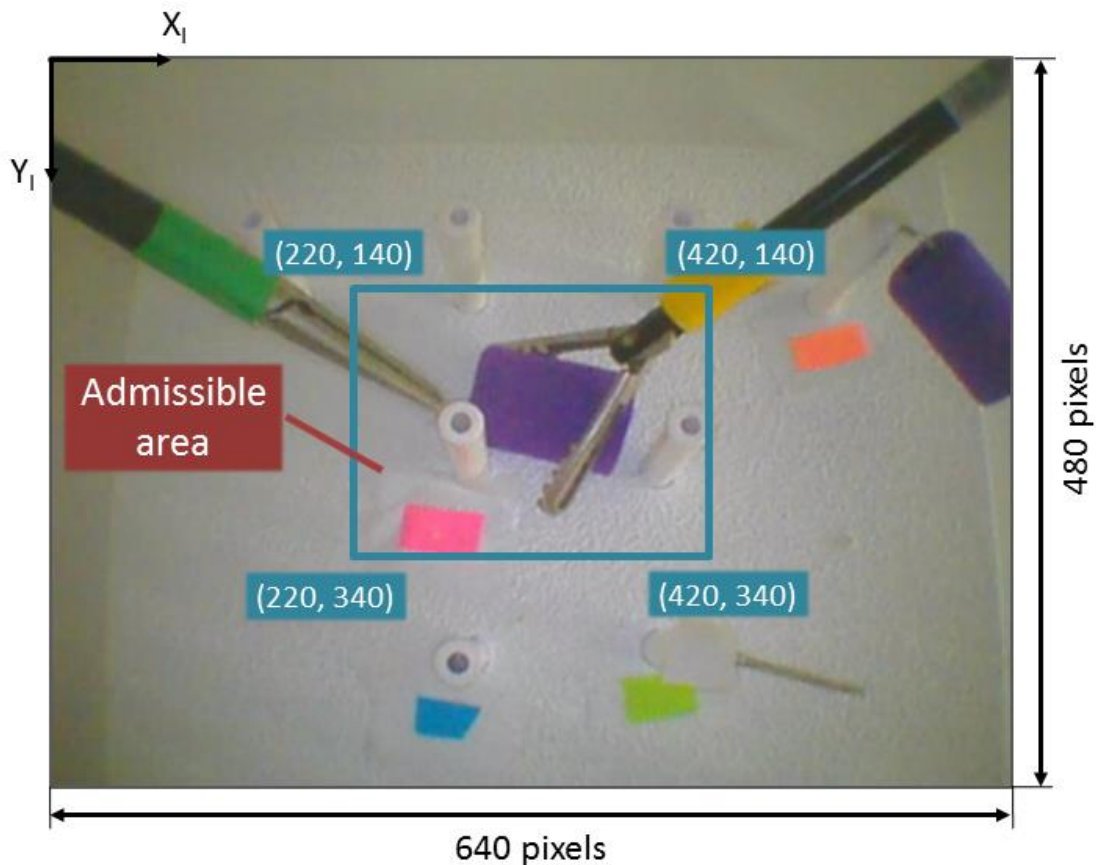


Figure 5.18 Admissible area within no camera displacement is necessary.

To guarantee image stability during the autonomous navigation of the camera, an admissible area has been defined that does not require any camera motion. This area is defined as a 200 x 200 pixels square in the center of the image, as depicted in Figure 5.18. Thus, if the tracking point P_{FoA} is within this area, no camera displacement occurs. Otherwise, equation (4.10) is used to compute camera displacements d_x and d_y . This filtering is necessary to have a stable and smooth motion of the camera. Otherwise, the camera would be continuously moving and it would negatively affect the quality of the image, resulting in a great discomfort for users.

5.5.4.3 Evaluation variables

Evaluation of the experimental results is done using two variables that allow an objective evaluation of the user performance:

- NoCommands: number of commands used by the users to correct the camera view during the performance of each state.
- Time: time spent in completing each state.

The number of commands is the most significant variable, as it gives a clear idea about the efficiency of the camera view provided by the robotic assistant. The higher the number of commands, the less efficient the navigation strategy, and vice versa. On the other hand, time is affected more by external factors but is also relevant to analyze the navigation strategy, as the more efficient it is, the more natural the camera view would be and the less time the user would spend performing the task.

In an attempt to isolate these variables to external factors, such as the users' skills in managing the teleoperating system and performing the task, each user has spent a training period before the experiment. The goal of this training was trying to minimize the influence of the number of trials, i.e. if the user is not skilled with the task, he/she would have a better performance in the last trial than in the first one independently of the camera behavior. However, if the user already skillfully performs the task, camera view would be the only factor affecting the performance of different trials.

5.5.4.4 Results

Figure 5.19 shows the experimental mean performance time and the mean number of corrections of the five users for each state of the task. It can be observed how both the time and the number of corrections are higher for manual control, decrease for reactive and proactive control, and result in the lowest values for dual control. These results demonstrate the efficacy of combining a reactive and a proactive behavior in the camera navigation strategy. Moreover, in such cases, the number of corrections is reduced to 0, allowing the user to concentrate on the important surgical task.

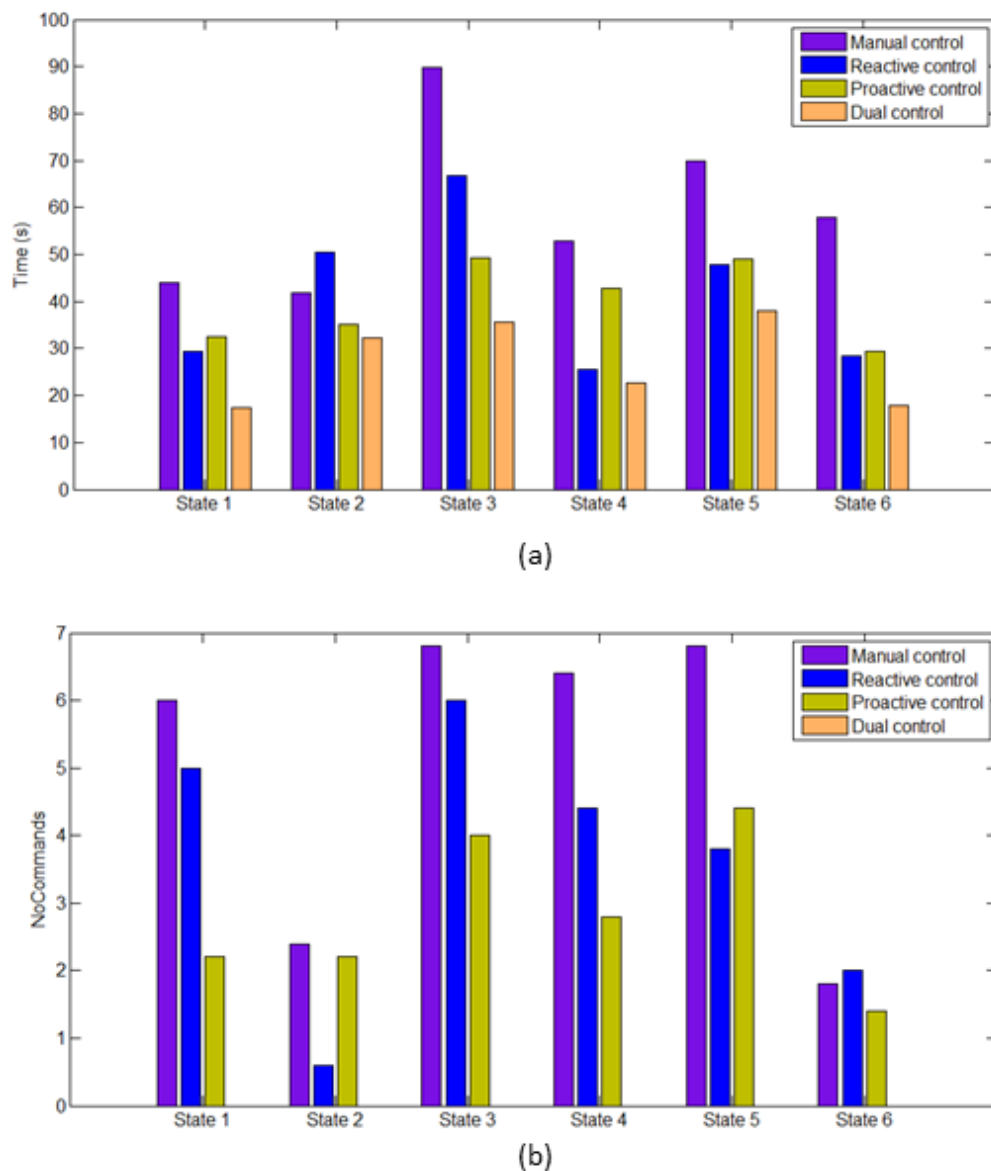


Figure 5.19 Results of Experiment 1: (a) mean performance time; (b) mean number of corrections.

On the other hand, an in-depth analysis of every state reveals that reactive and proactive control strategies are more useful depending on the task being performed. Picking and placing states, i.e. states 1, 3, 4 and 6, are performed with lower camera corrections using the proactive control, as these states are performed around a particular area and tools usually do not leave the camera field of view. However, in transferring states (2 and 5), both tools are interacting and may not always be moving around the same area, so a more reactive behavior results more comfortable for users. For example, ring transfer may be done around the picking peg or around the placing peg. Moreover, during the ring transfer it may happen that the object falls. This situation is not contemplated by the proactive control, but the reactive control will follow the tools to pick up the ring again. Such an unexpected situation will be further analyzed below. Hence, in these states, the reactive contribution is more critical than the proactive contribution. The performance time is less significant to compare the different control strategies as it is more affected by the user ability and the state difficulty. However, the tendency is similar than for the number of corrections.

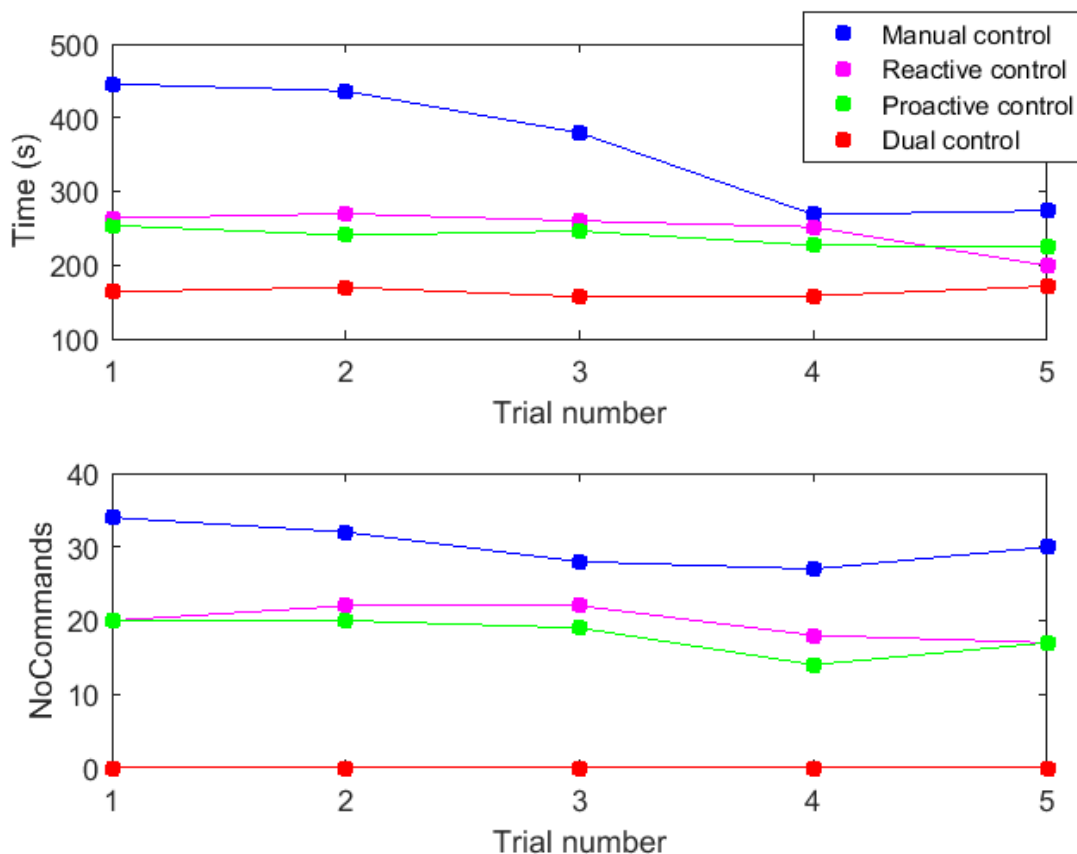


Figure 5.20 Comparison of the performance of a particular user during the five trials: time (up) and number of commands (down).

Figure 5.20 shows the total time spent in performing the overall task and the total number of commands of a particular user. The graphs show the evolution of the task performance during the different trials and provide a graphical comparison of the different behaviors during the overall task, instead of by states, as done in Figure 5.19. The graphs reveal the effect of the training in the performance of the task. Although users had spent a previous training period to get skilled with the system and the task, it can be appreciated how, in manual control, the overall time highly decreases in the last trials. This occurs because manual control is the first set of trials the users perform. This effect is no longer observed for the remaining set of trials with reactive, proactive and dual control, in which a similar performance is observed for the five trials. However, it is clear that the overall performance is much better for dual control than for the rest of the types of control, as both evaluation variables get the lowest values. Despite the effect of training, manual control shows the worst performance values, and reactive and proactive controls present similar results.

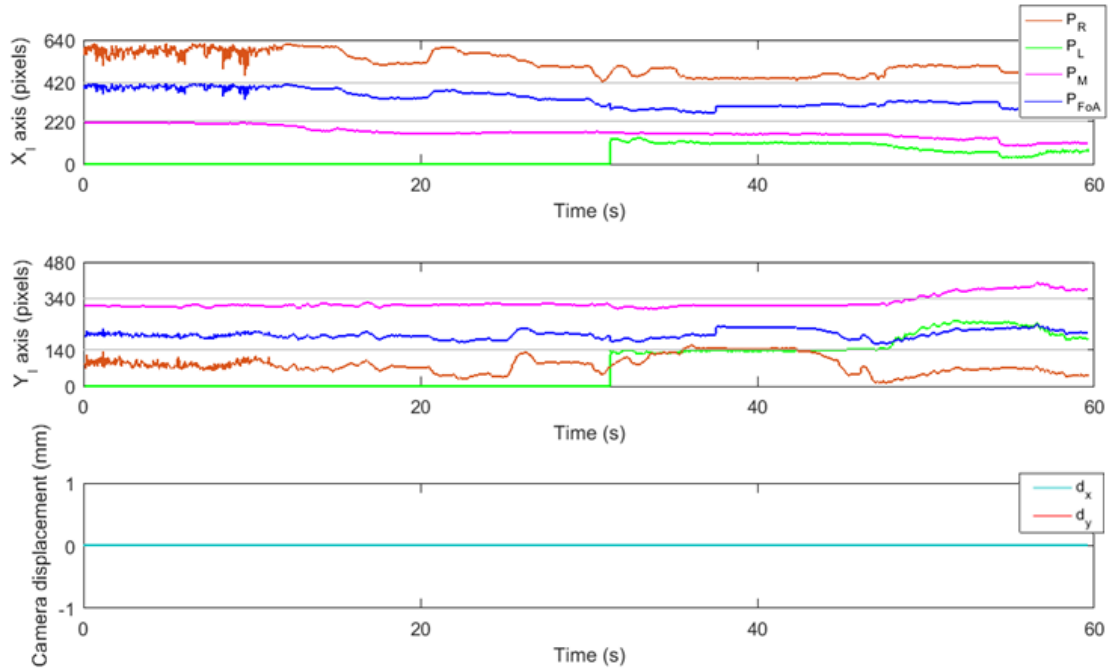


Figure 5.21 Marker tracking and camera displacement in State 2 in a normal situation.

Figure 5.21 shows a low-level analysis of the robot behavior during one of the trials of State 2. In particular, it shows the marker tracking in the X_I and Y_I axis, and the corresponding camera displacements d_x and d_y. During State 2, the vision algorithm of the perception system tracks the position of the right and left tool, P_R and P_L, respectively, and the position of marker M₃ (P_M) as stored in the semantic

unit S_2 (Table 5.3). Then, the tracking point P_{FoA} is computed following equation (4.6). As it can be observed in Figure 5.21, at the beginning of the state, the left tool remains still while the right tool approaches it ($P_L = 0$ means the tool is not moving, as δ_L of equation (4.5) is null). Then both tools slightly move during the ring transfer. During this entire process, P_{FoA} remains within the admissible area defined in Figure 5.18, so no camera displacement is required during the state.

On the other hand, Figure 5.22 shows the same data, also during State 2, but in this case, an unexpected situation occurs during the state performance. The state begins as in the previous case, with the right tool approaching the left tool. In this case, a slight camera movement is required to get P_{FoA} in the admissible area. Then, something unexpected occurs: the rubber ring is dropped during the transfer, and it goes out of the camera view. Thus, the user starts moving the left tool in the direction the object fell, and the camera moves to keep it within the field of view. As it can be appreciated, while the ring is being picked back up, which occurs approximately during seconds 40 and 100, the left tool stays on the left side of the image, while marker M_3 remains on the right side of the image, which keeps P_{FoA} more or less in the center of the image. Once the ring is picked back up, both tools perform the ring transfer.

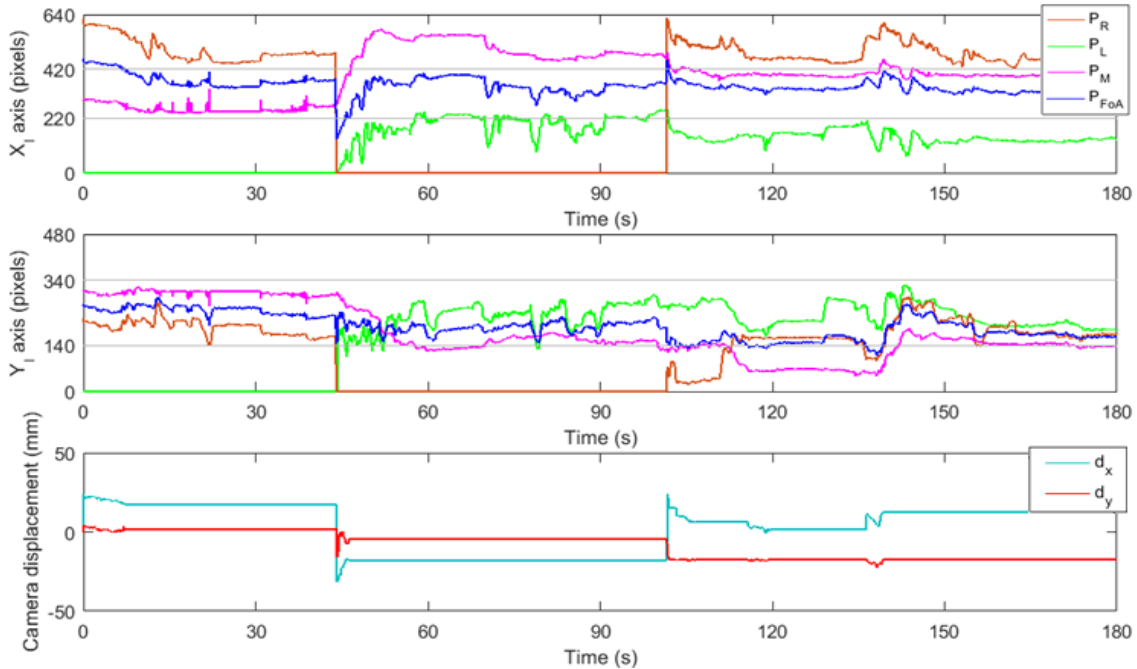


Figure 5.22 Marker tracking and camera displacement in State 2 during an unexpected situation.

5.5.4.5 Discussion

This experiment has evaluated the different behaviors of the robotic camera assistant in order to analyze the benefits of combining a reactive control that tracks the surgical tools with a proactive control that adapts the camera view to the conditions of each state. Results show that user performance is better when the navigation strategy combines both behaviors than when each behavior is isolated. Both the performance time and the number of corrections are lower in such a case. In particular, the number of corrections are reduced to zero, meaning that the user can concentrate on the surgical task instead of having to continuously give commands to the robotic assistant. Furthermore, results show that the desirable contribution of each control strategy depends on the task being performed, and therefore, should be made dependent on the current state.

Moreover, an unexpected situation in which the rubber ring is dropped during the transfer has been analyzed. Results have shown that by combining both reactive and proactive control strategies, the system is able to react to such a situation, adapting the camera view without requiring direct control of the user. With a purely reactive behavior, the camera would have followed the left tool and would have lost sight of the marker. So, after the transfer, the user would have had to command the camera to move back towards the placing peg. Conversely, with a purely proactive behavior, the camera would not have followed the tool during the recovery of the ring, also requiring direct commands from the user to follow the tool. However, the combination of both control behaviors has made it possible to overcome such an unexpected situation. Thus, a real autonomous camera navigation that overcomes the limitations of isolated reactive and proactive control approaches has been demonstrated.

5.5.5 Experiment 2: learning evaluation

This section describes the second experiment in regards to the camera navigation strategy, which is aimed at evaluating the reinforcement learning mechanism of the cognitive agent. Organization of this section follows the same structure as the previous one.

5.5.5.1 Objective

The previous experiment has revealed that the contribution of reactive and proactive control strategies, K_r and K_p , respectively, should be made dependent on

the current state. As stated in Section 4.5, the reinforcement learning algorithm implemented in the cognitive architecture chooses, for each state of the task, the values of K_r and K_p that maximize the system reward. Thus, the goal of this experiment is to analyze if the camera robotic assistant is able to learn the customized values of parameters K_r and K_p that most satisfy each user.

5.5.5.2 Procedure

This experiment has been performed by the same five users of the previous one. In this case, each user has performed 15 trials of the task. Contribution of each control strategy is initialized at $K_r = 0.5$ and $K_p = 0.5$. Then, for each trial, the learning mechanism chooses new contribution values according to the reinforcement algorithm. The algorithm has been designed with the following parameters: a learning rate (ρ) of 0.3, to consider past knowledge acquired but allowing the addition of new information, and a discount factor (μ) of 0.9, that makes the system strive for a long-term reward. In regards to the policy to choose the following action, a value of $\epsilon = 0.4$ is used for the first ten trials, to allow exploration of new actions, while the last five trials are performed with $\epsilon = 0.2$, to facilitate the convergence of K_r and K_p . In a surgical scenario, environmental conditions may randomly change from one intervention to another. Thus, long-term learning should prevail over the most recent information. Hence, the value of τ has been chosen so that old information prevails over new knowledge, and the value of μ makes the system strive for a long-term reward. Conversely, values of τ approaching 1 would make the system consider only the most recent information, and values of μ approaching 0 would consider only the current rewards. Moreover, the value of ϵ determines the learning speed of the algorithm. While a smaller value of ϵ favors the exploration of new rules, higher ϵ values favors the convergence of the algorithm.

5.5.5.3 Evaluation variables

Evaluation of the learning mechanism is done with the following variables:

- K_r and K_p : contribution of the reactive and the proactive behavior, respectively, to the global navigation strategy. These parameters are essential in the learning mechanism, as computation of its value is precisely the final aim of the reinforcement learning algorithm.
- Reward: the reward is computed with the fuzzy model described in Section 4.5. Negative reward values mean that the user is penalizing the camera

behavior. Thus, in this case, the system would not be learning the appropriate control strategy. Conversely, positive reward values mean that the user is satisfied with the camera behavior. Therefore, the objective of the reinforcement learning mechanism is to output the contribution parameters that provide a positive reward to the system. Moreover, the convergence of the reward value is important to provide a stable robotic assistant behavior. The reward ranges from -10 to 10, where -10 is the highest penalization the system may obtain, and 10 is the highest reward.

5.5.5.4 Results

Figure 5.23 shows the customized values of K_r for each user (please note that $K_p = 1 - K_r$), defined as the mode of the results of the 15 trials. As it can be seen, states 1, 3, 4 and 6 have K_r values lower or equal to 0.5, as for this states, users appreciate the proactive control contribution over the reactive one. Conversely, states 2 and 5 have K_r values closer to 1, as for these states, users feel more comfortable with the camera tracking the surgical tools. It can be appreciated that the value of K_r is slightly different among users. This is because of the particular preferences of each user, and because of the influence of the initial values of K_r output by the algorithm, as when a particular value has a positive reward, it is more likely to be chosen again. These values of K_r will be used by the procedural memory to set the global focus of attention during the normal performance of the system.

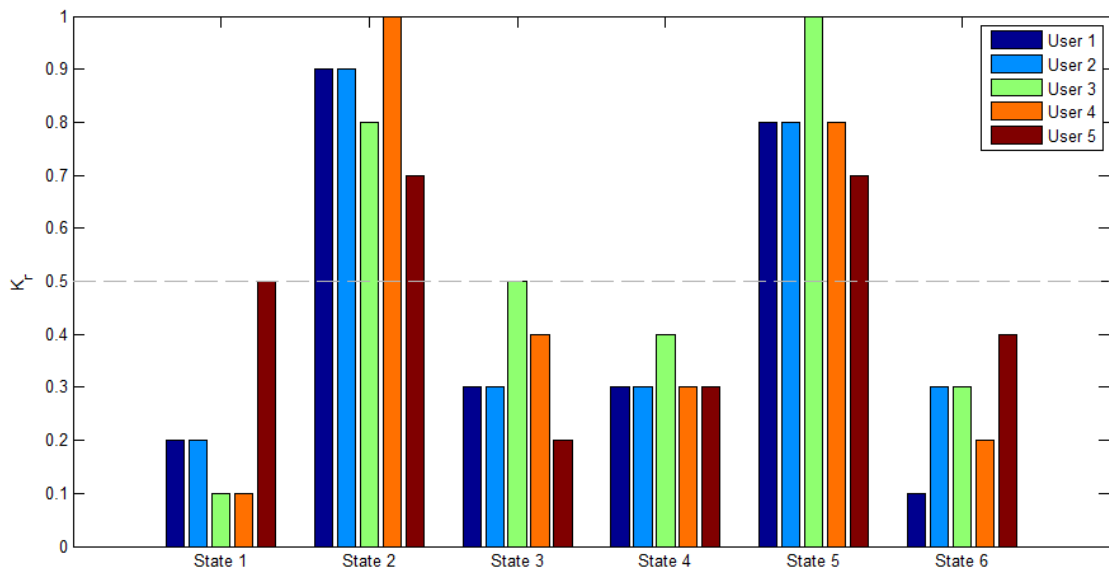


Figure 5.23 Customized values for K_r for each user and each state.

Figure 5.24 shows the frequency of the customized values of K_r for each user (the mean of the six states is represented). The purpose of this figure is to show the evolution of the election of the final customized value of K_r during the learning period. The red bar represents the global frequencies for the 15 trials, which are 64.4%, 61.1%, 70%, 58.9%, and 67.8% for Users 1 to 5, respectively. The other three bars represent the evolution of the data during the 15 trials. As can be seen from the figure, during the first five trials, the frequency of the customized value of K_r is lower and, as the system learns, the frequency increases, reaching the maximum for the last five trials.

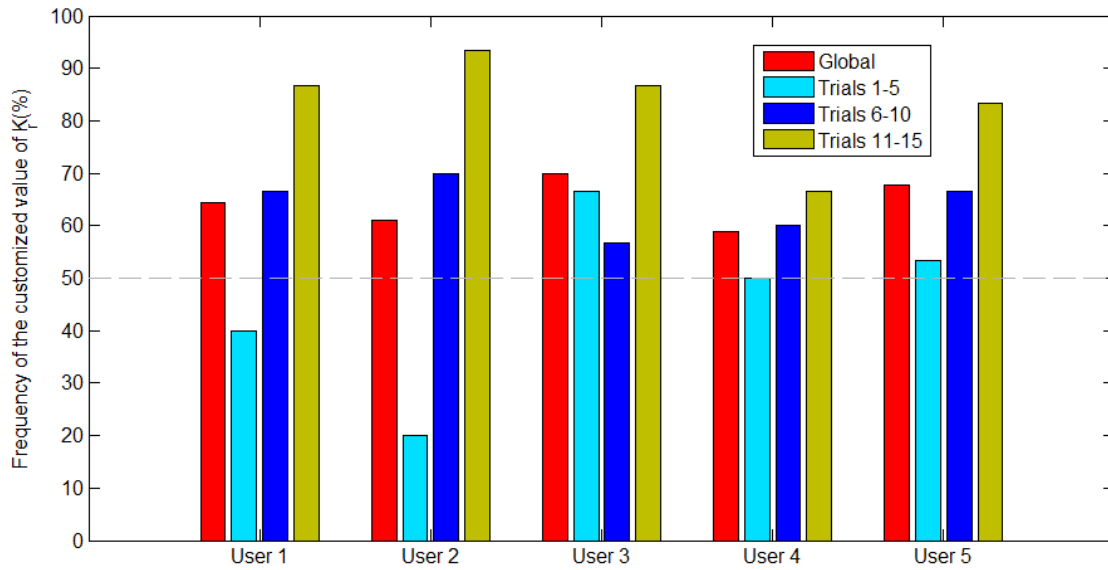


Figure 5.24 Frequency of the customized value for the 15 trials performed by each user.

Figure 5.25 shows the particular results for State 4 of User 4, with the value of K_r and the associated reward of each of them represented in blue and yellow, respectively (this is a representative case, but results of other states and users are similar). As can be seen in Figure 5.23, the customized value for User 4 and State 4 is $K_r = 0.3$. Figure 5.25 shows how this value has a higher reward than the other values of K_r . According to equation (4.14), a rule with a high reward has a higher utility value; thus the value of K_r associated with this rule is more likely to be chosen in following trials. This fact can be appreciated in the figure, as the most rewarded value, $K_r = 0.3$, is the most output value by the learning algorithm in the set of trials. However, owing to the reinforcement learning nature, even within the last five trials, new action exploration is presented. This is why the algorithm chose a random value of K_r in Trial 13, which in this case is 0.1. However, the user penalizes this value with a negative reward; therefore this value is highly unlikely to appear again.

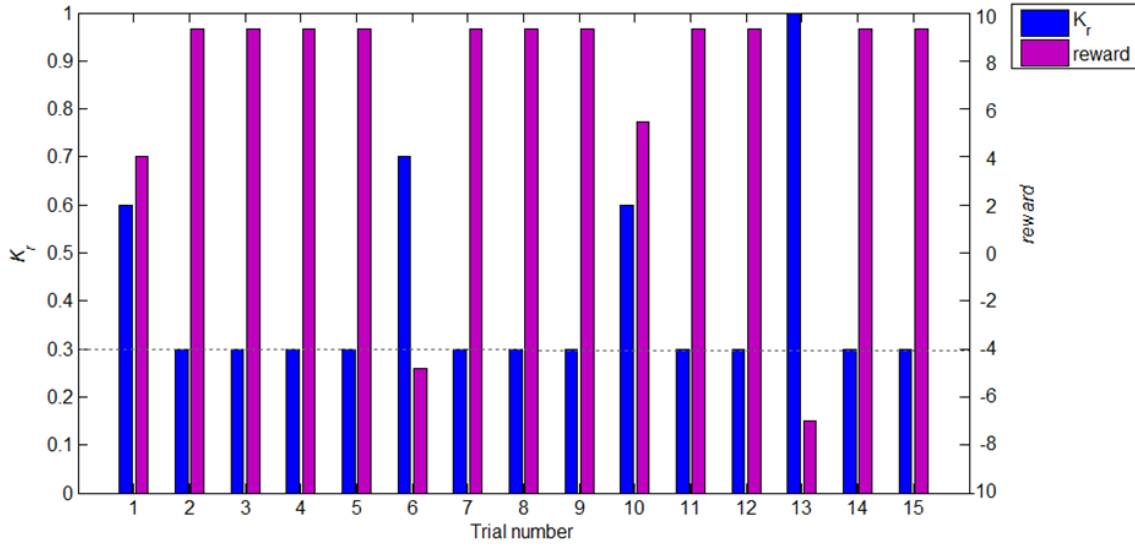


Figure 5.25 Reinforcement learning algorithm analysis for State 4 of User 4: K_r and reward for each trial of the experiment.

5.5.5.5 Discussion

The reinforcement learning algorithm makes it possible to adapt the contribution of each kind of control to the global behavior of the robot for each state, and for each particular user. Otherwise, predefined values would have to be used. As it was expected, the customized values of K_r and K_p are highly related to the nature of the task to be performed during each state: those states that are performed mostly around a particular area have higher values of K_p , while tasks that require large motion of the tools are better performed with a higher contribution of the reactive control.

Analyzing the results of the experiments, we can observe that, with the values chosen for parameters τ , μ and ε of equation 4.14, the speed of the learning algorithm prevails over its accuracy. Higher values of ε will make the algorithm less dependent on initial values, but appreciably slower. For the particular application of moving the camera in a laparoscopic procedure, a high accuracy of the customized values of K_r and K_p is not crucial, as similar values of these parameters will provide similar behaviors of the camera. However, it is important that the system is able to provide a comfortable camera view with a short learning period.

5.6 Conclusion

This chapter has presented the implementation of the theoretical concepts described in this thesis project, and its validation through a set of in-vivo and in-vitro experiments. First, the experimental setup is described, along with the hardware architecture that allows the connection of the different robots and devices used for the experiments. The software implementation of the system has been performed in a ROS network, which allows easy communication between the different elements of the system. Moreover, ROS networks allow testing every system component individually before the global integration, which results very practical in complex systems structures as the experimental setup described in this chapter. Furthermore, implementation in a ROS structure makes it possible to easily add new components to the system, and to export the concepts implemented in this work into another system or experimental setup. For example, the Barrett WAM could be effortlessly substituted by another external robot, as well as the CISOBOT platform, while concepts validated in this work could be integrated into a Da Vinci platform by substituting the nodes that manage the WAM Arm and the CISOBOT with a Da Vinci node.

The camera robot has been tested in an in-vivo experiment in a pig. This experiment has demonstrated the feasibility of substituting the conventional endoscope with a camera robot in a real surgical environment. Magnetic interaction has been proven safe and efficient, and image quality good enough to perform surgical tasks. The experiment also reveals that the camera robot does not mist up as conventional endoscopes do, avoiding the annoying constant cleaning of the camera. Furthermore, the camera robot provides different camera views and organ perspectives than a conventional endoscope, which results more natural and intuitive for surgeons, as the image comes from above as in a conventional open surgery. Thus, the camera robot can be used as the single vision source in a laparoscopic procedure, or it could also be used as a support camera view to get access to unreachable areas for the endoscope. This approach could augment the possibilities of laparoscopic surgery to procedures that currently can only be performed by open surgery.

The in-vitro experiments have validated the force-position control to displace the external robot along the abdominal wall and the smart camera navigation strategy. Experiments have demonstrated that combining a reactive and a proactive behavior results in a flexible and autonomous navigation, that does not require direct control of the surgeon, and that provides an efficient camera view able to help surgeons during the performance of surgical tasks. It has also been demonstrated that with the navigation strategy proposed in this work, the camera

robotic assistant is able to successfully overcome unexpected situations, similar to the way a human assistant would react. Finally, it has been validated that the learning mechanism allows the system to improve its behavior and adapt the camera view according to different surgeons' particular preferences and ways of working.

6 CONCLUSION AND FUTURE WORK

6.1 Conclusion

Laparoscopic surgery has become a widely accepted technique all over the world that provides many benefits for patients. However, it is still a more challenging technique for surgeons compared to conventional open surgery that largely limits the number of interventions that can be performed with this technique. The main challenges of laparoscopic procedures can be divided into visual and manipulation limitations. The only visual feedback surgeons have of the operating area comes from the image provided by an endoscope. Unlike vision in open surgery, these devices offer a planar and shadowless image of the anatomical structures, which considerably hinders the execution of surgical tasks. On the other hand, instrument manipulation in laparoscopic interventions is much more complex than operating in an open procedure. As instruments are manipulated through small incisions, the entry ports restrict the motion of the tools. Thus, instrument manipulation suffers from a loss of DoF that hinders not only the surgeons' dexterity but also the access to certain areas within the abdominal cavity.

Surgical robots have made an important contribution to the progress of laparoscopic surgery, as robotic systems such as the da Vinci (Haidegger, Sándor, and Benyó 2011) greatly facilitate the work of the physicians providing tremor filtering, improved dexterity, ability to scale motions, ergonomic position, better visualization, etc. (Lanfranco et al. 2004). In regards to vision, robotic camera assistants such as the EndoAssist (Gilbert 2009) or the AESOP (Kraft et al. 2004)

allow surgeons to operate without the need for an additional assistant that handles the endoscope during the intervention and offer advantages such as more image stability than human endoscope holding. However, current camera robotic assistants require constant monitoring and control by the surgeon, who has to release the surgical instruments to move the camera or may be distracted by commanding the robot for specific camera motions. Many researchers have focused their efforts on designing autonomous robots that navigate the camera without direct control from the surgeon. However, current navigation methods lack the intelligence and awareness to be considered autonomous, as they are based on very rigid and predefined behaviors (Pandya et al. 2014).

In this sense, this thesis project proposes a novel concept of a smart camera robotic assistant that augments the vision capabilities in laparoscopic procedures and provides a real autonomous camera navigation based on a cognitive architecture. The camera robotic assistant is composed of a camera robot magnetically controlled from the outside by an external robot. Placing the vision source in an intra-abdominal device enhances the field of view compared to conventional endoscopes, as camera motion is not restricted by the entry port. Besides the narrow field of view surgeons have to operate through, laparoscopic images suffer from a reduced perspective of the anatomical structures, as camera orientation is limited by the position of the entry port in the abdomen. The two internal DoFs of the camera robot make it possible to easily change the perspective from which a particular area is seen, which along with the enhanced field of view, opens the doors to procedures that currently are only performed through open surgery. The cable-driven actuation system avoids the need for incorporating motors to the device, which would augment both the size and the weight of the device. The experimental prototype of the intra-abdominal device has been tested in an in-vivo experiment in a pig. This experiment validated the insertion procedure in the abdominal cavity and the magnetic interaction approach to attach the device to the abdominal wall and to displace it along the surface without causing any harm to the patient. Moreover, the quality of the image has proven to be good enough to perform real surgical tasks.

Previous research works in intra-abdominal devices for surgical applications employ manual guidance of the external magnetic holders, thus requiring direct human control, from the surgeon or an additional assistant. This work proposes to attach the external holder to a robotic arm in order to be able to perform autonomous navigation of the intra-abdominal device. A cognitive architecture has been implemented in order to provide real autonomous camera navigation. On the one hand, the semantic memory stores the declarative knowledge of the system, essential for reasoning and making decisions. While on the other hand, the rules that govern the camera navigation strategy are stored in the procedural memory of

the system. Camera navigation has been improved in respect to previous work in the literature by combining a reactive behavior that tracks the surgical tools with a proactive behavior that adapts the camera view to the surgery workflow. Thus, navigation follows a more flexible algorithm that allows the robot to adapt to different ways of working and to react to unforeseen situations. The cognitive system includes two learning mechanisms: a semantic learning algorithm that allows the system to add new knowledge to the current knowledge base, and a reinforcement learning algorithm that learns the contribution of reactive and proactive behaviors to the global robot performance that is best suited for each state of the task and for each particular surgeon. Learning capabilities are essential for a real cognitive agent, and as far as the author's knowledge, no previous work has contemplated including learning techniques in camera navigation strategies.

The action system of the robotic assistant includes a hybrid force-position control with torque compensation for the displacement of the robot along the abdominal wall. Torque compensation ensures that the end effector of the external robot remains parallel to the contact surface. This is essential to ensure magnetic interaction between the external holder and the intra-abdominal device and also to ensure a safe and soft displacement of both devices along the abdominal wall. For the force controller, an elastic interaction model between the robot and the surface has been assumed, in which the stiffness matrix is estimated with a RLS algorithm that updates the value of K_x with new measures taken during the normal working of the robotic assistant.

A set of in-vitro experiments have been performed to validate the theoretical concepts proposed in this work. The experiments have demonstrated that combining a reactive and a proactive behavior results in a flexible and autonomous navigation, that does not require direct control of the surgeon, and that provides an efficient camera view able to help the surgeon during the performance of surgical tasks. It has also been demonstrated that with the navigation strategy proposed in this work, the camera robotic assistant is able to successfully overcome unexpected situations, similarly to how a human assistant would react. Finally, it has been validated that the learning mechanism allows the system to improve its behavior and to adapt the camera view according to different surgeons' particular preferences and ways of working.

Summarizing, this thesis project proposes a smart camera robotic assistant that enhances the camera view in laparoscopic procedures and provides an autonomous camera navigation similar to the collaboration between the surgeon and a human assistant. The main goal of this achievement is to decrease the workload of surgeons during laparoscopic interventions and avoid the need for additional medical staff in charge of handling the camera.

6.2 Future work

The work presented in this thesis could be expanded with the following contributions:

1. **Integration of the gesture recognition system in the implementation of the cognitive architecture**

The implementation of the gesture recognition system is out of the scope of this thesis because it has been the goal of other thesis projects within the research group of the author (Estebanez 2013). Thus, it would be convenient to integrate the previous work developed in the group within the framework of the work developed in the present thesis, to provide a complete surgical robotic platform.

2. **Dynamic model of the actuation system of the intra-abdominal device**

The performance of the cable-driven actuation system has been tested according to the needs of the present work. However, a complete study of the camera robot design that includes a dynamic model of the actuator should be carried out.

3. **Augmenting the cognitive capabilities of the robotic assistant including an episodic memory**

Incorporating an episodic memory that allows adding information from the on-line experiences of the robotic assistant would be interesting to augment the robot capabilities and to augment its knowledge base. Thus, errors committed in the camera guidance could be corrected in later performances.

4. **Improvement of the force-position control with a deep magnetic interaction analysis**

The force-position control of the action system could be improved with a deeper analysis of the magnetic interaction between the intra-abdominal device and the external holder. Thus, stiffness matrix estimation could be avoided with an appropriate interaction modeling.

5. **In-vivo experimentation with the complete robotic assistant**

This thesis offers in-vivo results regarding the intra-abdominal device. However, in-vivo experimentation should be augmented by testing the complete system, including the external robot, in a real surgical environment.

A INTUITIVE TELEOPERATION CONTROL

This appendix describes the intuitive teleoperation control implemented in the CISOBOT platform to teleoperate the surgical tools. This control is important in a teleoperated system in order to isolate the reference systems of the master side and the slave side to the user, especially when the user is teleoperating the slave side through visual feedback from a camera image. As stated in Section 5.2, for natural and intuitive teleoperation of the surgical tools, the configuration of the haptic devices and the monitor follows an arms-eyes configuration. Thus, when the user moves the left haptic device to the right, he or she expects a coherent motion of the left tool, as shown in Figure A.1. A coherent motion is a motion that results natural for human. Thus, the tool is expected to move to the right in the image. Therefore, an intuitive teleoperation control should isolate to the user the computation required to translate haptic motion in coherent motion of the surgical tools.

Thus, this appendix starts with the description of such intuitive control scheme, followed by an experimental validation. The teleoperation control was developed in The Birobotics Institute (Scuola Superiore Sant'Anna of Advances Studies, Pisa, Italy) during a research stay of the author, under the supervision of Professor Arianna Menciassi and Dr. Giuseppe Tortora. This appendix describes the modular robotic platform used to validate the control scheme and the experimental results. The work validated in this appendix can be directly exported to the experimental setup used in this thesis project (Figure 5.1), as the configuration of the robotic system is the same on both platforms: a camera robot and two slave manipulator for surgical tools.

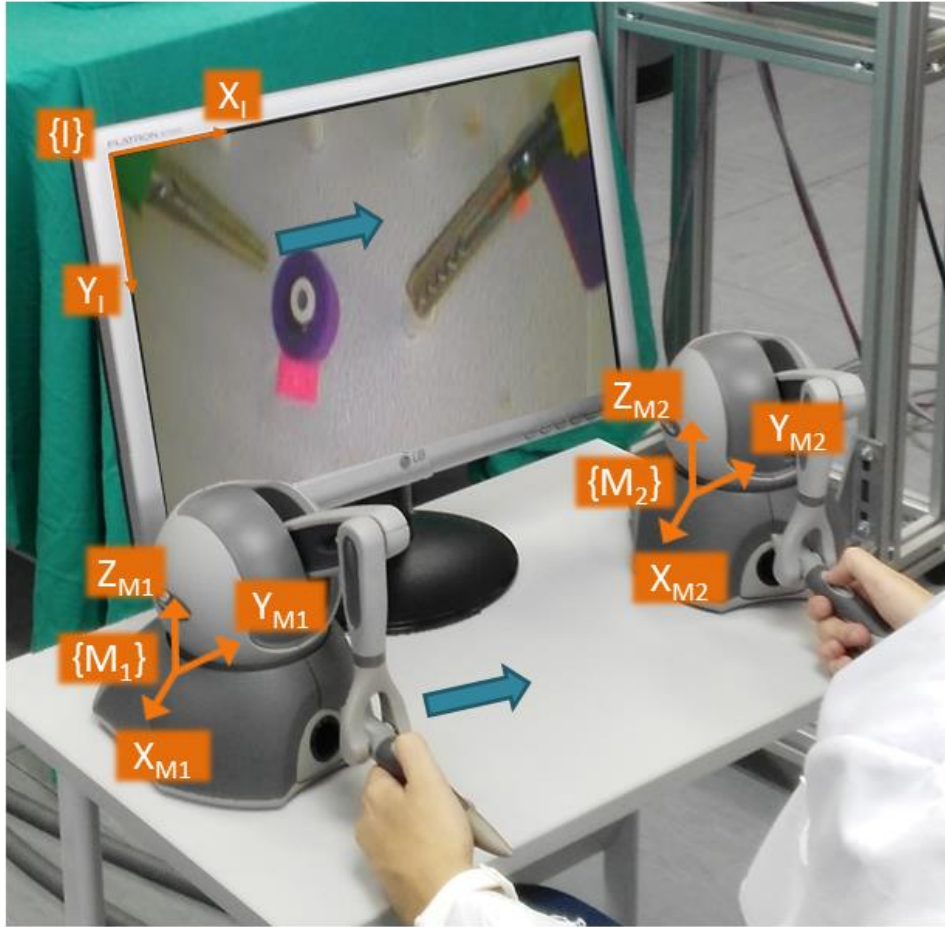


Figure A.1 Intuitive teleoperation of the surgical tools.

A.1 Control scheme

Figure A.2 shows the control scheme of the intuitive teleoperation control. The surgeon teleoperates the haptic devices, which associated references frames are $\{M_1\}$ and $\{M_2\}$, as shown in Figure A.1. For simplicity, Figure A.2 only represents the control of one manipulator. Thus, $\{M\}$ and $\{S\}$ represent the reference frames of the master side (haptic devices) and the slave side (surgical tools). The haptic devices output the incremental motion performed by the surgeon, ${}^M\Delta P$. A kinematic coupling module transforms this incremental motion from system $\{M\}$ to system $\{S\}$, ${}^S\Delta P$, so it can be sent to the slave manipulators. As manipulators work in the joints domain, inverse kinematics is used to transform the desired motion into the corresponding manipulators' articular configuration q . The real position of the manipulator in the Cartesian space cannot be measured in a real surgical environment, but the control loop is closed by the surgeon (man-in-the-loop), who can correct the position of the tools based on the visual information provided by the camera.

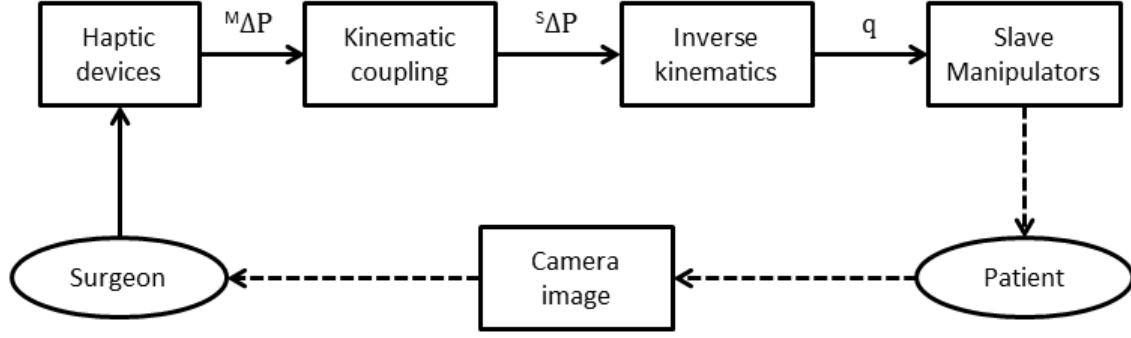


Figure A.2 Intuitive teleoperation control scheme.

The kinematic coupling module maps a haptic motion into a natural motion of the surgical tools. This coupling is done by connecting the master and the slave systems through the image system (the natural reference frame for the user) as follows:

$$^S\Delta P = K_e \cdot {}^S R_I \cdot {}^I R_M \cdot {}^M\Delta P \quad (\text{A.1})$$

where ${}^S R_I$ is the rotation matrix between systems $\{S\}$ and $\{I\}$, ${}^I R_M$ is the rotation matrix between systems $\{I\}$ and $\{M\}$, and K_e is a scale matrix that connects the workspaces of the master and the slave sides. On the one hand, ${}^I R_M$ depends on the relative orientation between the haptic devices and the camera. On the other hand, ${}^S R_I$ depends on the relative location of the slave manipulators and the camera. These rotation matrixes can be computed using a 3D position tracker, such as the Polaris Spectra (Northern Digital Inc.). Finally, K_e is necessary to connect the size of the workspaces of both teleoperating sides in a practical way. It is defined as follows:

$$K_e = \begin{pmatrix} e_x & 0 & 0 \\ 0 & e_y & 0 \\ 0 & 0 & e_z \end{pmatrix} \quad (\text{A.2})$$

where e_x , e_y and e_z are the factor scales applied in directions x , y and z , respectively.

A.2 Experimental validation

This section describes the experimental validation of the control scheme presented in the previous section. Firstly, the experimental setup is exposed, followed the kinematics configuration of the slave manipulators. Finally, the experimental results are presented and discussed.

A.2.1 Modular robotic platform

The experiments have been performed with the modular robotic platform developed by (Tortora, Dario, and Menciassi 2014), shown in Figure A.3. This platform has been designed for NOTES procedures, and it is composed of a set of miniaturized robotic units coupled in a magnetic anchoring frame, that allows magnetic anchoring to the abdominal wall thanks to an external magnetic handle. The triangular-shape anchoring frame enters the abdominal cavity through a 17 mm esophageal access port (Guardus, US endoscopy, USA) in an open configuration. Once inside the abdomen, Shape Memory Alloy (SMA) actuators are used to reach the triangular configuration. It has been demonstrated that SMA actuators are suitable in terms of effectiveness and safety (Salerno et al. 2013). A dedicated docking mechanism allows the anchoring of the miniaturized modular robotic units (Tognarelli et al. 2015; Tortora et al. 2011, 2013). One of the robots has a miniature camera at the end effector (camera robot), while the other two robots are provided with a grasper and an electro-cutter at the end effector (active robotic units).

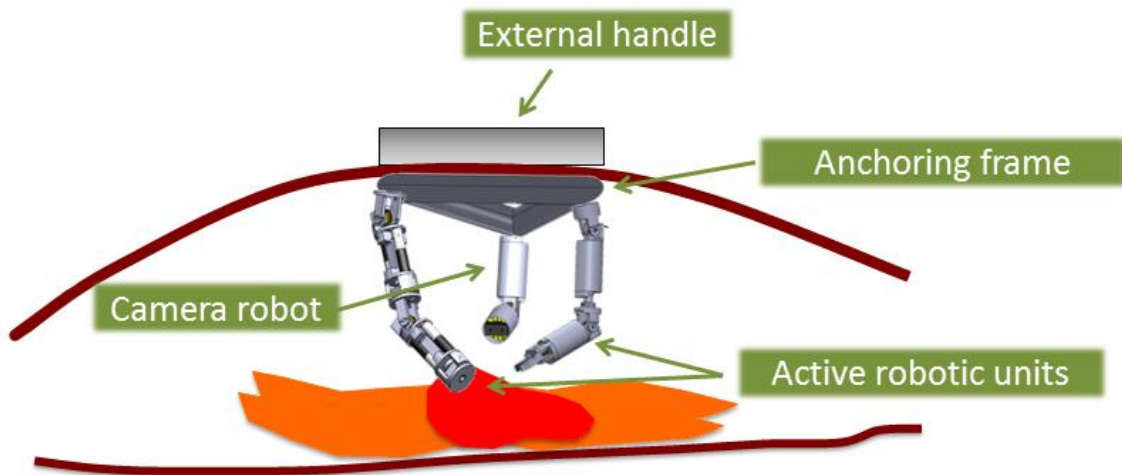


Figure A.3 Modular robotic platform developed by (Tortora, Dario, and Menciassi 2014).

The active robotic units, shown in Figure A.4, are made by connecting two basic robotic modules in a serial configuration, as described in (Tortora, Dario, and Menciassi 2014). Each basic module provides two DoFs, which can be Pitch (P) and Roll (R), or Pitch and End Effector (EE). The electro-cutter robot is composed of two P/R modules, so it is provided with a total of four DoFs. On the other hand, the grasper robot is composed of a P/R module assembled with a P/EE module.

The EE of this robot is an active grasper, so the EE DOF is responsible for opening and closing the grasper. Force on the tip is 0.65 N, which is enough for the execution of basic tasks in endocavitary surgery, while grasping force is about 5.3 N (Tortora et al. 2014). The diameter of the robots is 12 mm, which is a diameter compatible with the insertion through the esophageal access port. The motors of the robots (SBL04 by Namiki, Akita, Japan, reduction ratio 1:337) are controlled using wireless microcontrollers integrated into dedicated boards within the manipulators (CC2430 ZigBee, Texas Instruments, Dallas, TX, USA). Each board can control two brushless motors.

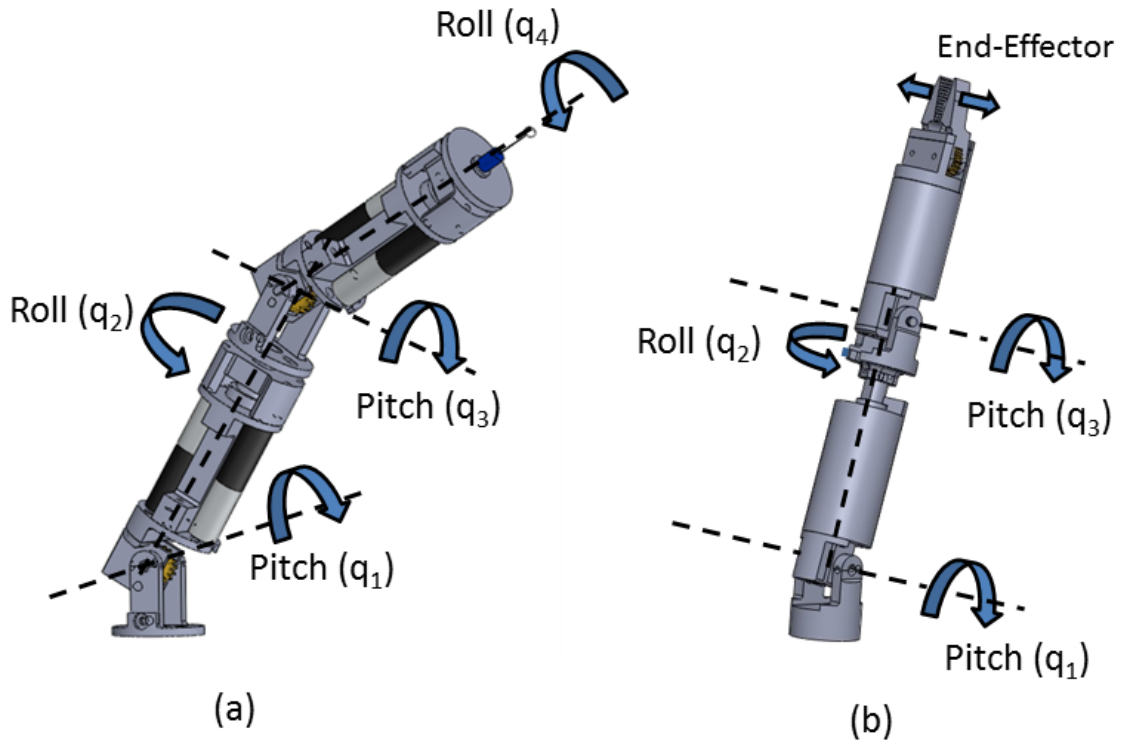


Figure A.4 Modular robotic units: (a) electro-cutter robot, and (b) grasper robot.

A.2.2 Kinematics configuration

Denavit-Hartenberg parameters of the robots are listed in Table A.1. It is worth noting that $q_4 = 0$ for the grasper robot, as the last motor is used to activate the grasper tool. Maximum bending for the first joint is $\pm 180^\circ$, while the third joint is limited to the range of $[0^\circ, 90^\circ]$ in order to avoid multiple solutions of the inverse kinematics. Inverse kinematics for an end effector position $P = (x, y, z)$ are shown in Table A.2. As end effector rotation does not affect position P , joint q_4 is not

considered in the inverse kinematics. A rotation matrix between the robotic units and the image, ${}^S R_I$, necessary in equation (A.1), is easily computed from the anchoring frame design, as the relative position between the active robotic units and the camera robot is fixed and known.

Table A.1 Denavit-Hartenberg parameters of the robotic units.

Link	α_i	a_i (mm)	d_i (mm)	θ_i
1	$-\pi/2$	0	0	q_1
2	$\pi/2$	0	40.85	q_2
3	$-\pi/2$	0	0	q_3
4	0	0	32.85	q_4

Table A.2 Inverse kinematics of the robotic units.

Joint	Equation
q_1	$\text{atan}\left(\frac{-(x(d_2 + d_4 \cos(q_3)) + z d_4 \cos(q_2) \sin(q_3))}{z(d_2 + d_4 \cos(q_3)) - x d_4 \cos(q_2) \sin(q_3)}\right)$
q_2	$-\text{asin}\left(\frac{y}{d_4 \cos(q_3)}\right)$
q_3	$\pi - \text{acos}\left(\frac{d_2^2 + d_4^2 - \sqrt{x^2 + y^2 + z^2}}{2d_2 d_4}\right)$

A.2.3 Experiments

To evaluate the feasibility and intuitiveness of the control scheme presented in the previous section, a pick and place experiment has been designed, similar to the one described in Section 5.5.1. Since only one grasper robot has been manufactured, the experiment has been adapted to be performed by the two robotic units of the modular platform. For the experiments, the electro-cutter has been replaced by a metallic hook. The experimental platform is a pegboard and the task is performed with a rubber triangular ring. The overall task has been divided into the three following states, depicted in Figure A.5:

- State 1: this state consists of picking the ring from one position of the pegboard using the grasper robot. This task is considered completed when

the ring has been completely removed from the peg.

- State 2: this states consists of placing the ring in a different peg of the pegboard. This task is completed when the grasper has completely released the ring.
- State 3: the last state consists of hitting the ring using the electro-cutter robot to make it fall. The task finishes when the ring falls out from the peg.

The task has been performed by 15 users, who have technical skills in robotics, but not medical skills, so they are not familiar with performing manipulation tasks under 2D vision. Two experiments have been carried out: the first one, performed by five of the 15 users, aimed at estimating the learning curve associated with the use of the robots, and the second one, performed by the other ten users, aimed at verifying the dexterity of the system by evaluating the time scored by the users to perform the experiments.

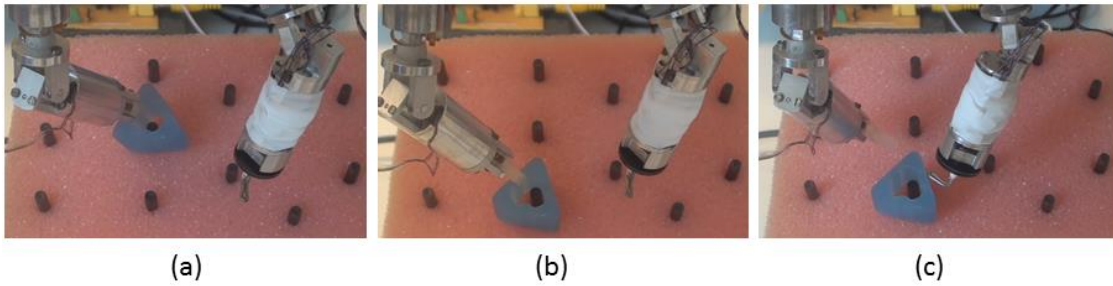


Figure A.5 Task protocol: (a) state 1, (b) state 2, and (c) state 3.

Experiment 1: learning curve

To estimate the learning curve associated with the use of the system, five users, who had never tried the system before, were asked to perform the experiment three consecutive times. Time spent on the development of each state was recorded. Figure A.6 shows the average time spent on completing each state with respect to the trial number. As it can be seen, the three curves decrease significantly with the number of trials, by approximately 70% for State 1, and by about 50% for State 2 and State 3. The higher decrease in State 1 is due to the fact that the first trial of this state is the very first contact of the users with the system.

Experiment 2: dexterity evaluation

To evaluate the dexterity of the system, ten additional users were asked to perform the test. Users were not previously familiarized with the system, but they had a short training period before the experimental session of about 5-10 minutes.

Recorded times for each task are presented in Table A.3. Mean times are 36, 46.7 and 17.1 seconds for state 1, state 2 and state 3, respectively. These values are considered acceptable if compared with other results with robots with more DoFs (Petroni et al. 2013). Standard deviation is 32.8, 23.5 and 21.7 for state 1, state 2 and state 3, respectively. These high values are due to the different innate skills of the users. In addition, a surgeon specialized in general surgery with experience in robotic-assisted laparoscopy tried the system. Times to perform each state were also recorded, resulting in 15, 17 and 29 seconds for State 1, State 2 and State 3, respectively. The surgeon expressed his satisfaction with the system and reported that it is intuitive to use.

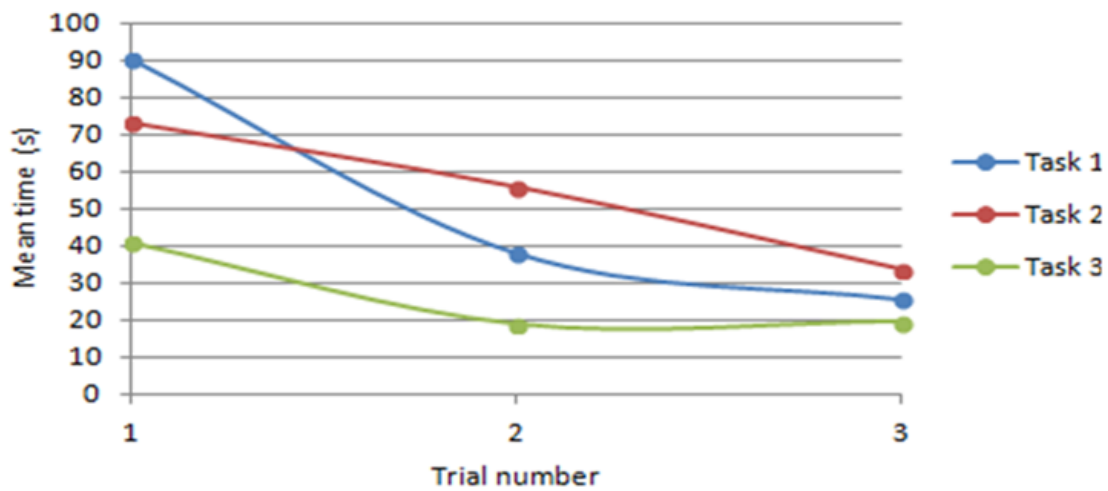


Figure A.6 Learning curve associated with the teleoperated system.

Table A.3 Dexterity evaluation experimental results.

User	State 1 (s)	State 2 (s)	State 3 (s)
1	23	93	19
2	19	38	5
3	26	26	19
4	119	65	8
5	10	24	13
6	52	52	9
7	55	74	77
8	14	30	9
9	24	31	3
10	18	34	9

B THE CISOBOT PLATFORM

As described in Chapter 5, the CISOBOT platform is composed of two six-DoFs manipulators manufactured by Robotnik Automation S.L. (Figure B.1). These modular robots have a spherical wrist configuration, which allows for the decoupling of the end effector position (defined by the first three joints) and orientation (defined by the last three joints). The rotational joint actuators are comprised of PowerCube servomotors from Schunk Corp. Each actuator includes a position and velocity PID controller that is configured to receive position and/or velocity references. Therefore, each joint is responsible for accomplishing its reference. Moreover, each actuator provides sensory information, such as position, velocity, and state of the joint. Communication with the actuators is performed by CANbus. This interface guarantees real-time communication and allows the use of a unique bus for each joint, making it possible to perform a joint decoupled control and sending the position and velocity references simultaneously to each joint.

Denavit-Hartenberg parameters of the manipulators are shown in Table B.1, where L is the length of the robotic graspers attached to the end effector of the manipulators. As the manipulators have a spherical wrist configuration, inverse kinematics is computed following the kinematics decoupling method, consisting in solving the position and the orientation problem independently, thus reducing the number of variables. The position problem has been solved using geometric techniques, while an algebraic solution is used for the orientation problem. The solution of the inverse kinematics is shown in Table B.2. This inverse kinematics may adopt four different solutions depending on the value of parameters b and c . These solutions are shown in Figure B.2. Parameter b has to do with the rotation of the first joint, being $b = 1$ and $c = 1$, complementary solutions for q_1 . On the other hand, parameter c has to do with the position of the elbow. Thus, $c = 1$ is called “elbow up” configuration, while $c = -1$ is called “elbow down” solution. Table

B.2 shows the sin and cosine of every joint, s_i and c_i , respectively. Then, joints values are computed as follows:

$$q_i = \text{atan}\left(\frac{s_i}{c_i}\right) \quad (\text{B.1})$$

Parameters R and L of the equations exposed in Table B.2 have the following values:

$$R = \sqrt{x^2 + y^2} \quad (\text{B.2})$$

$$L = \sqrt{R^2 + (z - d_1)^2} \quad (\text{B.3})$$

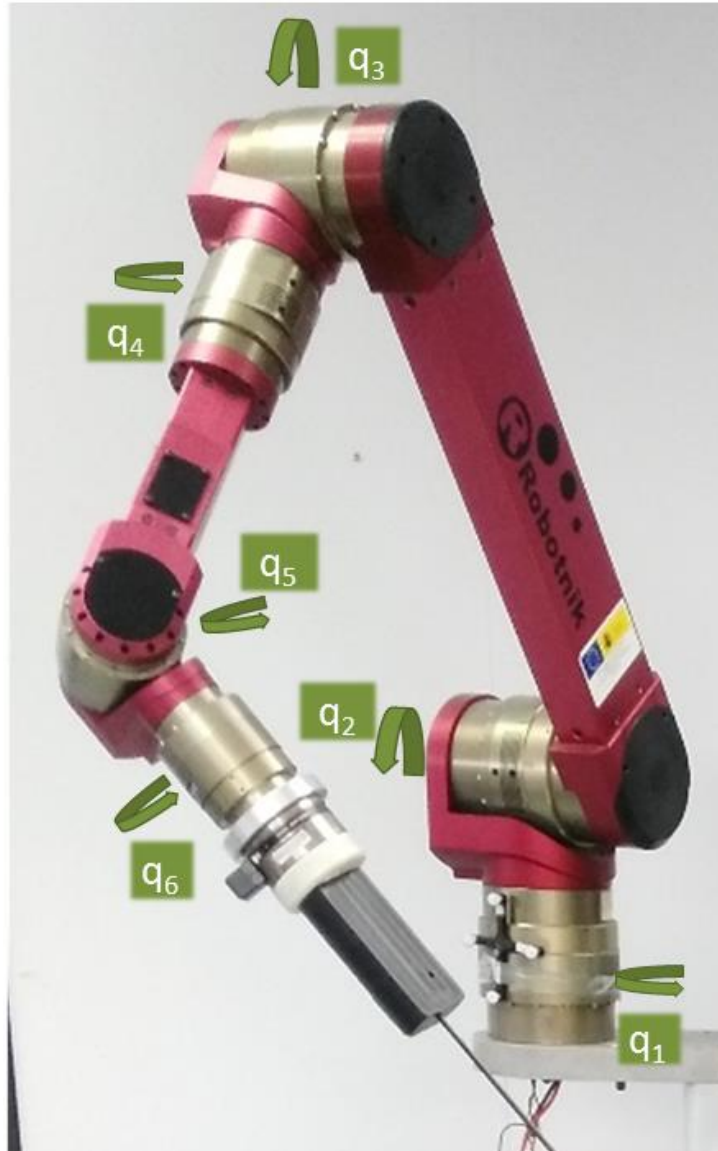


Figure B.1 Robotnik modular arm.

Table B.1 Denavit-Hartenberg parameters of the Robotnik modular arms.

Link	α_i	a_i (mm)	d_i (mm)	θ_i
1	$\pi/2$	0	240	q_1
2	0	540	0	q_2
3	$-\pi/2$	0	0	q_3
4	$\pi/2$	0	415	q_4
5	$-\pi/2$	0	0	q_5
6	0	0	$171.5+L$	q_6

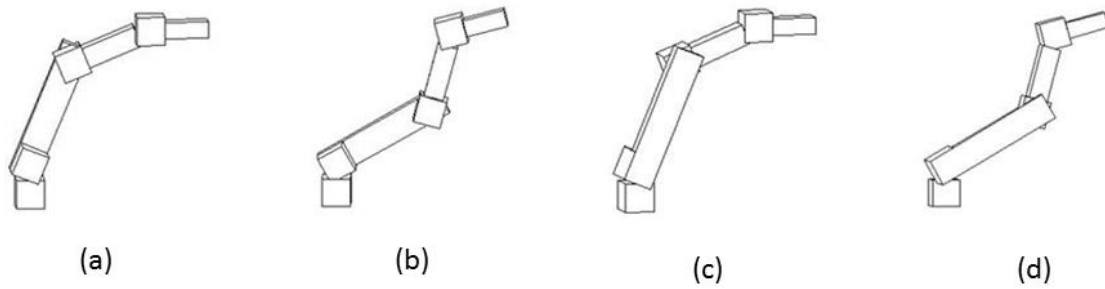


Figure B.2 Inverse kinematics solutions: (a) $b = 1$, $c = 1$, (b) $b = 1$, $c = -1$, (c) $b = -1$, $c = 1$, and (d) $b = -1$, $c = -1$.

Table B.2 Inverse kinematics of the Robotnik modular arms.

Joint	Equation
Q ₁	$s_1 = \frac{by}{R}$ $c_1 = \frac{bx}{R}$
Q ₂	$s_2 = b \left(c \frac{z - d_1}{L} \sqrt{1 - \left(\frac{a_2^2 + L^2 - d_4^2}{2a_2L} \right)^2} - \frac{R}{L} \frac{a_2^2 + L^2 - d_4^2}{2a_2L} \right)$ $c_2 = c \frac{R}{L} \sqrt{1 - \left(\frac{a_2^2 + L^2 - d_4^2}{2a_2L} \right)^2} + \frac{z - d_1}{L} \frac{a_2^2 + L^2 - d_4^2}{2a_2L}$
Q ₃	$s_3 = bc \sqrt{1 - \left(\frac{a_2^2 - L^2 + d_4^2}{2a_2d_4} \right)^2}$ $c_3 = - \frac{a_2^2 - L^2 + d_4^2}{2a_2d_4}$
Q ₄	$s_4 = - \frac{r_{23}}{\sqrt{r_{31}^2 + r_{32}^2}}$ $c_4 = - \frac{r_{13}}{\sqrt{r_{31}^2 + r_{32}^2}}$
Q ₅	$s_5 = \sqrt{r_{31}^2 + r_{32}^2}$ $c_5 = r_{33}$
Q ₆	$s_6 = - \frac{r_{32}}{\sqrt{r_{31}^2 + r_{32}^2}}$ $c_6 = \frac{r_{31}}{\sqrt{r_{31}^2 + r_{32}^2}}$

C ROBOTIC OPERATING SYSTEM (ROS)

ROS is defined as a flexible framework for writing robot software. It is a collection of tools, libraries, and conventions that aim to simplify the task of creating complex and robust robot behavior across a wide variety of robotic platforms (ROS.org 2016). The main characteristics of ROS are a distributed and modular design, open source software, hardware abstraction, low-level device control, implementation of commonly used functionality, message-passing between processes, and package management.

A ROS network consists of a number of processes connected at runtime in a peer-to-peer topology. The basic concepts of a ROS network are:

- **Nodes.** Nodes are processes that perform computation. A common robotic system usually comprises many nodes, each one controlling a different device or functionality. A ROS node is written using a ROS client library and accepts a variety of programming languages, such as Python, C++, Lisp or MATLAB. Nodes of the same network can be written in different languages.
- **Master.** The ROS Master is the central server of the network. Its function is to create the network and to register every node and message in the network. Thus, without this Master node, nodes would not be able to find each other, exchange messages or invoke services.
- **Messages.** Messages are the way nodes communicate among each other. A message is a data structure comprising typed fields. ROS offers standard predefined messages types, but messages can be created depending on each

system needs. A message can be sent through topics or through services.

- **Topics.** A topic is a name used to identify the content of messages. Messages are sent via a publisher/subscriber communication. A node sends out a message by publishing it on a given topic. In the same way, a node can subscribe to a particular topic to read the message within it. A node can publish and subscribe to multiple topics, and a topic can be published by different nodes.
- **Services.** Services are the way of communicating two nodes in a request/answer communication. A service is a pair of message structures: one for the request and one for the reply. A node may offer different services and other nodes can use this service by sending a message through it.

Figure C.1 shows the computational graph of a ROS network. Nodes connect to other nodes directly; the Master only provides lookup information. It stores topics and services registration information for the nodes. This architecture allows for decoupled operation, where the names are the primary means by which larger and more complex systems can be built.

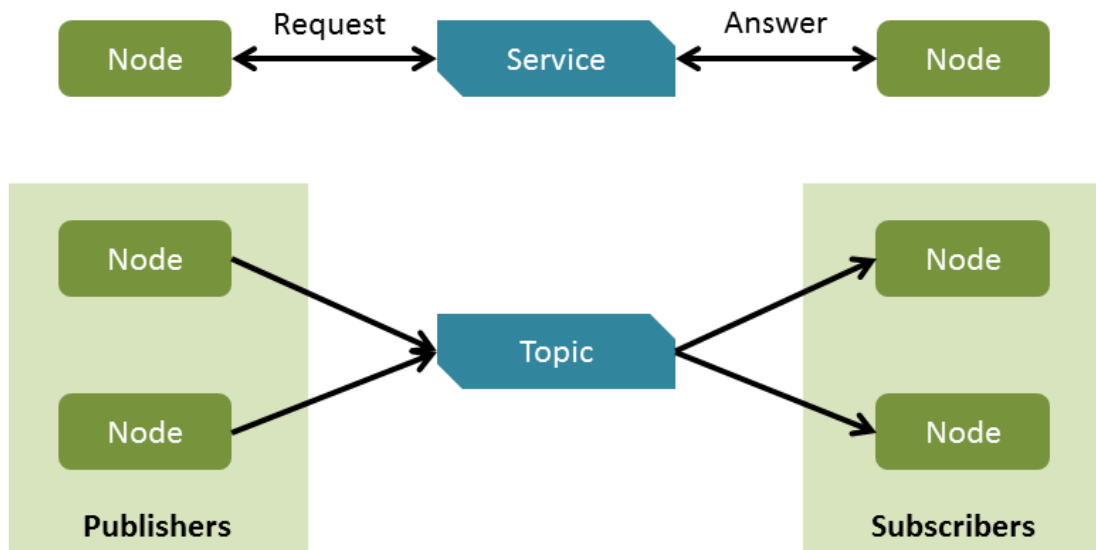


Figure C.1 ROS network.

D SOAR COGNITIVE ARCHITECTURE

Soar is a general cognitive architecture for developing systems that exhibit intelligent behavior (Soar Home 2016). It was developed by John E. Laird in 1983 and has evolved through many different versions to Version 9. The primary principle of Soar is that all decisions are made through a combination of relevant knowledge at run-time. Every decision is based on the current interpretation of sensory data, the contents of working memory created by prior problem solving, and any relevant knowledge retrieved from long-term memory. The architecture of Soar, Version 9, is shown in Figure D.1 (Laird 2008). It is composed of a set of long-term memories and a short-term memory. The long-term memory is divided into procedural memory, semantic memory, and episodic memory, and it is encoded as production rules. Rules provide a flexible, context-dependent representation of knowledge, with their conditions matching the current situation and their actions retrieving information relevant to the current situation. At the lowest level, Soar's processing consists in matching and finding rules. The short-term memory is encoded as a symbolic graph structure so that objects can be represented with properties and relations. It holds the agent's assessment of the current situation derived from perception and via retrieval knowledge from its long-term memory. Action in an environment occurs through the creation of motor commands in a buffer in short-term memory. The gesture recognition system selects operators and detects impasses. And the appraisal detector generates emotions, feelings, and an internal reward for reinforcement learning.

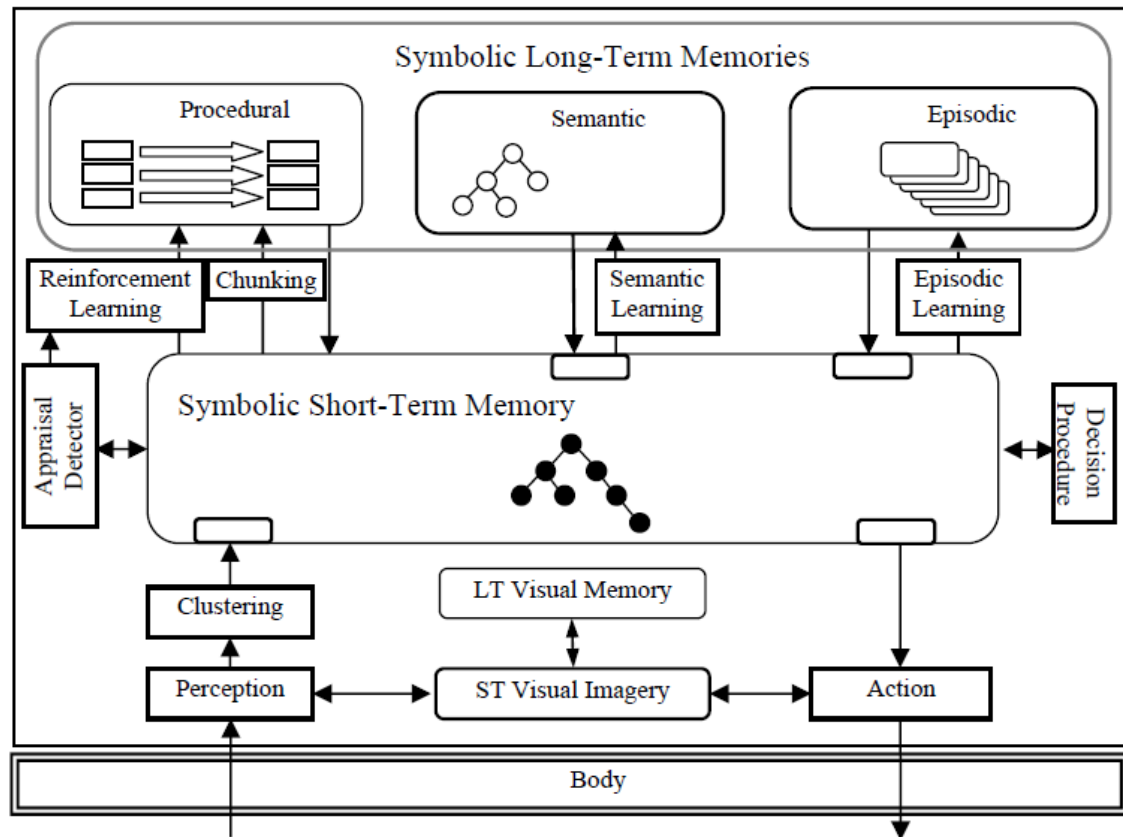


Figure D.1 Structure of Soar, Version 9 (Laird 2008).

Most rule-based systems choose a single rule to fire at a given time, but they do not use additional context-dependent knowledge to influence the decision. However, Soar allows additional knowledge to influence a decision by introducing operators as the locus for choice and using rules to propose, evaluate, and apply operators. In Soar, there are rules that propose operators that create a data structure in working memory representing the operator and an acceptable preference so that the operator can be considered for selection. There are also rules that evaluate operators and create other types of preferences that prefer one operator to another or provide some indication of the utility of the operator for the current situation. Finally, there are rules that apply the operator by making changes to working memory that reflect the actions of the operator.

The structure of problem-solving in Soar determines when new knowledge is needed, what that knowledge might be, and when it can be acquired. In Soar, impasses occur if the directly available knowledge is either incompliant or inconsistent. Therefore, impasses indicate when the system should attempt to acquire new knowledge. While problem-solving within a subgoal, Soar can discover information that will resolve an impasse. This information, if remembered, can avert similar impasses in future problem-solving. When a subgoal is completed, because its impasse has been resolved, an opportunity exists to add new knowledge

that was not already explicitly known. Chunking is the Soar learning mechanism to automatically learn new rules. When a subgoal is generated, a learning episode begins that could lead to the creation of a chunk. During problem-solving within the subgoal, information accumulates on which a chunk can be based. When the subgoal terminates, a chunk can be created. Each chunk is a rule (or set of rules) that gets added to the production memory. Reinforcement learning (RL) is a complementary learning mechanism of Soar that involves adjusting the selection of actions in an attempt to maximize a reward. RL applies to every operator selection, on every decision, even when there are no impasses, while chunking only learns rules through impasses. In addition, RL modifies existing rules by changing the value of numeric preferences, while chunking only adds new rules.

In contrast to semantic and procedural memory, which contains knowledge independent from when and where it was learned, and episodic memory, which contains memories of what was experienced over time. In Soar, it includes specific instances of the structures that occur in working memory at the same time, providing the ability to remember the context of past experiences as well as the temporal relationships between experiences. An episode is retrieved by the deliberate creation of a cue, which is a partial specification of working memory in a special buffer. Once a cue is created, the best partial match is found (biased by recency and working memory activation) and retrieved into a separate working memory buffer (to avoid confusion between a memory and the current situation). The next episode can also be retrieved, providing the ability to replay an experience as a sequence of retrieved episodes.

RESUMEN DE LA TESIS DOCTORAL

Introducción

En las últimas décadas, el campo de la cirugía ha evolucionado hacia técnicas mínimamente invasivas encaminadas a reducir el grado de invasión de las intervenciones. Así, la cirugía laparoscópica consiste en operar a través de pequeñas incisiones realizadas en la pared abdominal de los pacientes, a través de las cuales se introducen tanto los instrumentos laparoscópicos como un endoscopio. Esta forma de operar presenta numerosas ventajas para los pacientes, incluyendo beneficios tanto cosméticos como de tiempo de la recuperación (Romanelli, Mark, and Omotosho 2008). Sin embargo, estas nuevas técnicas conllevan una serie de inconvenientes para los cirujanos, que requieren de largos periodos de entrenamiento para adquirir destreza con este nuevo enfoque. Los procedimientos laparoscópicos han evolucionado hacia técnicas menos invasivas que mejoran las ventajas cosméticas para los pacientes, pero implican nuevos retos para los cirujanos: las técnicas de puerto único (SPAS en inglés), y la cirugía mediante orificios naturales (NOTES en inglés). En las técnicas de puerto único se utiliza una única incisión a través de la cual se introducen tanto los instrumentos como el endoscopio (Gascón Hove et al. 2014). Esta técnica requiere el uso de instrumentos especiales semiflexibles o curvos, que incrementan la curva de aprendizaje de los cirujanos. Además, esta forma de operar reduce el espacio de trabajo de los instrumentos debido a la cercanía de éstos comparten un espacio muy reducido

tanto dentro como fuera del abdomen. La cercanía entre los instrumentos y la cámara también provoca una pérdida de triangulación, que se traduce en una pérdida de sensación de profundidad en la imagen que recibe el cirujano. Por otro lado, las técnicas NOTES se realizan con instrumentos flexibles específicos para este tipo de procedimientos, que se introducen en la cavidad abdominal a través de orificios naturales del cuerpo (Wang et al. 2016). Sin embargo, esta técnica está actualmente estancada debido a la falta de instrumentos apropiados para su desempeño (Trejos et al. 2011).

En este sentido, la robótica ha encontrado un amplio campo de aplicación para superar las limitaciones de las técnicas de cirugía laparoscópica gracias a una mejora en las habilidades del cirujano en términos de alta precisión de movimientos y un manejo más intuitivo del instrumental. El mercado de la robótica quirúrgica ha sido monopolizado por la compañía Intuitive Surgical Inc. con el desarrollo del robot quirúrgico da Vinci. La compañía ha comercializado más de 3,000 unidades a lo largo del mundo, y se han realizado más de un millón y medio de intervenciones con esta plataforma robótica. De hecho, actualmente aproximadamente el 90% de las prostatectomías se realizan con el da Vinci (Haidegger, Sándor, and Benyó 2011). Sin embargo, este robot se encuentra actualmente obsoleto debido a las limitaciones de su control teleoperado, que se limita a replicar el movimiento de las manos del cirujano, pero no ofrece ningún tipo de autonomía. Actualmente, el uso de asistentes robóticos en intervenciones quirúrgicas se encuentra limitado debido a los siguientes factores: se requiere un mayor tiempo de operación, no existen herramientas adecuadas para intervenciones de gran complejidad, es necesario adaptar los quirófanos para la integración de los sistemas robóticos, no hay contacto directo entre el paciente y el cirujano, y los sistemas actuales no son capaces de trabajar con autonomía real que les permita trabajar codo con codo con el equipo médico ni reaccionar ante situaciones imprevistas, como un sangrado.

Para aumentar las capacidades de los robots quirúrgicos, muchos autores han desarrollado sistemas autónomos y semiautónomos capaces de realizar tareas automáticas que liberan al cirujano de carga de trabajo. En la literatura se pueden encontrar trabajos en los que se proponen métodos de navegación automática de la cámara (Ko et al. 2005; Weede et al. 2011), y trabajos relacionados con la automatización de tareas quirúrgicas como la sutura (Kang and Wen 2001), manejo de tejido (Patil and Alterovitz 2010) o planificación de movimientos para la inserción de la aguja (Alterovitz et al. 2009). Otros autores han propuesto escenarios colaborativos en los que el robot realiza parte de las maniobras mientras que el cirujano se centra en los movimientos más complejos (Bauzano et al. 2015; Padoy and Hager 2011). Sin embargo, estos sistemas aún requieren mucha intervención directa y supervisión del cirujano, y se limitan a realizar movimientos pre-programados. Por tanto, estos sistemas carecen de la inteligencia y conciencia para

ser considerados realmente autónomos (Pandya et al. 2014).

Bajo estas premisas, la evolución de los robots quirúrgicos debería ir encaminada al desarrollo de asistentes robóticos co-worker, que trabajen codo con codo con el cirujano de forma similar a como lo haría un asistente humano. Las arquitecturas cognitivas proporcionan la infraestructura necesaria para dotar a los robots con capacidades humanas. Existen numerosas arquitecturas cognitivas estándar que han sido aplicadas satisfactoriamente en diversos campos como la robótica móvil (Janrathitikarn and Long 2008; Laird et al. 2012), teoría de juegos (Choi et al. 2011; Kirk, Mininger, and Laird 2016) o el modelado de comportamiento humano (Liu et al. 2016; S. Zhang et al. 2014). Sin embargo, la aplicación de este tipo de arquitecturas en el campo quirúrgico es un área de investigación abierta en la que aún queda mucho por hacer. Un asistente robótico inteligente que pueda trabajar en un escenario quirúrgico co-worker requiere de la integración de diferentes tecnologías que proporcionen al robot medios para razonar y tomar decisiones, y para poder realizar tareas quirúrgicas de forma realmente autónoma. Así, las tecnologías de navegación se deben combinar con una interacción natural entre el robot y el cirujano que emule la comunicación entre humanos. Todo esto debe ser integrado en una arquitectura cognitiva que dote al robot de las capacidades cognitivas necesarias para realizar tareas de planificación de alto nivel a través de habilidades como el razonamiento y el aprendizaje, y una base de conocimiento apropiada.

Contribuciones

Esta tesis doctoral ofrece resultados tanto teóricos como experimentales relativos a un asistente robótico inteligente para técnicas de cirugía mínimamente invasiva. Este trabajo propone un nuevo concepto de asistente robótico camarógrafo que permite aumentar las capacidades de los sistemas actuales. Dicho asistente robótico se ha diseñado siguiendo una filosofía cooperativa, con una comunicación natural entre el cirujano y el robot que emula la interacción entre un equipo quirúrgico humano. Así, la inteligencia del sistema se ha basado en una arquitectura cognitiva con mecanismos de aprendizaje que dota al sistema de capacidad de toma de decisiones y navegación autónoma. En concreto, además de ofrecer un análisis profundo del estado del arte actual, esta tesis doctoral ofrece las siguientes contribuciones:

1. Nuevo concepto de asistente robótico camarógrafo para cirugía mínimamente invasiva sin restricciones holonómicas

Este trabajo propone un nuevo concepto de asistente robótico camarógrafo para cirugía mínimamente invasiva sin restricciones holonómicas en su movimiento. El asistente robótico está compuesto por un brazo robótico externo y un robot cámara intra-abdominal, cuyo movimiento a lo largo de la pared abdominal se controla mediante interacción magnética con el brazo externo. Así, la cámara puede moverse libremente por la cavidad abdominal gracias a los seis grados de libertad que ofrece el asistente: dos desplazamientos a lo largo de la pared abdominal y una rotación horizontal (actuados mediante el robot externo), y dos grados de libertad internos, giro e inclinación de la cámara, y un zoom digital (actuados mediante el dispositivo intra-abdominal). Este diseño permite aumentar el campo de visión de la cámara comparado con el de los endoscopios convencionales, y permite obtener diferentes perspectivas de las estructuras anatómicas internas, ayudando al cirujano a sobrellevar la pérdida de sensación de profundidad debida a la visión plana inherente a los procesos laparoscópicos, y ofreciendo una vista más natural del área de trabajo. Además, este enfoque de asistente robótico permite una navegación autónoma de la cámara, evitando la necesidad de un asistente humano únicamente destinado al manejo de la cámara.

2. Control híbrido de fuerza-posición con compensación de pares capaz de adaptar el movimiento de la cámara a la anatomía de la pared abdominal

El desplazamiento de la cámara a lo largo de la pared abdominal requiere un control de orientación activo capaz de adaptar el movimiento del robot a la anatomía de cada paciente, asegurando que el movimiento se realiza de forma segura, sin causar ningún tipo de daños, ya sean internos o externos, en el paciente. Con este objetivo, este trabajo propone un control híbrido de fuerza-posición con un módulo de compensación de pares que asegura una orientación adecuada del robot. Así, el esquema de control de posición controla el desplazamiento del robot en las direcciones tangentes a la superficie de contacto (pared abdominal), mientras que el control de la fuerza se realiza en la dirección normal a la superficie. Por otro lado, el módulo de compensación de pares asegura que el efector final del brazo externo se mantiene en todo momento paralelo a la pared abdominal durante el desplazamiento de la cámara, cuya anatomía es a priori desconocida y variable entre distintos pacientes.

3. Diseño de una arquitectura cognitiva para aplicaciones quirúrgicas con mecanismos de aprendizaje que emula el comportamiento humano

Las arquitecturas cognitivas proporcionan a los sistemas robóticos funcionalidades humanas, como capacidad de razonamiento, aprendizaje, resolución de problemas o toma de decisiones. En este trabajo, se ha adaptado una arquitectura cognitiva estándar para dotar al asistente robótico de una interacción hombre-máquina intuitiva y natural, y capacidad de toma de decisiones y de navegación autónoma que permitan al asistente trabajar codo con codo con el cirujano de forma similar a como lo haría un asistente humano. La arquitectura cognitiva también incluye mecanismos de aprendizaje que permiten al robot aumentar su base de conocimiento y mejorar su comportamiento en el tiempo.

4. Implementación del asistente robótico camarógrafo inteligente y resultados experimentales

Tanto la arquitectura cognitiva como el control híbrido de fuerza-posición se han validado mediante experimentación in-vitro que demuestra la validez de los conceptos teóricos propuestos en esta tesis doctoral. Además, el diseño del asistente robótico camarógrafo ha sido validado mediante experimentación in-vivo en un modelo porcino en el Centro IACE (Instituto Andaluz de Cirugía Experimental), mediante el que se han validado las principales características de diseño del robot cámara.

Contexto

Esta tesis doctoral se encuentra enmarcada dentro de las líneas de investigación del grupo de robótica médica del departamento de Ingeniería de Sistemas y Automática de la Universidad de Málaga. Además, la autora ha realizado una estancia de investigación de tres meses de duración en los laboratorios del Instituto de Biorrobótica della Scuola Superiore Sant'Anna (Pisa, Italia), bajo la supervisión de la profesora Arianna Menciassi.

Los resultados de esta tesis extienden estudios previos del grupo de investigación relacionados con asistentes robóticos en entornos colaborativos. Estos estudios formaron parte de las actividades e investigación que fueron llevadas a cabo en la Universidad de Málaga, cuyo principal logro fue el diseño e implantación de un asistente robótico que maneja un endoscopio, el cual ha sido utilizado con éxito en intervenciones quirúrgicas humanas (Munoz et al. 2006). Tras estos trabajos, el

grupo de investigación ha centrado sus investigaciones en el desarrollo de una plataforma robótica capaz de colaborar con el cirujano de forma autónoma en tareas quirúrgicas (Bauzano 2012) y en el desarrollo e implementación de un sistema de reconocimiento de maniobras quirúrgicas (Estebanez 2013). La última tesis doctoral desarrollada dentro del grupo de investigación se centra en la navegación del instrumental quirúrgico para técnicas de puerto único (Pérez del Pulgar 2015).

Esta tesis doctoral ha sido financiada mediante una beca de Formación de Personal Investigador (FPI) concedida por el Ministerio de Economía y Competitividad (EEBB-I-13-07552), asociada con el proyecto nacional DPI2010-21126-C03-01, cuyo principal objetivo ha sido el desarrollo de un asistente robótico para técnicas de cirugía SPAS/NOTES. La estancia de investigación de la autora de la presente tesis doctoral también ha sido financiada por el Ministerio de Economía y Competitividad en el contexto de ayudas a la movilidad para estudiantes de doctorado.

Estructura de la tesis

Esta tesis se divide en seis capítulos, cuatro apéndices y las referencias bibliográficas. Excepto este capítulo y el de conclusiones y trabajos futuros, cada capítulo comienza con una introducción que presenta el problema a resolver, y termina con unas conclusiones que resaltan las principales contribuciones y/o resultados obtenidos.

El capítulo 2, titulado *State of the art*, ofrece un estado del arte actualizado de las soluciones robóticas aplicadas a las necesidades actuales de las técnicas quirúrgicas, incluyendo el estado actual de las habilidades de los robots quirúrgicos. Posteriormente, se realiza un análisis de las arquitecturas cognitivas estándar más significativas, junto con los campos de aplicación de las mismas. El capítulo termina con una breve descripción de la propuesta de este trabajo de tesis doctoral, que va un paso más allá del estado del arte actual.

El capítulo 3, titulado *Control system of the robotic assistant*, presenta el esquema de control del asistente robótico camarógrafo. El capítulo comienza con una descripción general del asistente robótico, junto con las especificaciones de diseño del robot cámara. A continuación se realiza una descripción del modelo geométrico de la tarea. Posteriormente, se profundiza en el esquema de control del sistema, que se divide en el control del mecanismo de actuación del robot cámara y el control híbrido fuerza-posición con compensación de pares para el desplazamiento del robot externo.

El capítulo 4, titulado *Robot cognition*, describe la arquitectura cognitiva implementada en el asistente robótico inteligente. En primer lugar, se expone una descripción general de la arquitectura, seguida de un análisis en profundidad del bloque cognitivo del sistema. A continuación, se realiza una descripción tanto de la memoria semántica como de la memoria episódica del sistema, junto con el mecanismo de aprendizaje por refuerzo que permite mejorar el comportamiento del robot.

El capítulo 5, titulado *Implementation and experiments*, describe la implementación de los conceptos teóricos expuestos en los capítulos anteriores, y presenta los resultados experimentales de la presente tesis doctoral. Tras la descripción de la plataforma robótica empleada en los experimentos, se realiza una descripción de la arquitectura software basada en una red de ROS. A continuación, se presenta la validación in-vivo del robot cámara realizada en un modelo porcino. Posteriormente, se presentan los experimentos realizados para validar tanto el esquema de control del sistema como el método de navegación de la cámara inteligente basado en la arquitectura cognitiva descrita en el capítulo anterior.

El capítulo 6, titulado *Conclusion and future work*, destaca las contribuciones más relevantes de esta tesis doctoral y propone los trabajos futuros que continúan el presente trabajo.

Finalmente, los apéndices proporcionan un análisis más profundo del control teleoperado implementado en la plataforma de experimentación, y de los conceptos teóricos relacionados con las herramientas de programación implementadas en este trabajo.

Conclusiones

Actualmente, el mercado de los robots quirúrgicos se encuentra estancado debido a que los sistemas clásicos teleoperados, como el da Vinci, están obsoletos y no ofrecen la asistencia requerida por los cirujanos. Además, las soluciones mecatrónicas tradicionales, basadas en robots externos que manejan instrumental laparoscópico, no son válidos para las nuevas técnicas quirúrgicas que están surgiendo en los últimos tiempos. De esta manera, los investigadores están centrando sus esfuerzos en el desarrollo de dispositivos intra-abdominales, que reducen el grado de invasión de las intervenciones y solucionan las limitaciones de las nuevas técnicas laparoscópicas, ya que evitan los problemas de restricción de movimiento debidos al punto de entrada. Sin embargo, los enfoques actuales de este tipo de robots requieren de un asistente humano que controle el movimiento de los dispositivos intra-abdominales, lo que limita la aplicación de estos trabajos en

entornos co-worker en los que los robots puedan trabajar con autonomía.

La autonomía de los robots en entornos quirúrgicos ha sido estudiada por un gran número de autores, con el desarrollo de aplicaciones que van desde la navegación autónoma de la cámara hasta la automatización de tareas quirúrgicas. Sin embargo, estos trabajos requieren de la supervisión constante del cirujano y su capacidad de toma de decisiones y de adaptabilidad a escenarios dinámicos se encuentra aún muy limitada. Un asistente robótico inteligente que pueda colaborar con el cirujano en un entorno co-worker debe ir un paso más allá en cuanto a las habilidades actuales de los robots quirúrgicos, dotando al sistema con características humanas, como la representación de conocimiento, el razonamiento y la planificación, la interpretación del entorno, o mecanismos de aprendizajes. Algunos autores han diseñado arquitecturas cognitivas específicas para ciertas aplicaciones en un entorno quirúrgico, como el guiado del endoscopio, pero ninguno de estos trabajos incluye mecanismos de aprendizaje, una característica humana esencial. La adaptación de una arquitectura cognitiva estándar para aplicaciones quirúrgicas proporcionaría un marco general que podría ser implementado para diferentes tareas dentro del campo de la cirugía robótica, y sentaría las bases para el desarrollo de asistentes robóticos quirúrgicos.

Analizando las características particulares de las diferentes arquitecturas cognitivas estándar, SOAR parece ser la más adecuada para ser utilizada como base para construir una estructura general para robots quirúrgicos, ya que proporciona una gran flexibilidad y modularidad que permiten su implementación para una gran diversidad de aplicaciones, desde las tareas más sencillas como responder de forma autónoma a comandos específicos del cirujano, hasta escenarios colaborativos más complejos en los que se requiere de cierto grado de razonamiento y autonomía. SOAR ofrece diferentes niveles de memoria a largo plazo que permiten almacenar una amplia variedad de conocimiento: la memoria procedural permite almacenar comportamientos del robot; la memoria semántica permite almacenar conocimiento quirúrgico como los protocolos de la tarea o incluso realizar una representación semántica del entorno; y la memoria episódica permite almacenar y recuperar experiencias pasadas relativas, por ejemplo, con situaciones imprevistas que pudieran ocurrir durante una intervención, y permite también añadir nuevo conocimiento al sistema. Finalmente, SOAR está diseñada para permitir una fácil integración con otros componentes, como componentes robóticos o sensores.

Así, esta tesis doctoral propone una arquitectura cognitiva para un asistente robótico inteligente basada en SOAR, representada en la Figure 2.18. La cognición del sistema se compone de una serie de estructuras de memoria que permiten almacenar conocimiento, mecanismos de aprendizaje, y algoritmos de razonamiento y planificación de alto nivel. El sistema cognitivo hace uso de la información que

proviene del sistema de percepción, que recoge datos sensoriales del entorno quirúrgico, y envía los movimientos que debe realizar el robot al sistema de actuación. Por su parte, el módulo de actuación está compuesto por dos componentes: el asistente robótico y su sistema de control. Finalmente, el módulo de interacción humano-máquina permite la comunicación entre el cirujano y el sistema cognitivo. La forma más básica de comunicación es a través de un interfaz humano-máquina que permita al cirujano comandar de forma directa movimientos o comportamientos al robot, como comandos de voz, teleoperación directa, o un interfaz gráfico. Sin embargo, un asistente robótico inteligente diseñado para emular comportamiento humano, requiere de una forma de comunicación más natural. Dicha comunicación se realiza mediante un sistema de reconocimiento de gestos, que interpreta las maniobras que realiza el cirujano en cada momento de la operación para poder seguir el flujo de trabajo de la intervención completa. La arquitectura cognitiva propuesta se ha implementado para la aplicación particular de un asistente robótico camarógrafo.

El capítulo 3 de esta tesis describe un asistente robótico camarógrafo de 6 grados de libertad, que combina las ventajas de los asistentes robóticos convencionales y de los nuevos dispositivos intra-abdominales. Dicho asistente está compuesto por un dispositivo intra-abdominal dotado de una cámara de alta resolución, llamado robot cámara, y un brazo robótico externo. El robot cámara se introduce en la cavidad abdominal por una de las incisiones que realiza el cirujano para introducir el instrumental laparoscópico, y se adhiere a la pared abdominal por interacción magnética con un imán externo. Dicho imán se acopla al efector final del brazo robótico externo, de manera que el movimiento de la cámara en el interior del abdomen se controla mediante el desplazamiento del brazo externo por la pared abdominal exterior. Por un lado, el uso del robot cámara aumenta el campo de visión comparado con los endoscopios convencionales, ya que el movimiento de la cámara no se encuentra restringido por el punto de entrada. Por otro lado, el enfoque de acoplar el imán externo a un brazo robótico permite la implementación de estrategias de navegación autónoma de la cámara, liberando al cirujano o a un asistente adicional de esta tediosa tarea.

El robot cámara está dotado de dos grados de libertad internos, giro e inclinación de la cámara, que se actúan mediante un mecanismo actuado por cables. Estos grados de libertad adicionales permiten aumentar las capacidades de visión de la cámara, permitiendo obtener diferentes perspectivas de una misma escena, lo que ayuda a recuperar la pérdida de sensación de profundidad de la visión plana y permite obtener una perspectiva más natural del área de trabajo que la ofrecida por los endoscopios convencionales, cuya libertad de giro se encuentra muy limitada. El sistema de actuación mediante cables evita la necesidad de incluir motores en el robot cámara, lo que incrementaría tanto el peso como el tamaño del dispositivo.

Además, este sistema permite controlar los grados de libertad internos desde el exterior de forma sencilla.

El capítulo 3 también analiza el control del asistente robótico. En este capítulo se detallan las características del control híbrido de fuerza-posición con compensación de pares para el correcto desplazamiento de la cámara. La compensación de pares asegura que el efector final del brazo externo permanezca en todo momento paralelo a la superficie de contacto, dado que la anatomía de la pared abdominal es desconocida por el sistema, y además difiere entre diferentes pacientes. Esto es esencial para asegurar una correcta interacción magnética entre el imán exterior y el robot cámara, así como para asegurar que el desplazamiento de la cámara se realiza de forma segura, sin causar ningún tipo de daños sobre la piel del paciente. En dicho esquema de control, la fuerza y la posición del brazo externo se desacoplan en dos movimientos: un desplazamiento sobre la superficie de contacto, y una fuerza en la dirección perpendicular a dicha superficie. Para el control de fuerza, se ha asumido un modelo de interacción elástico entre el robot y la superficie de contacto (pared abdominal), cuya constante de elasticidad se estima mediante un algoritmo RLS que actualiza los valores de la constante elástica con nuevas medidas tomadas durante el normal funcionamiento del asistente robótico. De esta manera, se tienen en cuenta las características particulares de la pared abdominal de cada paciente, ya que el espesor de la pared abdominal difiere enormemente de un paciente a otro.

El capítulo 4 describe una arquitectura cognitiva para el asistente robótico inteligente que permite que el sistema colabore con los cirujanos en un entorno quirúrgico co-worker. La arquitectura, que está basada en la arquitectura estándar SOAR (Laird 2012), está compuesta por un módulo cognitivo como principal componente del conocimiento y el razonamiento del sistema, unos módulos de percepción y acción para la interacción del sistema con el paciente, y un módulo de interacción humano-máquina para la comunicación con el cirujano. La arquitectura ofrece una fácil integración de los diferentes módulos y una fácil adaptación a otras tareas quirúrgicas, aunque este trabajo se centra en un entorno colaborativo en el que el asistente robótico se encarga de manejar la cámara. El módulo de cognición incluye diferentes tipos de memoria para almacenar información, y algoritmos de razonamiento y toma de decisiones dependiendo de la información que el sistema percibe tanto del paciente como del cirujano.

Por un lado, la memoria semántica almacena el conocimiento declarativo del sistema, esencial para las funciones de razonamiento y toma de decisiones, ya que contiene información básica que permite al sistema seguir el flujo de trabajo de una intervención. Este conocimiento se codifica como una base de datos que contiene información necesaria para el reconocimiento e identificación de objetos, protocolos

quirúrgicos, y los comportamientos esperados de la cámara en función del estado actual de la tarea. Un algoritmo de aprendizaje semántico permite añadir nueva información a la base de conocimiento del sistema relativa a las preferencias y formas de trabajar de cada cirujano.

Por otro lado, la memoria procedural contiene la estrategia de navegación de la cámara. Dicha estrategia se ha mejorado respecto de los trabajos previos encontrados en la literatura científica mediante la combinación de un comportamiento reactivo, que realiza un seguimiento continuo de las herramientas quirúrgicas, y un comportamiento proactivo, que adapta el punto de vista al flujo de trabajo de la intervención. Así, la navegación de la cámara se fundamenta en un algoritmo flexible que permite al robot adaptar su comportamiento a la forma de trabajar y preferencias de diferentes cirujanos, y además le permite reaccionar ante situaciones imprevistas y no programadas a priori. Este método de navegación se mejora en el tiempo mediante un mecanismo de refuerzo por aprendizaje, capaz de aprender la contribución de cada uno de los comportamientos del robot, reactivo y proactivo, al comportamiento global del asistente. Estas contribuciones se aprenden para cada cirujano y para cada estado dentro de la intervención completa. La capacidad de aprendizaje es una característica esencial para un agente inteligente, que no ha sido considerada en ninguno de los trabajos previos encontrados en la literatura.

El capítulo 5 presenta la implementación de los conceptos teóricos desarrollados en la presente tesis doctoral, y su validación mediante una serie de experimentos tanto in-vivo como in-vitro. En primer lugar, se describe la plataforma de experimentación, describiendo en detalles toda la arquitectura hardware que permite conectar entre sí los diferentes sistemas robóticos utilizados y el resto de dispositivos necesarios durante la implementación. A continuación, se describe la arquitectura software implementada, que se ha llevado a cabo en el software robótico ROS, que permite una fácil comunicación e integración de diversos dispositivos. Además, ROS permite comprobar el correcto funcionamiento y programación de cada uno de los dispositivos de forma individual como paso previo a la integración completa, una característica muy útil cuando se trabaja con sistemas compuestos por un gran número de dispositivos diferentes. Además, esta plataforma permite añadir de forma sencilla nuevos dispositivos al sistema, e incluso exportar los conceptos implementados en el presente trabajo a otras plataformas de experimentación. Por ejemplo, el brazo robótico Barrett WAM, utilizado como brazo externo del asistente robótico camarógrafo, puede ser fácilmente sustituido por otro tipo de brazo sin necesidad de modificar el resto del sistema, por ejemplo, para poder realizar un experimento en un laboratorio diferente. Esto permitiría poder validar todos los conceptos desarrollados en esta tesis doctoral en una plataforma como el da Vinci.

En cuanto a la experimentación, por un lado, el robot cámara ha sido validado mediante experimentación in-vivo con un modelo porcino, gracias a la colaboración de los cirujanos Eduardo Sánchez de Badajoz y Pilar Sánchez Gallegos. Mediante este experimento se ha demostrado la viabilidad de sustituir un endoscopio convencional por un robot cámara en un entorno quirúrgico real. Se ha demostrado que la interacción magnética entre el robot cámara y el imán externo es segura para el paciente y eficiente, y la calidad de la imagen proporcionada por el robot cámara tiene una calidad suficiente como para realizar tareas quirúrgicas reales. El experimento también ha revelado que el concepto de robot cámara presenta la ventaja adicional de que no se empaña, como ocurre con los endoscopios convencionales, que es necesario limpiarlos continuamente durante una intervención. Además, el robot cámara permite obtener más puntos de vista y perspectiva de las estructuras anatómicas que los endoscopios convencionales, proporcionando una visión más intuitiva y natural del campo operatorio, ya que la imagen viene desde arriba, al igual que ocurre en cirugía abierta. De esta manera, el robot cámara se puede utilizar como sistema único de visión sustituyendo el endoscopio en intervenciones laparoscópicas, o bien como cámara de apoyo al endoscopio que permita acceder a áreas inaccesibles por la cámara principal, u obtener una vista, por ejemplo, de la parte trasera de un órgano. Este enfoque podría aumentar las posibilidades de los procedimientos laparoscópicos actuales, abriendo las puertas a intervenciones que actualmente únicamente se realizan mediante cirugía abierta.

Por otro lado, tanto el control híbrido de fuerza-posición como la estrategia de navegación inteligente de la cámara, han sido validados mediante experimentación in-vitro en los laboratorios de robótica médica de la Universidad de Málaga. El control del asistente robótico diseñado permite realizar un desplazamiento seguro de la cámara a lo largo de la cavidad abdominal. Por otro lado, se ha demostrado que la combinación de un comportamiento reactivo y un comportamiento proactivo, proporciona una estrategia de navegación de la cámara flexible y autónoma, que no requiere del control directo del cirujano, y proporciona un punto de vista eficiente del campo operatorio durante una intervención quirúrgica. También se ha demostrado que la estrategia de navegación propuesta permite al sistema reaccionar de forma eficiente ante situaciones imprevistas, de un modo similar a como lo haría un asistente humano. Finalmente, se ha validado el mecanismo de aprendizaje del sistema, demostrándose que permite mejorar el comportamiento del robot y adaptar el punto de vista dependiendo del cirujano con el que esté colaborando.

Como trabajos futuros de esta tesis doctoral, se proponen las siguientes contribuciones:

6. Incluir el reconocedor de gestos en la implementación de la arquitectura cognitiva, ya que en el presente trabajo no se ha realizado debido a que esta contribución pertenece a una tesis doctoral anterior del grupo de investigación. Por lo tanto, un paso futuro consistirá en integrar el trabajo de la tesis previa con los resultados de la presente tesis doctoral.
7. Realizar un modelo dinámico del sistema de actuación de los grados de libertad del robot cámara. En el presente trabajo se ha validado el funcionamiento del accionamiento mediante cables diseñado en el robot cámara de acuerdo con las necesidades de la tarea específica en la cual se ha aplicado el dispositivo. Sin embargo, en el futuro se realizará un estudio completo del diseño del robot que incluya un modelo dinámico del sistema de actuación.
8. Aumentar las capacidades cognitivas del asistente robótico incorporando una memoria episódica. Este tipo de memoria permitiría incorporar información de experiencias pasadas a los algoritmos de toma de decisiones. De esta manera, los errores cometidos durante el normal funcionamiento del asistente se podrían corregir de forma autónoma en experiencias posteriores.
9. Mejora del control híbrido fuerza-posición mediante un análisis en profundidad de la interacción magnética entre el dispositivo intra-abdominal y el imán externo. De esta manera, se podría mejorar la estimación de la constante elástica que modela la superficie de contacto.
10. Experimentación in-vivo del asistente robótico completo. Por cuestiones logísticas, esta tesis ofrece resultados in-vivo únicamente del dispositivo intra-abdominal, habiéndose validado el resto del sistema en un entorno de laboratorio. Por lo tanto, como trabajo futuro se contempla la validación del sistema completa en un entorno quirúrgico real.

GLOSSARY OF TERMS

DoF: Degree of Freedom

FDA: US Food and Drug Administration

HMI: Human Machine Interface

HMM: Hidden Markov Models

HRI: human-robot interaction

HSV: hue-saturation-value

LED: Light Emitting Diode

LMA: Local Magnetic Actuation

LS: Laparoscopic Surgery

MAGS: Magnetic Anchoring and Guidance Systems

MIS: Minimally Invasive Surgery

MM: Markov Models

NOTES: Natural Orifice Transluminal Endoscopic Surgery

PI: proportional-integrative controller

RGB: red-green-blue

RL: reinforcement learning

RLS: Recurrent least square algorithm

ROS: Robotic Operating System

SMA: shape memory alloy

SPAS: Single Port Access Surgery

SRTWT: Simulink real-time Windows target

NOTATIONS

d_a	Width of the abdominal wall
d_c	Height of the camera robot
d_e	Height of the external robot attachment component
d_h	Height of the holder
D_i	Pulley diameter
d_I	Distance between the camera and the image plane
d_x	Shift along x-axis
d_y	Shift along y-axis
h	Image height
h_z	Zoomed image height
${}^{S1}O_{S2}$	Origin of reference system $\{S1\}$ with respect to $\{S2\}$
${}^{S1}R_{S2}$	Rotation matrix between references systems $\{S1\}$ and $\{S2\}$
${}^{S1}T_{S2}$	Transformation matrix between references systems $\{S1\}$ and $\{S2\}$
w	Image width
w_z	Zoomed image width
α	Roll rotation
β	Tilt rotation
θ_i	Motor rotation
φ	Pan rotation
d_α	Image displacement due to a camera roll rotation
d_β	Image displacement due to a camera tilt rotation
S	Semantic unit
M	Color marker
HSV	HSV coordinates of color marker

P	Point position in the image
O_I	Center of the image
K_{pm}	Constant to transform pixels to mm
F	Force
δ_R	Binary variable for right tool
δ_L	Binary variable for left tool
K_r	Contribution of the reactive behavior to the overall camera behavior
K_p	Contribution of the proactive behavior to the overall camera behavior
τ	Torque
ϕ	Angle formed by force vector and end effector z-axis
Z_E	z-axis of external robot end effector
u	Vector of rotation
D_T, D_N	Matrixes that decoupled force and position actions
K_P, K_I	Position controller gains
K_x	Stiffness matrix of the contact surface

REFERENCES

- Adam, C. et al. 2016. "Social Human-Robot Interaction: A New Cognitive and Affective Interaction-Oriented Architecture." In Springer International Publishing, 253–63.
- Al-Dujaili, A., K. Subramanian, and S. Suresh. 2015. "HumanCog: A Cognitive Architecture for Solving Optimization Problems." In *2015 IEEE Congress on Evolutionary Computation (CEC)*, IEEE, 3220–27.
- Alishahi, M.S., M. Mejri, and N. Tawbi. 2015. "Clustering Spam Emails into Campaigns." In *International Conference on Information Systems Security and Privacy*, , 90–97.
- Alterovitz, R., K.Y. Goldberg, J. Pouliot, and I.-C. Hsu. 2009. "Sensorless Motion Planning for Medical Needle Insertion in Deformable Tissues." *IEEE Transactions on Information Technology in Biomedicine* 13(2): 217–25.
- Anderlini, E. et al. 2016. "Control of a Point Absorber Using Reinforcement Learning." *IEEE Transactions on Sustainable Energy* 7(4): 1681–90.
- Azizian, M., M. Khoshnam, N. Najmaei, and R.V. Patel. 2014. "Visual Servoing in Medical Robotics: A Survey. Part I: Endoscopic and Direct Vision Imaging - Techniques and Applications." *The International Journal of Medical Robotics and Computer Assisted Surgery* 10(3): 263–74.
- Baili, Z., I. Tazi, and Y. Salih Alj. 2014. "StapBot: An Autonomous Surgical Suturing Robot Using Staples." In *2014 International Conference on Multimedia Computing and Systems (ICMCS)*, IEEE, 485–89.
- Bascetta, L. et al. 2011. "Towards Safe Human-Robot Interaction in Robotic Cells: An Approach Based on Visual Tracking and Intention Estimation." In *2011 IEEE/RSJ International Conference on Intelligent Robots and Systems*, IEEE, 2971–78.
- Bauzano, E. 2012. "Robot Asistente Semiautónomo de Dos Brazos Para Intervenciones de Cirugía Laparoscópica." Universidad de Málaga.
- Bauzano, E., B. Estebanez, I. Garcia-Morales, and V.F. Muñoz. 2015. "Collaborative Human-Robot System for HALS Suture Procedures." *IEEE Systems Journal*: 1–10.
- Bauzano, E., V.F. Muñoz, and I. Garcia-Morales. 2010. "Auto-Guided Movements on Minimally Invasive Surgery for Surgeon Assistance." In *2010 IEEE/RSJ International Conference on Intelligent Robots and Systems*, IEEE, 1843–48.

-
- Becker, T., J.A. Fabro, A.S. Oliveira, and L.P. Reis. 2015. "Adding Conscious Aspects in Virtual Robot Navigation through Baars-Franklin's Cognitive Architecture." In *2015 IEEE International Conference on Autonomous Robot Systems and Competitions*, IEEE, 204–9.
- Van den Berg, J. et al. 2010. "Superhuman Performance of Surgical Tasks by Robots Using Iterative Learning from Human-Guided Demonstrations." In *2010 IEEE International Conference on Robotics and Automation*, IEEE, 2074–81.
- Best, S.L. et al. 2012. "Solo Surgeon Laparo-Endoscopic Single Site Nephrectomy Facilitated by New Generation Magnetically Anchored and Guided Systems Camera." *Journal of Endourology* 26(3): 214–18.
- Bihlmaier, A., and H. Worn. 2015. "Learning Surgical Know-How: Dexterity for a Cognitive Endoscope Robot." In *2015 IEEE 7th International Conference on Cybernetics and Intelligent Systems (CIS) and IEEE Conference on Robotics, Automation and Mechatronics (RAM)*, IEEE, 137–42.
- Brancadoro, Margherita, Selene Tognarelli, Gastone Ciuti, and Arianna Menciassi. 2017. "A Novel Magnetic-Driven Tissue Retraction Device for Minimally Invasive Surgery." *Minimally Invasive Therapy & Allied Technologies* 26(1): 7–14.
- Brett, P.N. et al. 2007. "A Surgical Robot for Cochleostomy." In *2007 29th Annual International Conference of the IEEE Engineering in Medicine and Biology Society*, IEEE, 1229–32.
- Bucher, P., F. Pugin, and P. Morel. 2008. "Single Port Access Laparoscopic Right Hemicolectomy." *International Journal of Colorectal Disease* 23(10): 1013–16.
- Burghart, C. et al. 2005. "A Cognitive Architecture for a Humanoid Robot: A First Approach." In *5th IEEE-RAS International Conference on Humanoid Robots*, IEEE, 357–62.
- Butt, A.J. et al. 2013. "The Soar of Cognitive Architectures." In *2013 International Conference on Current Trends in Information Technology (CTIT)*, IEEE, 135–42.
- Cadeddu, J.A. et al. 2009. "Novel Magnetically Guided Intra-Abdominal Camera to Facilitate Laparoendoscopic Single-Site Surgery: Initial Human Experience." *Surgical Endoscopy* 23(8): 1894–99.
- Cangelosi, A. 2010. "Grounding Language in Action and Perception: From Cognitive Agents to Humanoid Robots." *Physics of Life Reviews* 7(2): 139–51.
-

- Casals, A., J. Amat, and E. Laporte. 1996. "Automatic Guidance of an Assistant Robot in Laparoscopic Surgery." *IEEE International Conference on Robotics and Automation Minneapolis*: 895–900.
- Castro, C.A. et al. 2012. "MARVEL: A Wireless Miniature Anchored Robotic Videoscope for Expedited Laparoscopy." In *2012 IEEE International Conference on Robotics and Automation*, IEEE, 2926–31.
- Chen, Ch., D. Dong, Y. Dong, and Q. Shi. 2006. "A Quantum Reinforcement Learning Method for Repeated Game Theory." In *2006 International Conference on Computational Intelligence and Security*, IEEE, 68–72.
- Chin, W.H., and C.K. Loo. 2013. "Biologically Inspired Topological Gaussian ARAM for Robot Navigation." In *2013 Second International Conference on Robot, Vision and Signal Processing*, IEEE, 265–69.
- Choi, D., K. Kim, D. Kim, and B.J. You. 2011. "Problem Solving and Learning for a Humanoid Robot." In *2011 IEEE International Conference on Robotics and Biomimetics*, IEEE, 2499–2504.
- Chong, H.-Q., A.-H. Tan, and G.-W. Ng. 2007. "Integrated Cognitive Architectures: A Survey." *Artificial Intelligence Review* 28(2): 103–30.
- Chow, D.-L., and W. Newman. 2013. "Improved Knot-Tying Methods for Autonomous Robot Surgery." In *2013 IEEE International Conference on Automation Science and Engineering (CASE)*, IEEE, 461–65.
- Choy, I., and A. Okrainec. 2012. "Fundamentals of Laparoscopic Surgery-FLS." In *The SAGES Manual of Quality, Outcomes and Patient Safety*, Boston, MA: Springer US, 461–71.
- Chui, C.-K., B.P. Nguyen, and R. Wen. 2014. "Development of a Cognitive Engine for Balancing Automation and Human Control of Surgical Robotic System." In *2014 11th International Conference on Ubiquitous Robots and Ambient Intelligence (URAI)*, IEEE, 13–17.
- Deeba, Farah, Shahed K. Mohammed, Francis M. Bui, and Khan A. Wahid. 2016. "Learning from Imbalanced Data: A Comprehensive Comparison of Classifier Performance for Bleeding Detection in Endoscopic Video." In *2016 5th International Conference on Informatics, Electronics and Vision (ICIEV)*, IEEE, 1006–9.
- Dimeas, A.L., and N.D. Hatziargyriou. 2010. "Multi-Agent Reinforcement Learning for Microgrids." In *IEEE PES General Meeting*, IEEE, 1–8.

-
- Dogmus, Z., E. Erdem, and V. Patoglu. 2013. “ReAct! An Interactive Tool for Hybrid Planning in Robotics.”
- Dumpert, J. et al. 2009. “Semi-Autonomous Surgical Tasks Using a Miniature in Vivo Surgical Robot.” In *2009 Annual International Conference of the IEEE Engineering in Medicine and Biology Society*, IEEE, 266–69.
- Elek, R. et al. 2016. “Recent Trends in Automating Robotic Surgery.” In *2016 IEEE 20th Jubilee International Conference on Intelligent Engineering Systems (INES)*, IEEE, 27–32.
- Estebanez, B. et al. 2012. “Maneuvers Recognition in Laparoscopic Surgery: Artificial Neural Network and Hidden Markov Model Approaches.” In *2012 4th IEEE RAS & EMBS International Conference on Biomedical Robotics and Biomechatronics (BioRob)*, , 1164–69.
- Estebanez, B. 2013. “Diseño E Implantación de Un Sistema Multimodal Para Un Asistente Robótico.”
- Estebanez, B., P. Del-Saz-Orozco, V.F. Munoz, and I. Garcia-Morales. 2010. “Maneuvers Recognition System for Laparoscopic Surgery.” In *19th International Workshop on Robotics in Alpe-Adria-Danube Region (RAAD 2010)*, IEEE, 87–92.
- “F/T Sensor Datasheet.” 2016. http://www.barrett.com/DS_FTSENSOR.pdf.
- Faghihi, U., and S. Franklin. 2012. “The LIDA Model as a Foundational Architecture for AGI.” In Atlantis Press, 103–21.
- Fakhry, M., B. Gallagher, F. Bello, and G.B. Hanna. 2009. “Visual Exposure Using Single-Handed Magnet-Driven Intra-Abdominal Wireless Camera in Minimal Access Surgery.” *Surgical Endoscopy* 23(3): 539–43.
- Foka, A.F., and P.E. Trahanias. 2010. “Probabilistic Autonomous Robot Navigation in Dynamic Environments with Human Motion Prediction.” *International Journal of Social Robotics* 2(1): 79–94.
- Fowler, D.L. et al. 2010. “Initial Trial of a Stereoscopic, Insertable, Remotely Controlled Camera for Minimal Access Surgery.” *Surgical Endoscopy* 24(1): 9–15.
- Franklin, S., T. Madl, S. D’Mello, and J. Snaider. 2014. “LIDA: A Systems-Level Architecture for Cognition, Emotion, and Learning.” *IEEE Transactions on Autonomous Mental Development* 6(1): 19–41.
- Garbin, Nicolo et al. 2016. “Laparoscopic Camera Based on an Orthogonal Magnet
-

- Arrangement.” *IEEE Robotics and Automation Letters* 1(2): 924–29.
- Garbin, Nicolò et al. 2015. “Laparoscopic Tissue Retractor Based on Local Magnetic Actuation.” *Journal of Medical Devices* 9(1): 11005.
- Garcia-Martinez, Alvaro, Carlos G. Juan, Nicolas M. Garcia, and Jose Maria Sabater-Navarro. 2015. “Automatic Detection of Surgical Gauzes Using Computer Vision.” In *2015 23rd Mediterranean Conference on Control and Automation (MED)*, IEEE, 747–51.
- Gascón Hove, M. et al. 2014. “Single-Port Access Surgery Resection of a Presacral Schwannoma | SpringerLink.” *Techniques in Coloproctology* 18(4): 407–8.
- Gilbert, J M. 2009. “The EndoAssist Robotic Camera Holder as an Aid to the Introduction of Laparoscopic Colorectal Surgery.” *Annals of the Royal College of Surgeons of England* 91(5): 389–93.
- Griffiths, T.L., M. Steyvers, and J.B. Tenenbaum. 2007. “Topics in Semantic Representation.” *Psychological Review* 114(2): 211–44.
- Haddadin, S. et al. 2011. “Towards the Robotic Co-Worker.” In Springer Berlin Heidelberg, 261–82.
- Hagn, U. et al. 2010. “DLR MiroSurge: A Versatile System for Research in Endoscopic Telesurgery.” *International Journal of Computer Assisted Radiology and Surgery* 5(2): 183–93.
- Haidegger, T., J. Sándor, and Z. Benyó. 2011. “Surgery in Space: The Future of Robotic Telesurgery.” *Surgical Endoscopy* 25(3): 681–90.
- Hanford, S.D. 2011. “A Cognitive Robotic System Based on the Soar Cognitive Architecture for Mobile Robot Navigation, Search, and Mapping Missions.”
- Hu, D., Y. Gong, B. Hannaford, and E.J. Seibel. 2015. “Semi-Autonomous Simulated Brain Tumor Ablation with RAVENII Surgical Robot Using Behavior Tree.” In *2015 IEEE International Conference on Robotics and Automation (ICRA)*, IEEE, 3868–75.
- Hu, T., P.K. Allen, N. J. Hogle, and D.L. Fowler. 2009. “Insertable Surgical Imaging Device with Pan, Tilt, Zoom, and Lighting.” *The International Journal of Robotics Research* 28(10): 1373–86.
- Hynes, P., G.I. Dodds, and A.J. Wilkinson. 2005. “Uncalibrated Visual-Servoing of a Dual-Arm Robot for Surgical Tasks.” In *2005 International Symposium on Computational Intelligence in Robotics and Automation*, IEEE, 151–56.

-
- Iima, H., and Y. Kuroe. 2015. "Swarm Reinforcement Learning Methods Improving Certainty of Learning for a Multi-Robot Formation Problem." In *2015 IEEE Congress on Evolutionary Computation (CEC)*, IEEE, 3026–33.
- Infantino, I., A. Chella, H. Dindo, and I. Macaluso. 2005. "A Cognitive Architecture for Robotic Hand Posture Learning." *IEEE Transactions on Systems, Man and Cybernetics, Part C (Applications and Reviews)* 35(1): 42–52.
- Jackson, R.C., and M.C. Cavusoglu. 2013. "Needle Path Planning for Autonomous Robotic Surgical Suturing." In *2013 IEEE International Conference on Robotics and Automation*, IEEE, 1669–75.
- Jagodnik, K.M. et al. 2016. "Human-Like Rewards to Train a Reinforcement Learning Controller for Planar Arm Movement." *IEEE Transactions on Human-Machine Systems*: 1–11.
- Janrathitikarn, O., and L.N. Long. 2008. "Gait Control of a Six-Legged Robot on Unlevel Terrain Using a Cognitive Architecture." In *2008 IEEE Aerospace Conference*, IEEE, 1–9.
- Jansen, R. et al. 2009. "Surgical Retraction of Non-Uniform Deformable Layers of Tissue: 2D Robot Grasping and Path Planning." In *2009 IEEE/RSJ International Conference on Intelligent Robots and Systems*, IEEE, 4092–97.
- Kajdoci, L., and C.R. Pozna. 2014. "Review of the Most Successfully Used Cognitive Architectures in Robotics and a Proposal for a New Model of Knowledge Acquisition." In *2014 IEEE 12th International Symposium on Intelligent Systems and Informatics (SISY)*, IEEE, 239–44.
- Kamei, K., and Y. Kakizoe. 2016. "An Approach to the Development of a Game Agent Based on SOM and Reinforcement Learning." In *2016 5th IIAI International Congress on Advanced Applied Informatics (IIAI-AAI)*, IEEE, 669–74.
- Kang, H., and J.T. Wen. 2001. "EndoBot: A Robotic Assistant in Minimally Invasive Surgeries." In *Proceedings 2001 ICRA. IEEE International Conference on Robotics and Automation (Cat. No.01CH37164)*, IEEE, 2031–36.
- Kassahun, Y. et al. 2016. "Surgical Robotics beyond Enhanced Dexterity Instrumentation: A Survey of Machine Learning Techniques and Their Role in Intelligent and Autonomous Surgical Actions." *International Journal of Computer Assisted Radiology and Surgery* 11(4): 553–68.
- Kehoe, B. et al. 2014. "Autonomous Multilateral Debridement with the Raven
-

- Surgical Robot.” In *2014 IEEE International Conference on Robotics and Automation (ICRA)*, IEEE, 1432–39.
- Kim, B.G., Y. Zhang, M. van der Schaar, and J-W Lee. 2016. “Dynamic Pricing and Energy Consumption Scheduling With Reinforcement Learning.” *IEEE Transactions on Smart Grid* 7(5): 2187–98.
- Kirk, J., A. Mininger, and J.E. Laird. 2016. “Learning Task Goals Interactively with Visual Demonstrations.” *Biologically Inspired Cognitive Architectures*.
- Kleinmann, L., and B. Mertsching. 2011. “Learning to Adapt: Cognitive Architecture Based on Biologically Inspired Memory.” In *2011 6th IEEE Conference on Industrial Electronics and Applications*, IEEE, 936–41.
- Ko, S.Y., J. Kim, D.-S. Kwon, and W.-J. Lee. 2005. “Intelligent Interaction between Surgeon and Laparoscopic Assistant Robot System.” In *ROMAN 2005. IEEE International Workshop on Robot and Human Interactive Communication, 2005.*, IEEE, 60–65.
- Koubaa, Anis, ed. 2016. *625 Robot Operating System (ROS)*. Cham: Springer International Publishing.
- Kraft, B. M. et al. 2004. “The AESOP Robot System in Laparoscopic Surgery: Increased Risk or Advantage for Surgeon and Patient?” *Surgical Endoscopy* 18(8): 1216–23.
- Krupa, A. et al. 2003. “Autonomous 3-D Positioning of Surgical Instruments in Robotized Laparoscopic Surgery Using Visual Servoing.” *IEEE Transactions on Robotics and Automation* 19(5): 842–53.
- Laird, J.E. 2008. “Extending the Soar Cognitive Architecture.” In *Artificial General Intelligence 2008: Proceedings of the First AGI Conference*, eds. P. Wang and S. Franklin. IOS Press Inc., 224–35.
- Laird, J.E. 2012. *The Soar Cognitive Architecture*. MIT Press.
- Laird, J.E., K.R. Kinkade, S. Mohan, and J.Z. Xu. 2012. “Cognitive Robotics Using the Soar Cognitive Architecture.” In *8th International Workshop on Cognitive Robotics*, , 46–54.
- Lanfranco, A.R., A.E. Castellanos, J.P. Desai, and W.C. Meyers. 2004. “Robotic Surgery: A Current Perspective.” *Annals of Surgery* 239(1): 14–21.
- Langley, P., J.E. Laird, and S. Rogers. 2009. “Cognitive Architectures: Research Issues and Challenges.” *Cognitive Systems Research* 10(2): 141–60.

-
- Lehman, A.C. et al. 2008. "Surgery with Cooperative Robots." *Computer Aided Surgery* 13(2): 95–105.
- Lehman, A.C. et al. 2009. "Natural Orifice Cholecystectomy Using a Miniature Robot." *Surgical Endoscopy* 23(2): 260–66.
- Lehman, A.C. et al. 2011. "Dexterous Miniature Robot for Advanced Minimally Invasive Surgery." *Surgical Endoscopy* 25(1): 119–23.
- Lei, Y., and P.S. Yu. 2016. "Multi-Agent Reinforcement Learning for Service Composition." In *2016 IEEE International Conference on Services Computing (SCC)*, IEEE, 790–93.
- Leonard, S. et al. 2014. "Smart Tissue Anastomosis Robot (STAR): A Vision-Guided Robotics System for Laparoscopic Suturing." *IEEE Transactions on Biomedical Engineering* 61(4): 1305–17.
- Leong, Florence et al. 2016. "Magnetic Surgical Instruments for Robotic Abdominal Surgery." *IEEE Reviews in Biomedical Engineering* 9: 66–78.
- Li, Ning, Gregory J. Mancini, and Jindong Tan. 2016. "Hardware Design for a Cable-Free Fully Insertable Wireless Laparoscopic Robotic Camera." In *2016 38th Annual International Conference of the IEEE Engineering in Medicine and Biology Society (EMBC)*, IEEE, 5128–31.
- Liu, Y. et al. 2016. "Cognitive Architecture Based Platform on Human Performance Evaluation for Space Manual Control Task." In Springer International Publishing, 303–14.
- Martínez Rodríguez, J.L. 2004. *Control de Procesos Industriales*.
- Matlin, M.W. 2005. *Cognition*. ed. Inc. Crawfordsville: John Wiley & Sons.
- Mayer, H. et al. 2008. "Automation of Manual Tasks for Minimally Invasive Surgery." In *Fourth International Conference on Autonomic and Autonomous Systems (ICAS'08)*, IEEE, 260–65.
- Muñoz, V.F. et al. 2006. "Control Movement Scheme Based on Manipulability Concept for a Surgical Robotic Assistant." In *Proceedings 2006 IEEE International Conference on Robotics and Automation, 2006. ICRA 2006.*, IEEE, 245–50.
- Muñoz, V.F. et al. 2005. "Pivoting Motion Control for a Laparoscopic Assistant Robot and Human Clinical Trials." *Advanced Robotics* 19(6): 694–712.
- Muradore, R. et al. 2011. "Robotic Surgery." *IEEE Robotics & Automation*
-

- Magazine* 18(3): 24–32.
- Nageotte, F., P. Zanne, C. Doignon, and M. de Mathelin. 2009. “Stitching Planning in Laparoscopic Surgery: Towards Robot-Assisted Suturing.” *The International Journal of Robotics Research* 28(10): 1303–21.
- Natali, Christian Di, Alireza Mohammadi, Denny Oetomo, and Pietro Valdastri. 2015. “Surgical Robotic Manipulator Based on Local Magnetic Actuation.” *Journal of Medical Devices* 9(3): 30936-1-2.
- Niccolini, M., G. Petroni, A. Menciassi, and P. Dario. 2012. “Real-Time Control Architecture of a Novel Single-Port lapaRoscopy bimaNual roboT (SPRINT).” In *2012 IEEE International Conference on Robotics and Automation*, IEEE, 3395–3400.
- Noonan, D.P. et al. 2010. “Gaze Contingent Control for an Articulated Mechatronic Laparoscope.” In *2010 3rd IEEE RAS & EMBS International Conference on Biomedical Robotics and Biomechatronics*, IEEE, 759–64.
- Noonan, D.P., G.P. Mylonas, A. Darzi, and G.-Z. Yang. 2008. “Gaze Contingent Articulated Robot Control for Robot Assisted Minimally Invasive Surgery.” In *2008 IEEE/RSJ International Conference on Intelligent Robots and Systems*, IEEE, 1186–91.
- Osa, T., N. Sugita, and M. Mamoru. 2014. “Online Trajectory Planning in Dynamic Environments for Surgical Task Automation.” *Robotics: Science and Systems (RSS)*.
- Padoy, N., and G.D. Hager. 2011. “Human-Machine Collaborative Surgery Using Learned Models.” In *2011 IEEE International Conference on Robotics and Automation*, IEEE, 5285–92.
- Pandya, A. et al. 2014. “A Review of Camera Viewpoint Automation in Robotic and Laparoscopic Surgery.” *Robotics* 3(3): 310–29.
- Park, I.J. et al. 2009. “Multidimensional Analysis of the Learning Curve for Laparoscopic Colorectal Surgery: Lessons from 1,000 Cases of Laparoscopic Colorectal Surgery.” *Surgical Endoscopy* 23(4): 839–46.
- Park, Sangtae et al. 2007. “Trocarr-Less Instrumentation for Laparoscopy: Magnetic Positioning of Intra-Abdominal Camera and Retractor.” *Annals of surgery* 245(3): 379–84.
- Patil, S., and R. Alterovitz. 2010. “Toward Automated Tissue Retraction in Robot-Assisted Surgery.” In *2010 IEEE International Conference on Robotics and*

-
- Automation*, IEEE, 2088–94.
- Pérez del Pulgar, C. 2015. “Smart Navigation in Surgical Robotics.” Universidad de Málaga.
- Petroni, G. et al. 2013. “A Novel Robotic System for Single-Port Laparoscopic Surgery: Preliminary Experience.” *Surgical endoscopy* 27(6): 1932–37.
- Polet, R., and J. Donnez. 2008. “Using a Laparoscope Manipulator (LAPMAN) in Laparoscopic Gynecological Surgery.” *Surgical technology international* 17: 187–91.
- Profanter, S. 2012. “Cognitive Architectures.” *Hauptseminar Human Robot Interaction*.
- Raza, M., and V.V.S.S. Sastry. 2008. “Variability in Behavior of Command Agents with Human-Like Decision Making Strategies.” In *Tenth International Conference on Computer Modeling and Simulation (Uksim 2008)*, IEEE, 562–67.
- Reiley, C.E., E. Plaku, and G.D. Hager. 2010. “Motion Generation of Robotic Surgical Tasks: Learning from Expert Demonstrations.” In *2010 Annual International Conference of the IEEE Engineering in Medicine and Biology*, IEEE, 967–70.
- Rivas-Blanco, I. et al. 2016. “Full Vision System in Laparoscopy.” *Actas Urológicas Españolas* in press.
- Rodriguez-Molares, Alfonso, Lasse Lovstakken, Ingvild Kinn Ekroll, and Hans Torp. 2015. “Needle Detection by Image Source Localization.” In *2015 IEEE International Ultrasonics Symposium (IUS)*, IEEE, 1–4.
- Romanelli, J.R., L. Mark, and P.A. Omotosho. 2008. “Single Port Laparoscopic Cholecystectomy with the TriPort System: A Case Report.” *Surgical innovation* 15(3): 223–28.
- “ROS.org.” 2016. <http://www.ros.org/about-ros/>.
- Rosen, J. et al. 2006. “Generalized Approach for Modeling Minimally Invasive Surgery as a Stochastic Process Using a Discrete Markov Model.” *IEEE Transactions on Biomedical Engineering* 53(3): 399–413.
- Sahu, Manish, Anirban Mukhopadhyay, Angelika Szengel, and Stefan Zachow. 2017. “Addressing Multi-Label Imbalance Problem of Surgical Tool Detection Using CNN.” *International Journal of Computer Assisted Radiology and Surgery*.
-

- Salerno, M. et al. 2013. "Anchoring Frame for Intra-Abdominal Surgery." *The International Journal of Robotics Research* 32(3): 360–70.
- Shademan, A. et al. 2016. "Supervised Autonomous Robotic Soft Tissue Surgery." *Science Translational Medicine* 8(337).
- Shah, A., and A. Shah. 2008. "Minimally Invasive Surgery." *The Indian Journal of Pediatrics* 75(9): 925–29.
- Shiller, Z., O. Gal, and E. Rimon. 2010. "Safe Navigation in Dynamic Environments." In Springer Vienna, 225–32.
- Simi, M. et al. 2013. "Magnetically Activated Stereoscopic Vision System for Laparoendoscopic Single-Site Surgery." *IEEE/ASME Transactions on Mechatronics* 18(3): 1140–51.
- "Soar Home." 2016. <http://soar.eecs.umich.edu/> (October 20, 2016).
- Song, Y., Y.-B. Li, C.-H. Li, and G.-F. Zhang. 2012. "An Efficient Initialization Approach of Q-Learning for Mobile Robots." *International Journal of Control, Automation and Systems* 10(1): 166–72.
- Stolzenburg, J.-U. et al. 2011. "Comparison of the FreeHand® Robotic Camera Holder with Human Assistants during Endoscopic Extraperitoneal Radical Prostatectomy." *BJU International* 107(6): 970–74.
- Sun, R., and S. Helie. 2015. "Accounting for Creativity Within a Psychologically Realistic Cognitive Architecture." In Atlantis Press, 151–65.
- Sun, R., and Nick Wilson. 2011. "Motivational Processes Within the Perception–Action Cycle." In *Perception-Action Cycle*, New York, NY: Springer New York, 449–72.
- Sun, R., Nick Wilson, and M.F. Lynch. 2016. "Emotion: A Unified Mechanistic Interpretation from a Cognitive Architecture." *Cognitive Computation* 8(1): 1–14.
- Tanweer, M. R., S. Suresh, and N. Sundararajan. 2014. "Human Meta-Cognition Inspired Collaborative Search Algorithm for Optimization." In *2014 International Conference on Multisensor Fusion and Information Integration for Intelligent Systems (MFI)*, IEEE, 1–6.
- Taylor, R.H. 2006. "A Perspective on Medical Robotics." *Proceedings of the IEEE* 94(9): 1652–64.
- "The EUROSURGE Project." 2016. <http://www.eurosurge.eu/eurosurge/>.

-
- Tognarelli, S. et al. 2015. “A Miniaturized Robotic Platform for Natural Orifice Transluminal Endoscopic Surgery: In Vivo Validation.” *Surgical Endoscopy* 29(12): 3477–84.
- Tokic, M., and G. Palm. 2011. “Value-Difference Based Exploration: Adaptive Control between Epsilon-Greedy and Softmax.” In Springer Berlin Heidelberg, 335–46.
- Tortora, G. et al. 2011. “Design of Miniature Modular in Vivo Robots for Dedicated Tasks in Minimally Invasive Surgery.” In *2011 IEEE/ASME International Conference on Advanced Intelligent Mechatronics (AIM)*, IEEE, 327–32.
- Tortora, G. et al. 2013. “A Modular Magnetic Platform for Natural Orifice Transluminal Endoscopic Surgery.” In *2013 35th Annual International Conference of the IEEE Engineering in Medicine and Biology Society (EMBC)*, IEEE, 6265–68.
- Tortora, G. et al. 2014. “A Miniature Robot for Retraction Tasks under Vision Assistance in Minimally Invasive Surgery.” *Robotics* 3(1): 70–82.
- Tortora, G., P. Dario, and A. Menciassi. 2014. “Array of Robots Augmenting the Kinematics of Endocavitary Surgery.” *IEEE/ASME Transactions on Mechatronics* 19(6): 1821–29.
- Trejos, A.L. et al. 2011. “Force Sensing in Natural Orifice Transluminal Endoscopic Surgery.” *Surgical Endoscopy* 25(1): 186–92.
- Varela, J. Esteban, Samuel E. Wilson, and Ninh T. Nguyen. 2010. “Laparoscopic Surgery Significantly Reduces Surgical-Site Infections Compared with Open Surgery.” *Surgical Endoscopy* 24(2): 270–76.
- Voros, S. et al. 2010. “ViKY Robotic Scope Holder: Initial Clinical Experience and Preliminary Results Using Instrument Tracking.” *IEEE/ASME Transactions on Mechatronics*.
- “WAM ARM Datasheet.” 2016. http://www.barrett.com/DS_WAM.pdf. http://www.barrett.com/DS_WAM.pdf (September 30, 2016).
- Wang, C.J. et al. 2016. “Natural Orifice Transluminal Endoscopic Surgery-Assisted versus Laparoscopic Ovarian Cystectomy (NAOC vs. LOC): A Case-Matched Study.” *Surgical Endoscopy* 30(3): 1227–34.
- Wang, W., A.-H. Tan, and L.-N. Teow. 2016. “Semantic Memory Modeling and Memory Interaction in Learning Agents.” *IEEE Transactions on Systems, Man, and Cybernetics: Systems*: 1–14.
-

- Weede, O. et al. 2013. "Towards Cognitive Medical Robotics in Minimal Invasive Surgery." In *Proceedings of Conference on Advances In Robotics - AIR '13*, New York, New York, USA: ACM Press, 1–8.
- Weede, O., H. Monnich, B. Muller, and H. Worn. 2011. "An Intelligent and Autonomous Endoscopic Guidance System for Minimally Invasive Surgery." In *2011 IEEE International Conference on Robotics and Automation*, IEEE, 5762–68.
- Wei, G.-Q., K. Arbter, and G. Hirzinger. 1997. "Real-Time Visual Servoing for Laparoscopic Surgery. Controlling Robot Motion with Color Image Segmentation." *IEEE Engineering in Medicine and Biology Magazine* 16(1): 40–45.
- Whiteson, S. 2010. "Reinforcement Learning." In *Adaptive Representations for Reinforcement Learning*, Springer Berlin Heidelberg, 7–15.
- Wilkes, D.M. et al. 2010. "Heterogeneous Artificial Agents for Triage Nurse Assistance." In *2010 10th IEEE-RAS International Conference on Humanoid Robots*, IEEE, 130–37.
- Wilson, M. et al. 2010. "Psychomotor Control in a Virtual Laparoscopic Surgery Training Environment: Gaze Control Parameters Differentiate Novices from Experts." *Surgical Endoscopy* 24(10): 2458–64.
- Wilson, N.R., and R. Sun. 2014. "Coping with Bullying: A Computational Emotion-Theoretic Account." In *Proceedings of the Annual Conference of Cognitive Science Society*, , 3119–24.
- Wolf, D.F., and G.S. Sukhatme. 2008. "Semantic Mapping Using Mobile Robots." *IEEE Transactions on Robotics* 24(2): 245–58.
- Woolley, Gary. 2011. "Cognitive Architecture." In *Reading Comprehension*, Dordrecht: Springer Netherlands, 35–47.
- Xue, H-J, J-F Pang, Y-C Luan, and Y-Q Tie. 2012. "Computational Cognitive Modeling of Civil Aviation Pilots." In *International Conference on Automatic Control and Artificial Intelligence (ACAI 2012)*, Institution of Engineering and Technology, 668–71.
- Yan, Y., B. Zhang, and J. Guo. 2016. "An Adaptive Decision Making Approach Based on Reinforcement Learning for Self-Managed Cloud Applications." In *2016 IEEE International Conference on Web Services (ICWS)*, IEEE, 720–23.
- Yoon, S.M., W.J. Kim, and M.C. Lee. 2015. "Design of Bilateral Control for Force

-
- Feedback in Surgical Robot.” *International Journal of Control, Automation and Systems* 13(4): 916–25.
- Yu, Y.-X., and H.-P. Mang. 2002. “A Social Cognition Model Applied to General Combinatorial Optimization Problem.” In *Proceedings. International Conference on Machine Learning and Cybernetics*, IEEE, 1208–13.
- Zeltser, Ilia S. et al. 2007. “Single Trocar Laparoscopic Nephrectomy Using Magnetic Anchoring and Guidance System in the Porcine Model.” *The Journal of Urology* 178(1): 288–91.
- Zhang et al. 2010. “Integrating HTN Planner in Cleaning-Security Robot: Handling Planning with Memory and Problem Template.” In *2010 IEEE International Conference on Automation and Logistics*, IEEE, 55–60.
- Zhang, Lin, Menglong Ye, Po-Ling Chan, and Guang-Zhong Yang. 2017. “Real-Time Surgical Tool Tracking and Pose Estimation Using a Hybrid Cylindrical Marker.” *International Journal of Computer Assisted Radiology and Surgery*.
- Zhang, S. et al. 2014. “Recent Development of Modeling Simulated RVD Tasks in a Cognitive Architecture.” In *2014 Sixth International Conference on Intelligent Human-Machine Systems and Cybernetics*, IEEE, 223–26.
- Zhang, X., and N. Tanigawa. 2009. “Learning Curve of Laparoscopic Surgery for Gastric Cancer, a Laparoscopic Distal Gastrectomy-Based Analysis.” *Surgical Endoscopy* 23(6): 1259–64.
- Zhuang, Jinlei et al. 2014. “Video System Design of a Miniature Cable-Free Robot for LESS.” In *2014 IEEE International Conference on Mechatronics and Automation*, IEEE, 535–40.